UNCLASSIFIED

AD 261 041

UNCLASSIFIED

WADD TECHNICAL REPORT 60-518

THE DYNAMIC RESPONSE
OF ADVANCED VEHICLES

Q. R. Bohne
B. E. Clingan
C. W. deCeault
P. C. Deutschle

BOEING AIRPLANE COMPANY

SEPTEMBER 1960

FLIGHT DYNAMICS LABORATORY
WRIGHT AIR DEVELOPMENT DIVISION
AIR RESEARCH AND DEVELOPMENT COMMAND
UNITED STATES AIR FORCE

AF-WP-B-JUL 61 1 15

THE DYNAMIC RESPONSE
OF ADVANCED VEHICLES

Q. R. Bohne
B. E. Clingan
C. W. deCeault
P. C. Deutschle

BOEING AIRPLANE COMPANY

SEPTEMBER 1960

WRIGHT AIR DEVELOPMENT DIVISION

AIR RESEARCH AND DEVELOPMENT COMMAND
UNITED STATES AIR FORCE
WRIGHT-PATTERSON AIR FORCE BASE, OHIO

FOREWORD

The research reported herein was conducted by the Aero-Space
Division of the Boeing Airplane Company, Seattle, Washington, under
Air Force Contract No. AF33(616)-6597, Project No. 1370, "Dynamic
Problems in Flight Vehicles," Task No. 14000 "Dynamic Loads Design
Criteria" for the Dynamics Branch of the Flight Dynamics Laboratory,
Wright Air Development Division. Captain L. J. Wine and Mr. W. P. Dunn
administered the program as WADD Project Engineers.

In addition to the listed authors, many other members of the
Boeing Airplane Company too numerous to mention by name, made valuable
contributions to this report.

ABSTRACT

An analytical study program has been conducted in order to determine dynamic load conditions and governing parameters for the flight of advanced vehicles; and an assessment of the adequacy and the applicability of existing dynamic loads predictions methods has been made.

A typical two stage liquid fuel boost-glide configuration is assumed for the study, thus allowing for the interaction of such variables as fuel slosh, structural flexibility, aerodynamic forces and control system forces. The report is divided into sections which discuss dynamic loads in the following areas: pre-launch, launch, boosted flight, staging, re-entry and landing or recovery. Included in the Appendices are discussions of modal determination, simplified methods of analysis, computational techniques, and ground wind criteria. Also included is a development of flight equations of motion and an extensive bibliography of reference material.

As a general conclusion it might be stated that the most formidable problems associated with dynamic loads determination result from man's inability to define aerodynamic forces accurately. Although mathematical models are becoming more complex, involving time-varying coefficients and nonlinear terms, their solutions can be obtained by the use of digital and analog computers.

PUBLICATION REVIEW

This report has been reviewed and is approved.

FOR THE COMMANDER:

John P. Taylor
Colonel, USAF
Chief, Flight Dynamics Laboratory

TABLE OF CONTENTS

SECTION I

INTRODUCTION AND SUMMARY

A. BACKGROUND

The extension of vehicular performance to greater velocities, altitudes and ranges generally requires utilization of lighter, more flexible structures and low-aspect-ratio, slender-body configurations. Current design trends are also directed toward reducing factors of safety for both manned and unmanned vehicles in order to obtain desired performance. The design trends noted are such as to increase the importance of dynamic loads incurred by advanced vehicl Therefore, it is imperative that dynamic loading conditions and governing parameters be determined and that existing prediction methods be assessed for adequacy and applicability.

Although it is recognized that any proposed configuration will have unique dynamic load problems that cannot be solved in advance by general studies, a complete study of a selected vehicle will point out those areas that are apt to be most critical for the type of configuration considered. Therefore, the vehicle configuration and mission profile described in Appendix A are chosen as being representative of advanced boost glide vehicles. The significant characteristics of the configuration can be summarized by stating that a manned glide vehicle is boosted into a once around orbit by a two-stage liquid fuel booster. Thus the problem areas to be considered range from prelaunch loads to landing or recovery loads, and the effects of vehicle characteristics such as flexibility, fuel slosh, and control system parameters are to be investigated.

Because of the large scope of the study, the report is divided into sections which, as far as practicable, are independent of the material in the other sections. In cases where necessary detailed developments would interrupt the smooth presentation of the material, these developments are presented as Appendices.

B. SUMMARY OF RESULTS

1. GENERAL RESULTS

The major results of the entire study are summarized in this section and are given by section as they occur in the body of the report. Since the study is primarily concerned with an evaluation of methods, the magnitude of the answers is of secondary importance, especially where deficiencies exist in criteria or experimental data. None the less it is desirable to make some comparisons as to the relative criticality of various loading conditions. Therefore, the summary curve of Fig. I-1 is presented to show bending moments arising from different loading conditions along the trajectory, based on the best available environmental descriptions. It is evident that wind shear and gust loads during boost cause the largest loads.

---

2. PRELAUNCH LOADS

The prelaunch loads considered are those due to ground wind and ground shock. The ground wind studies include both discrete gust and random turbulence criteria. The random turbulence studies in general produce lower loads than those in which critically phased discrete gusts are considered. The oscillatory loads due to vortex shedding cannot be accurately predicted because of the lack of information describing the forcing function; hence only an illustrative example is shown. The loads due to a typical ground shock have been calculated. The shock spectra method used to determine ground shock effects is quite conservative since the absolute values of the maximum load responses in each mode are added directly.

3. LAUNCH LOADS

The launch loads considered are transverse loads due to a sudden relaxation of hold-down restraints and axial loads due to thrust initiation. The maximum transverse bending moments increase when the delay time in activating the control mechanism at release is increased. The addition of higher modes (above the second mode) in the analysis has a small effect on the transverse bending moments. The inclusion of nozzle inertia with a refined control law has no significant effect on the transverse bending moments. A procedure is suggested for estimating axial loads, and the maximum acceleration of the glider encountered during thrust initiation.

4. BOOST FLIGHT LOADS

The dynamic loads experienced during boost are the most critical encountered for a large portion of the structure. Loads due to wind shear, discrete gusts, and continuous random turbulence have been determined; and the effects of control system representation, structural representation and fuel slosh have been studied. The effects of variations in some of the control system parameters and glider lift curve slope on loads have also been determined.

The maximum bending moments are produced by the wind shear, although discrete gust loads are nearly as severe. Solutions have been obtained using a digital program, incorporating time-varying coefficients and using an analog program incorporating constant coefficients. The parameter studies have been conducted on the analog computer.

A very simple control system representation is shown to be adequate for the dynamic load studies, but a more refined representation is required to determine the stability boundaries. A method of determining the control gain settings required to give a certain frequency and damping in pitch, including the effect of flexibility, has been developed (Appendix D). Structural representations ranging from rigid body to three flexible modes are considered; two coupled modes are completely adequate in this study. For some purposes it is sufficiently accurate to use only one beam mode or to assume static deformation of the structure. A simplified method using an assumed mode shape has also been developed which may be accurate enough for preliminary estimates of bending loads (Appendix E). Fuel slosh response due to wind shear is large, but the effect of sloshing on the vehicle response is negligible. Bending loads, during boost, are quite sensitive to the glider lift curve slope. Therefore, improvement in the knowledge of the aerodynamic forces will allow corresponding improvement in the accuracy with which bending loads may be determined.

5. STAGING

The most severe loading condition, resulting from the staging process, occurs at the instant of start burn of the succeeding stage. This condition is critical in the extreme case of full vectoring of the engine nozzles to maintain a programmed attitude. The bending moment calculated for this condition is of such a magnitude (0.2×10^6 in-lbs at the mass center) that no serious load problem is expected from a staging process within the capabilities of the vehicle to maintain its stability. It appears that the real problem in staging is one of control to maintain stability, rather than of load.

6. RE-ENTRY

During re-entry the vehicle is subjected to elevated temperatures, maneuver loads, and atmospheric turbulence. Although elevated temperature effects constitute a serious detailed design problem, only the effect of temperature on material properties is considered significant in this study. The maneuver loads which might occur at elevated temperatures are more critical than loads due to atmospheric turbulence.

7. LANDING AND RECOVERY

The lower bound of the maximum deceleration that a vehicle is subject to upon landing is dependent on the square of the relative velocity normal to the landing surface at the instant of contact, and it is for this reason that the design of a parachute and/or air brake be included in the recovery system.

The lower bound of the maximum deceleration is inversely dependent on the maximum relative deformation normal to the landing medium (land, water,etc) of the landing gear or medium (water, etc) which takes place from the instant of contact to that instant when the relative normal velocity has been reduced to zero.

A priori no upper bound on the maximum deceleration can be placed, but it is estimated that by proper design of the landing mechanism, the deceleration should not exceed twice the lower bound.

The procedure outlined in this study should prove adequate for investigating the loads which result from a conventional landing approach on either land or sea. In particular, the treatment given for solving nonlinear landing gear problems can be easily extended to the rational analysis of complex landing gear-glider systems.

C. CONCLUSIONS AND AREAS FOR FUTURE RESEARCH

When embarking upon a general research study such as the one reported herein one is always hopeful of bringing together the needed data and analyses to reduce the problem to a routine operation. However, as is the case in this study, the end product all too often is a greater appreciation of the problems yet unsolved. Therefore, the following remarks are made concerning the results of this study.

1. Even during the time that this contract was being carried out, the concept of an "advanced vehicle" changed significantly. Therefore, caution must be exercised in applying the results to different configurations.

2. Control system parameters are found to have an important effect on loads and a more important effect on stability. On larger boosters with lower structural frequencies, adaptive control systems may be necessary to insure stability. It is important that these systems also be analyzed for transient load responses.

3. The nature of aerodynamic forces acting on vehicles in the launch position is not at present understood. This is strikingly demonstrated when one examines recent test results which show that very minor configuration variations change base bending moments very significantly. More experimental and theoretical research is needed to gain insight into the basic problems before analysis is justified.

4. Methods of computing unsteady and quasi-steady aerodynamic pressure distributions need to be improved for wing-body combinations such as the one studied. It is questionable as to what degree of mathematical complexity one should consider the problem when the basic forcing function can only be estimated crudely.

5. Modeling of a tandem arrangement of circular cylinders and flat plates, a typical idealization of the type of vehicle studied herein, presents complex but not insolvable problems in elasticity and computer technique. However, vehicles having clustered cylinders or unorthodox shells present quite formidable problems, not only in the two areas mentioned, but also in opening the door to three dimensional dynamics. Research into the three dimensional dynamics of complex vehicles might be warranted.

6. In view of the large loads generated by both wind shear and gusts, continued effort should be made to establish rational criteria for these environments. Particular emphasis should be given to methods of combining loads due to these effects.

7. The use of analog computers makes possible the solution of complex nonlinear dynamic equations which could not be economically solved by any other method. Further applications of differential analyzers and direct analogy computers to dynamics problems is suggested.

8. In considering the results of this study for design, one must recognize that a possible mode of structural failure is fatigue. The dynamic loads calculated in this study could be useful in arriving at estimates of fatigue loading.

   After the vehicle is erected, but prior to launch, significant fatigue loadings are caused by ground winds. These are due to a combination of oscillatory lift, oscillatory drag, and quasi-steady drag, as discussed in Section II. The time that a vehicle is in this prelaunch condition will most likely be much longer than the time during boost or re-entry and therefore, will result in a much greater number of occurrences of varying loads.

For the glider, re-entry and descent will be of major concern from a
fatigue standpoint. The occurrence of maneuvers and turbulence in
conjunction with elevated structural temperatures can be very detrimental
to structural life. When varying loads occur during the time of high
structural temperatures, rates and durations, as well as intensities, of
loadings can be significant. The problem becomes much more complex than
in other portions of the flight, because of the interaction effects of
fatigue, creep, thermal stresses, thermal cycling and varying physical
and mechanical properties of the structural materials.

It appears that the most critical sources of external loadings, from a
structural fatigue standpoint, are ground winds during prelaunch,
atmospheric turbulence and maneuvers during re-entry. Earthquake and
ground shock loads, launch loads, staging loads and landing loads appear
to be of secondary importance.
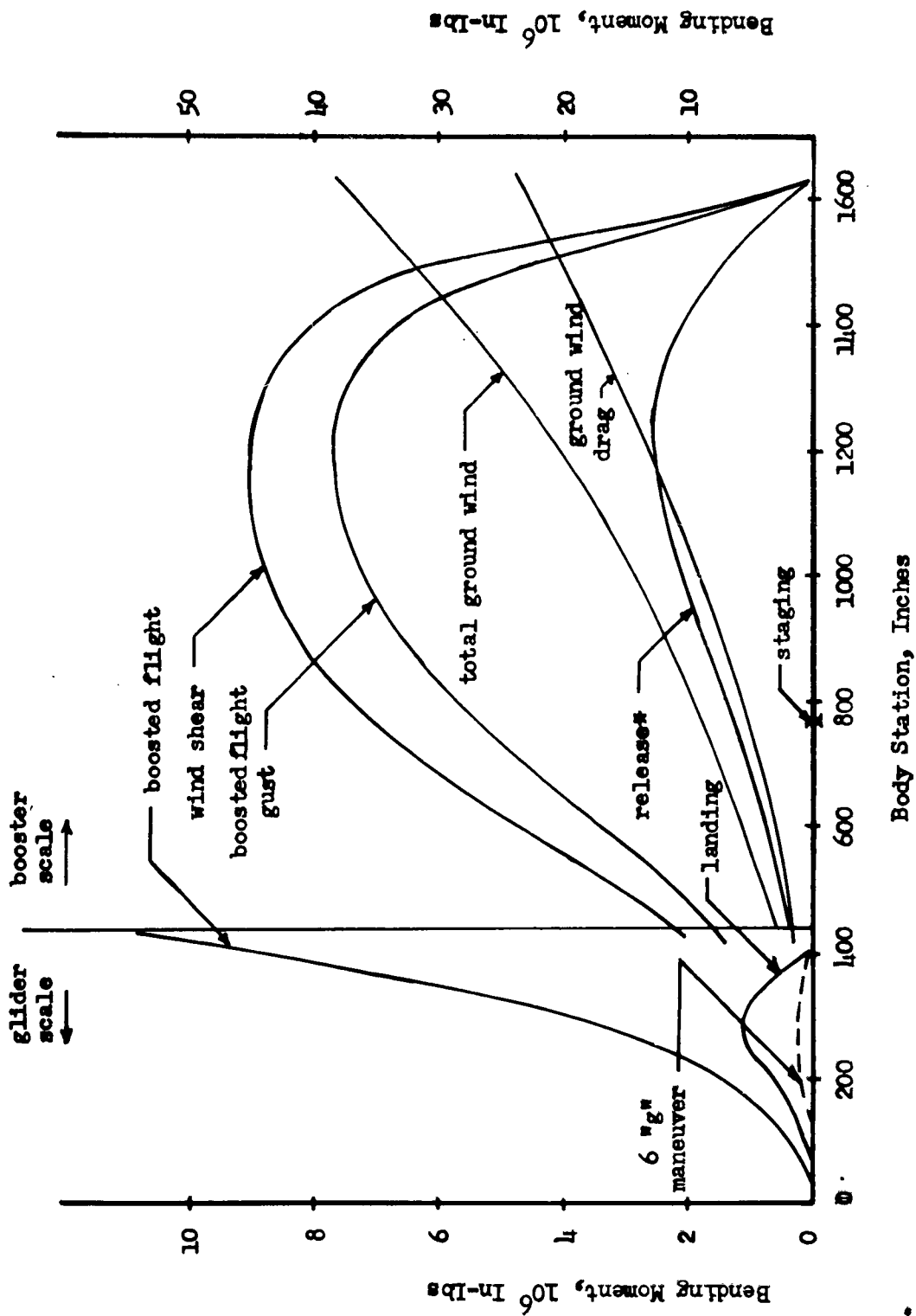
FIG. I-1 COMPARISON OF BENDING MOMENTS DUE TO VARIOUS ENVIRONMENTS

\# based on one second control system delay (see text)

II. PRELAUNCH LOADS

A. GENERAL DISCUSSION

Consider a fully loaded vehicle ready to be launched in the near vertical position. Some of the loading conditions associated with prelaunch result from ground wind, ground motion of the vehicle supporting structure and the noise environment due to the rocket engines. The first two loading conditions have been examined in this study with the major effort on ground wind.

The ground wind loading condition is divided into loads due to ground wind steady drag and loads due to vortex shedding which produces oscillatory loads in directions both parallel and perpendicular to the flow. The loads due to motion of the ground resulting from shock and earthquakes are considered briefly.

For the first part of the ground wind drag studies the vehicle is considered cantilevered, while for the second part a flexible base which allows rotation only is considered.

For most of the parameter studies a discrete-type input is used. However, it is possible through analog techniques to generate a wind which is random in nature. This type of wind is considered more realistic than the discrete-type wind.

Due to the lack of exact analytical methods to determine the forces due to vortex shedding, only a rough estimate of the responses has been determined for one case.

In all cases, except the random wind studies, the measure of response is bending moment. In the random wind studies, the best measure of response is dynamic magnification factor, which is defined as the dynamic bending moment divided by the static bending moment.

B. WIND DRAG

Design winds in the past have usually been specified by the government (85) to consist of a steady wind plus a gust. The magnitudes have varied depending upon site location and periods of exposure. One characteristic of the specified wind is that the maximum gust velocity is usually 50% of the steady wind velocity. Thus the specification 40-60 and 60-90 are common specifications which give the steady wind velocity and the steady wind-plus-gust velocity respectively. Unfortunately, the specifications do not indicate either the gust shape or period.

For this study two approaches are used. One approach considers the wind as a steady forty mph plus a one minus cosine type gust with a magnitude of twenty mph superimposed on it. The second approach considers the wind variation to be random in nature rather than discrete. The vehicle

is subjected to a random wind in which the level of turbulence is adjusted to give a peak value of approximately sixty mph every five minutes. The results are then interpreted with the aid of statistics. The philosophy of the random wind criteria is discussed in detail in Appendix F.

For both approaches the effects of including higher modes, damping, base flexibility, and linearizing the generalized forces are examined. In addition, for the discrete case only the effects of neglecting gravity and the effects of vehicle misalignment are examined.

In all cases the vehicle is represented by the vehicle beam modes. The vehicle is considered attached at station 1656 and is positioned such that station 1676 is ten feet above the ground.

1. DISCRETE GUST STUDIES

Equation of Motion

Consider the vehicle standing in the near vertical position, attached to a rigid base to prevent translation, and provided with a linear spring to resist rotation. The first two cantilever beam modes are used to represent the vehicle. A derivation similar to that presented in Appendix C based on Lagrange's equation of motion will result in the following equations.

$$
\begin{bmatrix} \Sigma m x^2 & \Sigma m x \phi_1 & \Sigma m x \phi_2 \\ \Sigma m x \phi_1 & \Sigma m \phi_1^2 & 0 \\ \Sigma m x \phi_2 & 0 & \Sigma m \phi_2^2 \end{bmatrix} \begin{Bmatrix} \ddot{q}_0 \\ \ddot{q}_1 \\ \ddot{q}_2 \end{Bmatrix} + \begin{bmatrix} 2\mathcal{F}_0 \omega_0 \Sigma m x^2 & 0 & 0 \\ 0 & 2\mathcal{F}_1 \omega_1 \Sigma m \phi_1^2 & 0 \\ 0 & 0 & 2\mathcal{F}_2 \omega_2 \Sigma m \phi_2^2 \end{bmatrix} \begin{Bmatrix} \dot{q}_0 \\ \dot{q}_1 \\ \dot{q}_2 \end{Bmatrix}
$$

$$
+ \begin{bmatrix} \omega_0^2 \Sigma m x^2 & 0 & 0 \\ 0 & \omega_1^2 \Sigma m \phi_1^2 & 0 \\ 0 & 0 & \omega_2^2 \Sigma m \phi_2^2 \end{bmatrix} \begin{Bmatrix} q_0 \\ q_1 \\ q_2 \end{Bmatrix} = \begin{Bmatrix} Q_{q_0} \\ Q_{q_1} \\ Q_{q_2} \end{Bmatrix} \qquad \text{(II-1)}
$$

where $\mathcal{F}_j$: fraction of critical damping

     q_0 : the angle of rotation at the base due to the rotation spring

     m : the mass at the ith station

     x : the distance from the point of attachment to the ith station

     ϕ_{ji} : the jth modal value of the cantilever mode at the ith station

q_j : the generalized coordinate of the $j^{\underline{th}}$ cantilever mode

ω_j : the frequency of the $j^{\underline{th}}$ cantilever mode

ω_θ : the frequency of the rotational mode

Inertia coupling results since the cantilever beam modes are not orthogonal with the rotational mode.

The generalized forces including gravity and drag are:

$$Q_{q_\theta} = \Sigma\, mg(\beta + q_\theta)x + \Sigma\, mg(\phi_1 q_1 + \phi_2 q_2)$$

$$+ \frac{\rho}{2}\Sigma C_D D \left[V - \dot{q}_\theta x - \phi_1 \dot{q}_1 - \phi_2 \dot{q}_2 \right]^2 x\Delta x$$

$$Q_{q_1} = \Sigma\, mg(\beta + q_\theta + \phi_1' q_1 + \phi_2' q_2)\phi_1$$

$$+ \frac{\rho}{2}\Sigma C_D D \left[V - \dot{q}_\theta x - \phi_1 \dot{q}_1 - \phi_2 \dot{q}_2 \right]^2 \phi_1 \Delta x$$

$$Q_{q_2} = \Sigma\, mg(\beta + q_\theta + \phi_1' q_1 + \phi_2' q_2)\phi_2$$

$$+ \frac{\rho}{2}\Sigma C_D D \left[V - \dot{q}_\theta x - \phi_1 \dot{q}_1 - \phi_2 \dot{q}_2 \right]^2 \phi_2 \Delta x \qquad (II-2)$$

where:

β : the angle due to misalignment

C_D : the steady-state drag coefficient

D : the dimension of the area transverse to the flow

As can be seen in Eqn. (II-2), the generalized forces are nonlinear. For our study the term

$$\left[V - \dot{q}_\theta x - \phi_1 \dot{q}_1 - \phi_2 \dot{q}_2 \right]^2 \qquad (II-3)$$

$$\approx V^2 - 2\, V\dot{q}_\theta x - 2V\phi_1 \dot{q}_1 - 2V\phi_2 \dot{q}_2$$

This approximation will be justified later.

Eqns.(II-1)and(II-2)are the basic equations for the ground wind study. By setting the appropriate terms equal to zero, the desired equations for each part are determined.

For steady-state drag, (81),C_D cylinder $\approx$ .33 and C_D plate $\approx$ 1.20 for high Reynolds numbers. Using these values for C_D and the correction factor (59) for V, which is shown in Fig. II-1, the summations in the equations of motion and load equations have been determined. The summations corresponding to the terms neglected in Eqn.(II-3)have also been determined.

The bending moments are determined, for all cases in the ground wind studies, by the force summation method.

Since it is desired to determine the response due to a gust superimposed on a steady forty mph wind, the equilibrium position of the vehicle due to a forty mph wind, has to be determined. This is done by setting the inertia terms and the response-velocity terms equal to zero and solving for the displacement terms.

Cantilever Case

For the first part of the analysis the vehicle is considered cantilevered, with no misalignment, and without the gravity terms. Four studies use this representation.

The equations of motion along with the load equations have been solved on a differential analyzer. Due to the fact that it is required to obtain the products of $V\dot{q}_1$, $V\dot{q}_2$ and V^2 this system has to be solved with a differential analyzer which has electronic multipliers. See Appendix G for a description of obtaining nonlinear terms on the analog.

The first study is made to justify the approximation made in Eqn. II-3. As mentioned before, all of the summations are determined. The coefficients of the terms deleted are of the same order of magnitude of those retained; therefore, it is only necessary to show that the products $\dot{q}_1\dot{q}_2$, $\dot{q}_1^2$, and $\dot{q}_2^2$ are small with respect to the products $V\dot{q}_1$, $V\dot{q}_2$, and V^2. As can be seen in Table II-2, this is true and deleting these terms is justified.

TABLE II-1

Maximum Measured Responses
Maximum Wind Speed -- 88 FPS

Forcing Frequency	V^2	$V\dot{q}_1$	$V\dot{q}_2$	$\dot{q}_1\dot{q}_2$	$\dot{q}_1^2$	$\dot{q}_2^2$
1 cps	7744.	308	20.24	.805	12.25	.0529
2.5 cps	7744.	202.4	79.20	2.07	5.29	.81

The second and third studies are made to evaluate the importance of the number of flexible modes and the importance of gust phasing on the dynamic response. The results, illustrated in Fig. II-2, indicate that the major portion of the response is in the first flexible mode, and the maximum base bending moment occurs when the frequency of the gust is equal to the frequency of the lowest cantilever mode of the vehicle.

In the fourth study the effect of structural damping on the response is determined. Fig. II-3 indicates that damping has little effect on the bending moment for a discrete input.

Flexible Base

Since in actuality, the vehicle might be spring suspended for protection against earthquakes or atomic blasts, let us consider a flexible base. The base springs, which allow rotation only, are chosen so as to yield base frequencies of $1/4$, 1 and 4 cps.

The equations of motion along with the load equations are solved on the differential analyzer using a method similar to that used in the cantilever case. The base bending moment is the only load determined.

The effects of a flexible base can be seen in Fig. II-4. This figure indicates that the maximum base bending moment occurs with the softest spring; therefore, this spring is used to examine other parameters. Two interesting effects can be seen in Fig. II-4. Since the cantilever frequencies and the base frequency are not the natural frequencies of the coupled system, the maximum base bending moment does not occur at one of these frequencies, which is to be expected. The natural frequencies of the coupled system have been computed and are compared in Table II-2.

TABLE II-2

Comparison of Frequencies in CPS

Frequencies Associated With The Nonorthogonal Modes			Frequencies Associated With The Orthogonal Modes		
ω_0	ω_1	ω_2	ω_1	ω_2	ω_3
0.25	.956	2.495	0.242	2.03	5.15
1.00	.956	2.495	0.699	2.21	5.36
4.00	.956	2.495	0.932	2.45	5.71

The other interesting effect which can be seen in Fig. II-4 is associated with the system with the base spring frequency of 1 cps. One would normally think that this system would yield higher base bending moments than the system with the base spring frequency of 4 cps, but because the first cantilever frequency and the base frequency are approximately equal, this

system forms, essentially, a two degree of freedom system in which the generalized mass associated with the base spring acts as a mass damper on the generalized mass associated with q_1.

With this result one is tempted to say that the best choice of a base frequency is that of the first cantilever mode of the vehicle. One must remember, however, that only drag due to ground wind has been considered.

The results plotted in Fig. II-5 indicate that the effect of structural damping on the maximum base bending moments is negligible. The maximum change in base bending moment is approximately 5% when the percent of critical damping is changed from 1% to 10%.

Fig. II-6 indicates that the gravity terms must be included to give accurate results for a flexible base. The gravity terms become increasingly important as the base spring becomes softer.

Fig. II-7 shows that the change in maximum base bending moment due to misalignment is within analog limits, the same for gusts as for a steady forty mph wind, i.e., the effect is one which can be accounted for by superposition.

As previously mentioned the generalized forces have nonlinear terms. If these nonlinear terms can be either replaced with linear terms or eliminated a nonlinear differential analyzer is no longer required. The nonlinear terms are $V\dot{q}_0$, $V\dot{q}_1$, and $V\dot{q}_2$. Two methods are used to examine the possibility of linearizing these terms. The first method replaces V with a constant value of 40 mph, while the second method deletes the nonlinear terms. Fig. II-8 indicates that the maximum base moment changes less than 5% when the results of the two methods, as outlined above, are compared.

2. RANDOM GUST STUDIES

In this part of the study the input is random; however, the equations of motion and the load equations retain the same form as those in the discrete studies. A white noise generator and a filter circuit are used to represent the atmospheric turbulence. The level of the turbulence is adjusted to give a peak value of wind velocity of approximately sixty mph every five minutes.

The results are interpreted by a statistical method as described in Appendix F. The vehicle is exposed to the turbulence for a long period of time, the recordings are divided into five minute intervals, and the maximum static bending moments, the maximum dynamic bending moments, and the maximum wind velocities are tabulated. Then, the following quantities are calculated.

$$\bar{\ell} = \frac{1}{N} \sum_{i=1}^{N} \ell_i$$

$$\sigma^2 = \frac{1}{N} \sum_{i=1}^{N} (\ell_i - \bar{\ell})^2$$

where $\quad \ell_i$: maximum quantity in the ith time interval

$\bar{\ell}$: mean value of maximum quantity

N : number of intervals

σ : variance of maximum quantity distribution

With the values calculated the dynamic magnification factors are calculated using the following expression:

$$\text{Dynamic Magnification Factor} = \frac{(\bar{\ell}+3\sigma) \text{ Dynamic}}{(\bar{\ell}+3\sigma) \text{ Static}}$$

The major effects examined are base flexibility, damping, number of degrees of freedom, and linearization. The method of obtaining the random type input can be found in Appendix G. The effect of gravity is included in all cases.

The results of the random-type studies can be seen in Tables II-3 and II-4.

As can be seen in Table II-3 the dynamic magnification factor is reduced when the input is changed from discrete to random. This is true for both values of base spring frequencies.

Changing the percent of critical damping from 1% to 10% changes the dynamic magnification factor very little. A reduction in the dynamic magnification factor is realized when three degrees of freedom instead of one degree of freedom are used to represent the elastic action of the vehicle. This is probably caused by the inertia coupling.

The same methods as outlined in the discrete studies are used to examine the removal of the nonlinear terms. The dynamic magnification factor increases approximately 2% when the nonlinear terms are replaced with linear terms and 27% when the nonlinear terms are dropped. This indicates that the equations can be linearized by linearizing the terms rather than deleting them.

TABLE II-3   RANDOM INPUT RESULTS

Base Spring Frequency, cps	Degrees of Freedom	% Critical Damping	Dynamic Magnification Factor Random Studies	Dynamic Magnification Factor Discrete Studies
1	3	1	1.113	1.227
1/4	3	1	1.125	1.193
1/4	3	10	1.137	-
1/4	1	1	1.148	-
1/4*	1	1	1.170	-
1/4 [⊥]	1	1	1.460	-

TABLE II-4   RANDOM INPUT STATISTICS

Base Spring Frequency, cps	Degrees of Freedom	% Critical Damping	Average Gust Factor	Standard Deviation	Number of Five Minute Intervals
1	3	1	1.52	0.125	61
1/4	3	1	1.56	0.101	53
1/4	3	10	1.49	0.117	60
1/4	1	1	1.53	0.093	60
1/4*	1	1	1.55	0.110	60
1/4 [⊥]	1	1	1.57	0.092	49

* Nonlinear terms replaced with linear terms

⊥ Nonlinear terms deleted

C. OSCILLATORY LOADS DUE TO VORTEX SHEDDING

1. INTRODUCTION

Any bluff body which is immersed in a moving fluid sheds vortices. Associated with this shedding there is a force which acts on the body in a direction perpendicular to the fluid flow. This force is due to the change in circulation around the body necessary to balance the vorticity shed into the wake.

The prediction of these forces are extremely difficult and are usually determined from wind-tunnel test. Even when the Reynolds number is sub-critical and the vortex shedding is periodic, little consistency can be found (63). Only meager information on the forces can be found (61) when the Reynolds number is supercritical and the shedding is random.

The following example can only be used for illustrative purposes since the lift force measured in supercritical flow is for a cylinder only, and nothing is known about the forces for other shapes and configurations. There is an indication (58) that the response can be reduced by a significant amount by the proper use of spoilers. In choosing the spoilers, however, one must rely on wind tunnel tests since an analytical solution does not exist.

2. ILLUSTRATIVE EXAMPLE

In Reference (61) the power spectrum $\Phi(S)$ of lift coefficient determined from experiments is given for several Reynolds numbers. In addition an analytic expression is given which fits the experimental data:

$$\Phi(S) = \frac{\overline{c_L^2} \, 2 \, \mathcal{L} \left[1 + 3 \, (2\pi \frac{\mathcal{L}}{d} S)^2 \right]}{d \left[1 + (2\pi \frac{\mathcal{L}}{d} S)^2 \right]^2} \qquad (\text{II-4})$$

where $\mathcal{L}/d$ = 2.4

$\mathcal{L}$: scale of turbulence

d : diameter

S : $\frac{fd}{V}$, Strouhal Number

f : frequency

V : velocity of flow

$\overline{c_L}$: root mean square lift coefficient

Since the above expression is for a constant diameter cylinder, it is necessary to reduce the vehicle to an equivalent constant diameter cylinder. A mean diameter based on the projected area exposed to the flow is used.

The system to be analyzed has the following properties. The vehicle is assumed to be in vertical alignment, gravity effects are included, and the vehicle is exposed to a steady wind velocity of 60 mph. The value of $\bar{C}_L$, determined from Reference (61), is 0.1292. The vehicle is considered to have a flexible base and an associated base frequency of one-quarter cycle per second. The modes are determined by using the small vibration theory and including the base spring. This yields a set of orthogonal modes of which the first three are used. The frequencies associated with these modes are .242, 2.03, and 5.15 cycles per second. A value of 1% critical damping in each mode is used.

The orthogonal beam modes determined in Part II-B are used since the inertia coupling terms are eliminated. The equations of motion are the following.

$$
\begin{bmatrix} m_1 & 0 & 0 \\ 0 & m_2 & 0 \\ 0 & 0 & m_3 \end{bmatrix}
\begin{Bmatrix} \ddot{q}_1 \\ \ddot{q}_2 \\ \ddot{q}_3 \end{Bmatrix} +
\begin{bmatrix} 2m_1 \mathcal{J}_1 \omega_1 & 0 & 0 \\ 0 & 2m_2 \mathcal{J}_2 \omega_2 & 0 \\ 0 & 0 & 2m_3 \mathcal{J}_3 \omega_3 \end{bmatrix}
\begin{Bmatrix} \dot{q}_1 \\ \dot{q}_2 \\ \dot{q}_3 \end{Bmatrix}
$$

$$
+ \begin{bmatrix} m_1 \omega_1^2 & 0 & 0 \\ 0 & m_2 \omega_2^2 & 0 \\ 0 & 0 & m_3 \omega_3^2 \end{bmatrix}
\begin{Bmatrix} q_1 \\ q_2 \\ q_3 \end{Bmatrix} =
\begin{Bmatrix} Q_{q_1} \\ Q_{q_2} \\ Q_{q_3} \end{Bmatrix} \qquad \text{(II-5)}
$$

where $\mathcal{J}_1 = \mathcal{J}_2 = \mathcal{J}_3 = .01$

$$
Q_{q_1} = \tfrac{1}{2}\rho V^2 \sum Dd \,\Delta\, \phi_1 C_L + \sum mg\phi_1'\phi_1 q_1 + \sum mg\phi_2'\phi_1 q_2 + \sum mg\phi_3'\phi_1 q_3
$$

$$
Q_{q_2} = \tfrac{1}{2}\rho V^2 \sum Dd \,\Delta\, \phi_2 C_L + \sum mg\phi_1'\phi_2 q_1 + \sum mg\phi_2'\phi_2 q_2 + \sum mg\phi_3'\phi_2 q_3
$$

$$
Q_{q_3} = \tfrac{1}{2}\rho V^2 \sum Dd \,\Delta\, \phi_3 C_L + \sum mg\phi_1'\phi_3 q_1 + \sum mg\phi_2'\phi_3 q_2 + \sum mg\phi_3'\phi_3 q_3 \qquad \text{(II-6)}
$$

The force summation method is used to determine the base bending moment.

To determine the mean diameter, the following expression is used:

$$
d_{mean} = \frac{\sum Dd \Delta}{L} \qquad \text{(II-7)}
$$

where   L = length of vehicle

$\sum D \, d\triangle$ = maximum area normal to the flow

$$d_{mean} = \frac{1460.99}{138.67} = 10.54 \text{ ft.}$$

Using the digital program discussed in Appendix G, the root-mean-square base bending moment, normal to the flow, is 6.71 million-in-lb. There is an oscillatory drag, associated with the oscillatory lift, due to vortex shedding. If one assumes that the normalized spectrum of the oscillating drag force is identical to the normalized spectrum of lift force, one can easily compute the root-mean-square bending moment, due to the oscillatory drag. The relation is the following:

$$BM_D = \frac{\overline{C}_D}{\overline{C}_L} \; \overline{BM}_L$$

For our case $\overline{C}_D$, from Reference (61), is 0.04; and therefore, the root-mean-square base bending moment, parallel to the flow, due to vortex shedding, is 2.1 million in-lbs. In order to combine the three components, the peak values, rather than the root-mean-square values, of the oscillatory bending moments should be used. It has been indicated (58) that the peak values are approximately three times the root-mean square; also it has been indicated (58) that the build-up of bending moments, due to vortex, is sufficiently rapid that the peak values should be added to the peak value of bending moment determined in the quasi-steady drag study, including dynamic effects. The maximum base bending moment obtained in Part 2, with a base spring of 1/4 cps., is 24.4 million in-lbs.

$$BM_T = \left[BM_{OL}^2 + (BM_{OD} + BM_{QSD})^2 \right]^{1/2} \text{ in-lbs.} \qquad (II-8)$$

where BM_{OL} : peak bending moment due to oscillatory lift

BM_{OD} : peak bending moment due to oscillatory drag

BM_{QSD} : peak bending moment due to quasi-steady drag

For this example the total base bending moment is:

$$BM = \left[(20.1 \times 10^6)^2 + (6.3 \times 10^6 + 24.4 \times 10^6)^2 \right]^{1/2} \text{ in-lbs}$$

$$BM = 36.7 \times 10^6 \text{ in-lbs}$$

This example, probably, is more suitable to a ballistic missile, rather than to a configuration similar to the one studied here, because the ballistic missile is closer to being a cylinder.
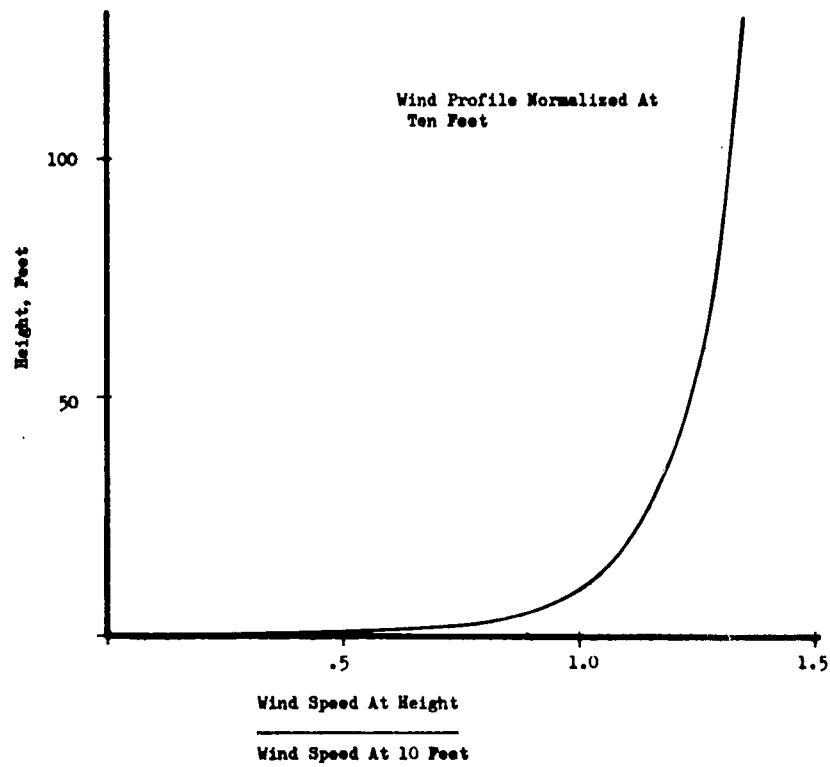
FIG. II-1 WIND PROFILE
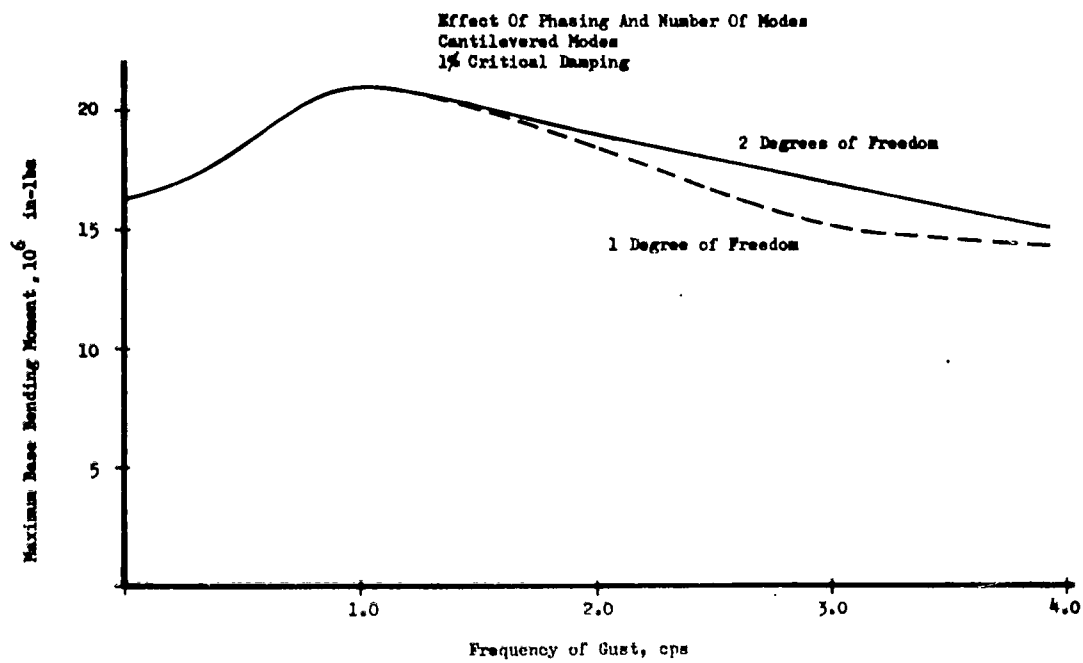
FIG. II-2 EFFECTS OF PHASING AND NUMBER OF MODES

Cantilevered Modes
Two Degrees of Freedom
Frequency of Gust, 1 CPS

Per Cent Critical Damping
1
2
4
6
8
10

FIG. II-5 EFFECT OF DAMPING

3 Degrees of Freedom
1% Critical Damping in All Modes
With Gravity Terms

$\omega_0 = \frac{1}{4}$ cps

$\omega_0 = 4$ cps

$\omega_0 = 1$ cps

Frequency of Gust, cps
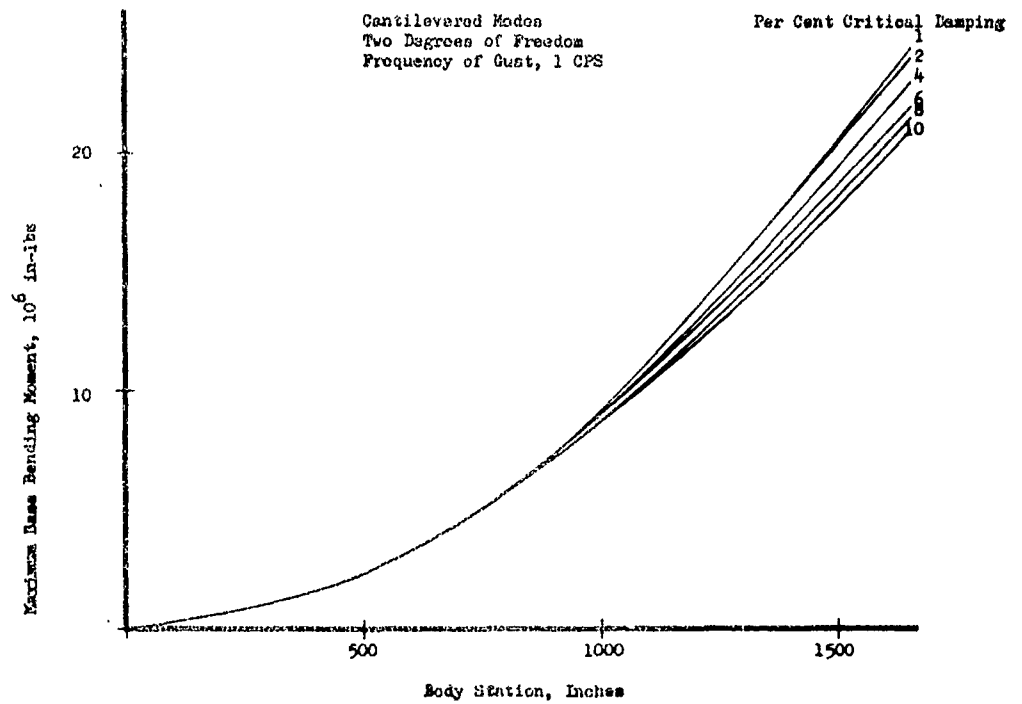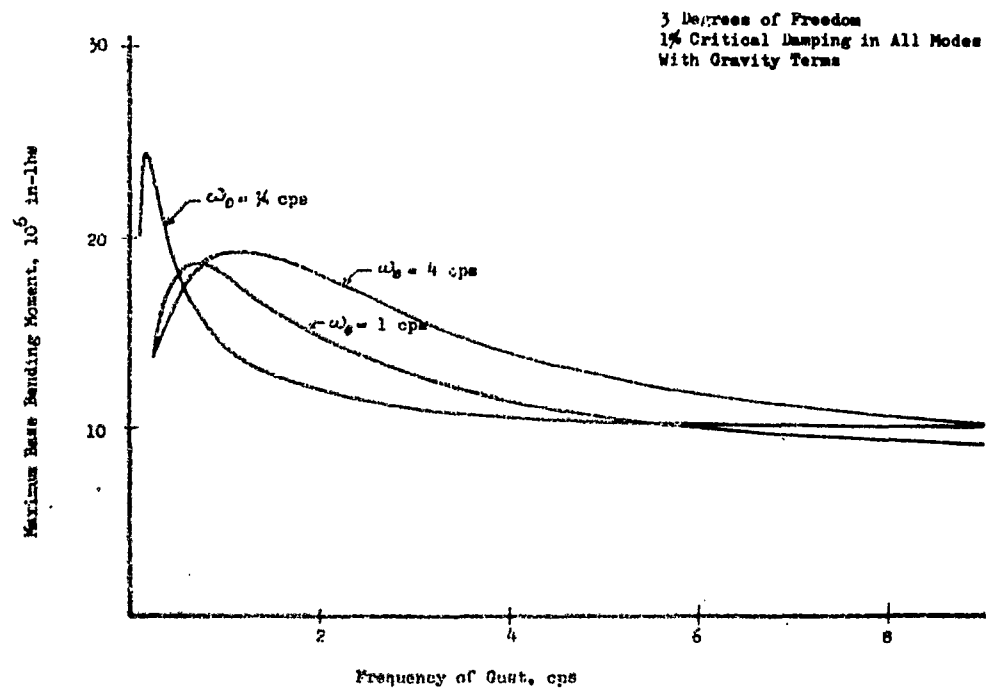
FIG. II - 4 EFFECTS OF FLEXIBLE BASE
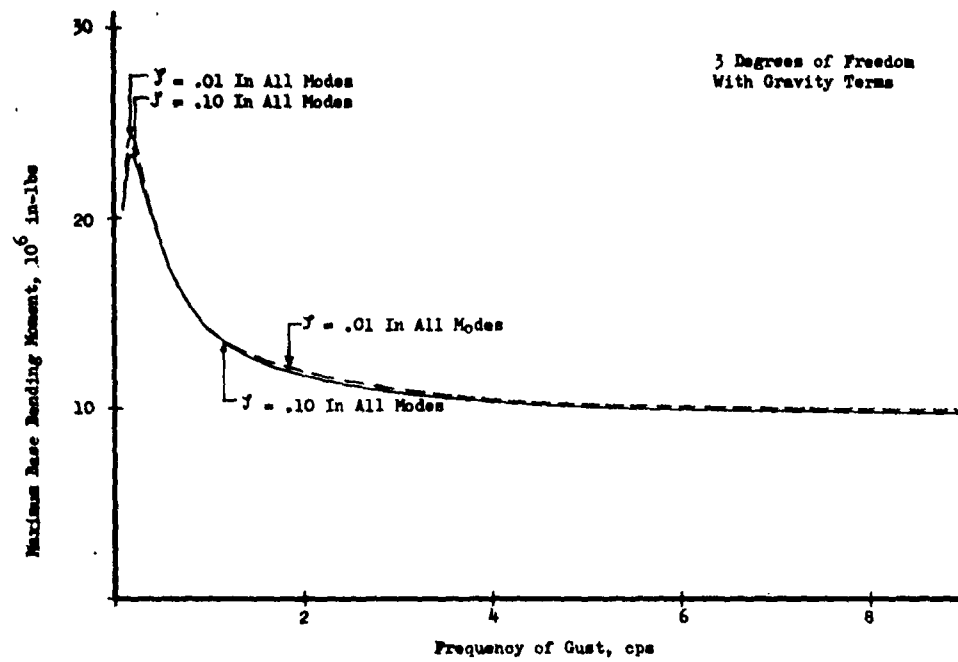
FIG. II-5   EFFECT OF DAMPING
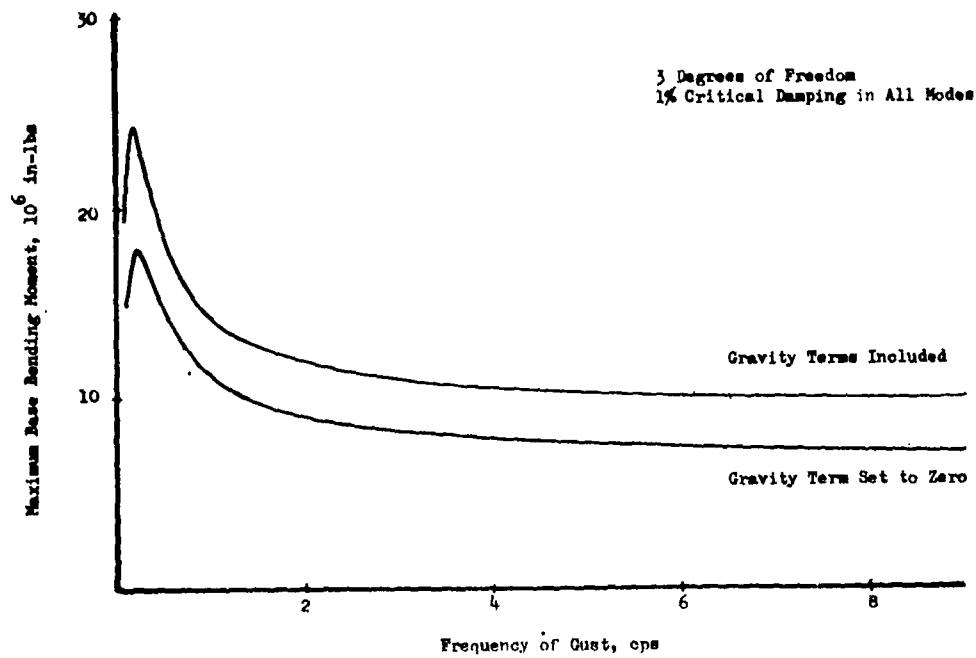
FIG. II-6   EFFECTS OF GRAVITY

3 Degrees of Freedom
1% Critical Damping in All Modes
With Gravity Terms

2° Misalignment

No Misalignment

Frequency of Gust, cps
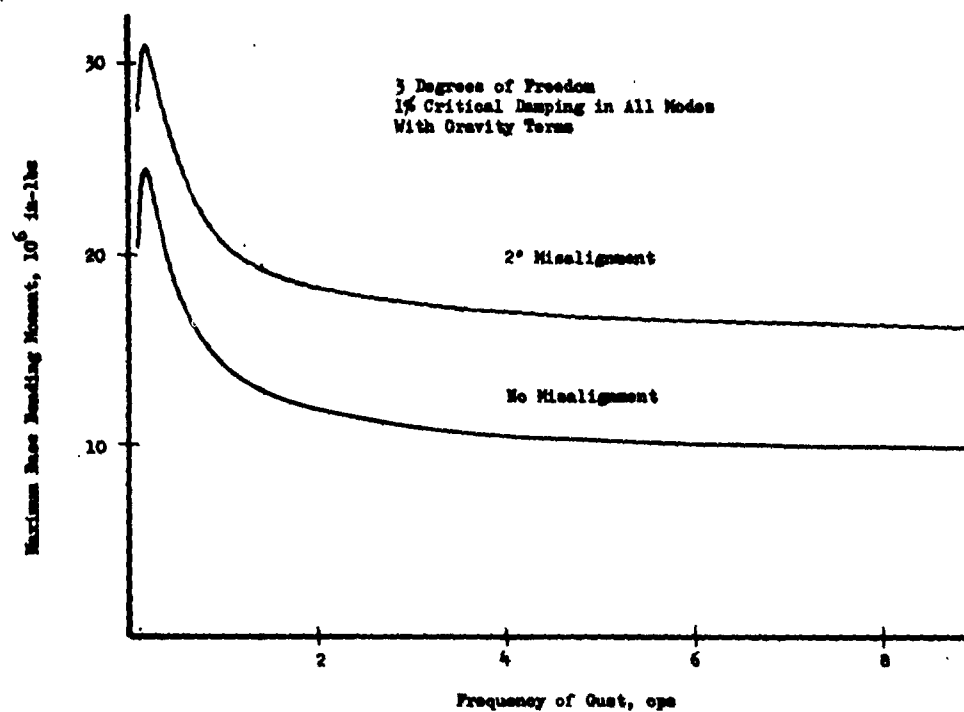
FIG. II - 7   EFFECT OF MISALIGNMENT

:3 Degrees of Freedom
1% Critical Damping in All Modes
With Gravity Terms

Equations With Nonlinear Terms Deleted
Equations with Nonlinear Terms Replaced By Linear Terms
Equations With Nonlinear Terms

Frequency of Gust, cps
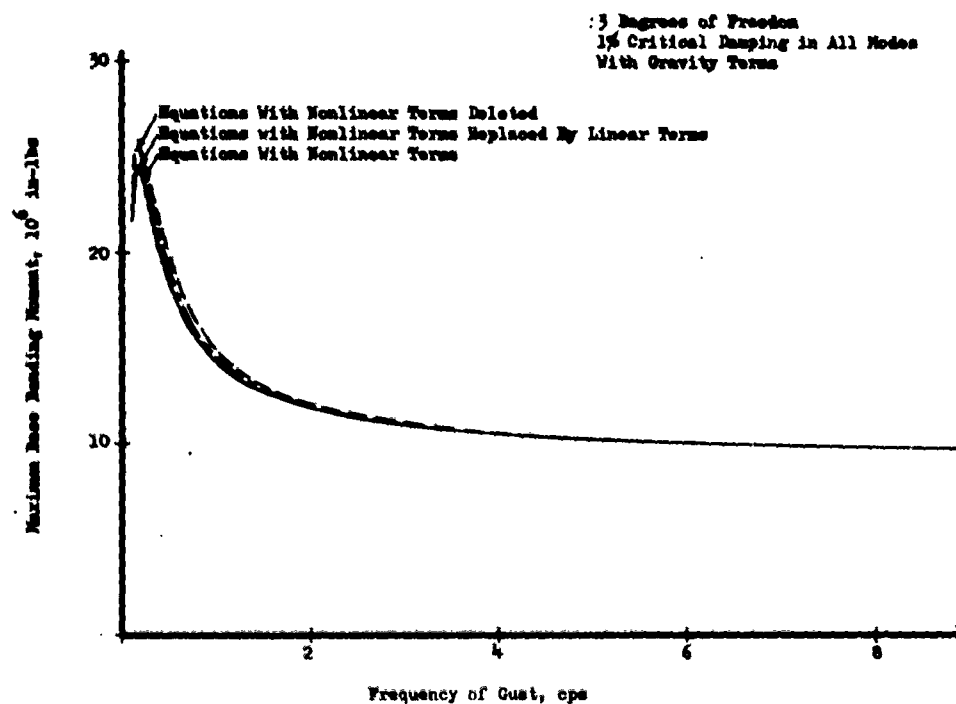
FIG. II-8   EFFECTS OF LINEARIZATION

D. EARTHQUAKE AND SHOCK LOADS

Because of their infrequent and unpredictable occurrence, earthquake and shock loads are not usually considered as design conditions. However, the method of computing loads due to these effects gives rise to problems which will be discussed in this report. The difficulty involved in obtaining shock measurements has led to the use of the shock spectra approach. This method is employed, when the exact nature of the shock cannot be determined. The remainder of this section will be devoted to a discussion of the shock spectra concept and an evaluation of loads obtained by the shock spectra method.

1. SHOCK SPECTRA METHODS

Certain disturbances, such as earthquake shocks and ground shock due to blast, produce transient accelerations which are rather hard to measure and hard to define. By a simple passive system (reed gages for example) it is possible to take measurements which will describe the shock by a shock spectrum that gives a measure of the frequency content and amplitude of the shock.

Consider a series of lumped mass reed gages of various frequencies to be placed in the ground in an earthquake area.
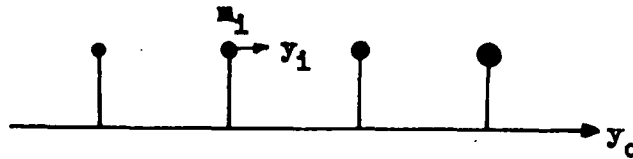
Let the lateral displacement of the earth due to the shock be y_o and let the relative displacement of a reed be y_i. The motion of a reed can be described by

$$m_i (\ddot{y}_i + \ddot{y}_o) + 2 \zeta_i m_i \omega_i \dot{y}_i + m_i \omega_i^2 y_i = 0$$

$$\ddot{y}_i + 2\zeta_i \omega_i \dot{y}_i + \omega_i^2 y_i = -\ddot{y}_o (t) \tag{II-9}$$

Let the maximum response of (II-9) be

$$\left| y_i (t) \right|_{max} = D (\omega_i)$$

We note that $D(\omega_i)$ can be measured quite easily.

We now define

$$A(\omega) = \omega^2 D(\omega)$$

where $D(\omega)$: displacement shock spectrum

$A(\omega)$: acceleration shock spectrum: equivalent static acceleration

The second definition can be visualized by letting $\ddot{y}_0(t)$ be a steady acceleration in Eqn. (II-9). Then $\omega^2 y = -\ddot{y}_0$

Now let the vehicle be subjected to the same shock and let its response be defined by the base motion plus two cantilever beam modes, as shown below.

$$\begin{bmatrix} \Sigma m & \Sigma m\phi_1 & \Sigma m\phi_2 \\ \Sigma m\phi_1 & \Sigma m\phi_1^2 & 0 \\ \Sigma m\phi_2 & 0 & \Sigma m\phi_2^2 \end{bmatrix} \begin{Bmatrix} \ddot{y}_0 \\ \ddot{q}_1 \\ \ddot{q}_2 \end{Bmatrix} + \begin{bmatrix} 0 & & \\ & 2\Sigma m \phi_1 \zeta_1 \omega_1 & \\ & & 2\Sigma m\phi_2\zeta_2\omega_2 \end{bmatrix} \begin{Bmatrix} \dot{y}_0 \\ \dot{q}_1 \\ \dot{q}_2 \end{Bmatrix} +$$

$$\begin{bmatrix} 0 & & \\ & \Sigma m \phi_1^2\omega_1^2 & \\ & & \Sigma m\phi_2^2\omega_2^2 \end{bmatrix} \begin{Bmatrix} y_0 \\ q_1 \\ q_2 \end{Bmatrix} = 0$$

(II-10)

We can rewrite the second and third equation as

$$\ddot{q}_1 + 2\zeta_1\omega_1\dot{q}_1 + \omega_1^2 q_1 = -\frac{\Sigma m \phi_1}{\Sigma m \phi_1^2} \ddot{y}_0 = -\lambda_1\ddot{y}_0$$

(II-11)

$$\ddot{q}_2 + 2\zeta_2\omega_2\dot{q}_2 + \omega_2^2 q_2 = -\frac{\Sigma m \phi_2}{\Sigma m \phi_2^2} \ddot{y}_0 = -\lambda_2\ddot{y}_0$$

where λ_j is called the kinematic factor.

Noting the similarity of Eqns. (II-11) and (II-9) we can say that

$$\left| q_1(t) \right|_{max} = \lambda_1 \, D(\omega_1)$$

$$\left| q_2(t) \right|_{max} = \lambda_2 \, D(\omega_2)$$

If the response at some point on the veh... is given by

$$y(x) = \phi_1(x) \; q_1 + \phi_2(x) \; q_2 + \ldots \; \phi_n(x) \; q_n$$

then an __upper bound__ on the maximum response is given by

$$\left| y(x) \right|_{max} = \sum_{j=1}^{n} \left| \lambda_j \, \phi_j(x) \; D \, (\omega_j) \right|$$

The __same__ type of upper bound can be placed on loads by the relationship

$$\left\{ \left| L_i \right|_{max} \right\} = \left[\left| \ell_{ij} \right| \right] \left[\lambda_j \right] \left\{ A(\omega_j) \right\} \tag{II-12}$$

where L_i = load at station i

ℓ_{ij} = load at station i due to a unit acceleration in the j mode.

This is recognized to be conservative, but the degree of conservatism is not known. In an attempt to determine the degree of conservatism a ground acceleration time history measured by Hudson and Housner (71) has been applied to the base of the vehicle by a direct analysis and by a shock spectrum analysis. Such a comparison cannot ordinarily be made, because time-histories are usually not available.

The ground acceleration trace, used in the comparison is shown in Fig. (II-9). The ground motion was measured approximately 370 yards from a 370,000 lb. charge of "nitromon" explosive; the explosive had been packed in several hundred feet of tunnel cut into the sloping side of a mountain. The acceleration shock spectrum shown on Fig. (II-10) has been computed from the trace on Fig. (II-9) by computing the response of "reed gage" systems. Since the shock spectrum is usually measured rather than the time history trace, no detailed description of the calculation of the shock spectrum is given.

The vehicle loads, due to the shock, have been computed using Eqn. (II-12) and Fig. (II-10). The results of the study are shown on Fig. (II-11) as envelopes of shear and bending moment. The influence of the number of modes used in the analyses is clearly shown. The addition of modes always raises the envelope, but the effect of higher modes such as the fourth and fifth modes is small.

If the response at some point on the vehicle is given by

$$y(x) = \phi_1(x)\ q_1 + \phi_2(x)\ q_2 + \cdots + \phi_n(x)\ q_n$$

then an upper bound on the maximum response is given by

$$\left| y(x) \right|_{max} = \sum_{j=1}^{n} \left| \lambda_j\ \phi_j(x)\ D\ (\omega_j) \right|$$

The same type of upper bound can be placed on loads by the relationship

$$\left\{ \left| L_i \right|_{max} \right\} = \left[\left| \ell_{ij} \right| \right] \left[\lambda_j \right] \left\{ A(\omega_j) \right\} \tag{II-12}$$

where L_i = load at station i

   ℓ_{ij} = load at station i due to a unit acceleration in the j mode.

   This is recognized to be conservative, but the degree of conservatism is not known. In an attempt to determine the degree of conservatism a ground acceleration time history measured by Hudson and Housner (71) has been applied to the base of the vehicle by a direct analysis and by a shock spectrum analysis. Such a comparison cannot ordinarily be made, because time-histories are usually not available.

   The ground acceleration trace, used in the comparison is shown in Fig. (II-9). The ground motion was measured approximately 370 yards from a 370,000 lb. charge of "nitromon" explosive; the explosive had been packed in several hundred feet of tunnel cut into the sloping side of a mountain. The acceleration shock spectrum shown on Fig. (II-10) has been computed from the trace on Fig. (II-9) by computing the response of "reed gage" systems. Since the shock spectrum is usually measured rather than the time history trace, no detailed description of the calculation of the shock spectrum is given.

   The vehicle loads, due to the shock, have been computed using Eqn. (II-12) and Fig. (II-10). The results of the study are shown on Fig. (II-11) as envelopes of shear and bending moment. The influence of the number of modes used in the analyses is clearly shown. The addition of modes always raises the envelope, but the effect of higher modes such as the fourth and fifth modes is small.

These results have been computed for a cantilever beam representation of the vehicle. If a spring support is used, care must be taken to compute the new orthogonal modes of the system and obtain the values of $A(\omega)$ at the proper frequencies. This results from the fact that the system does not respond naturally at its cantilever frequencies if the base is flexible, but rather responds at coupled frequencies.

2. DIRECT DYNAMIC ANALYSIS

In order to assess the accuracy of the shock spectra method, Eqns. (II-10) have been solved directly by using the ground acceleration trace on Fig. II-9 as an input. The loads have been computed by mode displacement and force summation methods by the following formulae:

$$\{L_i\} = \overbrace{[\ell_{ij}]\{\omega_j^2 q_j\}}^{\text{mode displacement}} \qquad (\text{II-13})$$

where ℓ_{ij} is the load (bending moment or shear) at the $i\underline{\text{th}}$ load point due to a unit acceleration of the $j\underline{\text{th}}$ mode.

$$\{L_i\} = \overbrace{\{\ell_{io}\}(-\ddot{y}_o) + [\ell_{ij}]}^{\text{force summation}} \{-\ddot{q}_j\} \qquad (\text{II-14})$$

Due to the absence of air loads, the two loads methods are seen to be quite similar.

3. DISCUSSION OF RESULTS

A comparison of Figs. II-12 and II-13 shows that bending moments are almost identical, using either the mode displacement or force summation method with one or more modes. This is not a general result and for most applications the force summation method is considered to be more accurate. In this study the time histories of loads by the two methods are different, but the maximum loads are the same because they happen to occur when the base acceleration is zero. An examination of Eqns. (II-13, II-14) shows that the loads will be the same by either method if $\ddot{y}_o = 0$ and the system is vibrating freely.

Shear calculations did not converge as rapidly as bending moment calculations especially near the base. The force summation and mode displacement methods gave different answers for maximum shear. This is due to the fact that maximum shear occurs when $\ddot{y}_o \neq 0$ in Eqn. (II-14).

The shock spectra method is expected to be conservative since it adds peak loads from each modal response as though all the peaks occurred simultaneously. A comparison of Figs. II-11 and II-13 shows that the

shock spectra method gave loads that were between 75% and 100% higher than the loads computed by direct methods. It is interesting to note that the shock spectra method and the mode displacement method give identical results for one mode, but that additional modes markedly increase the shock spectra results.

The numerical results of the study are not intended to be significant since the input used is only a simulated earthquake. The magnitude of the acceleration is roughly equivalent to that of a moderately strong earthquake. Some recorded strong earthquakes have had magnitudes from two to three times as large as the example accelerations, and the motion has lasted from 15 to 20 times as long.
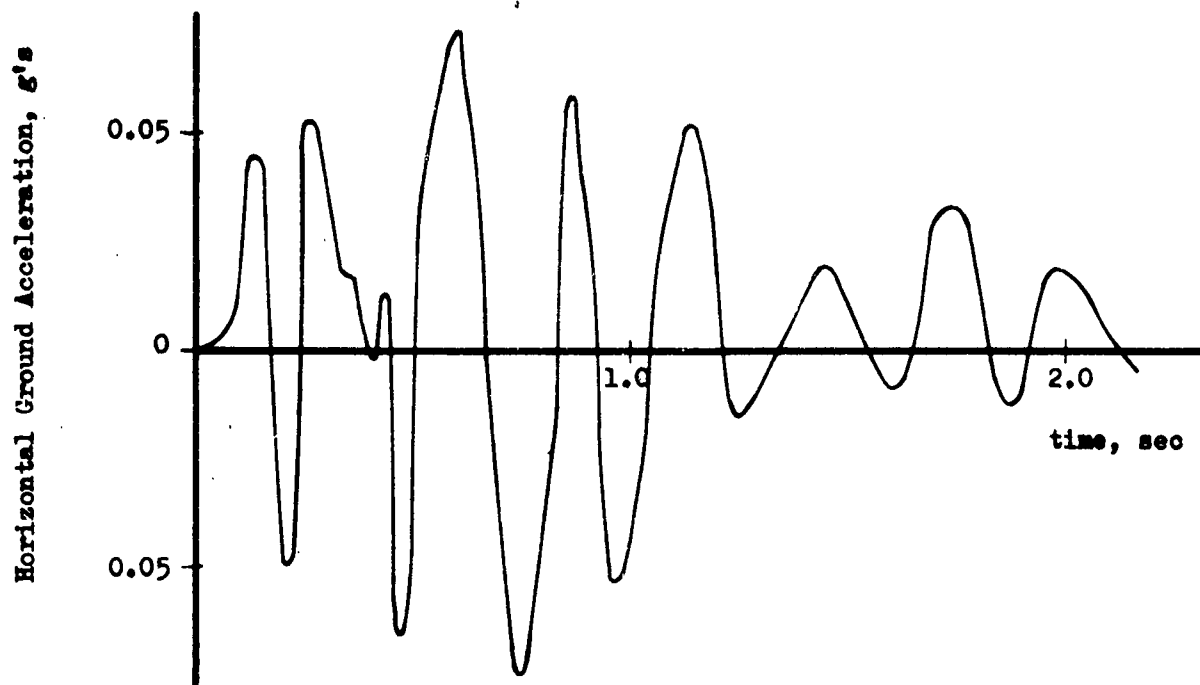
FIG. II-9   TYPICAL GROUND SHOCK ACCELERATION TRACE
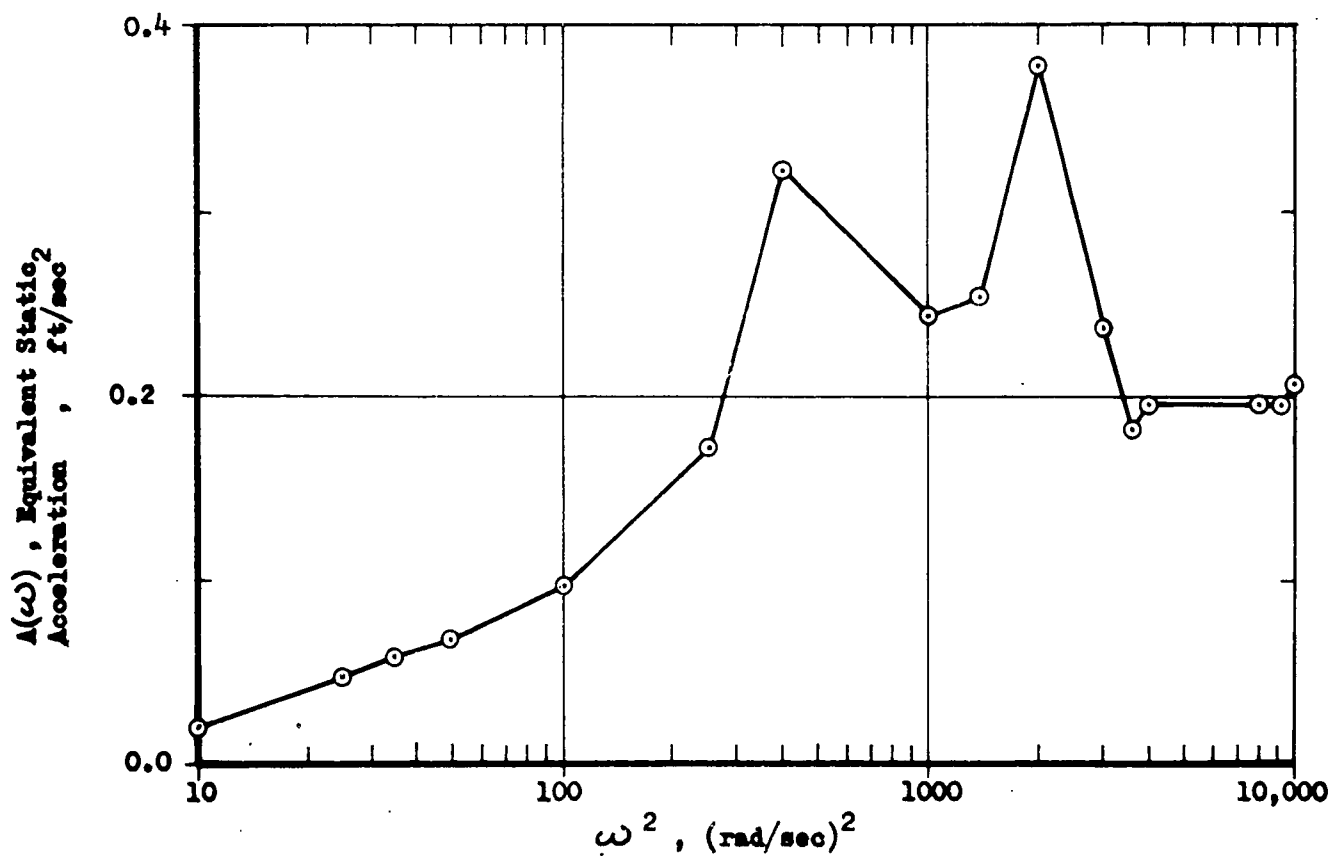
FIG. II-10   SHOCK SPECTRUM FOR TYPICAL GROUND SHOCK
ACCELERATION TRACE
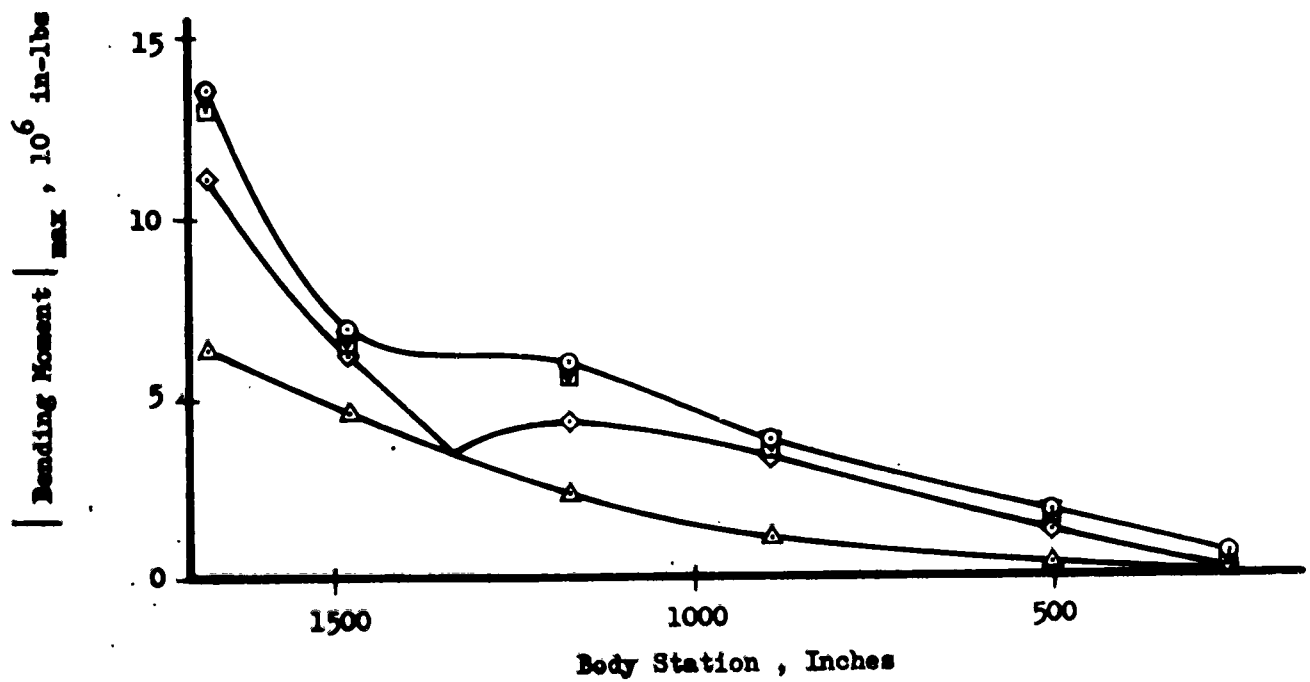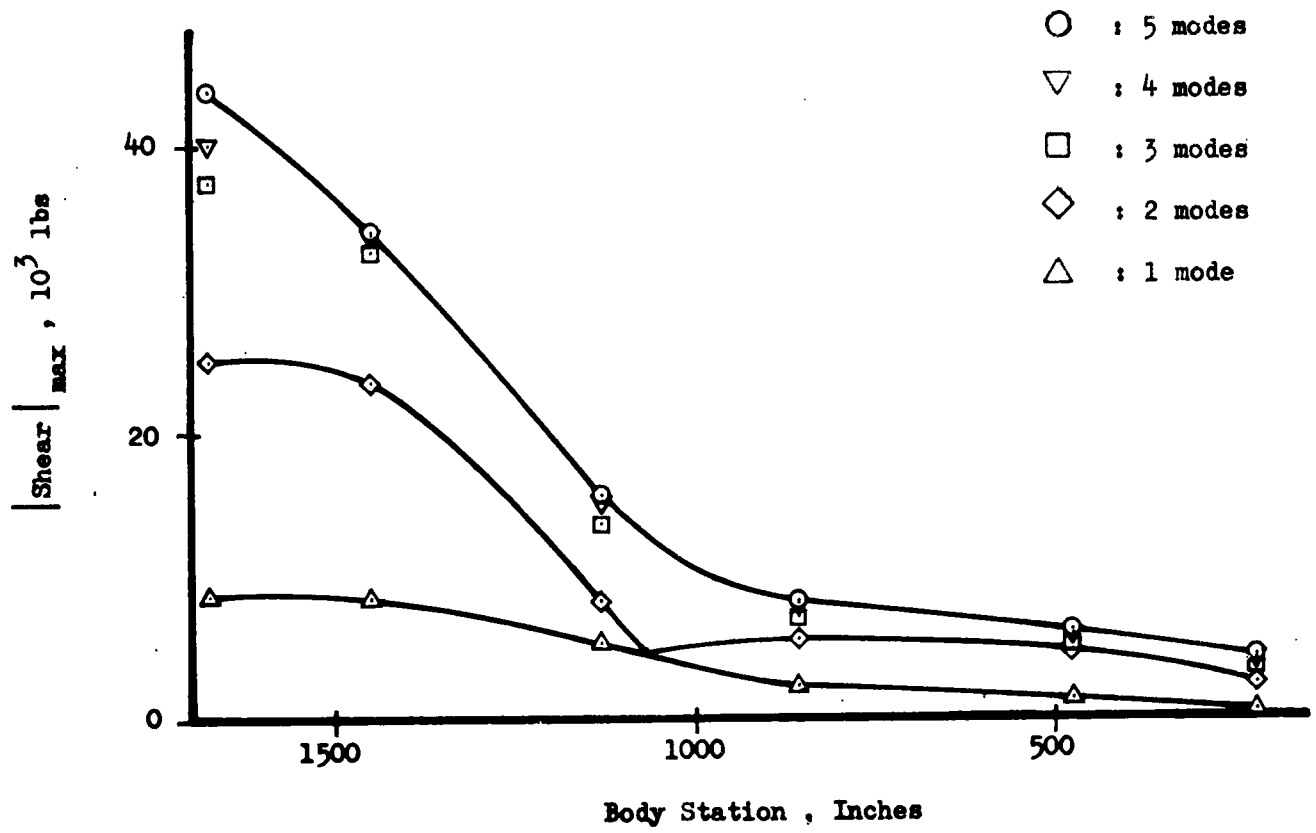
FIG. II-11   VEHICLE LOADS DUE TO SHOCK COMPUTED BY
SHOCK SPECTRA METHOD
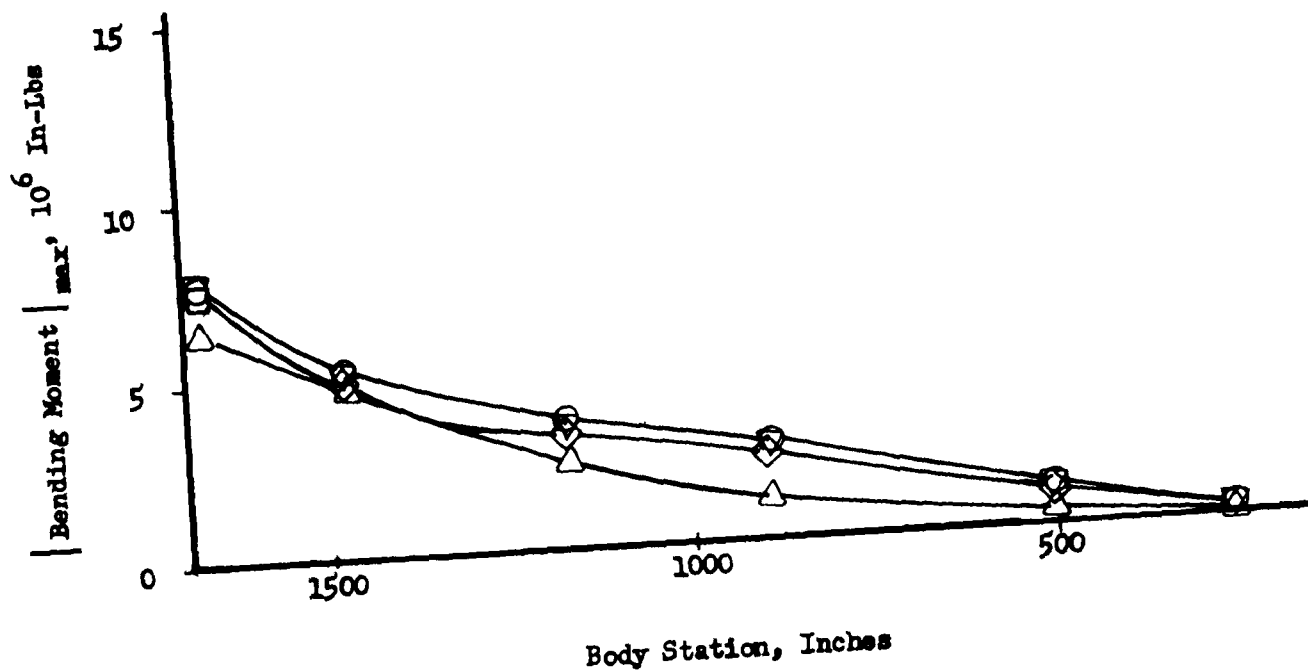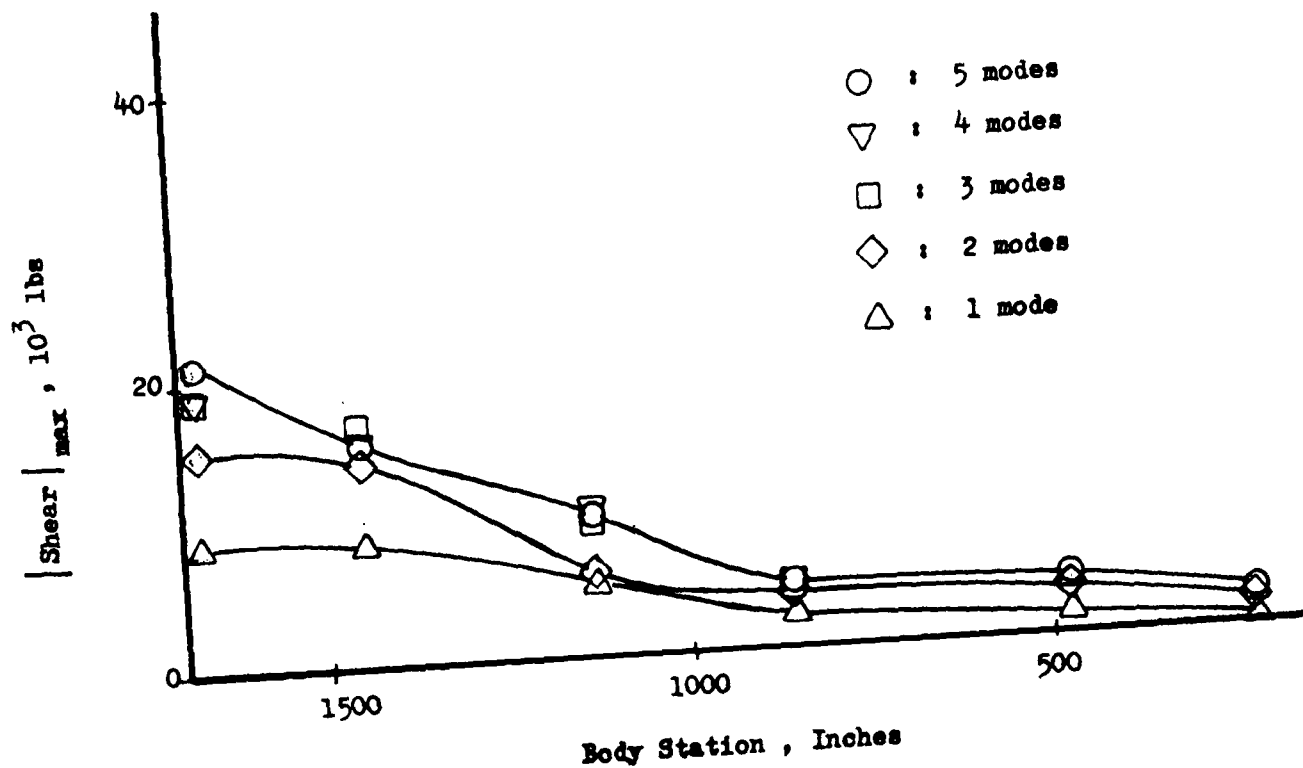
FIG. II-12 VEHICLE LOADS DUE TO SHOCK COMPUTED BY MODE DISPLACEMENT METHOD

Legend:
○ : 5 modes
▽ : 4 modes
□ : 3 modes
◇ : 2 modes
△ : 1 mode
0 : rigid body motion only

(Top plot) Y-axis: $|\text{Shear}|_{max}, 10^3$ lbs — values 0, 20, 40. X-axis: Body Station, Inches — 1500, 1000, 500.

(Bottom plot) Y-axis: $|\text{Bending Moment}|_{max}, 10^6$ In-lbs — values 0, 5, 10, 15. X-axis: Body Station, Inches — 1500, 1000, 500.
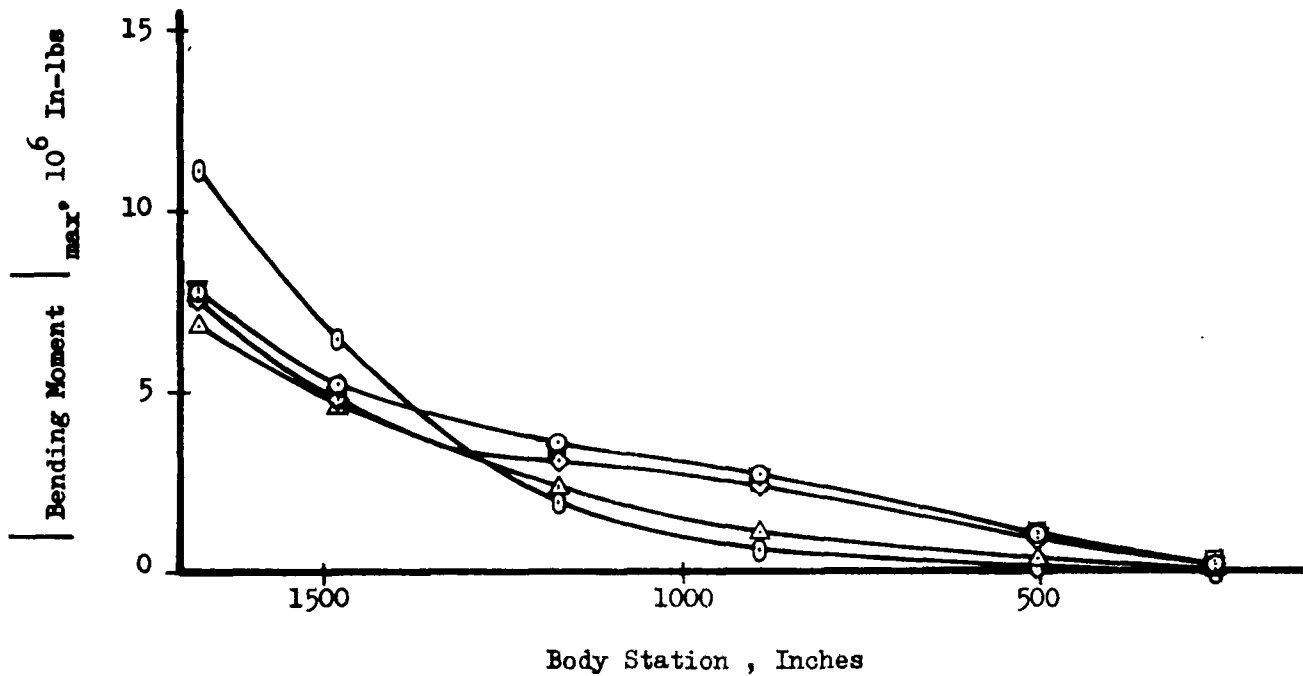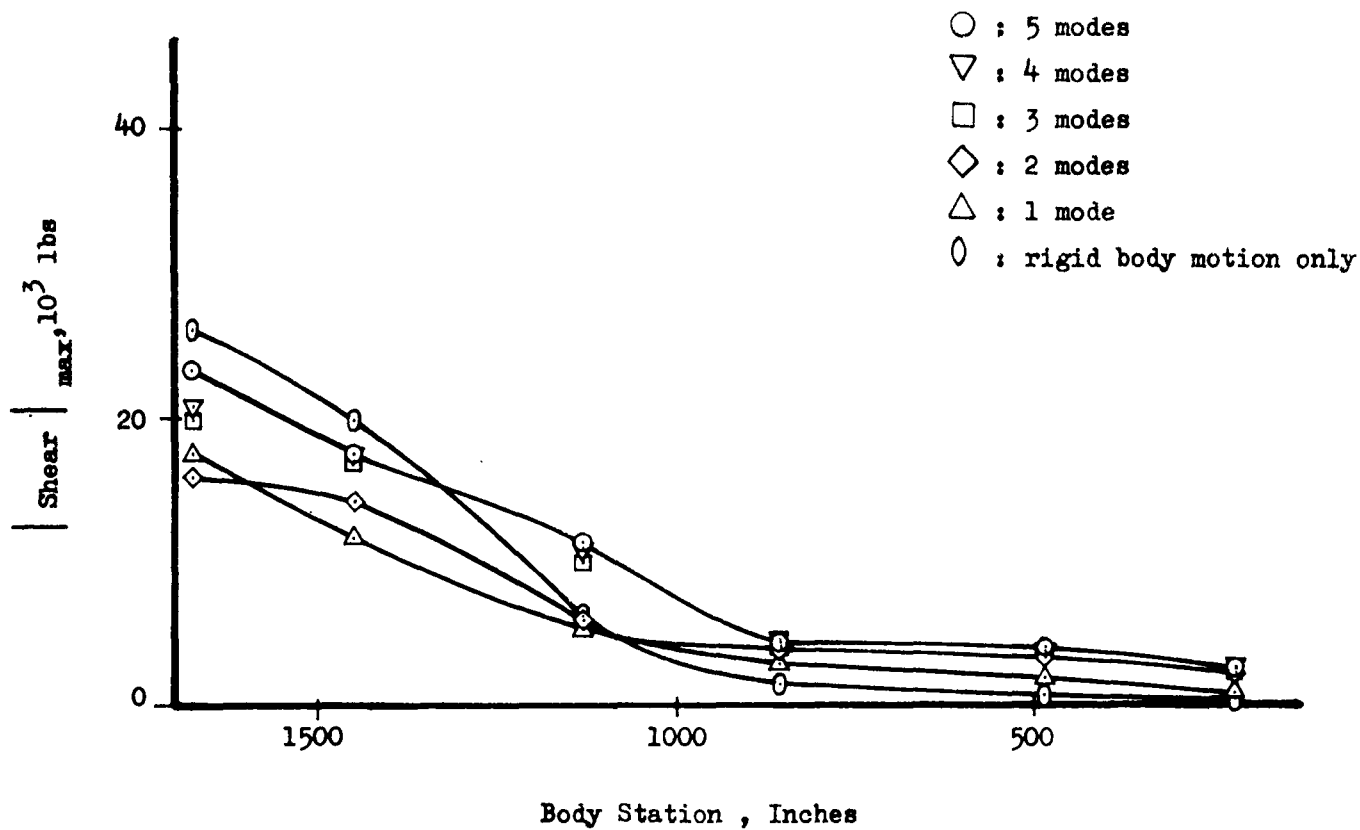
FIG. II-13   VEHICLE LOADS DUE TO SHOCK COMPUTED BY FORCE
SUMMATION METHOD

A. RELEASE

1. Introduction

The release problem is generated from the quick relaxation of the holding mechanism at a prescribed instant during the count down. Since the vehicle support is opposed to the forces and moments due to ground wind, this relaxation is equivalent to a sudden release of the shear and moment at the base.

The effects of different control laws, nozzle inertia, number of degrees of freedom required to accurately describe the motion, and delay time in activating the control system after release are examined.

2. Analysis

The first eight coupled free-free modes are used to represent the vehicle. In this part of the study the equations used follow directly from the perturbation equations referred to body fixed axis in Appendix C. Comparison of the following equations with those in Appendix C reveal by implication the assumption made in this part of the study.

$$\sum m\ddot{q}_z - m_o\ell\,\ddot{q}_\delta = Q_{q_z}(A) + T(q_\delta + \phi_1'(x_p)q_1 + \phi_2'(x_p)q_2) \tag{III-1}$$

$$\sum mx^2\ddot{q}_\theta - m_o\ell x_p\ddot{q}_\delta = Q_{q_\theta}(A) + Tx_p\,(q_\delta + \phi_1'(x_p)q_1 + \phi_2'(x_p)q_2) \tag{III-2}$$

$$M_j\ddot{q}_j - m_o(\phi_j)_n\ell\ddot{q}_\delta + 2\zeta_j\omega_j M_j\dot{q}_j + M_j\omega_j^2 q_j = Q_{q_j}(A)$$

$$+ T\phi_j(q_\delta + \phi_1'(x_p)q_1 + \phi_2'(x_p)q_2) \qquad (j = 1,2,\ldots\ldots8) \tag{III-3}$$

$$m_o\ell^2\ddot{q}_\delta - m_o\ell\ddot{q}_z - m_o x_n\ell\ddot{q}_\theta - m_o\ell(\phi_1)_n\ddot{q}_1 - m_o\ell(\phi_2)_n\ddot{q}_2$$

$$- m_o\ell(\ddot{q}_x + g\sin\psi)\left[q_\delta + \phi_1'(x_p)q_1 + \phi_2'(x_p)q_2\right] = Q_{q_\delta}(C) \tag{III-4}$$

The generalized forces are

$$Q_{q_z}(A) = \frac{\rho}{2}\sum c_D\,D\Delta x\left[V - \dot{q}_z\right]^2 \tag{III-5}$$

$$Qq_\theta \ (A) = \frac{\rho}{2} \Sigma C_D \ D \ x \Delta x \left[V - \dot{q}_z \right]^2 \qquad\qquad (III-6)$$

$$Qq_j \ (A) = \frac{\rho}{2} \Sigma C_D \ D \ \phi_j \Delta x \left[V - \dot{q}_z \right]^2 \qquad\qquad (III-7)$$

$$Qq_\delta \ (C) = m_o \ell^2 \omega_o^2 \ (\delta_a - q_\delta) - 2m_o \ell^2 \omega_o \mathcal{J}_o \ \dot{q}_\delta \qquad\qquad (III-8)$$

Where δ_a in Eqn. (III-8) is determined from the solution of:

$$\gamma_A = K_\theta \left\{ q_\theta + \phi'_{1A} \ q_1 + \phi'_{2A} \ q_2 \right\} \qquad\qquad (III-9)$$

$$\gamma_R = K_\theta^{\cdot} \left\{ \dot{q}_\theta + \phi'_{1R} \dot{q}_1 + \phi'_{2R} \dot{q}_2 \right\} \qquad\qquad (III-10)$$

$$\lambda + T_1 \dot{\lambda} = \gamma_A + \gamma_R = \gamma_s \qquad\qquad (III-11)$$

$$\delta_a + T_2 \dot{\delta}_a = \lambda \qquad\qquad (III-12)$$

and where: ρ : density at sea level

V : velocity of the wind = 40 mph

T : thrust at sea level

C_D : drag coefficient

D : dimension normal to the flow

γ_A : attitude sensor output

γ_R : rate sensor output

K_θ : attitude gain

$K_\theta^{\cdot}$: rate gain

λ : output of filter

T_1 = .034 seconds (time constant of filter)

δ_a : nozzle swivel angle commanded

T_2 : .035 second (hydraulic system lag)

$-x_p$: body fixed axial coordinate associated with the hinge point of the motor nozzles

ζ_j : damping ratio in the jth mode = .02

M_j : generalized mass of the jth mode

ω_j : frequency of jth flexural mode

M_0 : mass of nozzles

ℓ : distance from nozzle cg to nozzle swivel axis

ω_0 : natural frequency of nozzle swiveling

ζ_0 : nozzle damping ratio

ϕ'_{jA} : modal slope of the jth mode at attitude sensor location

ϕ'_{jR} : modal slope of the jth mode at rate sensor location

$(\phi_j)_n$: modal value of the jth mode at nozzle cg

$\phi'_j(x_p)$: modal slope of the jth mode at nozzle attachment point

ψ : angle of inclination of vehicle axis from the horizontal

$\phi_j(x_p)$: modal value of the jth mode at nozzle attachment point

The control system sensors are located as follows: rate sensor at body station 1636 and attitude sensor at body station 411. These locations are consistent with those in the boost-flight analysis.

The gain settings used throughout the release problem are K_Θ = 3.47 $\frac{rad}{rad}$ and $K_{\dot\Theta}$ = 1.33 $\frac{rad}{rad/sec}$. These gain settings are calculated by the method outlined in Appendix D. These gains provide a frequency and damping in pitch of one-half cps and .6 critical immediately after release.

The generalized forces, due to the quasi-steady drag, are linearized when $\left[V - q_z\right]^2$ is replaced by V^2, which will be justified later.

All coefficients remained constant, and the force summation method is again used to determine the bending moments.

To find the equilibrium position prior to launch, a force and a moment are applied at the base such that the translation at the base is zero and the slope at the base is proportional to the base moment. The base stiffness corresponds to a base frequency of one-fourth cps. Setting the inertia and response velocity terms to zero and writing the equations corresponding to the prescribed deflection and slope at the base, results in a set of nine algebraic equations with nine unknowns. The solution of the set yields the proper initial conditions.

The solution of this problem is divided into two parts. Part one uses the supposition that the control law completely filters out any frequency above 5 cps, and the mass of the engine is negligible, and there is no time delay between the angle of thrust vectoring required and applied. That is $T_1 = T_2 = 0$.

Part two considers the effects neglected in part one with the exception that only the first two flexible degrees of freedom in addition to pitch are sensed.

3. DISCUSSION OF RESULTS

a. Linearization Justification

The aerodynamic forces are linearized by neglecting the products of $V\dot q_z$ and $\dot q_z^2$. As can be seen in Fig. III-2, when the control law is activated at release, the bending moment becomes a maximum within .18 of a second after release. The trace of $\dot q_z$ also shown in Fig. III-2 shows that at .18 of a second after release $\dot q_z$ is equal to 5 in/sec. This is small compared with the wind velocity of 704 in/sec; and consequently linearization is justified.

b. Perfect Control Law and Massless Engines

A typical time history of bending moment distribution is shown in Fig. III-3 and Fig. III-4. The bending moment distribution becomes a maximum approximately at t = .18 seconds after release. The pictures

between t = .40 seconds and the steady-state condition are not shown, since they would only show an oscillating but converging bending moment distribution.

At some stations the bending moments due to release are twice the bending moments due to a steady 40 mph ground wind.

The bending moment distribution for four degrees of freedom and ten degree of freedom are compared in Fig. III-5. This figure indicates that four degrees of freedom are adequate to describe the motion.

c. Refined Control Law and Engine Inertia Studies

Both the effects of the refined control law with engine inertia and the delaying of the activation of the control law are illustrated in Fig. III-6. Adding the refined control law and engine inertia has little effect on the maximum bending moments. The reason for the scatter might be due to the phasing of applying the control thrust force and the motion of the flexible degrees of freedom. The delay time in activating the control law increases the maximum bending moment.

Typical control system signals for the release problem are shown in Fig. III-7. The general shape of the curves are identical. Each output lags by a small amount the preceeding output.

4. GENERAL CONCLUSIONS

a) Linearization of the equations of motion is justified.

b) Delaying the activation of the control system increases the bending moment.

c) Four degrees of freedom are adequate to describe the motion.

d) Using a refined control law and engine inertia has little effect on the maximum bending moment.

B. AXIAL LOADS

1. Introduction

The first axial loads of large magnitude, encountered by the vehicle, occur during launch. Large axial loads are also encountered at the termination and initiation of thrust during the staging process.

Under a nominally steady thrust, T, high frequency variations (screaming) of the order of 6000 cps and low frequency variations (chugging) of the order of 50 cps are known to occur in the thrust of rocket engines, the magnitude of the variation being on the order of 1% to 10% at full thrust. Resonance of the structure with a screaming or chugging engine could be the source for the production of large axial loads at specific body stations; fortunately the screaming and chugging frequencies do not persist for long periods of time nor are they of a strictly sinusoidal nature.

2. Analysis

The modeling of a liquid-fueled vehicle appears to present more difficulties than the modeling of a solid-propellant vehicle where a combination of linear springs and masses generally suffices. The major difficulty in modeling of the former type of vehicle comes about in defining the interaction between the liquid and the structure. A cursory investigation of this problem indicates that the structure should be considered separate from the liquid. The coupling between the two is in the pressure exerted by the liquid on the structure. In all but the most simple geometries, the analytical expressions for the interaction poses extremely difficult problems in shell theory as well as in potential flow theory. To circumvent the difficulties and yet provide simple numerical estimates of the maximum axial loads one might expect, the following method is suggested.

The analysis is based on the following assumptions:

1) The vehicle can be represented by two springs and a mass in tandem as shown in Fig. III-1. The spring constant of each spring is calculated using the average stiffness of the shell represented in each stage, Fig. A-6, and the mass is that of the glider.

2) The glider is assumed to be rigid.

3) The mass of the stage structure is neglected.

4) The interaction of the propellant (fuel + oxidizer) and the structure is assumed to be only in the pressure exerted by fluid resulting from the acceleration of the base of the spring, and the gravitational field. The lumping of the propellant (fuel + oxidizer) in each stage as acting as a single fluid in a single equivalent shell is an approximation that can be refined. The force F_i thus exerted on the base of each spring, is given by:

$$F_i = - M_i(g + \ddot{x}_i) \qquad (III-13)$$

where M_i : mass of the propellant in the ith stage

g : gravitational field acceleration

$g + x_i > 0$ is assumed

No interaction resulting from the exertion of lateral pressure on the shell by the fluid is assumed.

5) The instance considered assumes the vehicle to be in a vertical position at the instant of launch.

6) The application of a constant thrust, T, is assumed to take place instantaneously (unit step).
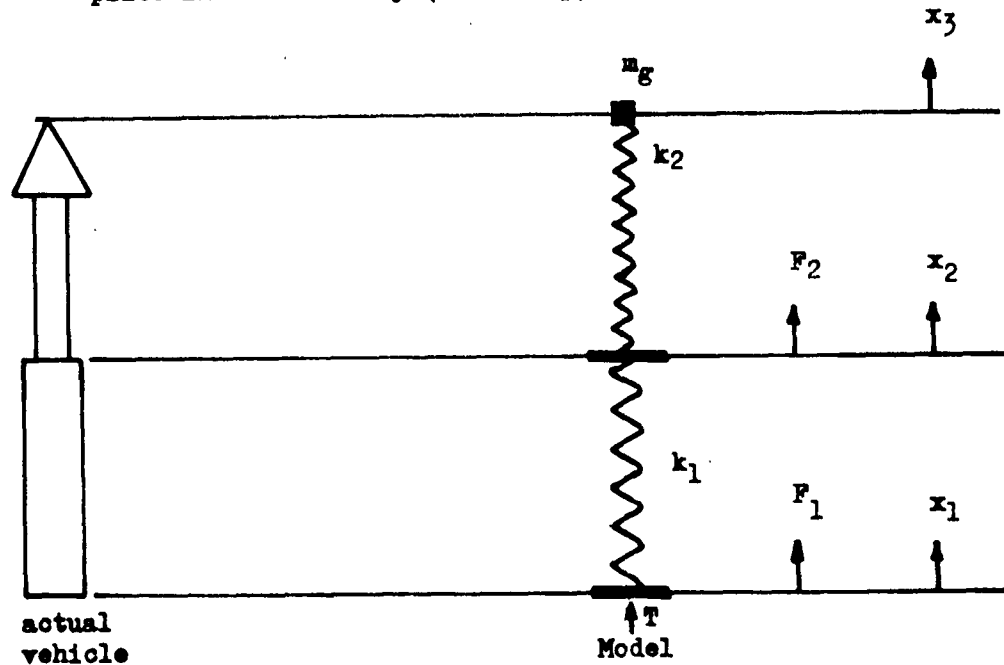
FIG. III-1 AXIAL LOAD ILLUSTRATION

The equations of motion

$$T + F_1 + k_1 (x_2 - x_1) = 0 \tag{III-14}$$

$$F_2 + k_2(x_3 - x_2) + k(x_1 - x_2) = 0 \tag{III-15}$$

$$m_G \ddot{x}_3 = k_2(x_2 - x_3) - m_G g \tag{III-16}$$

are solved for the maximum deformation, χ_i, possible in the springs (under the application of a unit step thrust) in excess of the deformation $\delta_i(e)$ resulting from the equilibrium prior to launch, and the deformation $\delta_i(ss)$ resulting from a steady state condition subsequent to launch. These values are compared in the following table, along with the steady state value of $\ddot{x}_3$, $\ddot{x}_3(ss)$, and the maximum value of $\ddot{x}_3$ possible.

î	k_i	$\xi_i(e)$	$\xi_i(ss)$,	$\chi_i max$,	$\ddot{x}_3(ss)$	$\ddot{x}_3 max$,
	10^6 lb/in	inches	inches	inches	g	g
1	1.15	.046	.0710	.0520		
					0.54	5.0
2	0.865	.0104	.0160	.0178		

The above values are based on the assumption that the eigenvalues of the system are commensurate and on the important restriction that $g + \ddot{x}_i > 0$, which is not generally satisfied, hence a more exacting analysis would require

$$F_i = -W_i (g + \ddot{x}_i) \qquad g + \ddot{x}_i \geq 0$$

$$0 \qquad g + \ddot{x}_i < 0$$

This problem can be solved by an electric analog with little difficulty.

Four Degrees of Freedom
2% critical damping in flexible modes
massless engine - simple control law
velocity of wind 58-67 fps

Translational Velocity

Bending Moment at Station 587
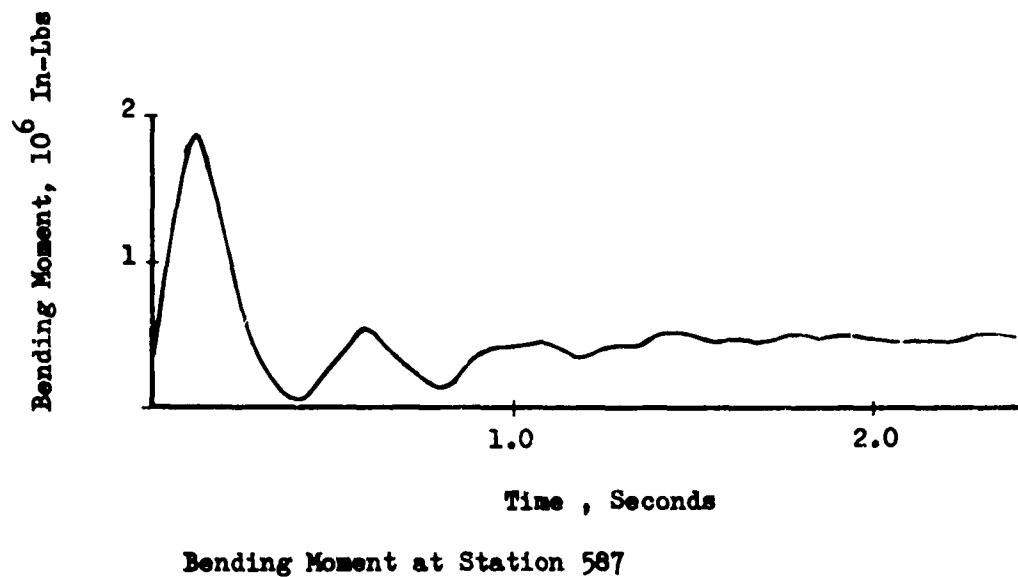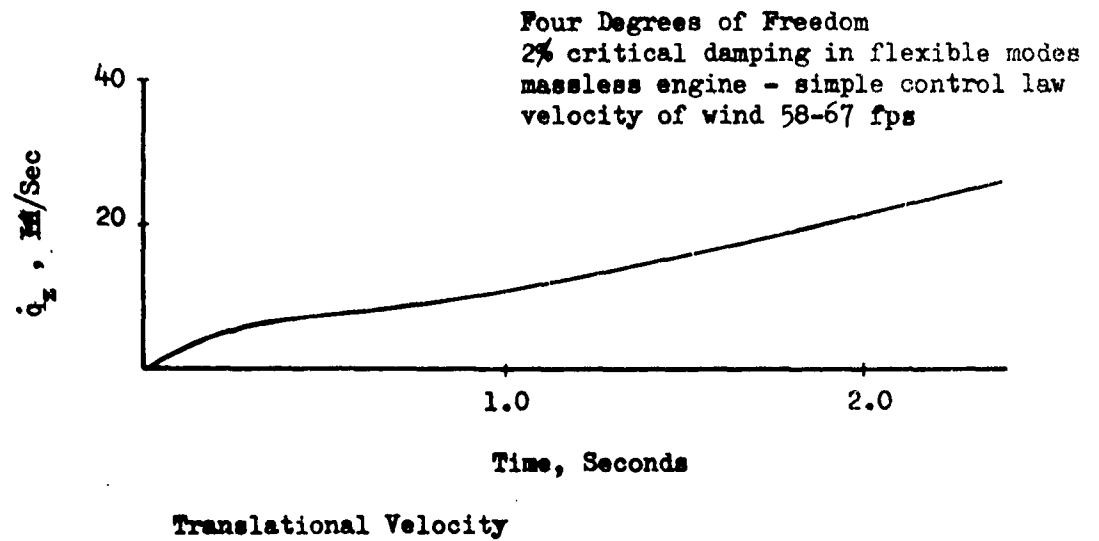
FIG. III-2   LINEARIZATION JUSTIFICATION

Four Degrees Of Freedom
Control Law Applied at Release
Massless Engine - Simple Control Law
2% critical damping in flexible modes
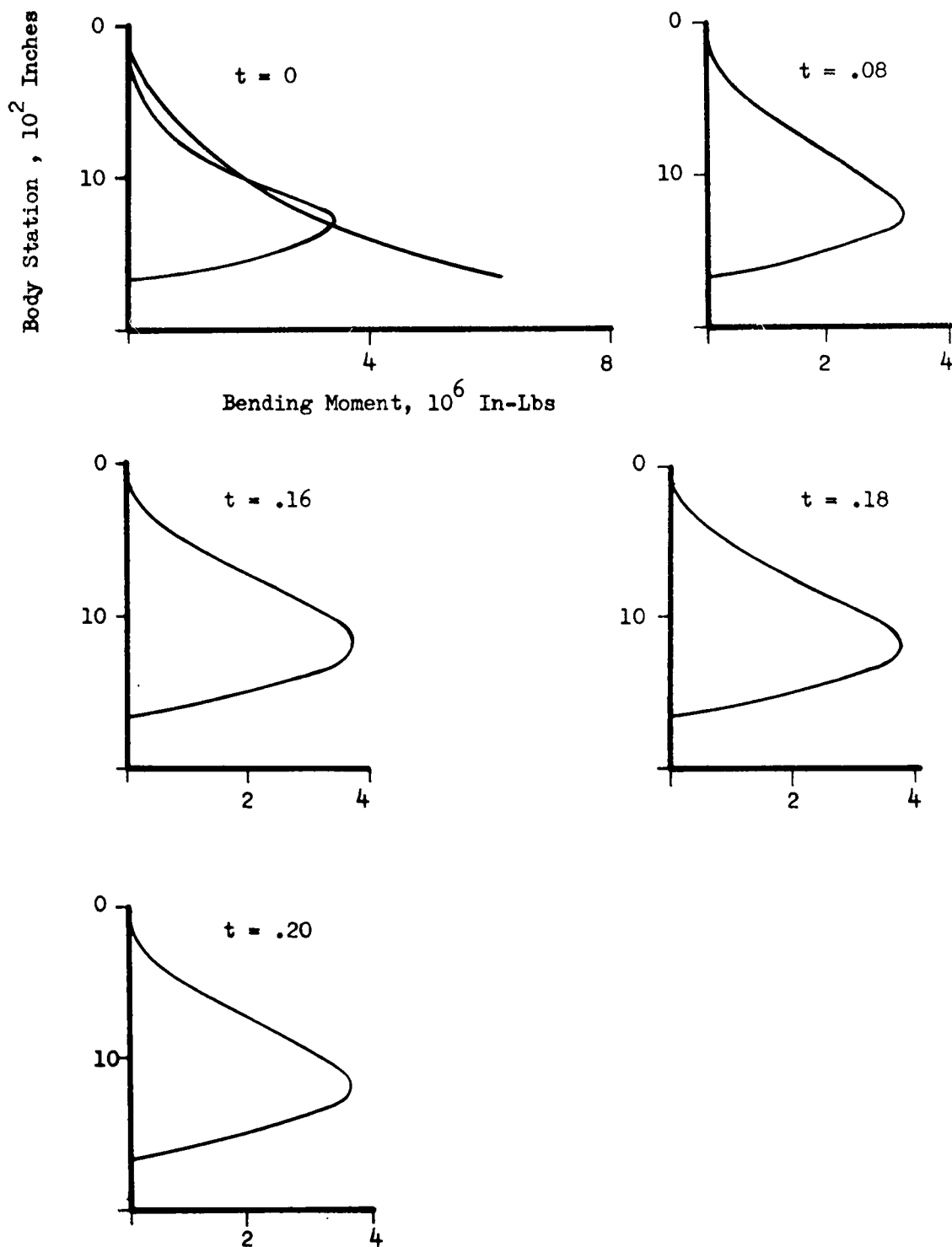
FIG. III-3   TIME HISTORY OF BENDING MOMENT DISTRIBUTION
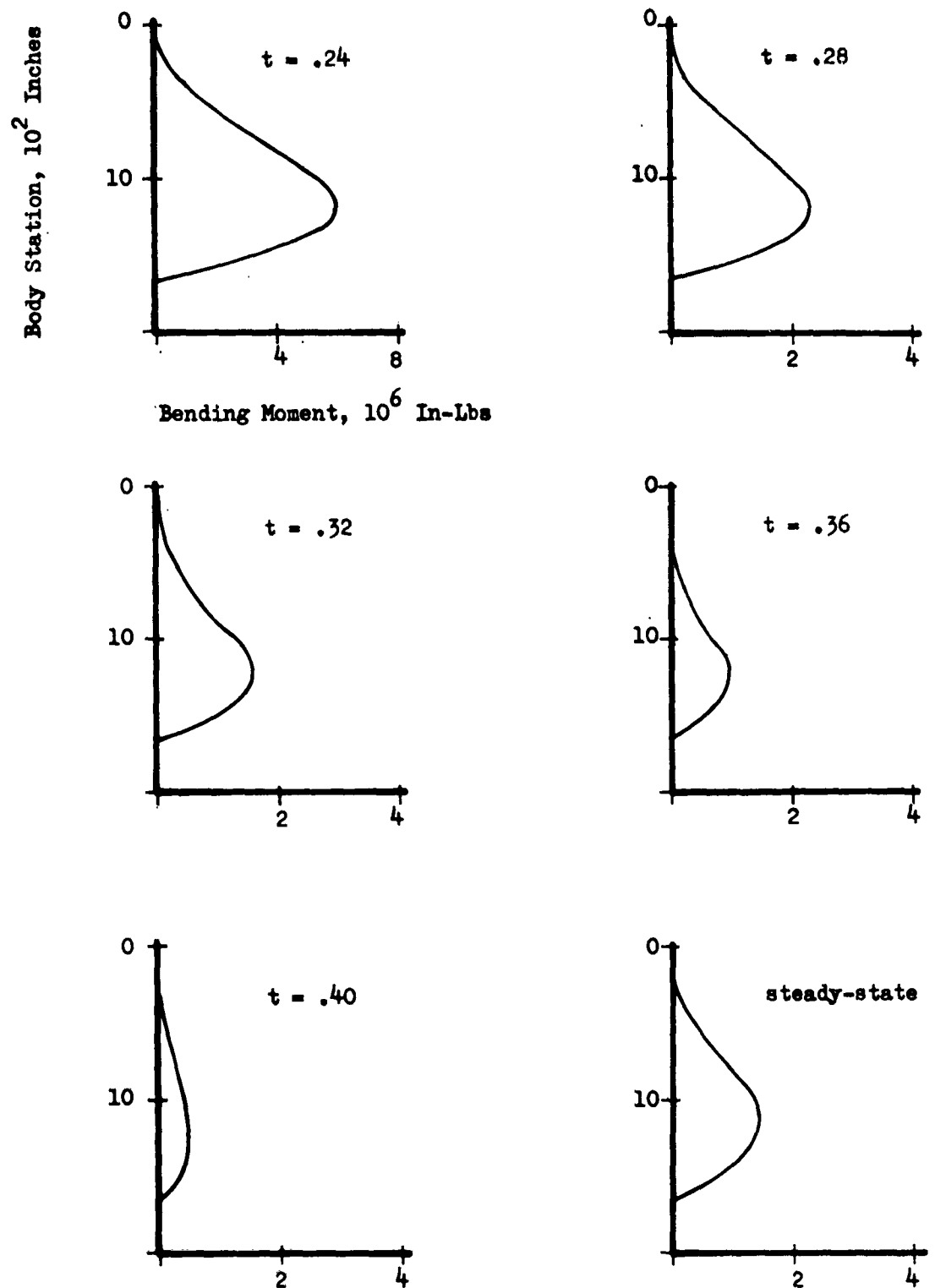
FIG. III-4   TIME HISTORY OF BENDING MOMENT DISTRIBUTION

Bending Moment at Release
2% Critical Damping in·Flexible Modes
Simple Control - Massless Engine

10 degrees of freedom←   ←4 degrees of freedom

Body Station , Inches
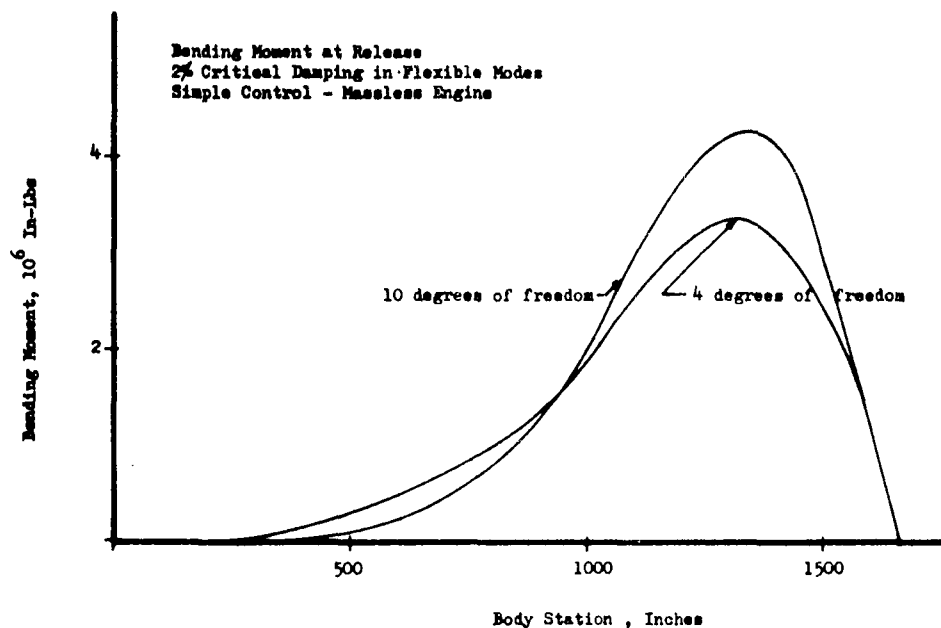
FIG. III-5   EFFECT OF ADDITIONAL DEGREES OF FREEDOM

Four Degrees of Freedom
2% critical damping in flexible modes

△ engine with mass and refined control law
O massless engine and simple control law

body station 1027

body station 505
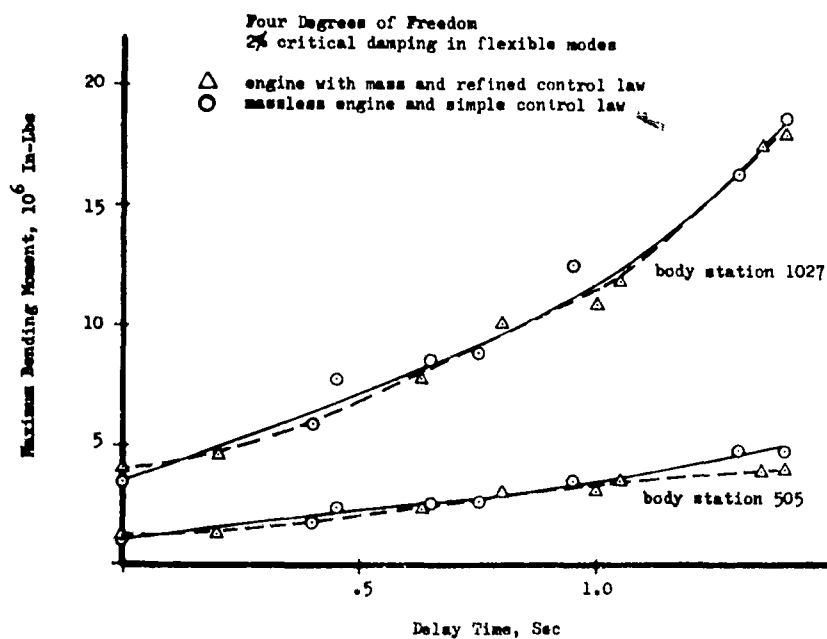
Delay Time, Sec

FIG. III-6   EFFECTS OF DELAY TIME IN ACTIVATION OF THE CONTROL SYSTEM

Four Degrees of Freedom
2% Critical Damping in Flexible Modes
Refined Control Law and Engine Inertia
Control Law Applied at Release
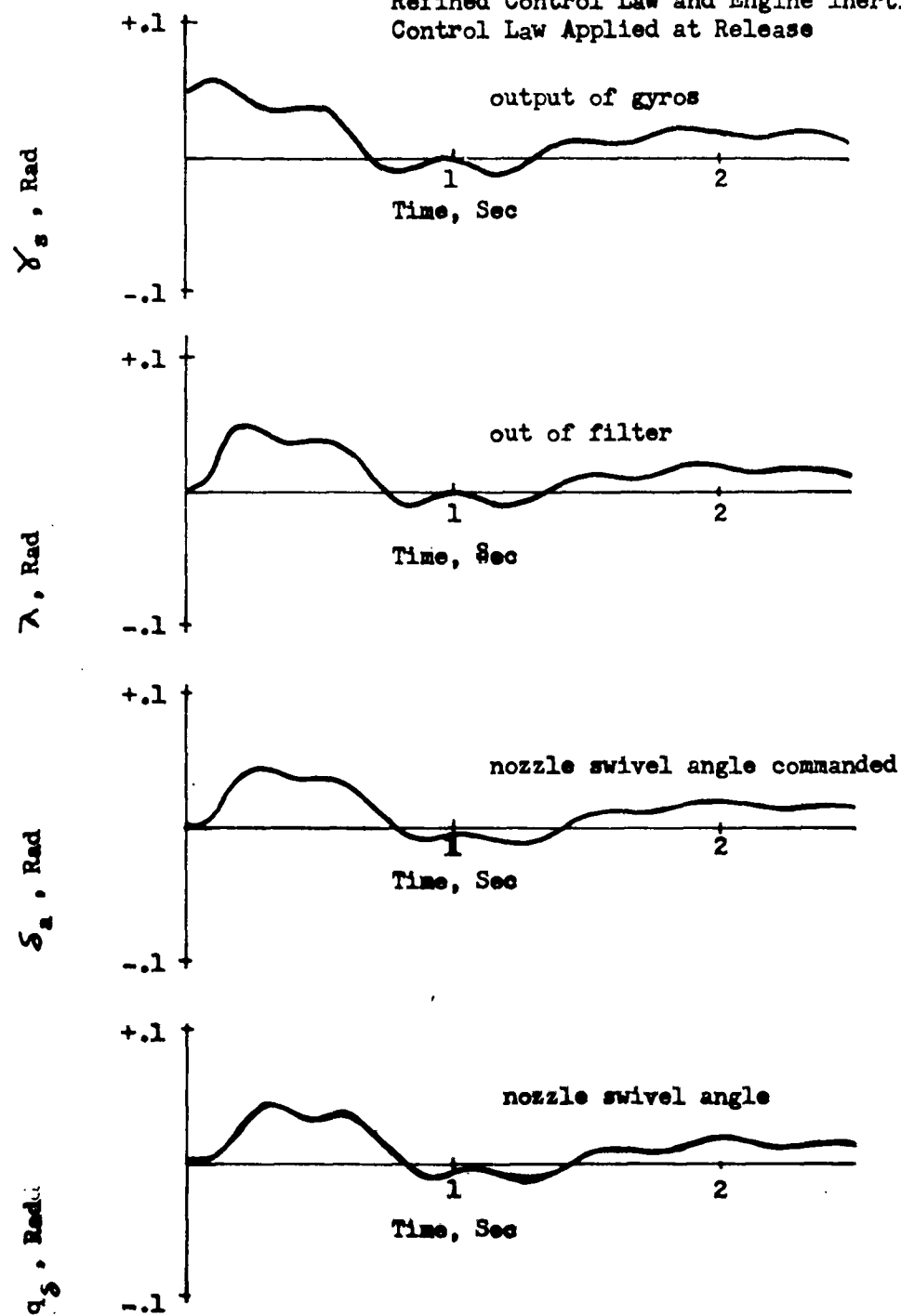
FIG. III-7   TYPICAL CONTROL RESPONSES

IV   BOOST FLIGHT LOADS

A.   GENERAL DISCUSSION

Introduction

A large percentage of the structure of a boost-glide vehicle is designed by loads occurring during the boost phase of the trajectory. Axial loads due to thrust, internal pressurization loads, and transverse bending moments due to atmospheric turbulence, wind shear, and maneuver combine to produce the critical loading conditions. Bending loads are likely to be large in boost-glide vehicles having a lifting surface near the nose of the vehicle.

A significant portion of the glider itself may also be designed by loads occurring during boost. Angles of attack due to wind shear, gusts, and maneuver encountered at high dynamic pressures during boost are likely to produce critical loads; and axial accelerations during boost are considerably higher than those due to re-entry for vehicles of the type being studied.

The thrust and pressurization loads depend on the thrust, drag, weight, weight distribution, geometry, and internal pressure. These essentially static loads may be calculated in a straightforward manner, since external disturbances such as turbulence and wind shear have little effect on them except insofar as internal pressurization requirements are determined by bending loads. Bending moments arise from programmed maneuvers, atmospheric turbulence, and wind shear. Maximum bending moments usually result from a combination of turbulence and wind shear reversal associated with a jet stream wind. A comprehensive dynamic analysis is required to accurately predict the bending loads due to wind shear and turbulence.

The Load Producing Environment

Wind shear is probably the most important contributor to bending loads produced during boost. The development of wind shear design criteria will continue as more data on winds aloft and wind shear become available and are analyzed.

Sissenwine (105, 115, 116, 117) has published several synthetic wind profiles which have been widely used for design purposes. Fig. IV-2 shows the Sissenwine revised one percent synthetic wind profile which has been used to compute wind shear loads in the present study. Presumably, a vehicle designed to this profile would exceed the design wind shear loads only once per hundred flights in the area and the season to which the profile is applicable. Another design wind profile recommended by AvIdyne Research (108) is also shown in Fig. IV-2. In using any of these profiles,

the wind is assumed to be blowing from the most adverse direction. The altitude at which the peak velocity occurs is also shifted between 30,000 and 45,000 feet to the most critical altitude within this band.

Atmospheric turbulence produces bending loads during boost which combine with wind shear loads. Turbulence may be represented for design purposes either as random continuous turbulence having a specified power spectrum and certain probability distribution functions or as a discrete gust of specified velocity and profile. In references 113 and 114 Press defines atmospheric turbulence power spectra and probability distribution functions, as well as procedures for determining probable load exceedances which have been used in gust load studies of several types of airplanes. However, the application of the power spectral method to vehicles having high vertical velocity components is questionable, since most of the data upon which the atmospheric power spectra and probability distributions functions are based were gathered by airplanes in essentially horizontal flight. Also the power spectral method gives loads in terms of root mean square values and probable number of exceedances of given load levels per unit time or distance; and there is considerable uncertainty as to how these loads should be combined with rapidly time varying discrete wind shear loads.

If the discrete gust approach is used, the loads due to a specified discrete gust are added to the wind shear loads. In the past, a one minus cosine shaped gust whose wave length is adjusted to produce maximum loads has been used extensively. The design maximum gust velocity is, of course, somewhat arbitrary, but the selection should be based on a probability encounter commensurate with the probability of encountering design wind shear loads. Therefore, it seems reasonable that a gust which would be encountered only once in one hundred flights should be used for design when a one percent probability wind profile is used.

Objectives

The objectives of the boost flight loads analyses conducted in the present research program are two fold. The first and perhaps the primary objective is to study and evaluate existing methods of dynamic loads prediction. In particular, the effects of various refinements in the mathematical representation of the system as well as variations in some of the parameters are determined. The second objective of the boost loads studies is to obtain quantitative results so that the loads occurring during boost can be compared with loads arising from other conditions. The mathematical representations studied range from a rigid vehicle with a simple idealized control system and no fuel slosh to representations including up to three elastic structural degrees of freedom, two liquid slosh degrees of freedom, and up to three control system lags. Parameter variations studied include control system gains, sensor locations, and assumed glider lift curve slope. The effect of configuration and trajectory changes are not studied, since these are considered fixed in the present research study. Wind shear and discrete gust loads are determined. A power spectral analysis of gust loads during boost is conducted to provide load occurrence data suitable for fatigue life studies.

B. ANALYSIS

General Approach

The major effort in the study of the boost phase is concentrated on the wind shear problem. Wind shear is the major contributor to bending loads, and an evaluation of analysis techniques and of the importance of various parameters should lead to more efficient solution of this important and rather complicated dynamic loads problem.

The dynamic loads analysis of a boosted vehicle differs from an airplane dynamic loads analysis primarily in that the boosted vehicle mass, velocity, air density, and Mach number all vary rapidly with time. The boosted vehicle is represented mathematically by a set of differential equations with time varying coefficients. Solution of these equations may be accomplished by a step by step integration procedure utilizing high speed digital computing equipment. Machine limitations as well as the magnitude of the effort required to determine time histories of a large number of coefficients make it desirable to limit the number of degrees of freedom in this problem to as few as possible. During most of the first stage boost, the horizontal wind velocity varies rather slowly with time; hence the response of the vehicle is primarily a rigid body translation response and a few degrees of freedom are adequate. However, in the vicinity of the peak of the wind profile, the horizontal wind velocity varies rapidly with time; and adequate representation of elastic mode response, nozzle inertia, fuel slosh, etc., may require a large number of degrees of freedom. This situation suggests a two-part approach. One part consists of obtaining the response to the portion of the wind profile which varies slowly with time. The spike is replaced with a straight line across the base of the spike. The vehicle is represented by three degrees of freedom, and the coefficients are varied with time. Solution is accomplished by means of a digital computer program. In the second part, the assumption is made that the coefficients can be considered constant during the passage through the wind spike. The response to the spike is obtained from an analog computer simulation in which a large number of degrees of freedom are included. Using this approach wind shear loads are determined by superposition of the loads due to the slow time-varying portion of the profile and the loads due to the spike. The use of the principle of superposition is, of course, applicable only for linear systems. When a nonlinearity consisting of limiting the nozzle angle is included in the problem, the values of the variables determined from the slow time-varying solution at the point corresponding to the start of the wind spike are used as initial conditions for the analog solution. The nonlinearity is simulated only on the analog in this analysis.

Both of the approaches described above depend on the assumption that all the coefficients may be considered constant during the passage through the spike. For comparison purposes, digital solutions have also been obtained for the response to the complete profile with time-varying coefficients. The advantages of the larger number of degrees of freedom included in the analog simulation are weighed against possible loss in accuracy due to the assumption of constant coefficients.

The analysis shows that the assumption of constant coefficients does indeed noticeably affect the results, and that as few as four degrees of freedom are adequate for predicting the response to the wind spike. Therefore, a digital solution of the equations of a four degree of freedom system with time-varying coefficients for the response to the spike has been obtained. Final wind shear loads have been determined by super-position of the responses to the spike and to the slow time-varying portion of the profile, both obtained by digital solution of equations with time-varying coefficients.

The studies designed to investigate the effects of the number of degrees of freedom, control system lags and nozzle inertia, fuel slosh, and parameter variations on loads have been conducted on the analog making the assumption of constant coefficients.

Although wind shear is the major contributor to bending loads, gusts also produce significant bending loads. In the gust problem, the vehicle is represented mathematically by the same set of differential equations used in the wind shear analysis. The forcing function consists of either a discrete gust profile or a random gust velocity defined in terms of its power spectrum and probability distributions. The assumption of constant coefficients is made in both the discrete and power spectral gust studies. The discrete gust solutions have been obtained on the analog, and the power spectral analysis has been accomplished by means of a digital computer program which computes the frequency response functions, the integrated output power spectra, and the characteristic frequencies of loads. The boost phase is divided into altitude bands, and the coefficients for each power spectral solution are based on the average conditions within a band.

Formulation of Equations

A derivation of the basic flight equations of motion of the vehicle is given in Appendix C using body-fixed axes.

The motions of the system in the flight loads problem are described in terms of the following degrees of freedom: translation normal to the vehicle axis, pitch, elastic deformation in the normal vibration modes, the first slosh modes in the first stage fuel and oxidizer tanks, and swiveling of the engine nozzles. All motions are assumed to be in the plane of the trajectory, and no extensional modes were included. The external forces acting on the system are aerodynamic forces due to wind, gusts, and the motions of the vehicle. The engine thrust due to exit pressure and mass efflux from the system is treated as an external force. The nozzles are considered hinged at the swivel axis location; but they are restrained by the hydraulic actuator linkage. With the hydraulic valves which supply fluid to the actuator cylinder closed, the nozzles can be forced to swivel by straining the elastic linkage and trapped hydraulic fluid. The nozzles have a certain natural swiveling frequency with the valves closed which is dependent on the moment of inertia of the nozzles about the swivel axis and the spring effects mentioned above.

The position of the actuator piston can be changed by allowing hydraulic fluid under pressure to flow to the appropriate side of the piston in the cylinder while unpressurized fluid is pushed out of the other side of the cylinder. The means by which the hydraulic flow is controlled will be discussed later.

Equations for vehicle bending moments and net panel loads on the glider are derived by the force summation method. In this method, panel loads are determined by summing the aerodynamic and inertia forces, expressed as functions of the generalized coordinates, their derivatives, and the wind velocity.

Bending moments are found by a summation of panel loads times appropriate moment arms. For the four aft bending moment stations, the loads aft of the station are summed. Therefore, components of the thrust force due to thrust vectoring and bending times appropriate moment arms are included in the summation for the bending moments at these stations.

The equations of motion used in the boost flight loads analysis are obtained from Eqn. (C-35) through (C-40). The following assumptions are made:

1) The solution of Eqn. (C-36) is assumed known.

2) $I_o = 0$. The rotary inertia of the engine nozzles about their own c.g. is assumed zero. This is consistent with the assumption made in calculating the mode shapes: that the rotary inertias of the individual masses about their own c.g.'s are zero.

3) $\dot{m} \left[\dot{q}_\theta \, (\ell_1 - x_p) - \sum_j \phi_j \dot{q}_j + \ell_1 (\dot{q}_S + \sum_j \phi'_j(x_p) \, \dot{q}_j) \right] = 0$. The terms arising from this quantity are very small in comparison to the parts of $Q(A)$ and $Q(C)$ which are functions of $\dot{q}_\theta$, $\dot{q}_j$ and $\dot{q}_S$.

4) $\gamma_i = 0$. Structural damping is neglected, since it is very small compared to aerodynamic damping.

The generalized forces of aerodynamic origin are:

$$Q_{q_z} \ (A) = \sum_i N_i \tag{IV-1}$$

$$Q_{q_\theta} \ (A) = \sum_i N_i x \tag{IV-2}$$

$$Q_{q_j} \ (A) = \sum_i N_i \phi_j \tag{IV-3}$$

where N_i = normal aerodynamic force on segment i.

x = distance from the centroid of segment i to the vehicle mass center, positive forward.

ϕ_j = modal value at the centroid of segment i in the jth mode.

The aerodynamic forces on the glider segments are:

$$N_i = \frac{\rho V^2}{2} \, S_i \, C_{N_\alpha} \alpha_i \qquad (i = 1 \text{ to } 30) \qquad \text{(IV-4)}$$

where

ρ = air density

V = velocity of air stream relative to the vehicle

S_i = planform area of ith segment

C_{N_α} = rate of change of normal force coefficient with angle of attack (lift curve slope)

α_i = local angle of attack on i^{th} segment

The air density is obtained assuming a standard atmosphere. In the wind shear problem the parallel component of the wind velocity is included in the relative velocity. The variation of lift curve slope with Mach number used in the analysis is shown in Figure IV-3. The local angle of attack in terms of the generalized coordinates and the wind velocity is:

$$\alpha_i = -\frac{\dot{q}_z}{V} - \sum_j \frac{\phi_j}{V} \dot{q}_j - \frac{x}{V} \dot{q}_\theta + \sum_j \phi_j' q_j + \frac{V_W}{V} \sin \theta_1 \qquad \text{(IV-5)}$$

The lift on each segment is assumed independent of the lift on the other segments. Unsteady lift effects are not included.

The aerodynamic forces on the booster are:

$$N_i = \left[\pi \frac{\rho V^2}{2} \int_{\Delta \ell_i} b \frac{db}{d\ell} \, d\ell \right] \alpha_i + \frac{\pi \rho}{4} \int_{\Delta \ell_i} b^2 d\ell \left[-V^2 \sum_j \phi_j'' \, q_j \right.$$

$$+ \ 2V\dot{q}_\theta + 2V \sum_j \phi_j' \, \dot{q}_j - (\ddot{q}_z + \dot{q}_x \dot{q}_\theta) - x\ddot{q}_\theta - \sum_j \phi_j \ddot{q}_j \left. \right]$$

$$(i = 31 \text{ to } 47) \qquad \text{(IV-6)}$$

where α_i is as defined above and b and ℓ are shown below.
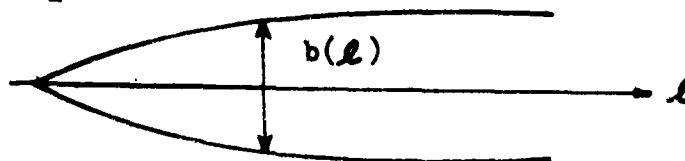
Equation IV-6 is derivable from momentum theory.

The generalized forces for the nozzle swiveling degree of freedom are:

$$Q_{q_\delta} (C) = -2 m_o \ell^2 \mathcal{Y}_o \omega_o \dot{q}_\delta - m_o \ell^2 \omega_o^2 (q_\delta - \delta_a) \qquad \text{(IV-7)}$$

where δ_a = actuator position measured in terms of nozzle swivel angle commanded.

Q_{q_δ} (C) is treated as an external moment acting about the nozzle swivel axis. The values of $\mathcal{Y}_o$ and ω_o used are typical of engines of this size.

The equations of motion as used in the boost flight loads analysis appear as written below. Certain equations are omitted in some of the studies, as indicated in the subsequent discussions.

Equations of Motion:

$$(\sum_i m_i)(\ddot{q}_z + \dot{q}_x \dot{q}_\theta) - m_o \ell \ddot{q}_\delta - \sum_{\ell=1}^{2} m_{\ell 1} h_{\ell 1} \ddot{q}_{\ell 1} =$$

$$(\sum_i m_i)(g \sin\theta_1) q_\theta + T(q_\delta + \sum_j \phi'_j(x_p) q_j) + \sum_i N_i$$

$$(\sum_i m_i x_i^2)\ddot{q}_\theta - m_o \ell x \ddot{q}_\delta - \sum_{\ell=1}^{2} m_{\ell 1} h_{\ell 1} x \ddot{q}_{\ell 1} =$$

$$- m_o \ell (\ddot{q}_x + g \sin\theta_1) q_\delta - \sum_{\ell=1}^{2} m_{\ell 1} h_{\ell 1} (\ddot{q}_x + g \sin\theta_1) q_{\ell 1} \qquad \text{(IV-8)}$$

$$+ T x_p (q_\delta + \sum_j \phi'_j(x_p) q_j) + \sum_i N_i x$$

$$M_j(\ddot{q}_j + \omega_j^2 q_j) - m_o \ell \phi_j \ddot{q}_\delta - \sum_{\ell=1}^{2} m_{\ell 1} h_{\ell 1} \phi_j \ddot{q}_{\ell 1} =$$

$$m_o \ell \phi'_j(x_p)(\ddot{q}_x + g \sin\theta_1) q_\delta + \sum_{\ell=1}^{2} m_{\ell 1} h_{\ell 1} \phi'_j(x_{\ell 1})(\ddot{q}_x + g \sin\theta_1) q_{\ell 1}$$

$$+ T \phi_j(x_p)(q_\delta + \sum_j \phi'_j(x_p) q_j) + \sum_i N_i \phi_j$$

$$m_{\ell 1} h_{\ell 1} \left[h_{\ell 1} \ddot{q}_{\ell 1} - (\ddot{q}_z + \dot{q}_x \dot{q}_\theta) - x \ddot{q}_\theta - \sum_j \phi_j \ddot{q}_j \right] =$$

$$- m_{\ell 1} h_{\ell 1} \left[(\ddot{q}_x + g \sin\theta_1)(q_{\ell 1} + \sum_j \phi'_j(x_{\ell 1}) q_j) + (g \sin\theta_1) q_\theta \right]$$

$$m_o \ell \left[\ell \ddot{q}_\delta - (\ddot{q}_z + \dot{q}_x \dot{q}_\theta) - x \ddot{q}_\theta - \sum_j \phi_j \ddot{q}_j \right] =$$

$$= m_o \ell \left[(\ddot{q}_x + g \sin\theta_1)(q_\delta + \sum_j \phi'_j(x_p) q_j) + (g \sin\theta_1) q_\theta \right]$$

$$- m_o \ell^2 \left[2 \mathcal{Y}_o \omega_o \dot{q}_\delta + \omega_o^2 (q_\delta - \delta_a) \right]$$

Aerodynamics

Several theories are considered for calculating the aerodynamic forces on the vehicle for the boost phase. The Mach number from launch until the vehicle has passed through the altitude band where high wind shear is encountered varies from zero to about 2.0. Aerodynamic forces at much higher Mach numbers are not of interest since the dynamic pressure drops off rapidly as altitude and Mach number increase. The theories considered are momentum theory, piston theory, linear first order supersonic theory, and a semiempirical theory which assumes a piston theory lift distribution with a lift curve slope based primarily on experimental data.

The aerodynamic forces on the booster are in all cases calculated by momentum theory. In this particular configuration, the aerodynamic forces on the booster are almost insignificant when compared to those on the glider. Therefore, any theory which predicts the correct order of magnitude of the aerodynamic forces on the booster is considered satisfactory, and no time has been spent studying other possible methods of calculating these forces.

Flight loads are found to be quite sensitive to the aerodynamic forces on the glider; hence, considerable thought is given to glider aerodynamics. The aspect ratio of the glider is low enough so that momentum theory is considered applicable. However, momentum theory has several shortcomings. First, this theory predicted significant lift forces due to angle of attack only on the portion of the glider in which the span increased with glider length. Thus the large area lying between the straight wing tips has no angle of attack dependent aerodynamic forces on it. Second, momentum theory in its simple form does not reflect changes in the aerodynamic forces due to spanwise elastic deformations on the wing. Third, momentum theory does not reflect the effect of Mach number on angle of attack dependent aerodynamic forces.

Although the Mach number range of interest in the flight loads analysis is below the range of applicability of piston theory, this theory is considered attractive because of its simplicity and because the effect of elastic deformations on local angle of attack and the resulting aerodynamic forces can be included. The lift distribution calculated using piston theory appears somewhat more reasonable than the distribution predicted by momentum theory.

In order to have a basis for evaluating the lift distributions predicted by momentum theory and piston theory, which are considered the most easily adaptable theories for dynamic aeroelastic studies, a steady state lift distribution for the rigid glider has been calculated using linear first order supersonic theory. The calculation has been made for several angles of attack so that the rate of change of normal force with angle of attack can be determined. This calculation has been made for only one Mach number, that corresponding to the maximum dynamic pressure during boost. Although this theory predicts the pressure distribution more realistically than either piston theory or momentum theory, it is not easily adapted to describing aerodynamic forces on an elastic body whose shape is varying with time.

The approach finally decided upon for calculating the aerodynamic forces is a semiempirical theory which assumes a piston theory distribution with a lift curve slope based on the rigid glider lift curve slope calculated by linear supersonic theory for one Mach number and based on experimental wind tunnel data from similar configurations for other Mach numbers. Fig. IV-3 shows the estimated variation of glider lift curve slope with Mach number which is used in the flight leads analyses. Plots of glider lift curve slope versus Mach number for piston theory and momentum theory are also shown for comparison. The zero Mach number lift curve slope is based on the experimental point indicated. In the subsonic regime a typical Prandtl-Glauert variation is assumed, and a typical transonic variation is also assumed. The low supersonic part of the curve is drawn through the point based on linear first order supersonic theory. As the Mach number increases, the assumed curve approaches the piston theory curve which agrees quite well with the experimental data for Mach numbers between three and four. Although the assumed curve is based on a rather limited quantity of data, it is probably better than either of the theoretical curves shown. It is expected that in general sufficient wind tunnel data to define such a curve would be available before a final loads analysis is required.

Fig. IV-4 shows a comparison of glider lift distributions based on various methods. Two possible assumptions which would improve the momentum theory lift distribution are considered. In one of these, the leading edge is swept back further to form a delta wing of the same span as the actual planform, and in the other triangles are added to the tips to form a large delta wing. In the case where the leading edge is swept back further, the total lift predicted remained the same as that predicted by applying momentum theory to the original planform. Since the effect of local angle of attack variation due to the elastic deformation can be accounted for easily using the piston theory, and the total lift can be adjusted as desired by using a value of C_{N_α} other than $4/M$, it is decided to use the piston theory with a modified C_{N_α} for calculating aerodynamic forces on the glider.

Critical Altitude and Wind Direction

Since the most critical altitude from the standpoint of bending loads is not always most critical from the standpoint of combined loads, it is sometimes necessary to determine wind shear loads resulting from several wind profiles with the altitude of the spike varied between 30,000 and 45,000 feet. However, one of the altitudes at which the spike should be located is the one which will produce the maximum bending loads. In the present study wind shear loads due to a complete wind profile are determined only for the profile with the spike located at this most bending critical altitude, since one such analysis is sufficient to illustrate methods and investigate effect of refinements and importance of parameters.

In determining the altitude at which to locate the spike, it is assumed that bending moments will be highest if the spike is at the altitude which produces the greatest incremental lift on the glider due to a

given wind velocity. The altitude band of 30,000 to 45,000 feet is considered, since the present wind criteria make no provision for locating the spike outside this band. Further research may indicate that in some cases a spike located outside this band with a reduced maximum wind velocity should be used. The lift on the glider due to the wind velocity is:

$$L_w = 1/2 \rho (V_a + V_w \cos \psi) \ C_{N_\alpha} \ S \ V_w \ \sin \psi \qquad (\text{IV-9})$$

where

L_w = incremental lift due to the wind velocity

ρ = air density

V_a = velocity of the vehicle relative to the earth

V_w = horizontal wind velocity

ψ = inclination of vehicle from horizontal

C_{N_α} = glider lift curve slope

S = glider wing area

The above expression is evaluated at a number of altitudes within the 30,000 to 45,000 foot band, holding V_w constant at 300 feet per second and letting V_a, ρ, ψ, and C_{N_α} vary according to the altitude. The largest value of L_w within the band occurred at the lower limit of the band, 30,000 feet; therefore, the wind spike is located at 30,000 feet for the wind shear analysis.

It is assumed that maximum bending moments will be produced by a wind profile if the vehicle is oriented so that the component of the wind normal to the glider lifting surface is a maximum. Since launching into the wind tends to increase the dynamic pressure, the most critical direction for launch is directly upwind.

Although the launch directly upwind is considered most critical for booster bending moments and also glider panel loads, an analysis of the cross wind condition should be conducted to determine the loads on the vertical fins on the glider. The same methods as the bending loads analysis should be used. However, the numerical values of the coefficients in the equations of motion and load equations will be different. Such an analysis is not performed since nothing new would be illustrated by it.

C. PARAMETER STUDIES

1. CONTROL SYSTEM

The results of analog computer studies of dynamic loads on the boost-glide vehicle due to passage through a layer of high wind shear indicate

that control system characteristics have a significant effect on loads.
An investigation is made to determine the degree of refinement in control
system representation required to give sufficiently accurate dynamic
loads solutions. The effect of variations in control system gains and
sensor locations on loads is also studied. A simple method of choosing
control system gains for use in dynamic loads analyses in the absence of
detailed control system design information is developed and is presented
in Appendix D. The method considers the effect of flexibility on control
gain requirements.

Since the vehicle is statically unstable in pitch without controls,
it is necessary to design a pitch control system before any flight loads
studies can be attempted. Lacking any detailed information on control
requirements for this vehicle, it is decided that the pitch control system
should provide an undamped natural pitch frequency of one half cycle per
second and a damping in pitch of six tenths critical. The choice of fre-
quency and damping is somewhat arbitrary; however, the values chosen are
typical of those which provide a desirable short period response in manned
aircraft.

Description of Control System Representations

In the boost-glide vehicle being studied, pitch control is provided
by means of thrust vectoring. In the simplest representation of the con-
trol system, the nozzle swiveling angle is given by the following equation:

$$q_\delta = K_\theta q_\theta + K_{\dot\theta} \dot{q}_\theta \qquad \text{(IV-10)}$$

where

q_δ = nozzle swiveling angle

q_θ = incremental pitch angle (the difference between
the actual pitch attitude and the programmed
pitch attitude)

$\dot{q}_\theta$ = pitch rate

K_θ = attitude gain

$K_{\dot\theta}$ = rate gain

Although the system described by Eqn. (IV-10) is not a physically
attainable system, it is frequently used in preliminary dynamic loads
analyses in which the control system dynamics are not of primary interest.

The first refinement included in the representation of the control
system is to locate the sensors on the vehicle and allow them to sense
the pitch attitude and rate of the stations on the vehicle at which they
are located. Thus slope and rate of change of slope in the flexible modes
are sensed in addition to rigid pitch and pitch rate. The equations for
the pitch attitude and rate sensed are:

$$\theta_s = q_o + \sum_j \phi'_{jA} \, q_j \qquad \text{(IV-11)}$$

$$\dot{\theta}_s = \dot{q}_o + \sum_j \phi'_{jR} \, \dot{q}_j \qquad \text{(IV-12)}*$$

where:

θ_s = incremental pitch attitude sensed

ϕ'_{jA} = slope of the jth mode shape at the attitude sensor station

ϕ'_{jR} = slope of the jth mode shape at the rate sensor station

q_j = generalized coordinate for the jth flexible mode.

For the above system, Eqn. (IV-10) is modified by replacing rigid pitch and pitch rate with the pitch attitude and rate sensed.

$$q_\zeta = K_\theta \, \theta_s + K_{\dot{\theta}} \, \dot{\theta}_s \qquad \text{(IV-13)}$$

The system described by Eqn. (IV-13) also represents a very idealized control system, not physically attainable. The next step is to consider a typical control system in which the nozzles are swiveled by means of a hydraulic actuator. In this system, the signals from the sensors are added and then passed through a filter designed to attenuate the high frequency signals due to response in the higher flexible modes. The filtered signal is combined with a feedback proportional to the nozzle actuator position to produce a hydraulic error signal which commands a valve position. The valve allows a hydraulic flow rate proportional to valve position, and the rate of change of nozzle actuator position is in turn proportional to the hydraulic flow rate. The nozzle is driven by the actuator, and the nozzle position differs from the actuator position by an amount proportional to the strain in the actuator. Nozzle inertia, damping, and the restoring torque due to the axial acceleration of the vehicle (pendulum effect) resist the swiveling of the nozzles by the actuator. The equations representing the above system are:

$$\gamma_s = K_\theta \, \theta_s + K_{\dot{\theta}} \, \dot{\theta}_s \qquad \text{(IV-14)}$$

$$T_1 \dot{\lambda} = \gamma_s - \lambda \qquad \text{(IV-15)}$$

$$T_2 \dot{\delta}_a = \lambda - \delta_a \qquad \text{(IV-16)}$$

*It is noted that $\dot{\theta}_s$ is not the time derivative of θ_s except in the special case where the sensors are located at the same station.

$$m_o \ell^2 \ddot{q}_\delta + \text{(inertia coupling terms)} = -2\, m_o \ell^2 \omega_o \zeta_o \dot{q}_\delta \qquad \text{(IV-17)}$$

$$-m_o \ell^2 \omega_o^2 (q_\delta - \delta_a) + \begin{array}{l}\text{(moments due to carried field}\\ \text{acceleration)}\end{array}$$

where:

γ_s = sum of the sensor outputs

λ = filtered sum of the sensor outputs

δ_a = actuator position measured in terms nozzle swivel angle commanded

T_1 = time constant of the filter

T_2 = hydraulic lag

$m_o \ell^2$ = nozzle swiveling inertia

ω_o = natural swiveling frequency of nozzles with hydraulic valve closed

ζ_o = nozzle damping ratio

In transfer function form, the above control system is represented as

$$\frac{q_\delta}{\theta_s}(s) = \frac{K_\theta + K_{\dot{\theta}}\, s}{(1 + T_1 s)(1 + T_2 s)\left(1 + \dfrac{2\zeta_o}{\omega_o}\, s + \dfrac{s^2}{\omega_o^2}\right)} \qquad \text{(IV-18)}*$$

where

s = Laplace transform variable.

The hydraulic system lag arises because the filtered sensor signal essentially commands a swiveling rate proportional to the difference between the desired and actual actuator position instead of commanding a position. The swiveling frequency used in Eqn. (IV-18) includes the effect of hydraulic fluid compressibility as well as actuator compliance.

Although the control system described by Eqn. (IV-18) is much more realistic than those described by Eqn. (IV-10) and (IV-13), many effects have been left out which will have to be included if the emphasis is on the servo-system instead of dynamic loads. However, the first order lags which are neglected are small in comparison with the lags which have been included, and the frequencies associated with the effects which are neglected are above the frequency spectrum of interest in dynamic loads problems. Among the effects neglected are gyro lags, dead zones, drift, and frequency response, valve dynamics, and hydraulic fluid leakage.

*The transfer function notation, although not strictly correct unless $\dot{\theta}_s$ is the time derivative of θ_s, is used in the figures to conserve space.

Also, in an actual system the shaping networks would probably consist of more than a single simple filter circuit. Reference 49 describes in more detail a control system similar to the one described here. Simple modifications in the analog circuit are used to vary the control system from the very simplest as described by Eqn. (IV-10) to the complete system as described by Eqn. (IV-18). Degrees of freedom are easily added or removed from the simulation by turning off the appropriate amplifiers. The first order lags are included or removed by modifying amplifier feedbacks. The analog simulation for the control system is shown in Appendix G.

Results

The effects on the transient responses and maximum loads of variations in complexity of control system representation, gains, and sensor locations are investigated. It is found that the addition of a flexible mode or an additional complexity in control system representation has a marked effect on the responses, but in each case proper adjustment of the gains brings the frequency and damping back to approximately what they are for the rigid vehicle with the simplest control system representation. Therefore, it is considered desirable to develop a method for predicting the proper gain settings in advance for any given representation of the vehicle and control system. Such a method would find application in the selection of gains for digital solutions of flight loads problems, where it would be uneconomical to use a trial and error method. A method of predicting gain settings to provide the desired pitch frequency and damping including the effect of flexibility is developed in Appendix D. The method is based on the assumption that the response in the flexible modes is essentially static.

The gains to provide 1/2 cps and .6 critical damping in pitch for the rigid vehicle with the simplest control system representation are $K_\theta = 7.2$ and $K_{\dot\theta} = .919$. When these gain settings are used with a simulation including one flexible mode in which rigid pitch only is sensed, the pitch frequency and damping are both greatly reduced. When a second flexible mode is added to the simulation, the frequency and damping are increased slightly. The reason for this is that the second mode is primarily a wing plate mode which deforms under load so as to reduce angle of attack and therefore reduces the destabilizing aerodynamic pitching moment on the vehicle. The first mode is primarily a vehicle beam bending mode which increases the glider angle of attack and therefore increases the destabilizing pitching moment. The gains required for the flexible vehicle predicted by the method of Appendix D are 10.23 and 1.076 as compared to the 7.2 and .919 used.

Next the sensors are allowed to sense bending as well as rigid pitch. In this case, the attitude sensor is located in the glider and the rate sensor is located at the nozzle swivel axis location. When the attitude sensor is located in the glider, the ratio of θ_e to θ_g is such that the effective attitude gain is higher than the gain setting. Thus, in this case, the gain setting of 7.2 provides adequate pitch stiffness whereas it does not in the cases where only rigid pitch is sensed. The response time histories for this case are shown in Fig. IV-5.

In Fig. IV-6, a comparison is made of the maximum bending moment diagrams for the various representations of the vehicle with the simple nonlagged control system. The effect on loads of adding one and two flexible modes to the rigid vehicle simulation and effect of sensing bending as well as rigid pitch are shown. The addition of each flexible mode to the simulation has a marked effect on loads. Allowing the sensors to sense bending as well as rigid pitch also has a marked effect on loads, since the effective gains are changed when bending is sensed.

Next the effects of adding first order lags and nozzle inertia to the control system representation are investigated. It is found that the effect of each first order lag and nozzle inertia is to reduce damping. The original balue of $K_{\dot{\theta}} \cong .919$ does not provide sufficient damping for stability if more than one lag is included. However, this loss of damping is compensated for by increasing $K_{\dot{\theta}}$, and setting $K_{\dot{\theta}} = 2.4$ provides a satisfactory response when both first order lags and nozzle inertia are included. The time histories of the responses for this case are shown in Fig. IV-7.

Fig. IV-8 shows a comparison of maximum bending moment diagrams for the representations of the control system with lags. Two flexible modes are included in each of these simulations, and bending is sensed as well as rigid pitch in each case. The differences between these cases are in the number and order of lags in the control system and in the adjustment of the rate gain setting. The maximum bending moments are not greatly affected by the control system lags, provided the gain settings are properly adjusted. The one curve that lies considerably above the others corresponds to the case where $K_{\dot{\theta}}$ is not increased to compensate for the loss in damping due to the addition of a lag. The gain settings for these cases are determined by trial and error on the analog.

Fig. IV-9 shows a comparison of bending moment diagrams similar to those in Figs. IV-6 and IV-8. The gains used in obtaining these solutions are predicted by the method described in Appendix D. These loads are due to the 150 fps spike shown on the figure, whereas the loads in the previous cases are due to a 76 fps spike. The agreement of the bending moment diagrams in Fig. IV-9 for all cases in which bending is sensed is so close that differences can not be shown in the comparative plot. The control systems in which bending is sensed range in complexity from a nonlagged system to one in which two first order lags and nozzle inertia are included. The close agreement of the bending moments for the flexible vehicle shows that the method satisfactorily predicts the gain settings required for the various control system representations used. One may also conclude from these curves that a fairly simple control system representation is adequate for loads studies, since the lags and nozzle inertia do not have a large effect on the loads if the gain settings are properly adjusted. It is not intended here to imply that a simple control system would be adequate for determining stability boundaries. Also, nozzle inertia may be more important in other configurations having more massive engines relative to their total mass.

A study of the effect on loads of variation of gain settings is made with the control system representation which includes two first order lags, the nozzle swiveling degree of freedom, and sensors located in the glider (attitude sensor) and at the nozzle swivel axis location (rate sensor). First K_θ is varied throughout the stable range keeping the ratio $K_\theta/K_{\dot\theta} = 1.96$. The loads have been recorded and the results are plotted in Fig. IV-10. The loads are greatly affected by the variation in K_θ, and increasing K_θ reduces the loads. The minimum loads are obtained with the maximum K_θ which provides stability. One might expect that a gain setting well within the stable range will provide minimum loads, but this does not prove to be the case. Slightly below the low gain stability boundary the transient response is a divergent pitching oscillation in which the second peak is higher than the first, and so on. However, in the vicinity of the high gain stability boundary, the maximum load occurs on the first peak, in phase with the wind spike. Then, if the gain is slightly above the stability boundary, a divergent pitching oscillation of higher frequency gradually builds up. The amplitude of the first peak decreases as the gain setting increases; therefore, the maximum gain setting which provides stability gives the minimum loads.

Fig. IV-11 essentially shows the effect of pitch damping on loads. In this figure K_θ is held constant at 6.452 and $K_{\dot\theta}$ is varied throughout the stable range. A reduction in damping has the effect of increasing loads, as would be expected. The breaks in the curves in Figs. IV-10 and IV-11 occur at the gain settings for which the first and second peaks in the transient response are of equal amplitude. To the left of the break the maximum load occurs on the second peak; to the right the maximum load occurs on the first peak.

The location of sensors is also varied and the effect on loads has been recorded. Fig. IV-12 shows a tabulation of sensors locations and a comparison of the bending moment diagrams for these locations. The system is unstable for locations for which bending moments are not shown. A nonlagged control system which senses bending is used for the study. The gain settings have been calculated for each sensor location to provide one half cps and six tenths critical damping in pitch by the method developed in Appendix D. As noted previously, the method by which the gains are calculated is based on the assumption that the modes deflect statically and structural dynamic effects may be neglected. If this were strictly true the curves in Fig. IV-12 would be identical and all nine pairs of sensor locations would provide a stable response. Examination of the transient responses for each of the nine cases shows that a noticeable component at the first bending frequency appears in only three cases. These cases are also the only three in which the rate sensor is located forward of the antinode in the first mode. Assuming no phase shift between the rate sensor signal and the component of the nozzle motion proportional to this signal, a rate sensor located forward of the antinode of the first mode provides negative damping in that mode. Of course, some positive aerodynamic damping exists, so the net damping may be either positive or negative. In two of the three cases (cases 7 and 8) the oscillations at the first bending frequency diverge. In the other case (case 6) the ocillation dies out.

Although it has been concluded that a simple control system representation is adequate for the dynamic analysis of flight loads during boost, it does not follow that a simple representation will suffice for stability studies. It can be seen in Fig. IV-9 that the very simplest representation, which does not even include the sensing of bending by the sensors, gives almost the same solution for bending moments as the most refined representation considered. However, it has been shown that for certain sensor locations the system is unstable. Bending must be sensed in order to discover these instabilities. Here is an instance in which the determination of the stability of the system is an indispensable part of the loads problem. Dynamic loads determined using the simple control system representation are meaningless if the system being studied is actually unstable. Nevertheless, the simple representation is useful in preliminary design work, where accurate estimates of loads may be required before the sensor locations are known.

In the investigation of the effect of variation of gain settings on dynamic loads due to wind shear, instabilities occur when the attitude gain setting is either too high or too low. The effect of control system representation, rate gain setting, and overall structural stiffness on the boundaries of the stable range of attitude gain settings is determined. Since minimum loads result when the attitude gain setting is the highest which provides stability, it is necessary to accurately determine the stability boundary in order to optimize the control system from the standpoint of minimizing loads.

In the present analysis, only one point on the trajectory is studied—the one corresponding to the wind spike altitude during boost. Stability boundaries have been determined by adjusting the attitude gain setting and observing the transient response to a disturbance on the analog. The results are presented in the form of stability profiles showing the boundaries of the stable region on the attitude gain setting versus structural stiffness plane. No local stiffness changes have been investigated, since this would involve recalculating mode shapes. Overall stiffness changes are easily accomplished by changing the natural frequencies of the flexible modes. In these stability studies, the sensor locations are not changed, the attitude sensor being in the glider and the rate sensor at the nozzle swivel axis location. Other combinations of sensor locations will of course produce different stability profiles.

Fig. IV-13 shows the effect of control system representation on stability boundaries. The three profiles for representations where bending is sensed show an upper boundary as well as the lower. The primary effect of each additional lag included is to lower to upper boundary, decreasing the stable range of attitude gain setting. The profile for the simple representation in which bending is not sensed does not have an upper boundary. Instead the upper branch of the curve is asymptotic to a vertical line representing the structural stiffness at which a static aeroelastic divergence will occur. The lower branch is asymptotic to a horizontal line representing the minimum attitude gain setting below which the vehicle would be unstable in pitch. It is noted that the minimum attitude gain setting is considerably higher

when bending is not sensed, particularly in the low stiffness region. The reason for this is that the effective attitude gain is higher than the gain setting in the cases where bending is sensed and the attitude sensor is located in the glider.

The effect of changes in rate gain setting on the stability boundaries has also been studied. As would be expected, increasing the damping has the effect of enlarging the stable region.

The gain settings required for one half cycle per second pitch frequency as a function of overall structural stiffness are also shown in Fig. IV-13 for two control system representations. The gain setting required is lower in the case where bending is sensed, since the effective gain is increased when the sensor is forward in the glider.

The region above the upper branch of the stability profile is an unstable region due to structural and control system coupling. The above results show that the location of this upper branch is influenced by damping and by control system representation. Each refinement in the mathematical representation of the control system has the effect of lowering the upper boundary, decreasing the maximum stable gain setting for a given structural stiffness. As mentioned earlier, from a loads standpoint, it seems desirable to choose a gain setting quite close to this upper boundary. In order to do this, it is necessary to locate the upper boundary quite accurately. This requires a very good mathematical representation of the control system, much more refined than the simple representation which is found adequate for determining loads. The stability of the vehicle must be determined along the entire trajectory and not just at one point as is done in the present study.

One of the criteria that is used to avoid instabilities due to structural and control system coupling is to require that a certain minimum ratio of structural frequency topitch frequency be maintained. The one half cycle per second pitch frequency used in the present study yields frequency ratio of greater than five to one. Increasing attitude gain setting and thereby approaching the upper stability boundarylowers the above frequency ratio, and an accurate knowledge of this boundary would permit the determination of the minimum frequency ratio which would provide stability. An adaptive autopilot which continuously maintains the maximum gain setting providing stability would be very desirable since it would minimize dynamic loads. The increasing size of boosters make the attainment of a high frequency ratio increasingly difficult, and the attainment of a stable configuration will become correspondingly difficult.

2. STRUCTURAL REPRESENTATION

The structural representations of the vehicle used in the wind shear analysis vary from a simple rigid body to an elastic body whose motions are defined in terms of three normal vibration modes as well

as the rigid body degrees of freedom. The elastic modes have been added to the simulation one at a time, and the effect on the bending loads due to passage through the wind spike has been observed. Fig. IV-14 shows a comparison of the bending moment diagrams resulting from the various structural representations. Neglecting flexibility altogether results in a serious underestimation of the bending loads. The first flexible mode is primarily free-free bending of the booster, with very little wing deformation. When vehicle motion or wind produces a lifting force on the glider, the booster bends under the load so as to increase the glider angle of attack, thus increasing the lifting force and also the bending moment. The second flexible mode is primarily a wing mode in which the wing deforms under load so as to reduce local angle of attack and thereby alleviate the aerodynamic load on the glider. Therefore, the bending moments decrease slightly when both the first and second modes are included in the analysis. The addition of the third normal mode has very little effect on the bending loads, and it is concluded that two modes are sufficient to represent the elastic structure of this vehicle in the wind shear loads problem.

Considerable time and effort have been expended in calculating the normal vibration modes which include both wing and booster flexibility. A simple program is available for calculating the vehicle free-free beam bending modes in which the wing is assumed to contribute to the beam mass and stiffness and conform to the beam in chordwise bending. No spanwise wing deflection is accounted for in these beam modes. The calculation of wing plate modes requires two programs, one which determines the wing influence coefficient matrix, and one which determines the mode shapes and frequencies. Still another program is required to couple the wing plate modes and beam bending modes to determine the normal modes of the vehicle. A discussion of the modal calculations and tabulations of mode shapes are given in Appendix B.

In order to see whether it is necessary to expend the extra effort required to include wing plate deformations, bending loads due to passage through the wind spike with and without wing plate deformations have been compared. Equations of motion and loads equations have been derived using the free-free beam bending modes instead of the coupled wing and beam modes, and solutions using one and two beam modes are compared with the solutions using one and two coupled modes. The results are plotted in Fig. IV-15. The one mode solutions are practically the same, since the first coupled mode is primarily a beam bending mode with very little wing spanwise deformation. The two mode solutions do not show such close agreement, since the second coupled mode is primarily a wing mode. Thus the beam mode solution does not show the alleviation of bending moments due to wing deformation that is shown in the coupled mode solution. Considering the limited accuracy with which the aerodynamic forces are known, the use of the simpler beam modes may be justified in some cases. Certainly if only one flexible mode is included, no advantage would be gained by using the coupled mode. If two modes are included, coupled modes should be used.

As mentioned earlier, it has been observed that even in response to the abrupt shear reversal at the wind spike the flexible mode response is essentially a static deformation at the pitch frequency with very little vibration at the natural structural frequencies. This suggests that the structural representation could be simplified by neglecting structural dynamics but allowing the structure to deform statically under load. This may be accomplished by dropping the first and second derivatives of the generalized coordinates for the flexible modes out of the equations and revising the analog computer simulation accordingly. Fig. IV-16 shows a comparison of the bending moment diagrams with and without structural dynamics. Two flexible modes are considered, and the loads shown are due to passage through a wind spike. It can be seen that neglecting structural dynamics has the effect of slightly reducing the predicted bending moments, but that the difference is not large. If structural dynamics are neglected, the calculation of modes will not be necessary; a set of influence coefficients for the structure will suffice. In view of the limited accuracy with which the aerodynamic forces are known, the neglect of structural dynamics may be justified in flight loads analyses of boost glide vehicles, provided the static deformation of the elastic structure is accounted for.

3. FUEL SLOSH

Two fuel slosh degrees of freedom are included in the simulation of the boost-glide vehicle for the wind shear problem. These are the first slosh modes of the fuel and oxidizer tanks for the first stage booster. Other tanks are considered full. The higher order slosh modes have not been included because of analog equipment limitations, although their effects could have been investigated by making simplifications elsewhere in the simulation had the effect of sloshing proved important in this configuration.

The pendulum analogy, discussed in Appendix C, is used in deriving the equations for fuel slosh.

The dynamic response and loads due to passage through the wind profile spike have been obtained with and without fuel slosh modes using the differential analyser to effect the solutions. The effect of fuel slosh on loads is negligible. The transient responses in the rigid and flexible structural modes are somewhat different when slosh is included, but the maxima are not affected to any significant degree. This difference in the transient response noted is not striking, but it is noticeable in a direct comparison of the responses. The slosh response itself as evidenced by angular displacements of the pendula is fairly large. The slosh response time histories are shown in Fig. IV-17. The maximum angular displacement of the fuel tank pendulum in response to a 150 foot per second wind spike is 31.9 degrees. The maximum angular acceleration of this pendulum is 3.94 radians per sec^2. This produces a side force at body station 1557 of only 4800 pounds as compared to the maximum side force at body station 1636 of about 183,000

pounds due to thrust vectoring in response to the same wind spike. The
large angles traversed by the pendula representing the slosh modes are
well beyond the range in which a linear approximation is valid. The
pendulum analogy itself is applicable only for small slosh amplitudes;
and in cases where the dynamic response of the system is significantly
affected by slosh, a more refined analysis of sloshing may be required.
More study is required in this area.

The possibility that a particularly fortunate choice of slosh frequency
has accidentally been made is considered. Therefore, slosh frequency has
been varied from about .7 to 1.5 times the calculated frequency. Physically
this can be accomplished by changing the tank diameter or acceleration due
to thrust. The responses have been recorded for these slosh frequencies,
and the results show that the amplitude of the response (and therefore the
loads) is insensitive to slosh frequency.

4. GLIDER LIFT CURVE SLOPE

In view of the uncertainty as to the exact value of the glider lift
curve slope, it is necessary to determine the effect of variations in this
parameter on loads. Equations of motion and loads equations have been cal-
culated for values of glider C_{N_α} ranging from about .08 to 1.5 times the
estimated value, and these equations have been solved on the analog computer
for the loads due to the wind spike. The variation in maximum bending
moment at a given station with lift curve slope is shown in the Fig. IV-1.
If better information on the lift curve slope becomes available at some
later date, it will be possible to revise the wind shear loads without re-
peating the entire analysis, by referring to Fig. IV-1.
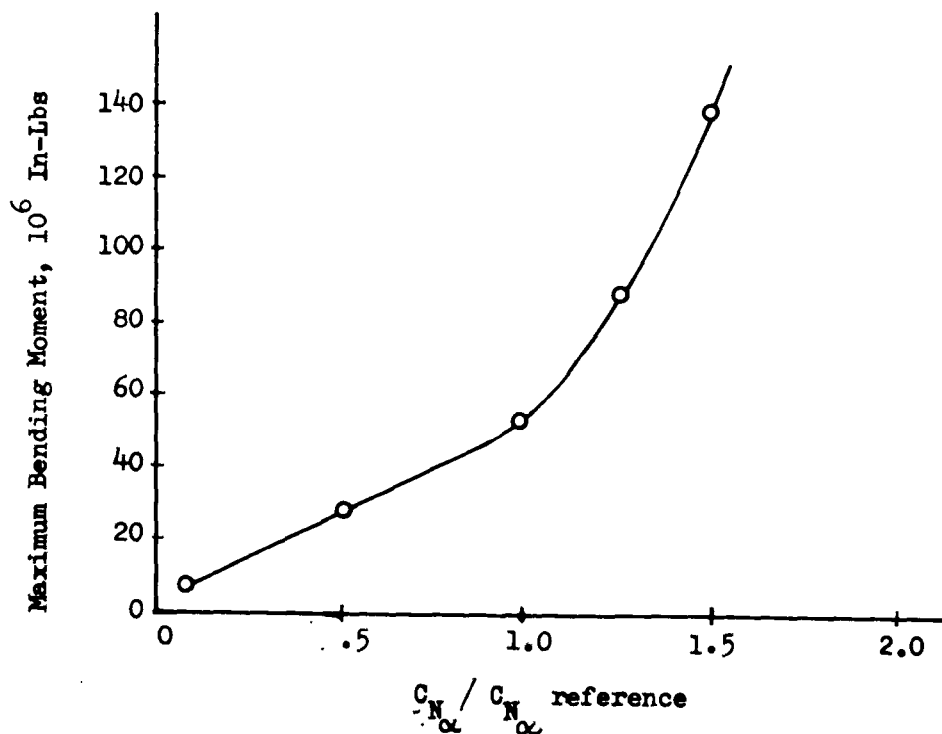
FIG. IV-1   EFFECT OF C_{N_α} ON MAXIMUM BENDING MOMENT

D. QUANTITATIVE RESULTS

The main purpose in obtaining numerical values for the loads is
to determine the relative criticalness of the various loading con-
ditions studied. In the boost flight loads analysis beam bending
moments at seven body stations and net loads on each of the thirty
glider panels have been determined. Since the panel loads are functions
of time, the set of loads to be transformed into stresses must be a
set that occurs at the same instant of time. If the panel loads are
not in phase, it may be difficult to choose the instant of time which
produces maximum stress in a given member. The panel loads during
boost are in phase and experience maximum load simultaneously. There-
fore, the set of maximum panel loads would be the proper set to use in
a stress analysis. The foregoing remarks are intended only to indicate
how the various loads would be used, since the determination of the
stresses is outside of the scope of the present study.

1. WIND SHEAR LOADS

The Sissenwine wind profile shown in Fig. IV-2 is taken as the design
wind profile for this study. Bending moments only have also been calcula-
ted for comparison purposes using the profile recently developed by AviDyne
Research under contract with WADD. The wind shear loads have been computed
by several methods, as described in the analysis subsection of the boost
flight loads section.

Superposition Method

The wind profile is broken down into two parts, one of which is
referred to as the slow time-varying portion and the other as the spike.
The response to the slow time-varying portion is obtained by solving
the equations having time-varying coefficients by means of the digital
computer program. Three degrees of freedom, two rigid body modes and
the first free-free beam bending mode are used to represent the motions
of the vehicle. The control system representation is the simplest one
considered in the study. Constant gain settings based on conditions
at the spike altitude are used. Actually, the gain settings used during
the portion of the flight up to the spike are unimportant. Solutions
obtained using time-varying gain settings which provided one-half cps
and six-tenths critical damping in pitch from the ground up yield
results almost identical to the constant gain solution. The response
to this portion of the profile is primarily a normal translation with
the normal component of the wind. Any reasonably tight pitch control
which provides stability causes the vehicle to drift with the wind with
a very small angle of attack up until the time the spike is encountered.
If a more refined control system representation is used, the relatively
high gain settings based on spike conditions may be too high for sta-
bility during the early portion of the flight. Thus, in any actual

design some programmed variation in the gain settings will probably be necessary. However, knowledge of the gain-settings during the early portion of the flight is not necessary in order to determine wind shear loads.

The response to the spike has first been obtained by solving the equations having constant coefficients based on the spike conditions by means of the analog computer. Analog circuitry utilized in obtaining the solutions described here is shown in Appendix G. The degrees of freedom used to describe the motions of the vehicle in the analog solution are two rigid body modes, the first two coupled flexible modes, and nozzle swiveling. In addition, two first order lags are included in the control system representation. Gain settings are determined by the method described earlier to provide one-half cps and six-tenths critical damping. Control system studies reported earlier show that this much refinement in the representation of the control system is unnecessary; but since the complete analog circuitry has already been set up, it has been utilized.

The loads based on these digital and analog solutions have been obtained by superposition of the loads due to the slow time-varying portion of the profile and the loads due to the spike. Fig. IV-18 shows the bending moment response at body station 1027 obtained by superposition as well as the response due to the slow time-varying portion only. The net panel loads obtained by superposition of the loads due to the spike and those due to the slow time-varying portion are shown in Fig. IV-19.

The superposition method as described above assumes that the variations in the coefficients during the few seconds in which the spike is passed are not rapid or large enough to significantly affect the results.

Comparison of time histories obtained by superposition using a constant coefficient, three degree of freedom spike solution with a three degree of freedom digital solution for the response to the complete profile using time-varying coefficients indicates that the assumption of constant coefficients noticeably changes the response to the spike. Therefore, the response to the spike has been obtained by means of a digital solution of equations for a four degree of freedom vehicle with time-varying coefficients. The motions of the vehicle in this solution are described in terms of the rigid body modes and the first two coupled flexible modes. A nonlagged control system in which bending is sensed is used. The sensor locations are as in case one in the sensor location study, and the gain settings are chosen to give one-half cps and six-tenths critical damping in pitch based on the spike conditions. Fig. IV-20 shows the bending moment response at body station 1027 obtained by superposition of the loads due to the slow time-varying portion and the loads due to the spike of the wind profile as determined by the four degree of freedom digital solution.

Analog Solution with Nonzero Initial Conditions

The superposition method described above depends on the assumption of linearity. When a nonlinearity in the form of a limit on the maximum nozzle swivel angle is investigated, the principle of superposition can not be used. The limit on the nozzle swivel angle is easily simulated on the analog computer as shown in Appendix G, and nonzero initial conditions representing the conditions existing at the start of the wind spike are calculated by means of the digital program. Two rigid body modes, one flexible mode, and the simplest control system representation have been used in the digital solution for the initial conditions. An additional flexible mode as well as a refined control system representation having two first order lags and nozzle inertia have been included in the analog simulation. The initial conditions for the additional flexible mode have been calculated by assuming that deformations in this mode are static. It is necessary to adjust the initial conditions for the flexible modes slightly by trial and error on the analog so that no transients at the flexible mode frequencies result when the problem is turned on. This assures that the deformations in the flexible modes at the start of the spike are compatible with the vehicle angle of attack and nozzle swivel angle existing at the start of the spike.

The responses to the wind spike with various nozzle swivel angle limits have been obtained. Even a small restriction on the angular deflection of the nozzle has a marked effect on the res onses. When the limit is set at $\pm 23^\circ$, the nozzle does not contact the stops at all; yet when the allowable deflection is reduced to $\pm 21^\circ$, insufficient control is available to prevent a pitch divergence. As soon as the nozzle contacts the stop, the effective positive pitch spring due to the thrust vectoring begins to soften, whereas the negative pitch spring due to aerodynamic forces remains constant. If the pitching velocity at the time the stop is contacted in greater than a certain value, the pitch excursion reaches the angle at which the effective net pitch spring becomes negative and the vehicle continues to pitch until failure occurs. It is also interesting to note that a significant vibratory response in the flexible modes occurs when the thrust is vectored rapidly as the nozzle comes off the stop. A typical response is shown in Fig. IV-21.

The method has the disadvantage that constant coefficients are used, but a digital program capable of handling the nonlinearity is not always available. Even when the limit is not incorporated, the assumption of linearity is not very good for the large angles encountered in response to the wind profile. A function generator can be used to transform the nozzle swivel angle into the sine of the angle on the analog. This has not been done, however, since it is felt that in any practical design the vehicle would have to be modified in some way to avoid the requirements for such large control moments. One possibility would be the use of tail fins to reduce the destabilizing aerodynamic pitching moments.

Digital Solution for Response to Complete Profile

The third method used to determine wind shear loads is the digital solution for the response to the complete profile. Three degrees of freedom and time-varying coefficients are used, as in the solution for the response to the slow time-varying portion of the profile described earlier. This method is simpler than either of the methods previously discussed, and it depends on the assumption that a few degrees of freedom are sufficient. In this study, three is considered the maximum number of degrees of freedom that can efficiently be used in obtaining a digital solution for the response to the complete profile. The number of coefficients for which time histories must be calculated increases as the square of the number of degrees of freedom, and machine time also increases greatly with additional degrees of freedom.

The study of the effect of structural representation on wind shear loads indicates that a fairly good prediction of the bending moments can be made with only one flexible mode. Fig. IV-22 shows a time history of bending moment at station 1027 obtained by solving the three degree of freedom equations on the digital computer for the response to the complete profile. The time histories obtained by superposition of the slow time-varying digital solution and the digital and the analog spike solutions are also shown in Fig. IV-22 for comparison. The results obtained by superposition of three and four degree of freedom digital solutions are considered the most accurate obtained.

For some purposes, the three degree of freedom solution may be adequate, although in this case the loads are considerably overestimated. Fig. IV-23 shows a comparison of bending moments due to the Avipyne profile with those due to the Sissenwine profile. Both solutions have been obtained using the three degree of freedom digital solution for the response to the complete profile. The three degree of freedom solution is considered adequate for determining the relative severity of various profiles, as in the present example.

Fig. IV-24 shows a comparison of the bending moment diagrams obtained by the methods discussed above.

2. GUST LOADS

Discrete Gusts

The responses to one minus cosine shaped discrete gusts of various wave lengths have been obtained on the analog computer. The equations of motion and loads equations are identical to the equations used in the wind shear analysis except for the forcing function. Discrete gust loads have been computed for the 30,000 foot altitude during boost, the altitude at which the wind spike is encountered. Fig. IV-25 shows the effect of gust frequency on maximum bending moment at body station 1027, and that the maximum bending response occurs when the gust frequency is about .8 cycle per second.

In the vehicle analysed, the gains are chosen so that the pitch
frequency and damping are .5 cps and .6 critical respectively. Thus,
it appears that the one minus cosine discrete gust which produces
maximum bending response has a frequency about equal to the frequency
which would produce maximum forced amplitude response in the pitch
mode. The maximum bending moments are produced by critically phasing
with pitch.

Fig. IV-26 shows the maximum bending moment diagram resulting
from critically phased 40 fps, one minus cosine shaped, discrete gust.

Combination of Discrete Gust and Wind Shear Loads

Since a one percent synthetic wind profile is used for determining
wind shear loads, it seems most rational for design purposes to use a
gust load which is exceeded only once per hundred flights. In practice
it may be very difficult to determine a one in a hundred gust load,
since existing probability density functions may not adequately describe
clear air turbulence associated with wind shear. A 40 fps one minus
cosine shaped critically phased discrete gust has been recommended as
an interim design criterion. (109) For illustration purposes, the
load due to this descrete gust is taken as a one percent gust load.
The loads die to this gust are quite severe. It is somewhat surprising
that the 40 fps gust produces loads almost as large as the 150 fps wind
spike. The explanation of this is that the gust wave length used is
chosen to produce maximum bending moments by exciting a maximum dynamic
pitching response. The wave length of the wind spike is quite long
compared to that which would excite maximum pitching response.

In combining the one percent wind shear load with the one percent
gust load, it should be recognized that the probability of these ex-
treme loads occurring simultaneously is much less than once in one
hundred flights; therefore, adding them directly would produce unduly
severe design loads. On the other hand, it would be unconservative
to use wind shear loads as desing loads with no increase to account for
turbulence. Design loads should probably lie somewhere between the two
extremes. A great deal more research is needed to develop rational
design criteria for wind shear and gusts for advanced vehicles. Ex-
cessive conservatism will result in serious penalties in performance
or payload, whereas, unconservatism can lead to an unacceptably low
probability of successful completion of the mission.

Power Spectral Gust Loads

The boosted flight from 0 to 50,000 feet is divided into the five
altitude bands shown in Table IV-1. Equations of motion and loads
equations for each of these bands have been written with constant co-
efficients representative of average conditions in the band. Three
degrees of freedom including two rigid body modes and one free-free

beam bending mode are used. The control system representation is the simplest one studied, with gain settings calculated to give one half cps and six tenths critical damping in pitch. The equations have been solved by means of a digital program (see Appendix G) for the normalized integrated output power spectra A^2 and characteristic frequencies $N(0)$ of bending moments for a normalized input power spectrum of atmospheric turbulence having a scale length of $L = 1000$ feet. These results as well as the distance traveled in each of the five bands are shown in Table IV-1. The number of exceedances of a given bending moment per unit distance within a given altitude band are given by the integral

$$N(\xi) = N(0) \int_o^{\infty} \hat{f}(\sigma_u) e^{-\frac{\xi^2}{2A^2 \sigma_u^2}} d\sigma_u \qquad \text{(IV-14)}$$

where $\hat{f}(\sigma_u)$ = probability density function of σ_u

σ_u = rms gust velocity

Fig. IV-27 shows plots of the integral $N(\xi)/N(0)$ versus the parameter $\xi^2/2A^2$ for various altitude bands based on probability density functions given in (113). The number of exceedances of various bending moments per unit distance for each altitude band has been obtained by evaluating the integral of Eqn. (IV-14) using Fig. IV-27. An alternative procedure is given in reference (114), in which simple forms of $\hat{f}(\sigma_u)$ are assumed such that Eqn. (IV-14) can be integrated in closed form. The number of exceedances of various bending moments per flight has been found by summing the exceedances in each of the five altitude bands. The resulting exceedance curves are shown in Fig. IV-28. These curves show exceedances of positive bending moment only and may be interpreted to give the number of bending moment cycles exceeding various amplitudes. The number of cycles in the amplitude range ξ to $\xi + \Delta \xi$ is equal to the difference between the number of exceedances of $\xi + \Delta \xi$ and the number of exceedances of ξ. This information can be used in preparing load spectra for fatigue tests or analyses.

TABLE IV-1

Time from Launch (sec.)	Altitude Band (ft.)	Distance Flown (ft.)	Load Station (in.)	$A^2 \times 10^{-10}$ $\frac{(in-lbs)^2}{(ft/sec)^2}$	$N(0)_1 \times 10^3$ ft.$^{-1}$
20	0- 5000	5200	587	.215	3.84
			896	.829	3.67
			1343	.792	2.22
33.75	5-15,000	11,200	587	.918	1.677
			896	3.50	1.579
			1343	3.69	.942
45.5	15-25,000	12,600	587	2.49	.870
			896	9.39	.819
			1343	10.45	.511
56	25-38,000	17,900	587	3.35	.579
			896	12.50	.545
			1343	13.24	.360
67.5	38-50,000	18,800	587	1.047	.629
			896	3.85	.589
			1343	3.59	.353

E. CONCLUSIONS

The important conclusions resulting from the boost flight loads study are summarized below:

1. A simple idealized control system representation, in which rigid pitching motions only are sensed and lags and nozzle inertia are neglected, is adequate for dynamic loads analyses provided gain settings which give the desired pitch frequency and damping are used.

2. A method of selecting gain settings to provide a desired short period response has been devised which accounts for the effects of flexibility and control system lags. The method depends upon the assumption that the response of the flexible modes is essentially static.

3. Loads due to wind shear and gusts are greatly influenced by control system gain settings. In general the highest attitude gain setting providing stability yields minimum loads. Since control system gain settings have a marked effect on dynamic loads, these gain settings should be chosen within the range satisfactory from the stability and control standpoint to minimize loads.

4. A simple control system representation is not adequate for investigating system stability. Sensor locations, lags, nozzle inertia, and structural stiffness as well as rate gain setting have an important effect on the stability boundaries.

5. Limiting the maximum nozzle swivel angle even a slight amount has a marked effect on the response. In response to the wind profile, the nozzle does not contact the stops if they are set at 23 degrees. If the stops are set at 21 degrees, the control moment available is insufficient to prevent the vehicle from tumbling. In any actual design of a boost-glide vehicle, it appears desirable to reduce the requirements for large control moments by reducing the destabilizing aerodynamic pitching moments.

6. No significant increase in accuracy is obtained by using more than two flexible modes in the flight loads analysis. Structural dynamics may be neglected provided the static deflection of the structure under aerodynamic and thrust vectoring loads is accounted for. The use of beam modes which include no glider wing mode components yields slightly conservative results. If beam modes are used instead of coupled modes, the use of more than one flexible mode is not justified.

7. The effect of fuel slosh on dynamic loads is negligible, although the slosh amplitudes are large due to passage through the wind spike.

8. Maximum bending loads due to wind shear are quite sensitive to glider lift curve slope.

9. Wind shear loads have been determined by several methods. The most attractive from the standpoint of maximum accuracy without an excessive amount of labor and machine time is the superposition of loads

due to the slow time-varying portion of the profile and loads due to the spike as obtained on the digital computer. Superposition is used because a smaller number of degrees of freedom can be used for the slow time-varying portion. The assumption of constant coefficients, during passage through the spike necessary in the analog solutions, changes the response sufficiently to affect the accuracy of the results. However, the analog is a valuable tool for the investigation of parameter variations, nonlinearities, and refinements in the mathematical representation of the system.

10. Maximum discrete gust loads are produced by phasing the one minus cosine gust with the pitch mode. Loads due to the 40 fps critically phased gust at 30,000 feet are quite large, almost as large as the maximum wind shear loads.

Sissenwine 1% synthetic wind
profile applicable to:

1) Area of USA with strongest
   30 to 45 thousand feet winds.
2) Windiest season.
3) Vehicles with sharp maximum
   wind response between 30 and
   45 thousand feet.

1% shears associated with peak

$\pm$ 1000 ft layer .076 sec^{-1}
$\pm$ 3000 ft layer .050 sec^{-1}
$\pm$ 5000 ft layer .033 sec^{-1}

AviDyne 1% profile maximum
shear .050 sec^{-1}
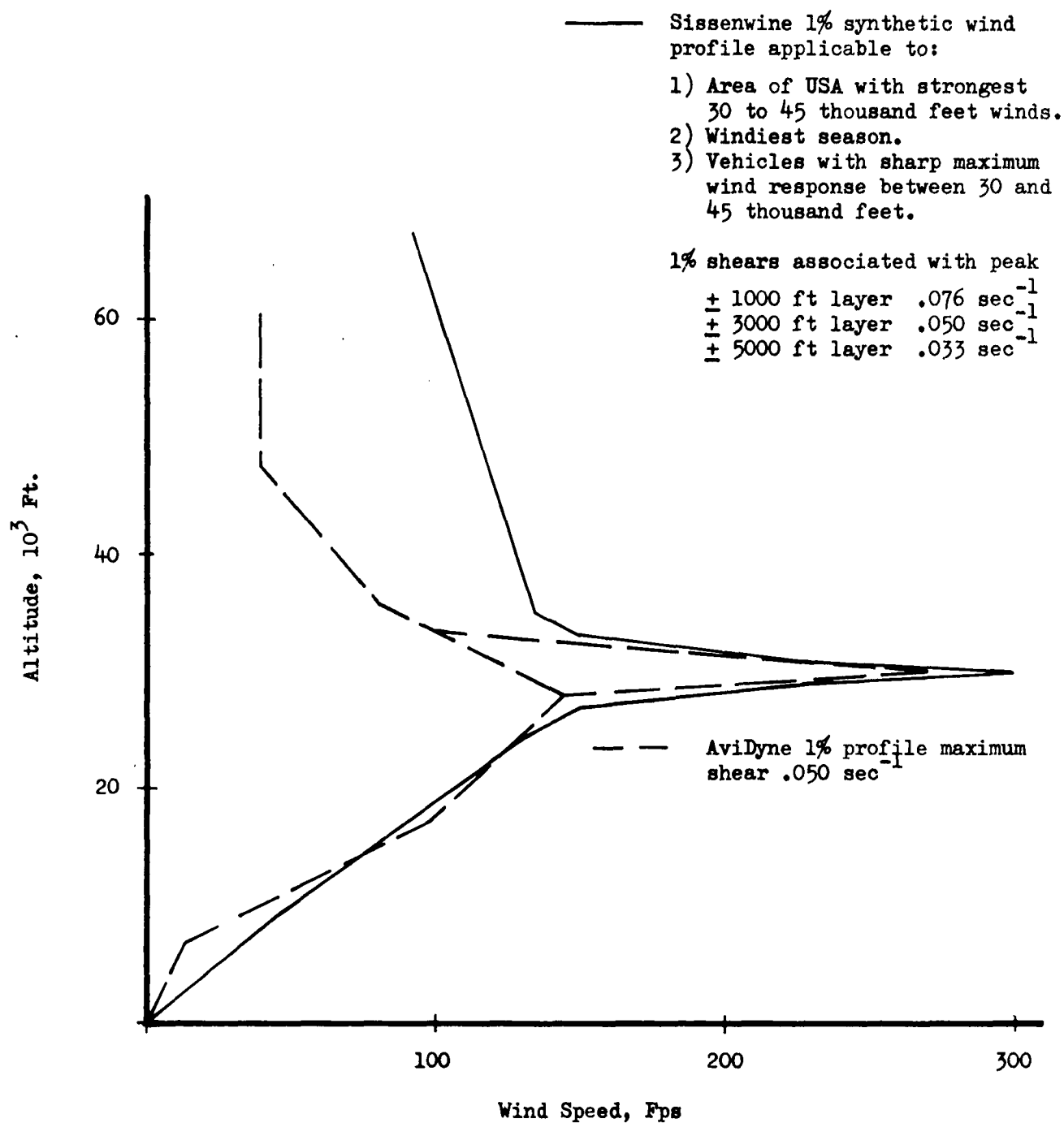
FIG. IV-2   1% SYNTHETIC PROFILES
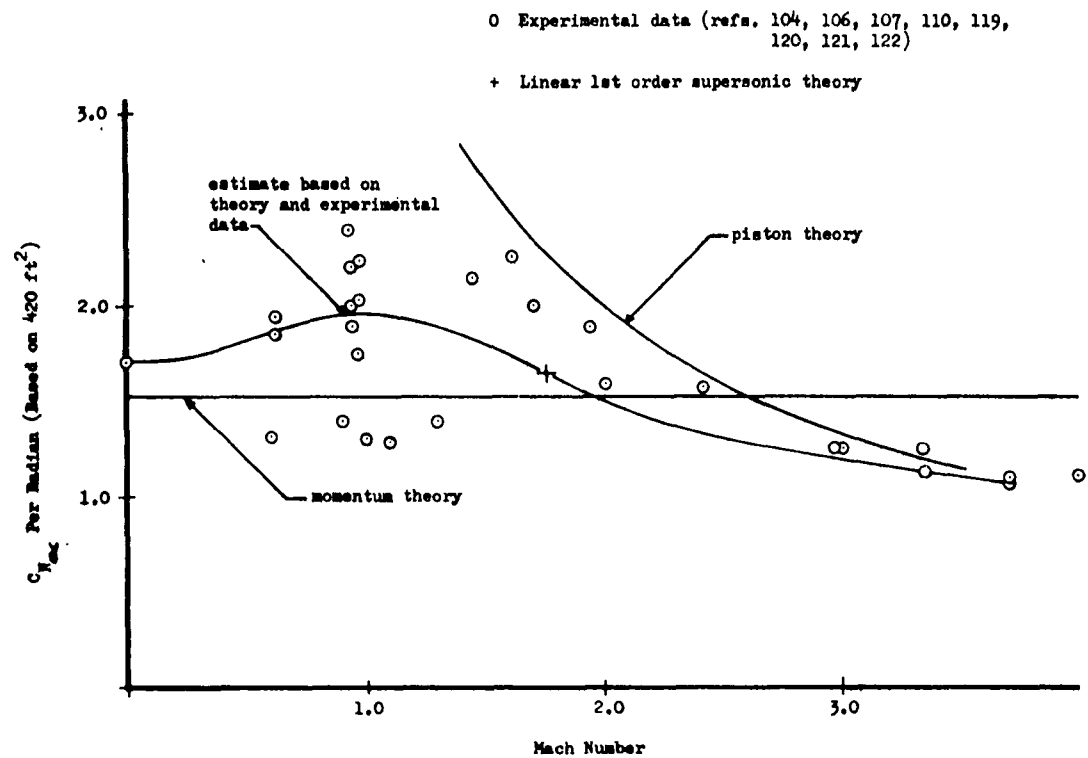
FIG. IV-3   VARIATION OF GLIDER C_{N_α} WITH MACH NUMBER
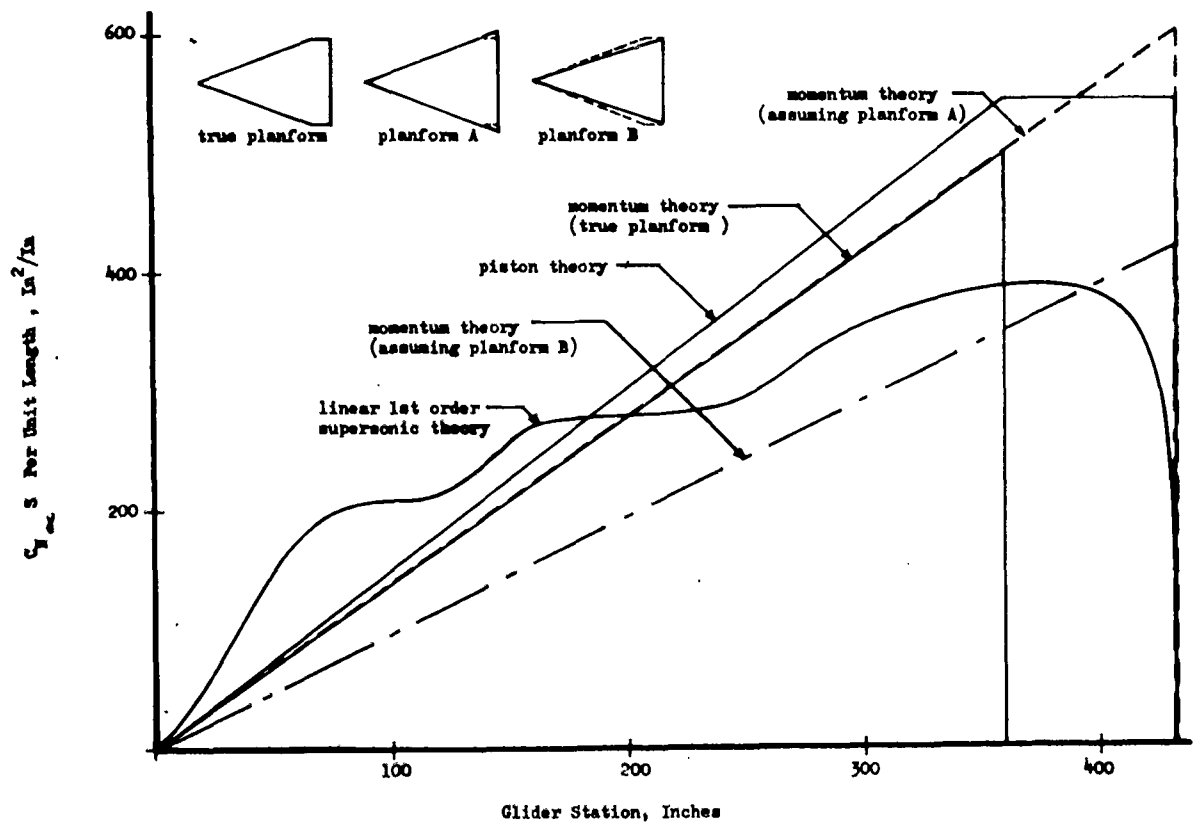
FIG. IV-4   RIGID GLIDER LIFT DISTRIBUTION AT MACH NO. 1.76 BY VARIOUS THEORIES

$$\frac{q_{\mathfrak{z}}}{\Theta_s} = 7.2 + .919 \, s$$

two flexible modes
bending sensed
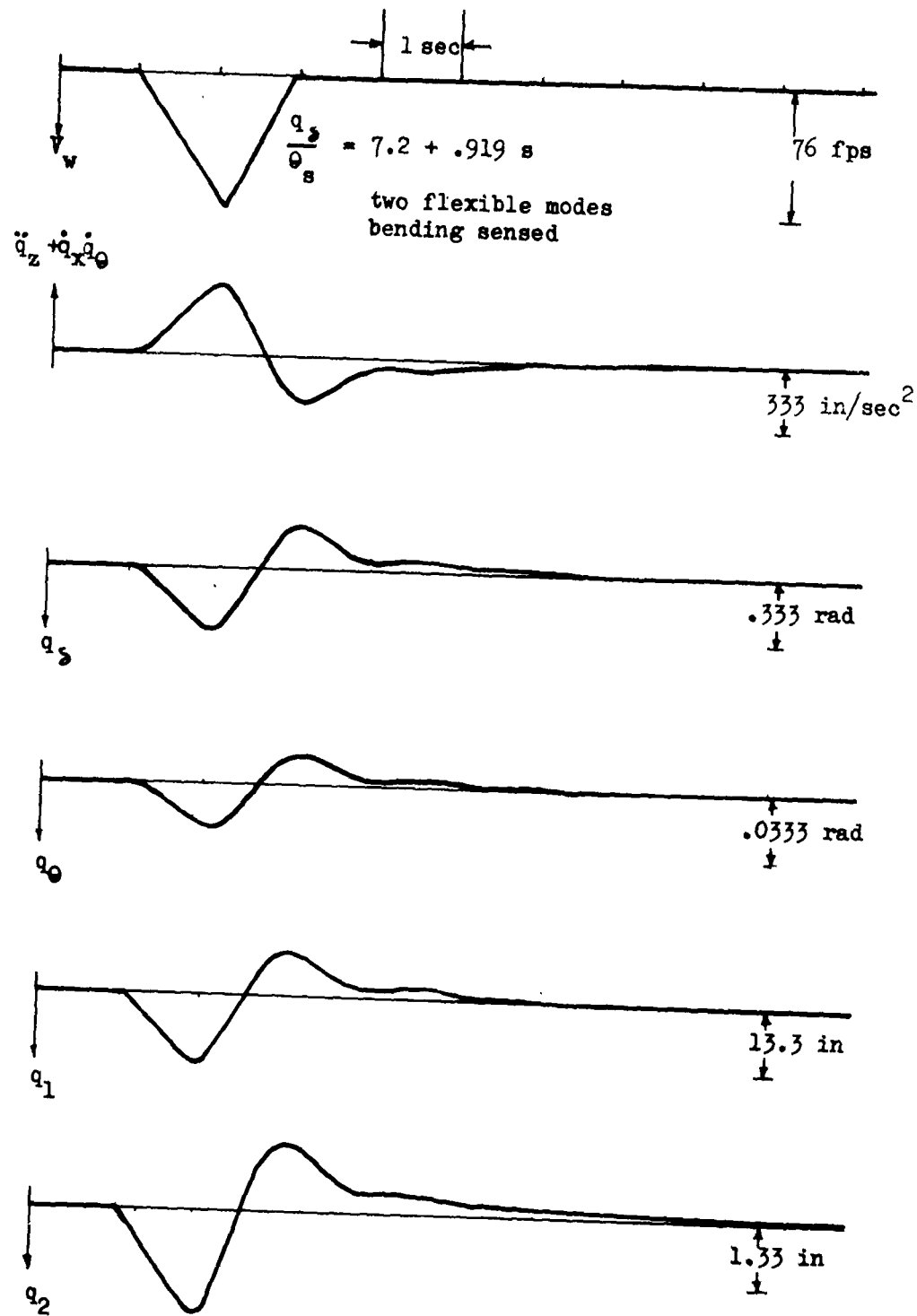
FIG. IV-5   TYPICAL RESPONSE TIME HISTORIES-
SIMPLE CONTROL SYSTEM

one flexible mode

two flexible modes

two flexible modes
(bending sensed)

rigid vehicle

$\dfrac{q_\delta}{q_\theta} = 7.2 + .919 \, s$

or

$\dfrac{q_\alpha}{\theta_s} = 7.2 + .919 \, s$

76 fps wind spike

Body Station , Inches

500   1000   1500

Bending Moment , 10^6 In-lbs

0   50   100
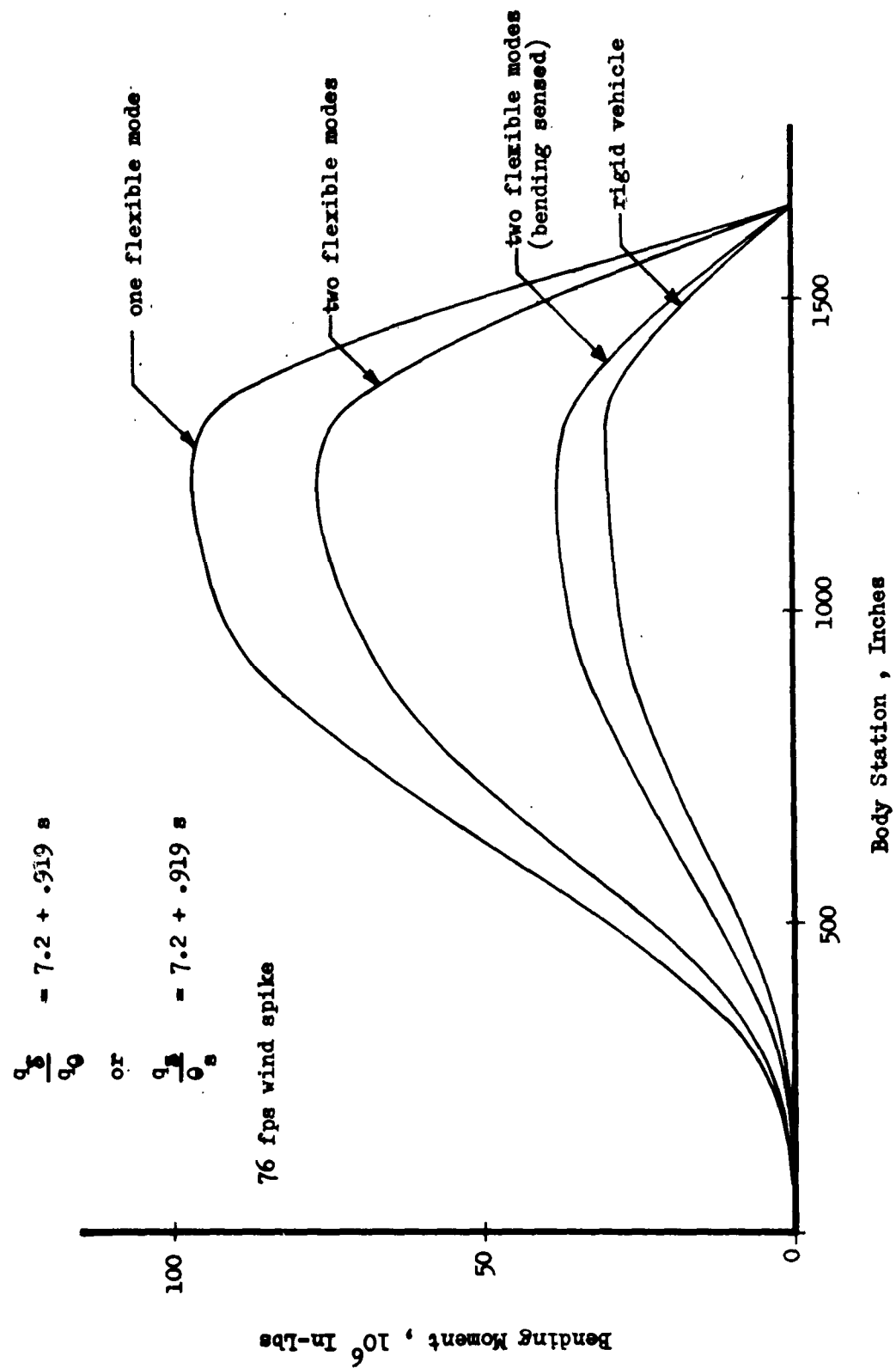
FIG. IV-6   EFFECT ON BENDING MOMENTS OF INCLUDING FLEXIBLE MODES
WITHOUT COMPENSATING ADJUSTMENT OF GAINS

$$\frac{q_\delta}{\Theta_s} = \frac{7.2 + 2.4s}{(1+.034s)(1+.035s)(1+2(.7)s \frac{s^2}{60} + \frac{s^2}{60^2})}$$
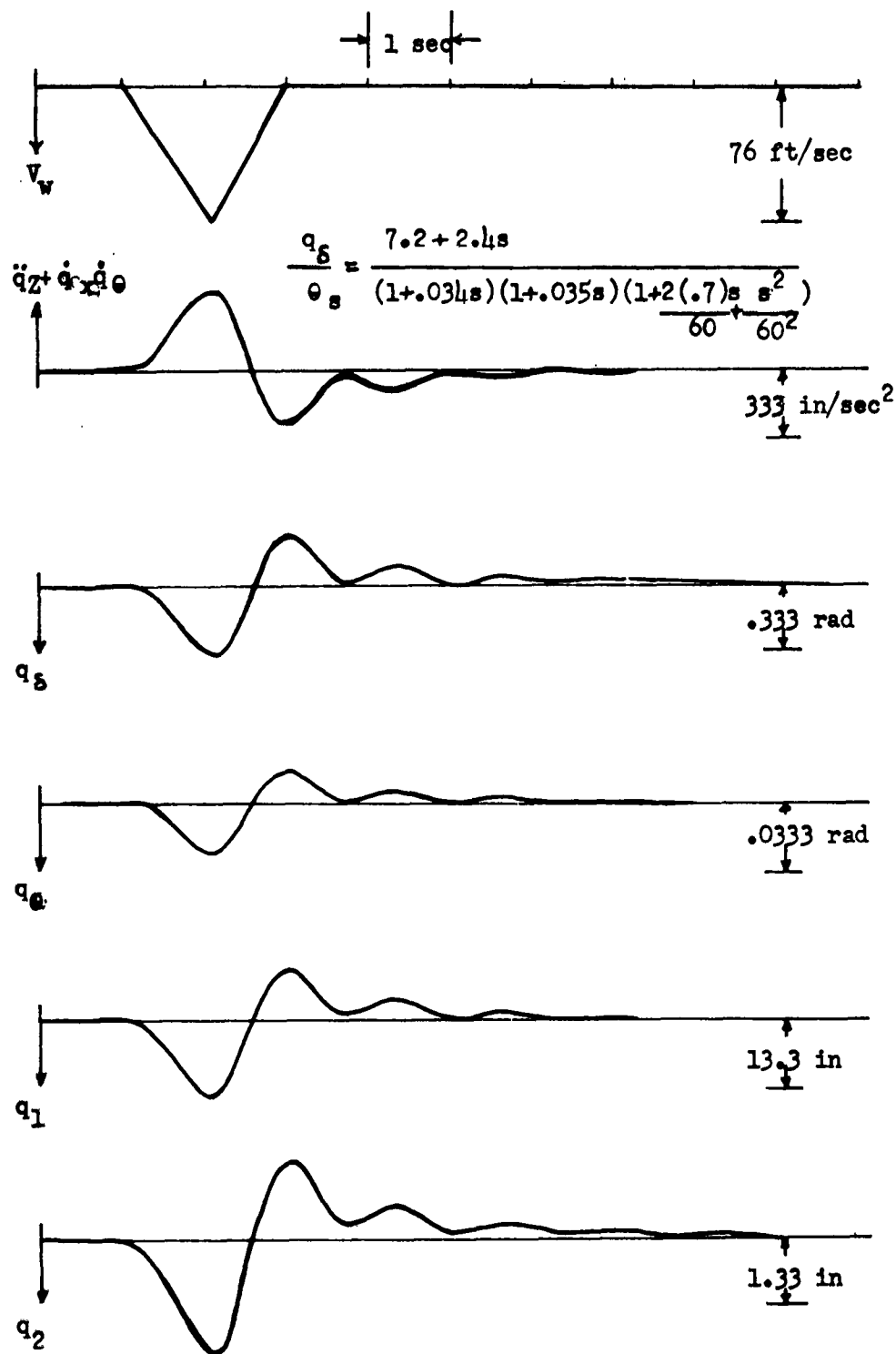
FIG. IV-7   TYPICAL RESPONSE TIME HISTORIES --
LAGGED CONTROL SYSTEM
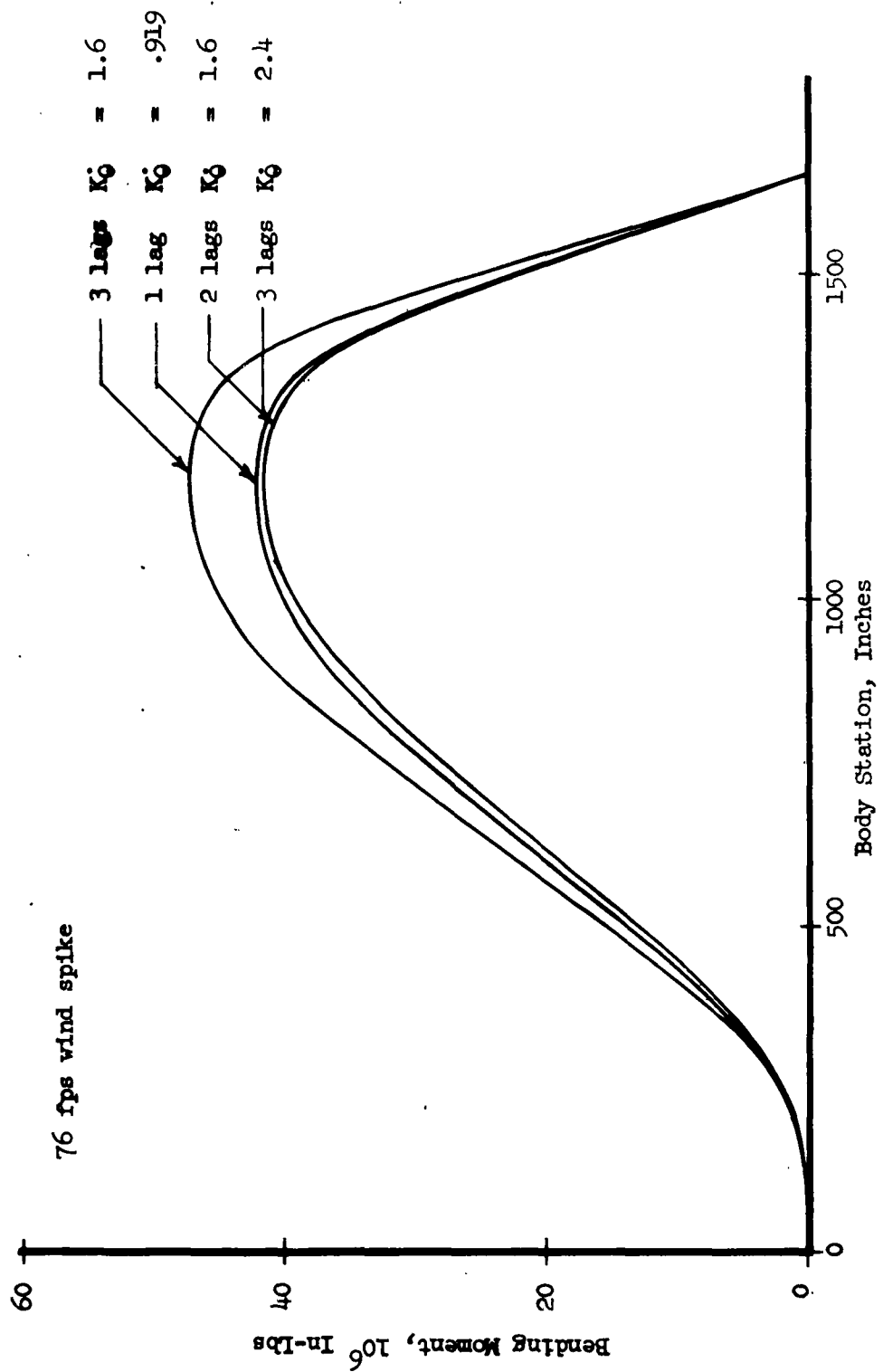
FIGURE IV-8   BENDING MOMENT DIAGRAMS WITH LAGGED CONTROL SYSTEMS --

TWO FLEXIBLE MODES K_θ = 7.2
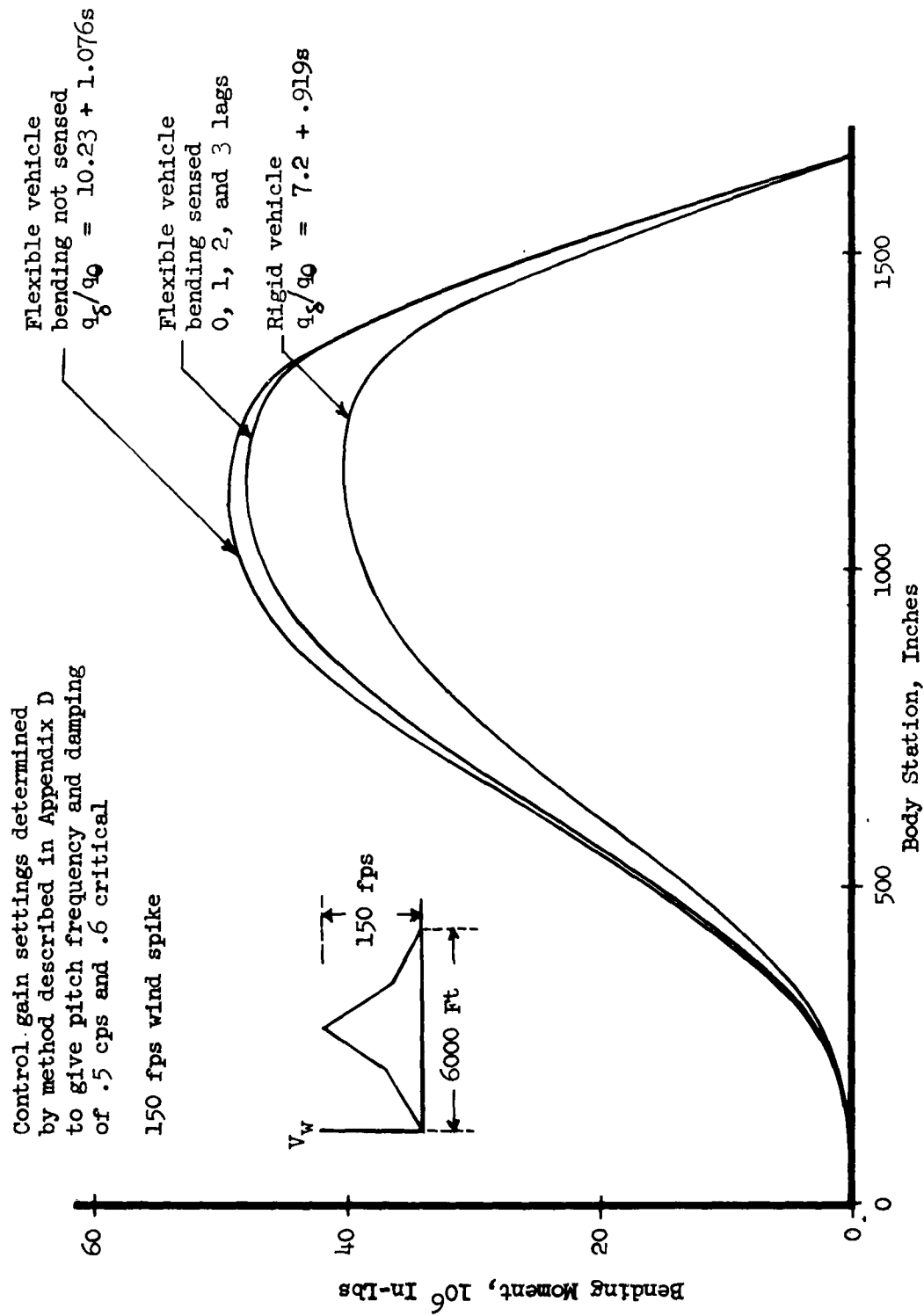
FIG. IV-9 BENDING MOMENT DIAGRAMS FOR VARIOUS VEHICLE
AND CONTROL SYSTEM REPRESENTATIONS

Control System

$$\frac{q_{\beta}}{\sigma_e} = \frac{K_Q \ (1 + s/1.96)}{(1 + .034s)(1 + .035s)(1 + \frac{2(.7)s}{60} + \frac{s^2}{60^2})}$$

150 fps wind spike

BS 1027
BS 1343
BS 896
BS 587
BS 1541
BS 505
BS 327

unstable

unstable

Bending Moment, 10^6 In-Lbs

Attitude Gain Setting, K_Q
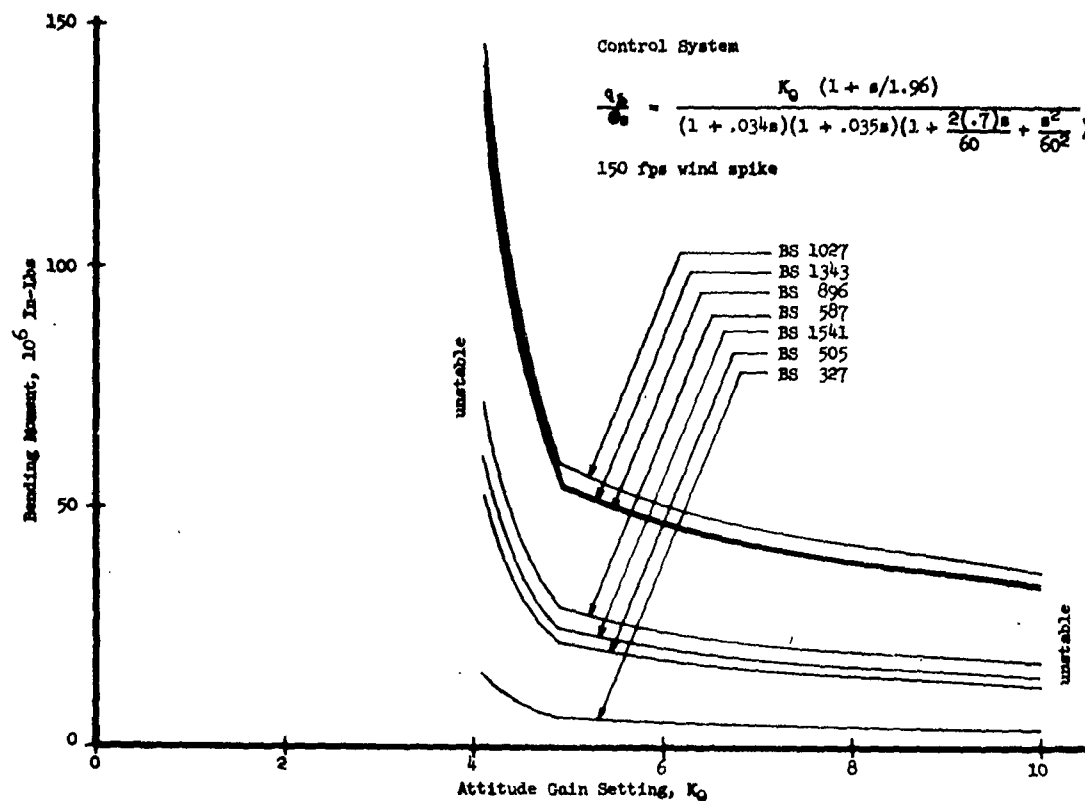
FIG. IV-10 EFFECT OF VARIATION OF ATTITUDE GAIN SETTING ON BENDING MOMENTS

Control System

$$\frac{q_{\beta}}{\sigma_e} = \frac{6.452 + K_{\dot{\phi}}}{(1 + .034s)(1 + .035s)(1 + \frac{2(.7)s}{60} + \frac{s^2}{60^2})}$$

150 fps wind spike

BS 1027
BS 1343
BS 896

BS 587
BS 1541
BS 505

BS 327

Unstable

Unstable

Bending Moment, 10^6 In-Lbs

Rate Gain Setting, $K_{\dot{\phi}}$
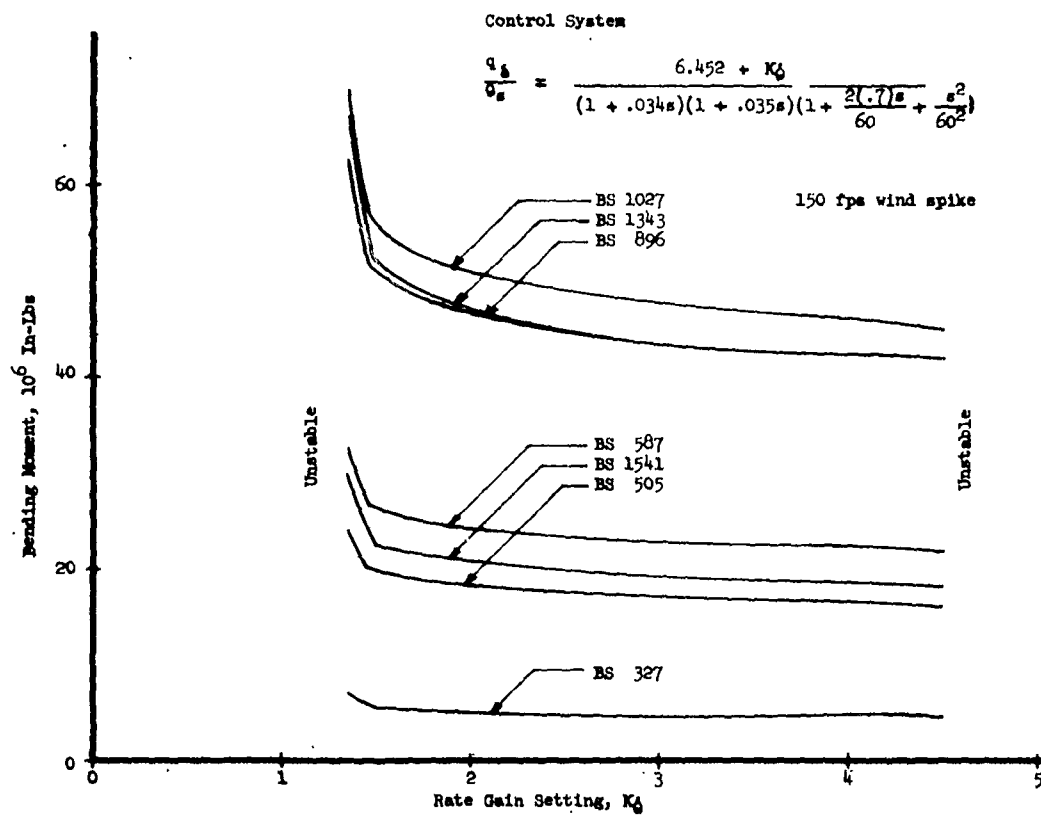
FIG. IV-11 EFFECT OF VARIATION OF $K_{\dot{\phi}}$ ON BENDING MOMENTS
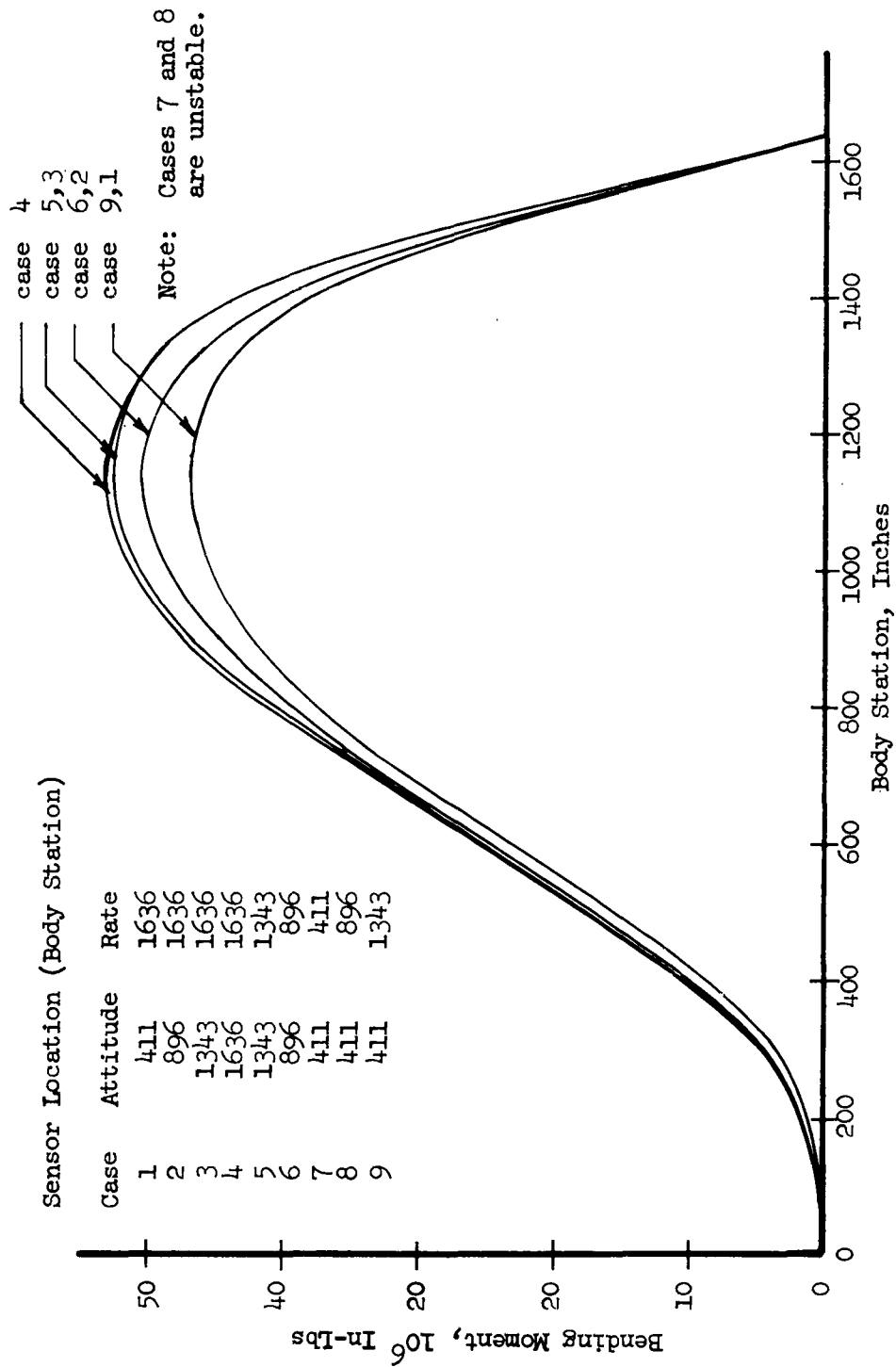
FIG. IV-12 EFFECT OF SENSOR LOCATION ON BENDING MOMENTS

$$q_\delta/\theta_s = K_\theta + K_{\dot\theta} s$$

Sensor Location (Body Station)

Case	Attitude	Rate
1	411	1636
2	896	1636
3	1343	1636
4	1636	1636
5	1343	1343
6	896	896
7	411	411
8	411	896
9	411	1343

case 4
case 5,3
case 6,2
case 9,1

Note: Cases 7 and 8 are unstable.
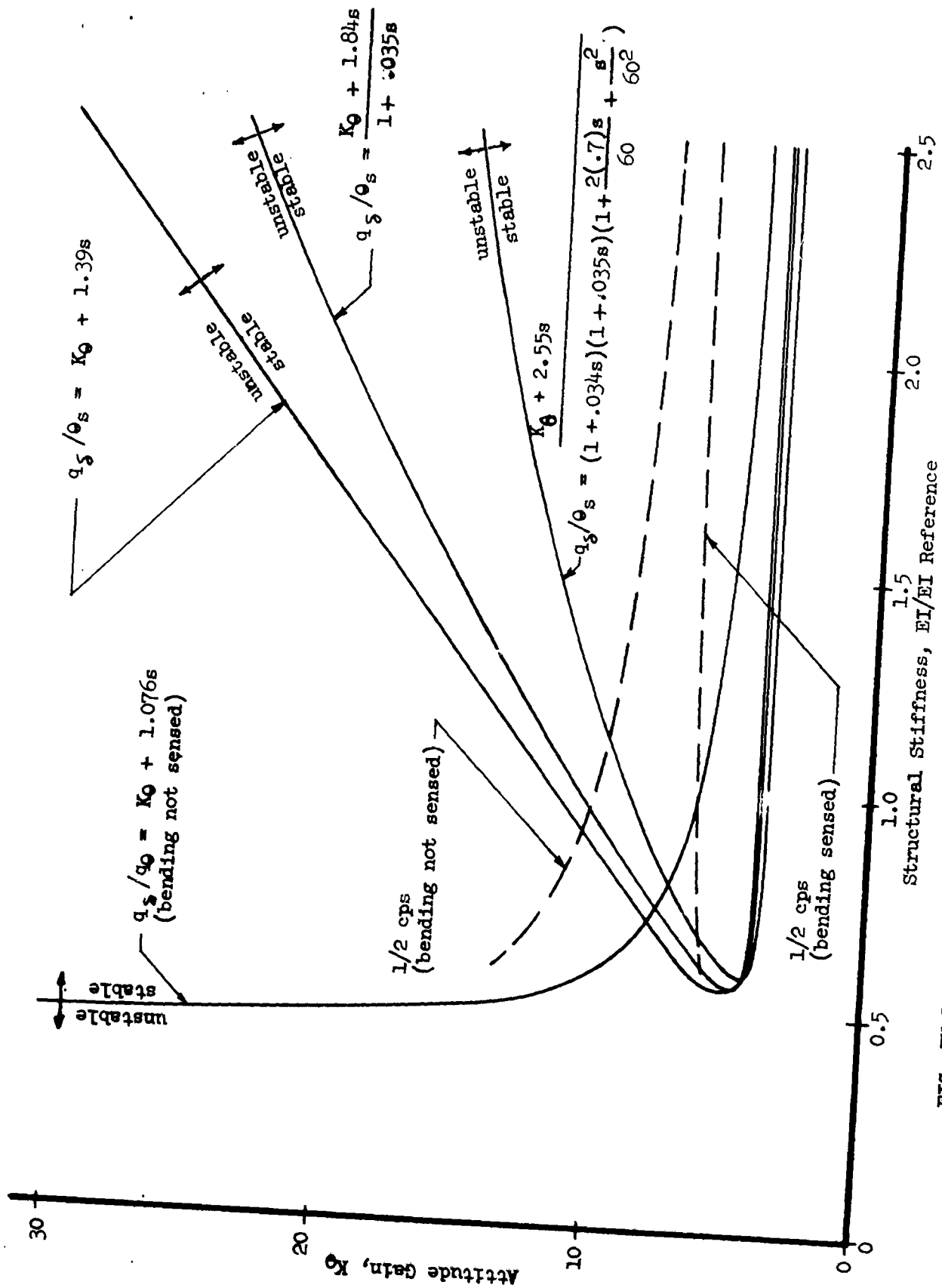
FIG. IV-13 STABILITY BOUNDARIES FOR VARIOUS CONTROL SYSTEM REPRESENTATIONS
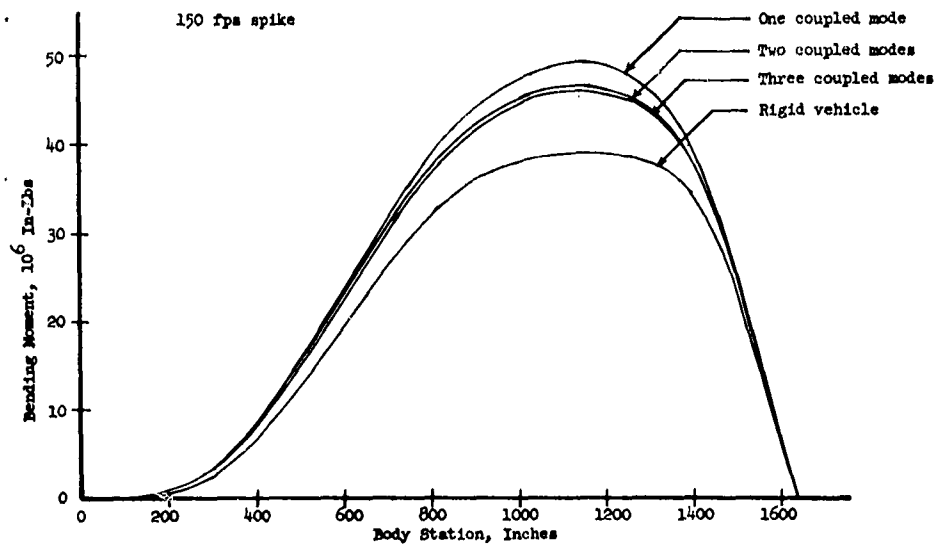
FIG. IV-14 EFFECT OF NUMBER OF MODES ON MAXIMUM BENDING MOMENTS
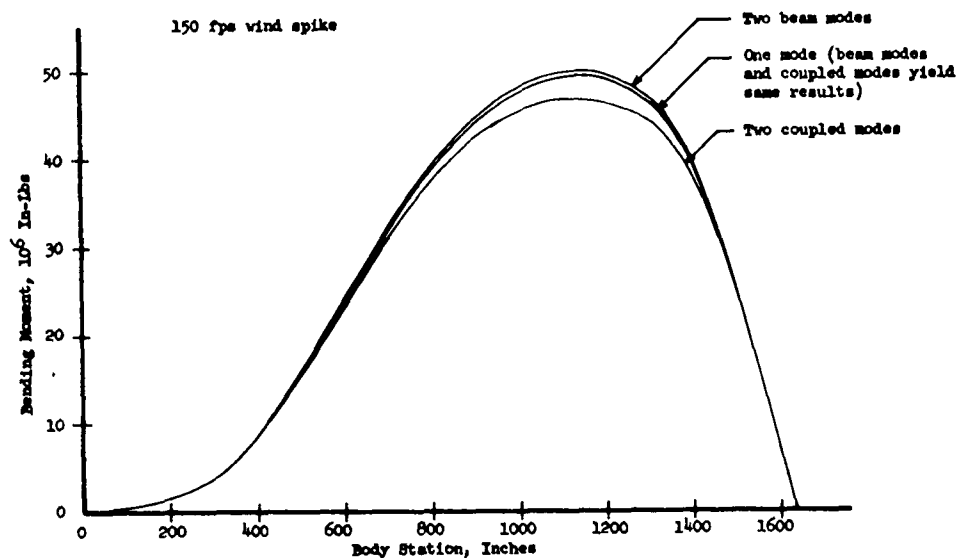
FIGURE IV-15 COMPARISON OF BENDING MOMENTS PREDICTED USING BEAM
MODES OR COUPLED MODES
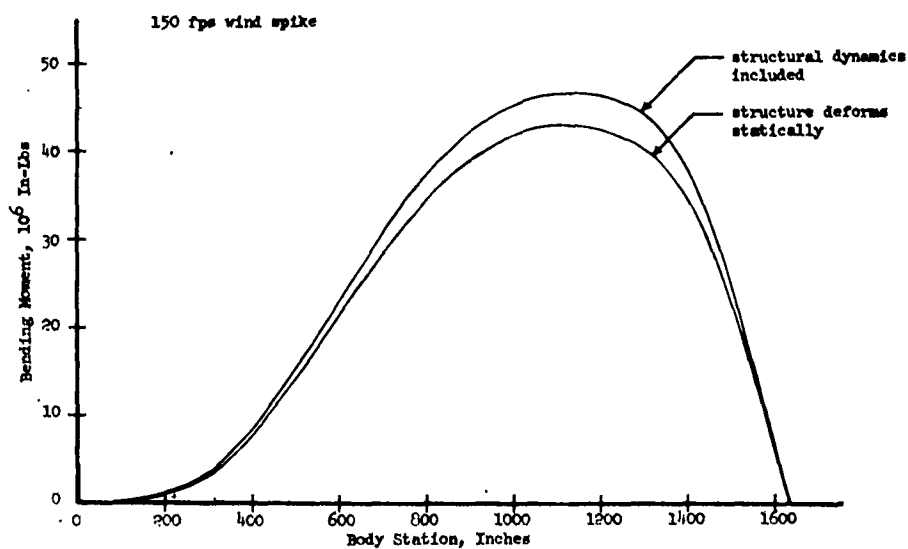
FIGURE IV-16 EFFECT OF STRUCTURAL DYNAMICS ON PREDICTED BENDING MOMENTS
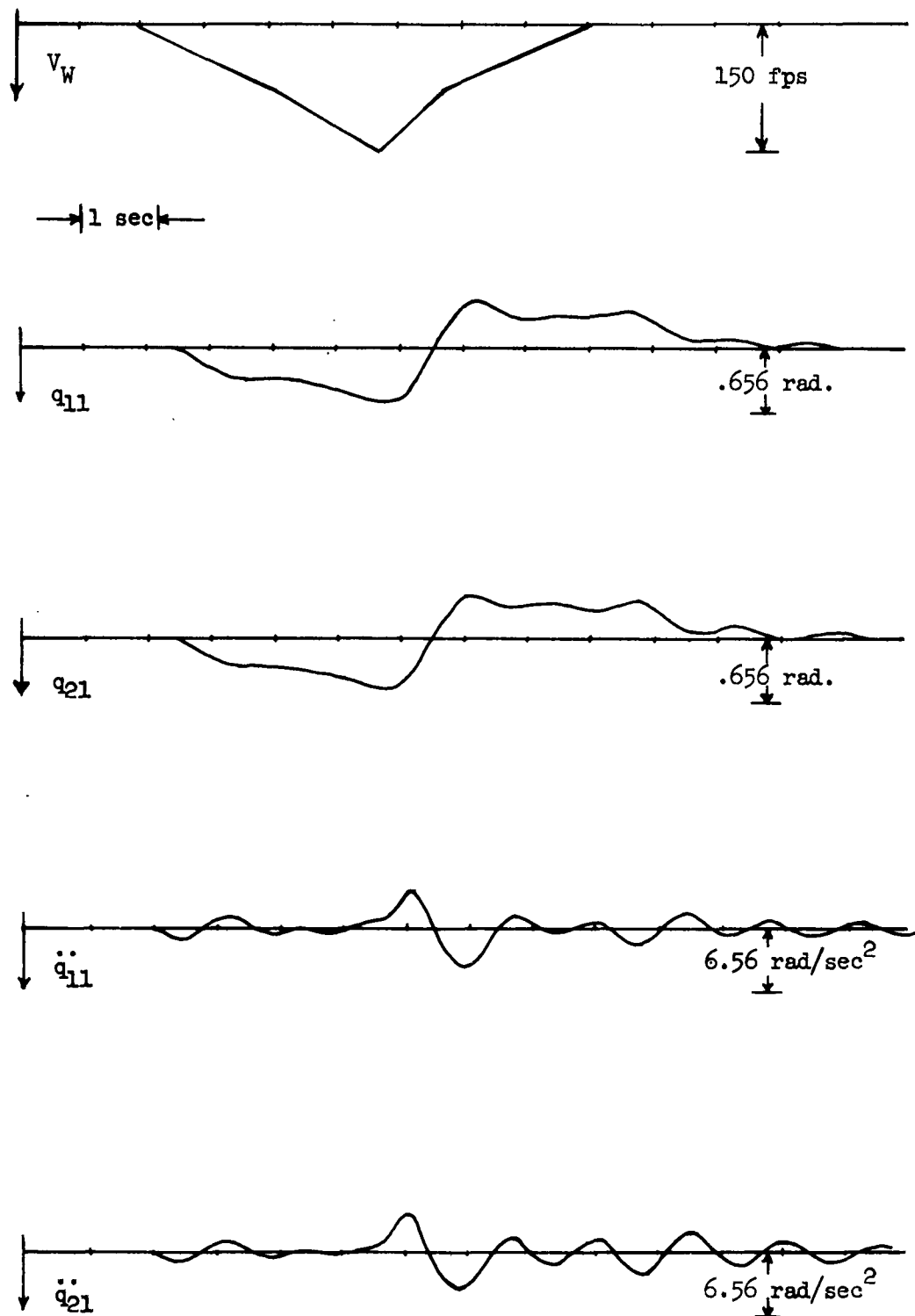
FIGURE IV-17   SLOSH RESPONSES
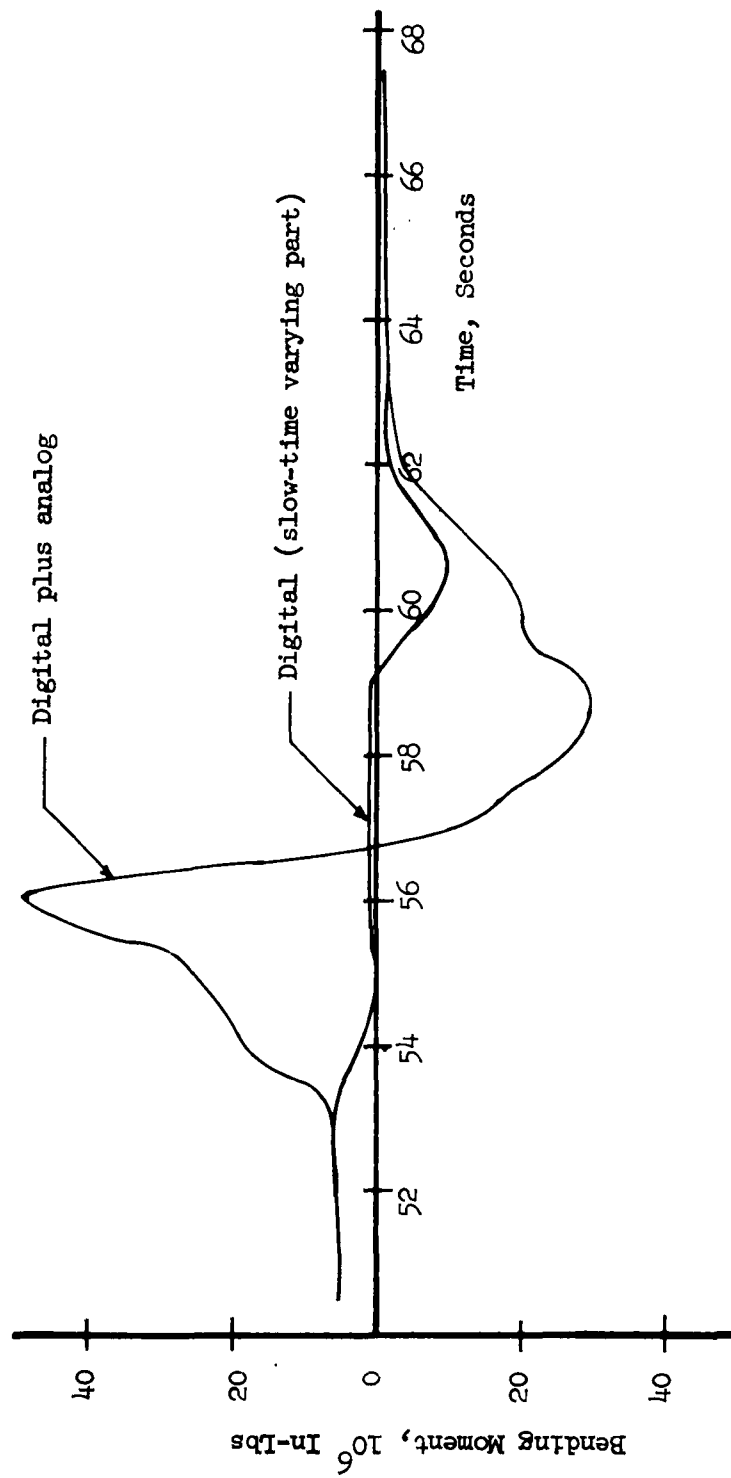
FIGURE IV-18 BS 1027 BENDING MOMENT TIME HISTORY BASED ON SUPERPOSITION OF DIGITAL AND ANALOG SOLUTIONS (SISSENWINE WIND PROFILE)

Net panel load (lbs/in²) = aerodynamic load + inertia load.

Note: 1. The loads on all the panels are in phase, and the maximum loads occur at the same time.

2. Loads determined by superposition of analog spike solution and digital slow time-varying solution.

FIGURE IV-19 MAXIMUM NET PANEL LOADS ON GLIDER DUE TO REVISED 1% SISSENWINE WIND PROFILE
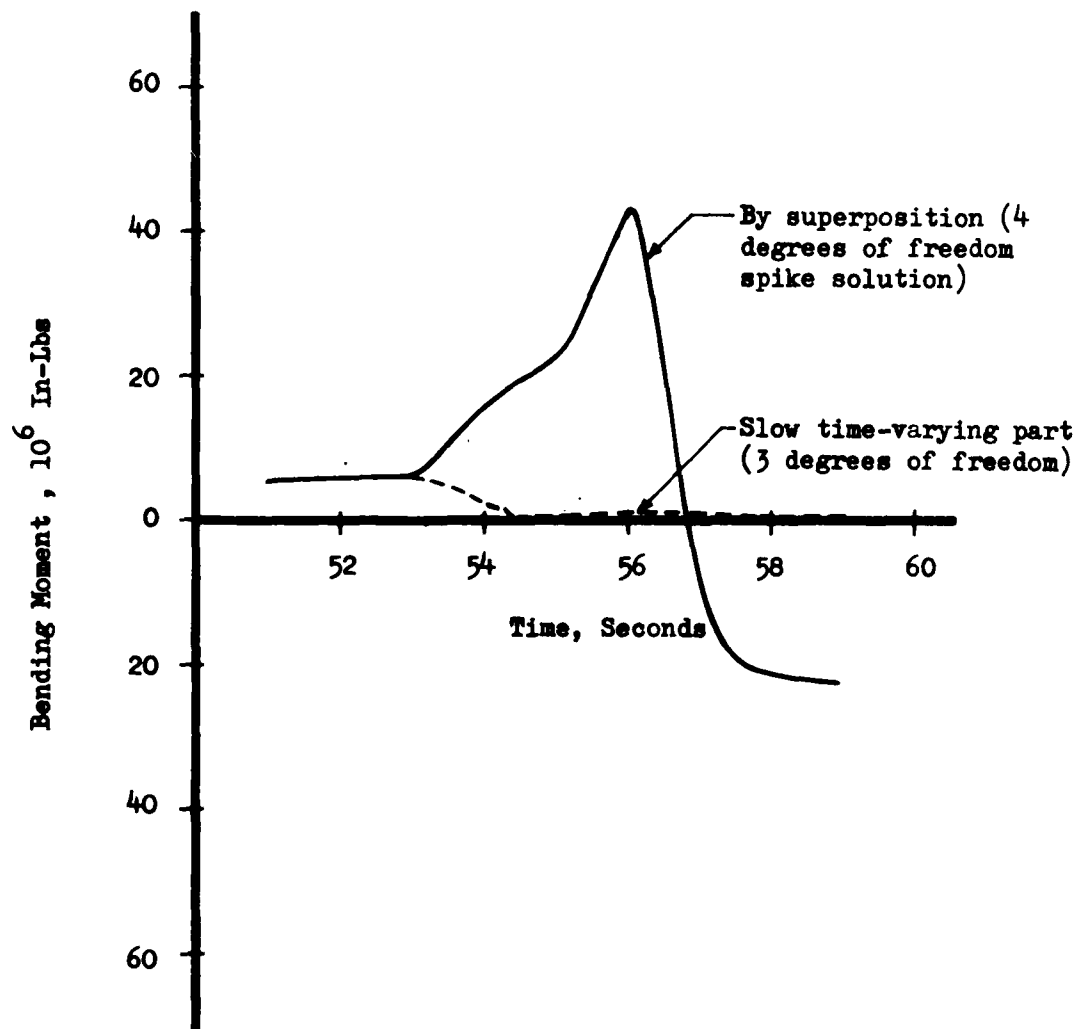
FIG. IV-20   BS 1027 BENDING MOMENT TIME HISTORY BASED
ON SUPERPOSITION OF DIGITAL SOLUTIONS
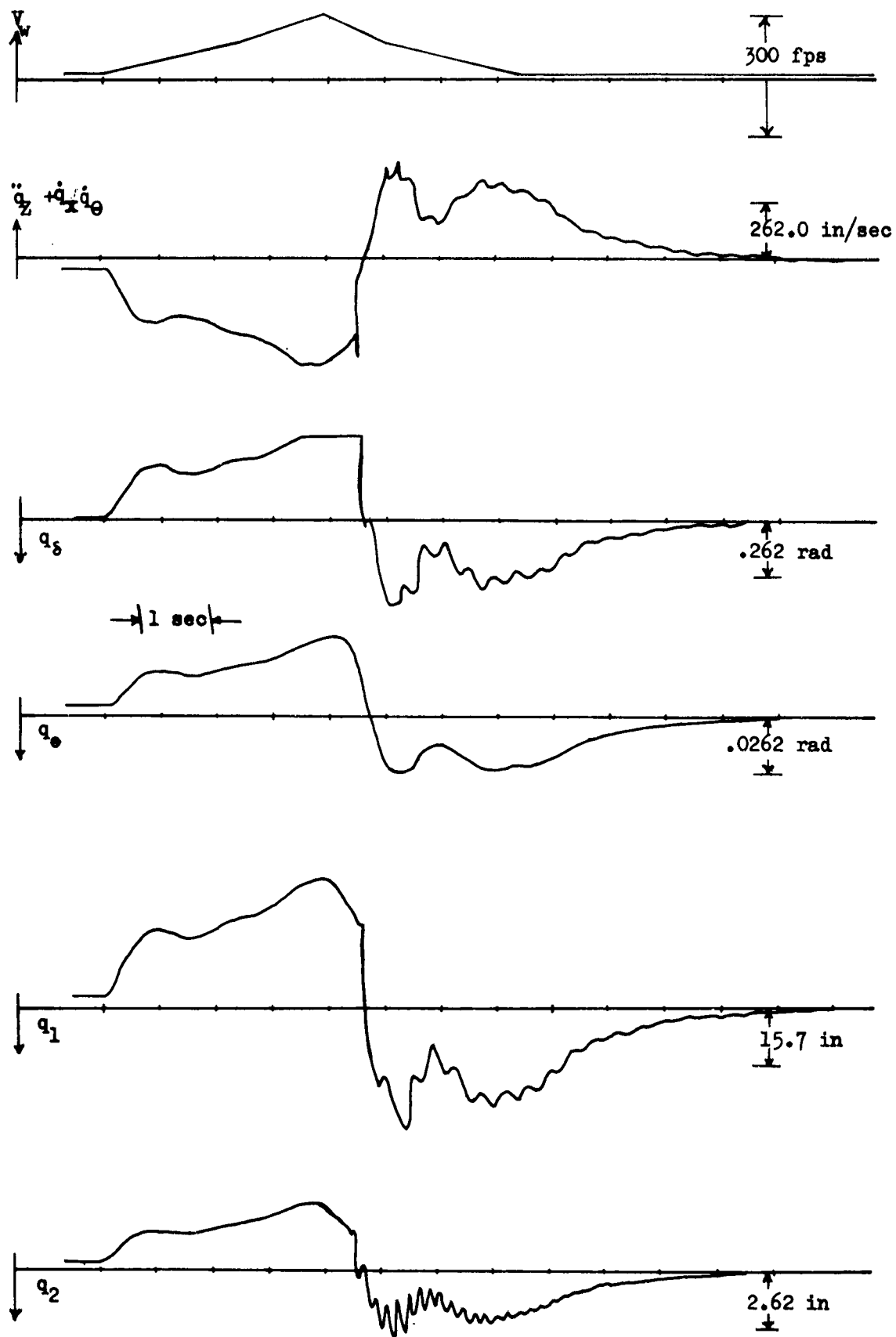
FIG IV-21   RESPONSE TIME HISTORIES -- NOZZLE SWIVEL ANGLE LIMIT 21.5°
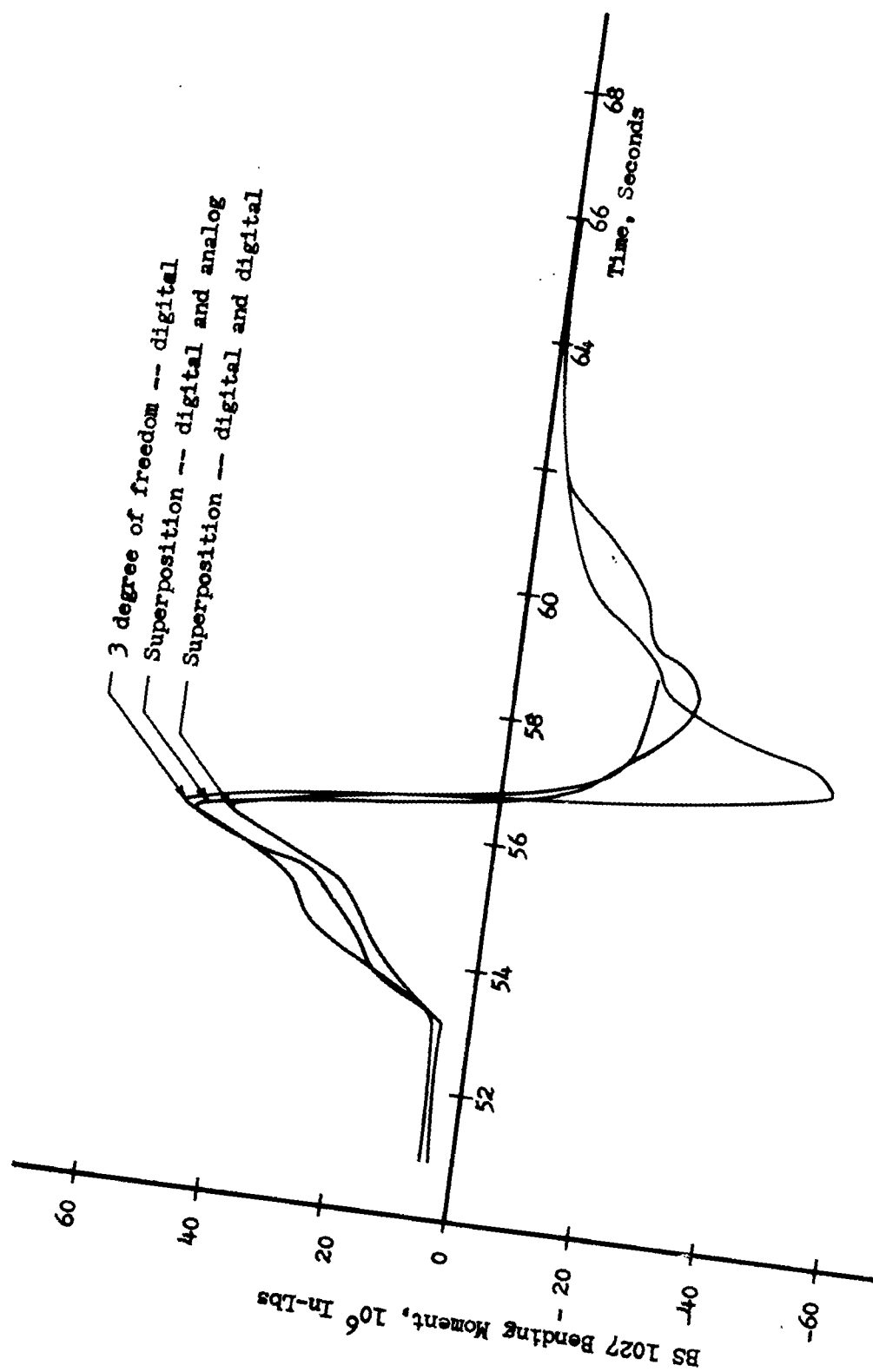
FIG. IV-22 COMPARISON OF BENDING MOMENT TIME HISTORIES COMPUTED BY VARIOUS METHODS

3 degree of freedom -- digital
Superposition -- digital and analog
Superposition -- digital and digital

Time, Seconds

BS 1027 Bending Moment, 10^6 In-Lbs

WADD TR 60-518

90
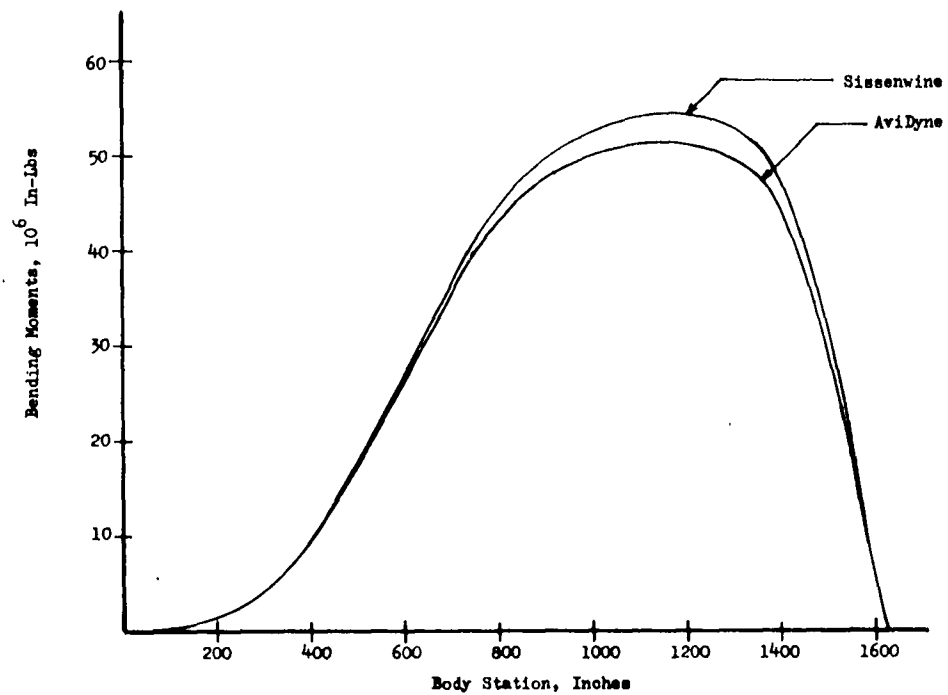
FIG. IV-23   COMPARISON OF BENDING MOMENTS DUE TO SISSENWINE AND
             AVIDYNE 1% WIND PROFILES
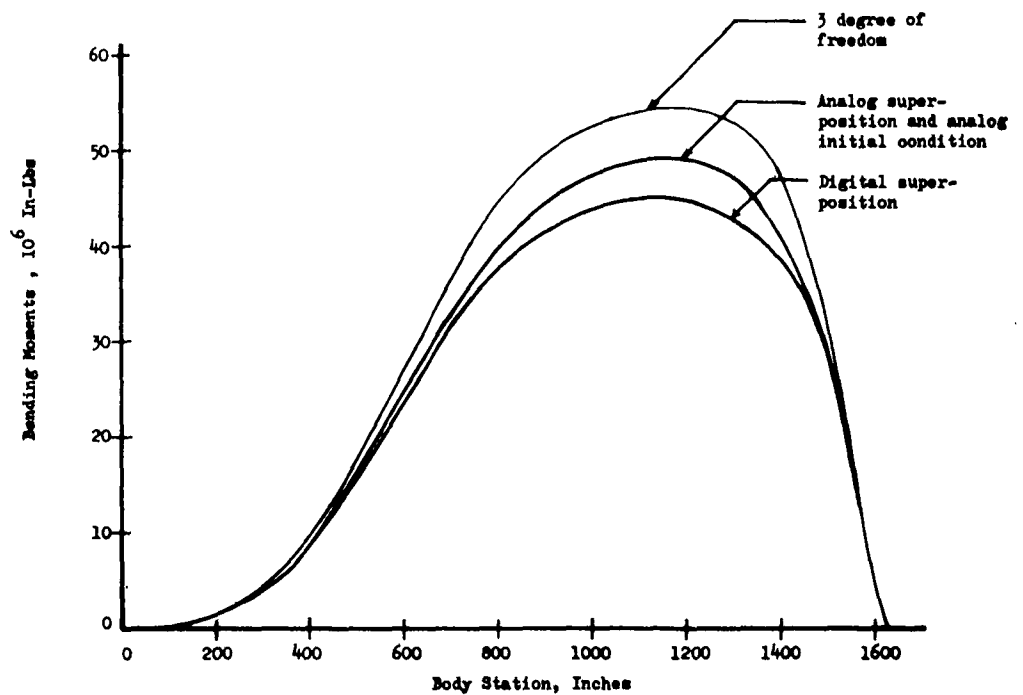
FIG. IV-24   BENDING MOMENTS DUE TO WIND SHEAR CALCULATED BY VARIOUS METHODS
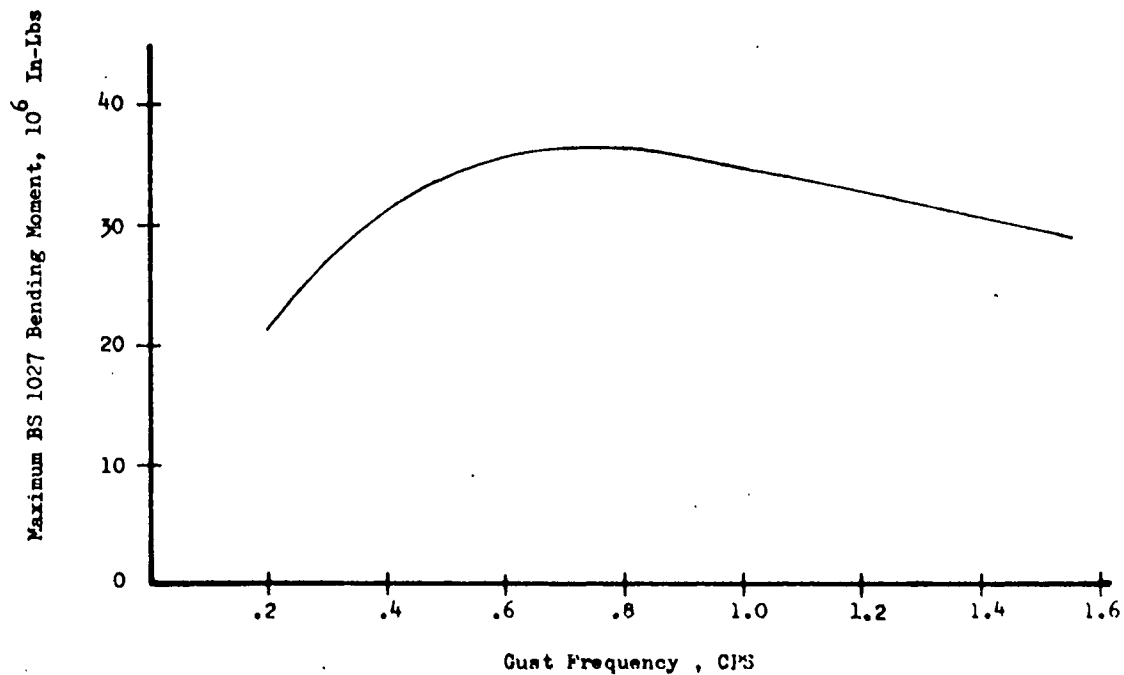
FIG. IV-25   VARIATIONS OF DISCRETE GUST LOADS WITH GUST FREQUENCY

40 ft/sec discrete gust
encountered at 30,000 ft
during boost
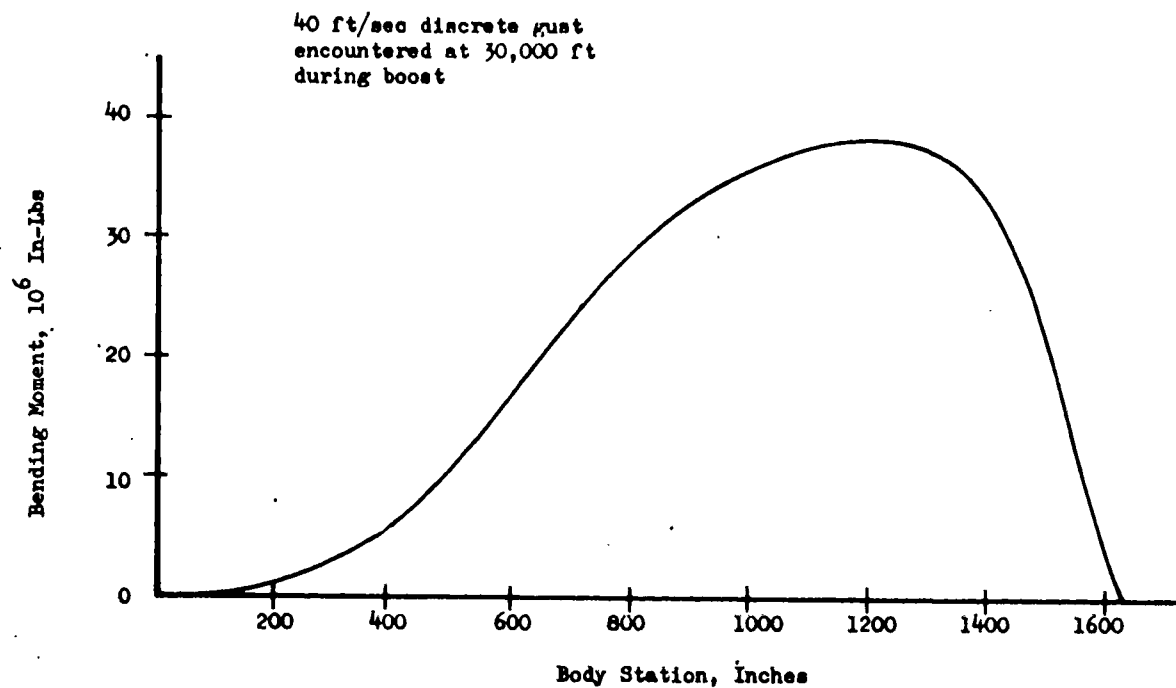
FIG. IV-26   MAXIMUM BENDING MOMENTS DUE TO A CRITICALLY
PHASED ONE-COSINE DISCRETE GUST
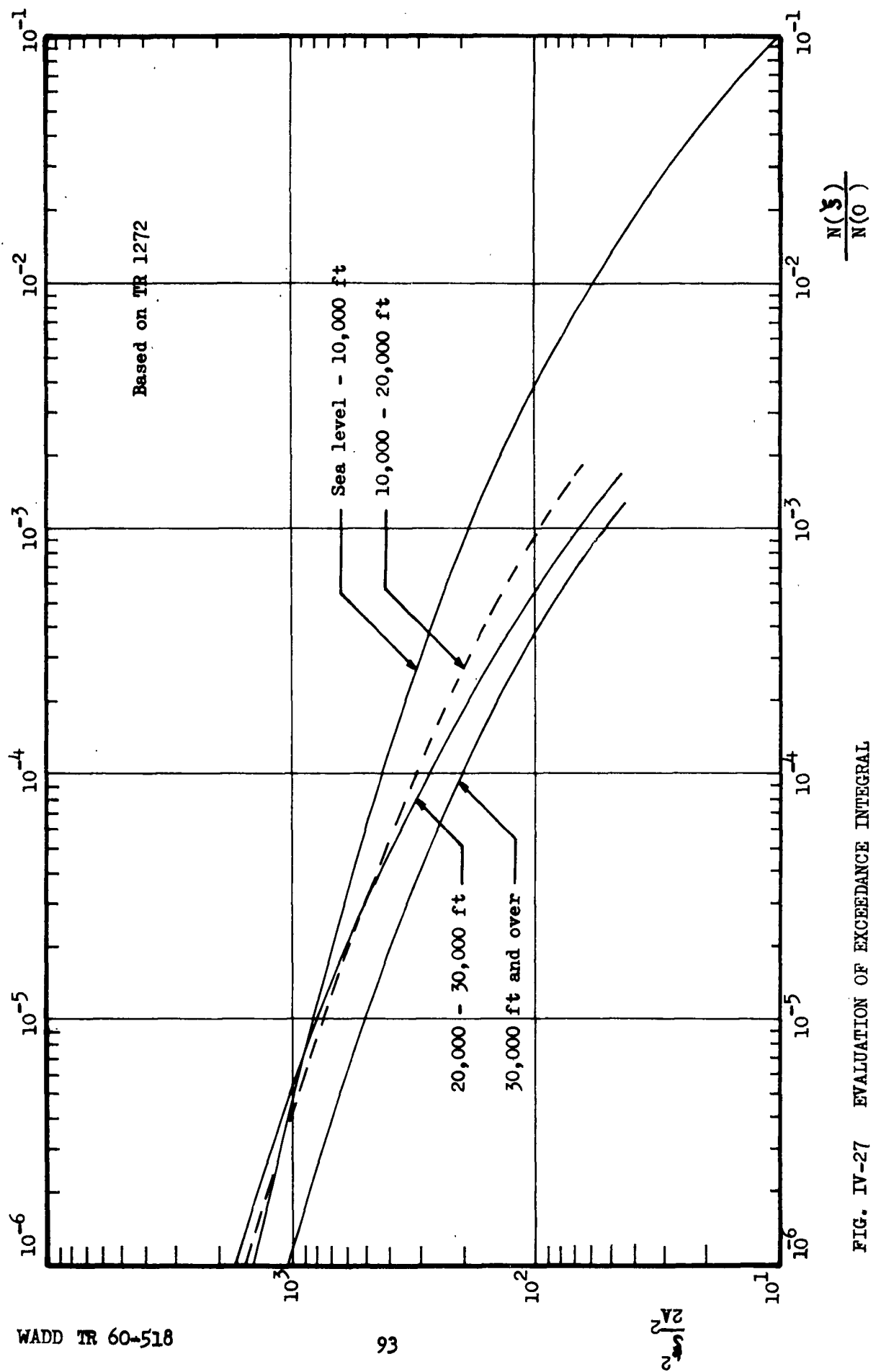
FIG. IV-27   EVALUATION OF EXCEEDANCE INTEGRAL

Based on TR 1272

Sea level - 10,000 ft

10,000 - 20,000 ft

20,000 - 30,000 ft

30,000 ft and over

$$\frac{N(\bar{\zeta})}{N(0)}$$

$$\frac{\zeta^2}{2A^2}$$
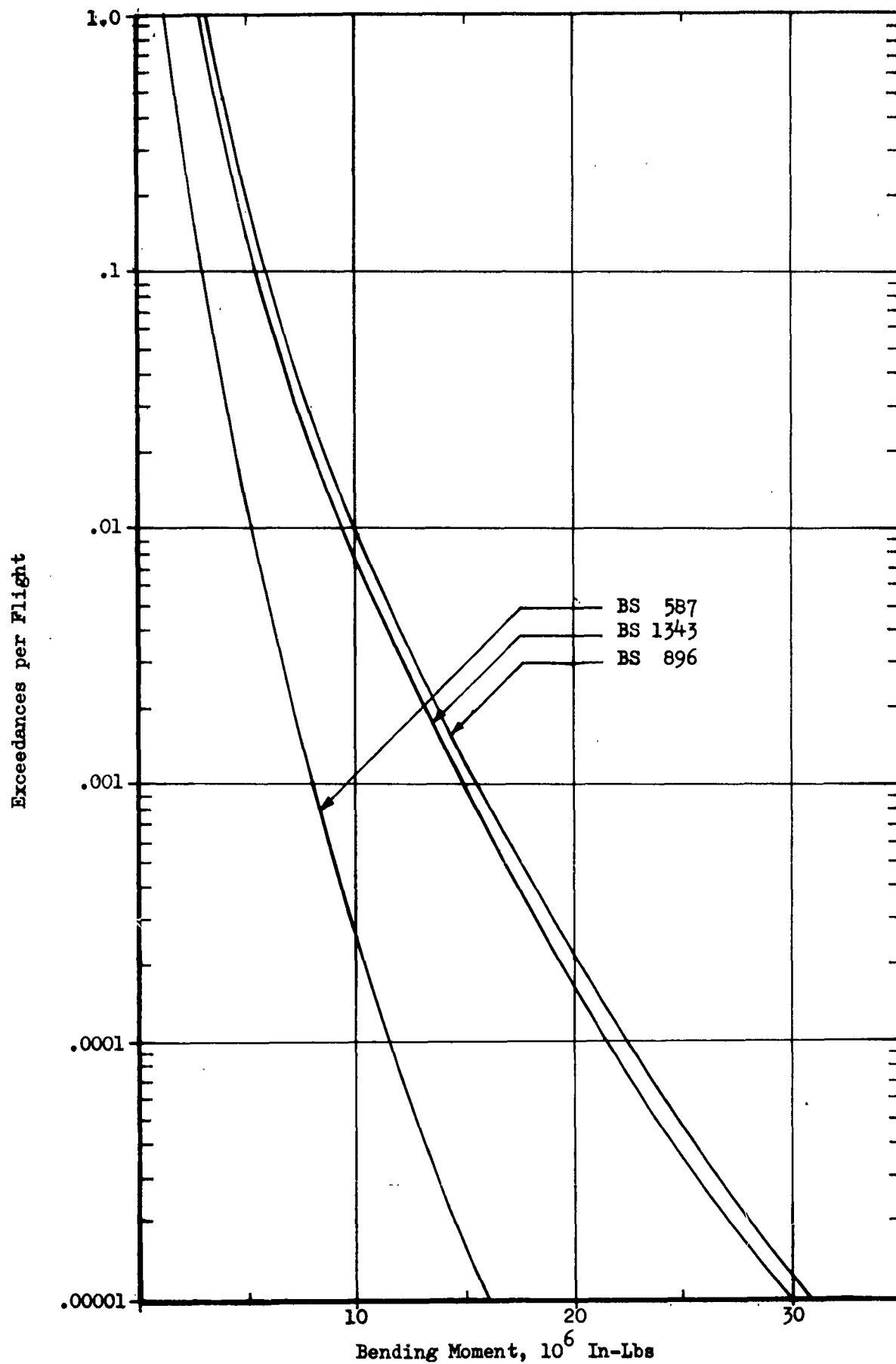
FIG. IV-28   BENDING MOMENT EXCEEDANCES DUE TO ATMOSPHERIC TURBULENCE

A.   INTRODUCTION

To determine the initial conditions occurring at the instant of
thrust decay in stage I, it is necessary to follow the motion of the
vehicle from the instant of release, through the wind shear spike and
turbulence to the altitude at which the thrust decay initiates. Normal-
ly this would be the case, however, the geometry of the vehicle under
consideration, namely, the large glider, coupled with the control system
provides a means of dissipating to the atmosphere large amounts of energy
in relatively short periods of time. Presuming that no significant dis-
turbance occurs between the encounter of the wind shear spike and the
initiation of thrust decay, it follows that one might reasonably expect
(analog records support this, see Section IV) that at the instant of
thrust decay the vehicle is entirely undisturbed. This would imply that
all initial conditions on perturbated quantities such as translation,
pitch, and the flexural modes are zero, and hence the decay of thrust
would induce no lateral loads (bending moments). However, if even a
slight deviation from this zero perturbation state exists, it would have
serious consequences since there exists at the altitude (180,000 ft) at
which the first staging occurs an aerodynamic pressure (40 psf) suffi-
cient to cause the system to be unstable. For long coast periods this
small destabilizing moment may cause initial conditions at the time of
second stage thrust build-up to be so large that the control system can-
not achieve stability. Even under ideal control conditions, the free
fall of the vehicle during coast would produce a velocity transverse to
the vehicle axis, thereby inducing an aerodynamic lift on the glider and
a destabilizing moment. Further, slight imperfections in the control
system on the mechanical alignment of the aerodynamic surfaces, motor
nozzle arrangements, etc., can provide additional sources from which non-
zero initial conditions can occur.

Finally, whatever the source of a nonzero initial condition or
destabilizing moment, the forces acting on the vehicle after the decay
of first stage thrust are gradually varying during the initial coast
period; hence it would seem that a simple quasi-static loads analysis
would be quite adequate.

The initial conditions on the coordinates specifying the motion of
the second stage portion of the vehicle result from the linear and angular
impulse occurring at separation as well as the destabilizing conditions
which occur during the coast periods preceding and following separation.

The most critical, and from a practical point of view, the most im-
portant lateral loads during the staging process result from the initia-
tion of thrust in the second stage booster with the nozzles in the "hard-
over" or extreme control position, since the survival of the second stage
depends on the ability of the control system to re-establish the program-
med attitude after the staging process. The following analysis is directed

toward determining the lateral loads (bending moments) induced by those initial conditions on the attitude and attitude rate which require a full vectoring of the motor nozzles at the ignition of the engines in the second stage.

B. FORMULATION OF THE PROBLEM

1. EQUATIONS OF MOTION

The perturbation equations of Appendix C, written with respect to body axes, are modified as follows:

$$I_o = m_{\ell k} = g = \text{coefficients of } \dot{m} = 0 \qquad (\text{V-1})$$

$$j = 1 \text{ (first coupled beam mode is used)} \qquad (\text{V-2})$$

$$\zeta_j = 0 \text{ (no structural damping)} \qquad (\text{V-3})$$

The thrust term in the equations of motion is modified to account for a ramp-type build-up; the term $T_o + (P_e - P_o) A$ is replaced by T_{max}:

$$T = \begin{cases} 0 & t < 0 \\ T_{max} \left(\dfrac{t}{\tau} \right) & 0 \leq t \leq \tau \\ T_{max} & t > \tau \end{cases} \qquad (\text{V-4})$$

where T_{max} : full thrust developed by the second stage booster at altitude.

τ : time required for build-up of thrust to full value.

$t = 0$: ignition of second stage engines.

2. GENERALIZED FORCES RESULTING FROM AERODYNAMIC FORCES

Simple first order piston theory is used to estimate the aerodynamic force acting on the glider; no aerodynamic forces are assumed to act on the booster. Only rigid body motion of the glider is taken into account in the calculation of the aerodynamic force.

$$Q_{q_z} = \frac{4A_G}{M_o} q_\varphi \left(\frac{\dot{q}_x^2}{2} \right) \qquad (\text{V-5})$$

$$Q_{q_\bullet} = \frac{4A_G}{M_o} \ q_\theta \left(\frac{\rho \dot{q}_x^2}{2}\right) x_c \qquad (V\text{-}6)$$

$$Q_{q_1} = \frac{4A_G}{M_o} \ \phi_1 \ (x_c) \ q_\bullet \left(\frac{\rho \dot{q}_x^2}{2}\right) \qquad (V\text{-}7)$$

$$Q_{q_s} = 0 \qquad (V\text{-}8)$$

$$\dot{q}_x = \text{constant (see Appendix A)} \qquad (V\text{-}9)$$

where A_G : planform area of the glider

M_o : Mach number

ρ : air density of 180,000 ft.

x_c : position of centroid of glider area with respect to mass center of second stage system.

3. GENERALIZED FORCE RESULTING FROM CONTROL SYSTEM

The control law used in this part of the study is similar to that described in Appendix D, however, the damping terms are neglected. The generalized force is given by:

$$Q_{q_\varsigma} = -K \left[q_\varsigma - K_\bullet(q_\theta + \phi_1'(x_A) \ q_1) - K_{\dot{\bullet}}(\dot{q}_\bullet + \phi_1'(x_R) \ \dot{q}_1) \right] \qquad (V\text{-}10)$$

where

$$K = (m_o \ \ell^2)\omega_n^2$$

ω_n : natural swiveling frequency of nozzles with hydraulic valve closed

$K_\bullet$: attitude gain

$K_{\dot{\bullet}}$: rate gain

4. INITIAL CONDITIONS

The initial conditions chosen are:

$$q_z(0) = \dot{q}_z(0) = q_1(0) = \dot{q}_1(0) = q_\delta(0) = \dot{q}_\delta(0) = 0 \qquad \text{(V-11)}$$

In conjunction with these, two distinct sets of initial condition on the perturbed angle, q_θ and $\dot{q}_\theta$ are:

$$\text{i)} \quad q_\theta(0) = 0 \qquad\qquad\qquad \text{(V-12)}$$

$$\dot{q}_\theta(0) \le \dot{q}_{\theta_0}$$

$$\text{ii)} \quad \dot{q}_\theta(0) = 0 \qquad\qquad\qquad \text{(V-13)}$$

$$q_\theta(0) \le q_{\theta_0}$$

where q_θ and $\dot{q}_\theta$ are such that a full vectoring of the motor nozzles are required to stabilize the vehicle.

5. SOLUTION OF THE EQUATIONS

An electronic analog, as described in Appendix G, has been used to solve the equations of motion; although a closed form solution can be obtained, the analytical determination of the initial conditions on q_θ and $\dot{q}_\theta$ specified above has been more economically gotten by the analog approach.

6. RESULTS

The maximum bending moments at the mass center of the second stage resulting from the sets of initial conditions and two values of τ are given in Fig. V-1.

Recorded on these figures for comparison is the calculated maximum quasi-static bending moment; the agreement indicates that a simple procedure for estimating maximum bending moment resulting from a "hard over" vectoring is sufficient.

The quasi-static bending moment (BM) is determined as follows:

$$\text{BM} = \sum_{x_i \ge 0} m_i \left(x_i \ddot{q}_z + x_i^2 \ddot{q}_\theta \right) \qquad \text{(V-14)}$$

where

$$\ddot{q}_z = \frac{T_{max}\,^q\mathfrak{S}\,max}{\displaystyle\sum_i m_i}$$

$$\ddot{q}_\Theta = \frac{T_{max}\,^q\mathfrak{S}\,max\ |x_T|}{\displaystyle\sum_i m_i x_i^2}$$

$\displaystyle\sum_{x_i \geq 0}$: a summation over all values of the integrand for which $x_i \geq 0$

C. CONCLUSIONS

The bending moment obtained under "hard over" vectoring of the motor nozzles is of such magnitude $(0.2 \times 10^6$ in-lbs) that no serious load problem will be expected from a staging process within the capabilities of the vehicle to maintain its stability. It appears that the real problem in staging is one of control to maintain stability, rather than of load.
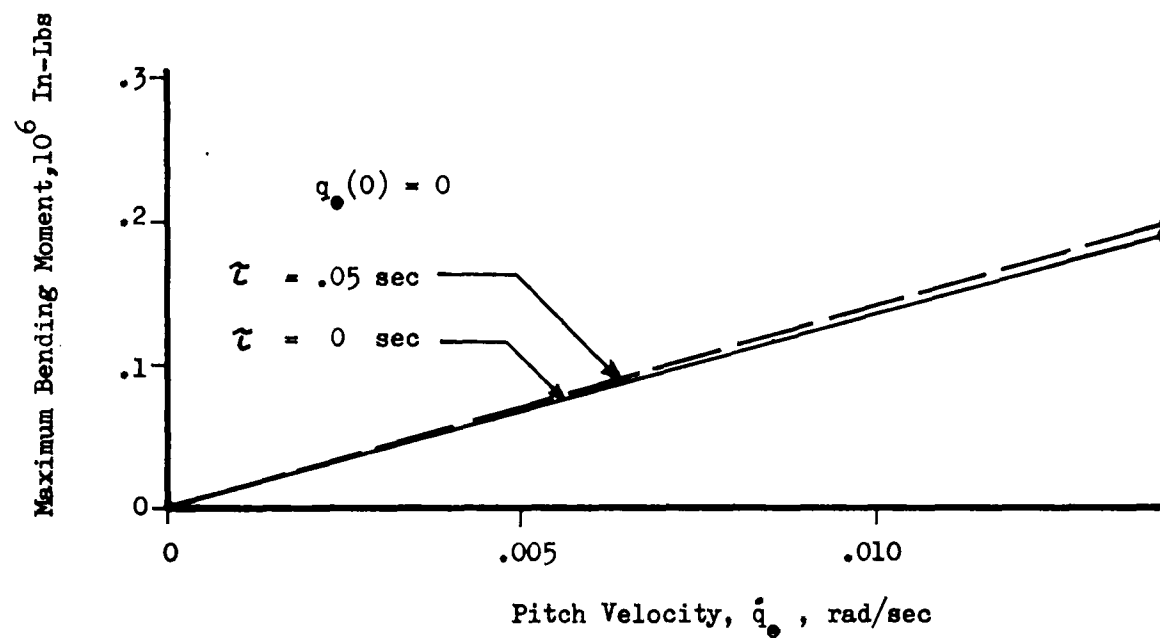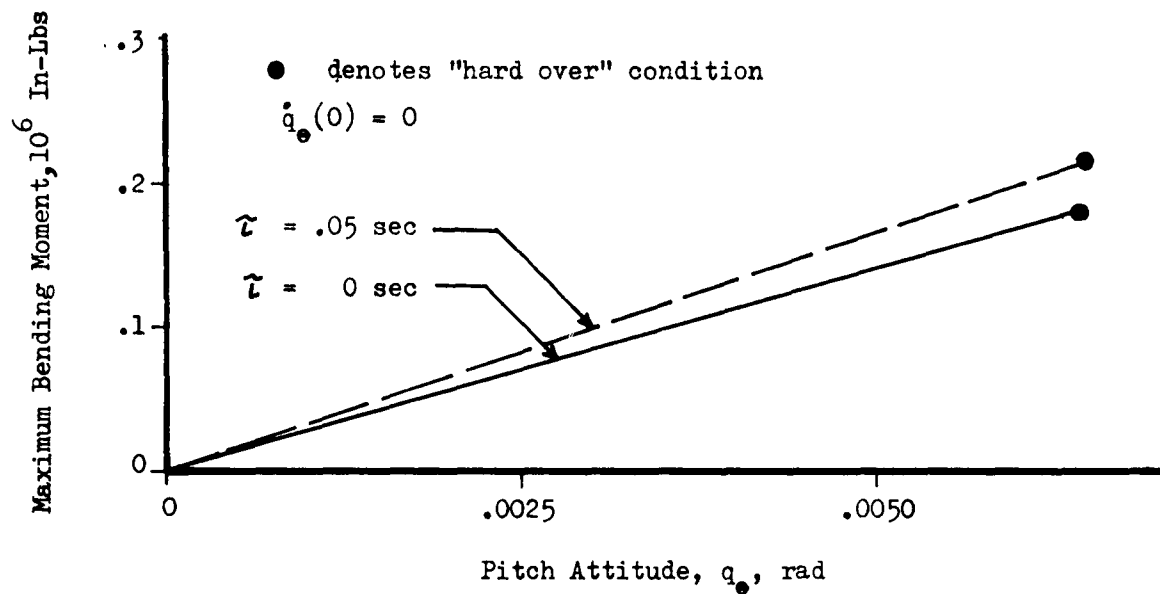
FIG. V-1   MAXIMUM BENDING MOMENT DUE TO PITCH ATTITUDE AND VELOCITY
DURING STAGING (STATIC "HARD-OVER" BENDING MOMENT = 200,000 IN-LBS)

SECTION VI

RE-ENTRY

A. GENERAL DISCUSSION

The re-entry problem can be divided into two flight regimes.
One regime is the flight through the stratosphere in which the major
concern is the temperature environment. The other regime is the
flight through the troposphere in which the major concern is the
atmospheric turbulence.

On the flight through the stratosphere the major problem is
to design a structure to withstand the elevated temperatures and
possible maneuvers. Even if the loads seem small due to possible
re-entry maneuvers, it must be remembered that the allowables have
been reduced considerably due to the elevated temperatures.

As the glider descends, the structure will cool and will be sub-
jected to a more conventional loading problem, namely air turbulence.

In this section the effects of elevated temperatures are discussed,
maneuver loads are calculated and loads due to atmospheric turbulence
are calculated. The major emphasis is on loads due to atmospheric
turbulence.

B. THERMAL ENVIRONMENT

Actually the thermal environment is more a detailed design problem
than a dynamic loads problem. It is the structural designer's problem
to determine the details such that the glider will withstand the thermal
environment.

1. EQUILIBRIUM TEMPERATURES

For the purpose of illustration some work has been done to show
the effects of temperatures on a typical re-entry trajectory. Appendix
A specifies the reference trajectory. Rather than restrict the glider
to the specified trajectory, some leeway is allowed. This leeway
allows the glider to be 10,000 feet below the specified trajectory
at any velocity. For the lower altitude limit a 20° angle of attack
is used while a 45° angle of attack is used for the reference tra-
jectory. This angle results from a short transient maneuver.

The equilibrium temperatures have been calculated using the methods
described in Reference 127. Listed in Table VI-1 are the values of
velocity, altitude, and angle of attack investigated. In addition,
the stagnation temperatures that have been calculated are listed. The
first set of parameters included in Table VI-1 corresponds to a point

in the boost trajectory chosen for the purpose of showing that the thermal effects are negligible.

TABLE VI-1 STAGNATION TEMPERATURES

Velocity, fps	Altitude, ft	Angle of attack, Degrees	Stagnation temp Degrees, F.
1,875 Boost	35,000	0	200
21,400	230,000	45	4400
21,400	220,000	20	4600
16,100	190,000	45	4150
16,100	180,000	20	4330
3,800	100,700	45	1050
3,800	90,700	20	1100

Typical plots of equilibrium temperatures for angles of attack of 45° and 20° can be seen in Figure VI-1 and VI-2. The equilibrium temperatures that have been calculated at some points on the glider appear to be large. Practical design would require that these temperatures be reduced by changing the trajectory, configuration, or by incorporating a suitable refractory material.

2. REDUCTION OF THE MODULUS OF ELASTICITY

One effect of elevated temperature is the reduction of the modulus of elasticity and the consequent reduction of natural frequencies of the glider. However, for the glider studied, the frequencies are sufficiently high that the reduction is not detrimental. For a typical re-entry material the change in frequency with temperature is shown below.

ω_0 = Frequency at room temp.

ω_t = Frequency at temp. t

$$\frac{\omega_t}{\omega_0}$$

1

500°   1000°   1500°   2000°   2500°
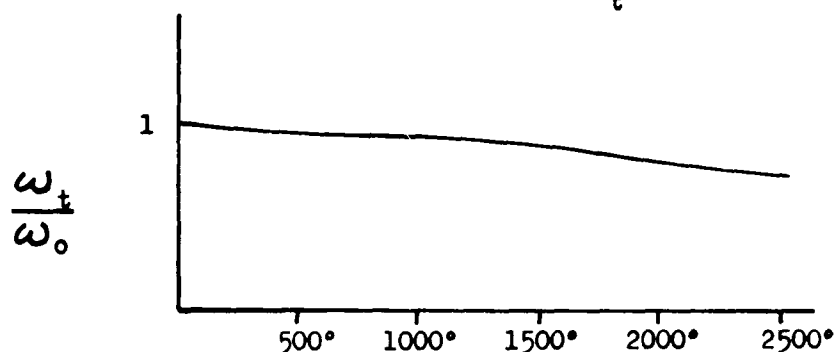
3. REDUCTION OF ALLOWABLES

As illustrated below, the reduction of allowable stress in the re-entry material used above is the most significant effect of temperature.

$(F_{Ty})_o$ = Tension yield stress at room temp.

$(F_{Ty})_t$ = Tension yield stress at temp. t.
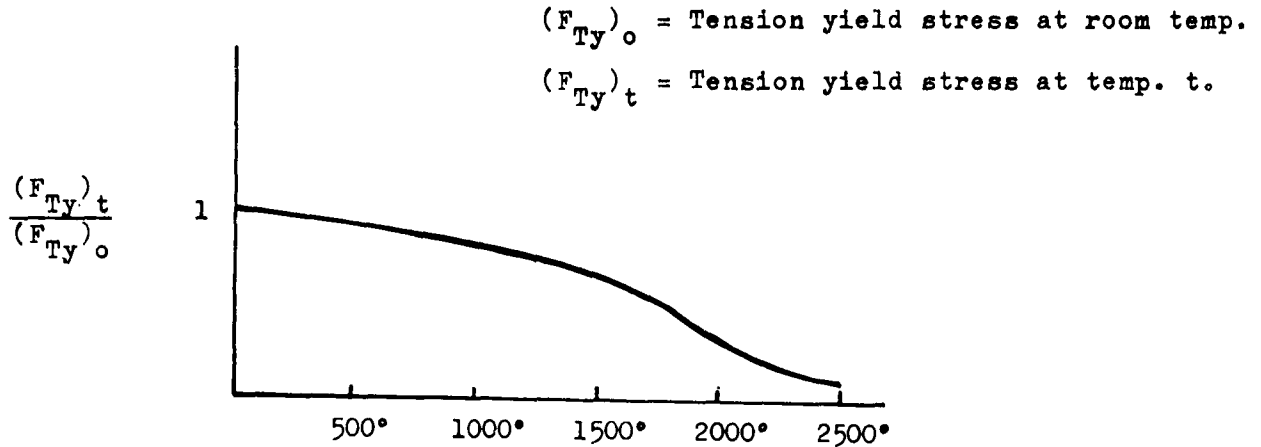
C. MANEUVER

A static aeroelastic analysis of maneuver loads has been conducted. The results in panel load per g are shown in Figure VI-3.

D. GUSTS

1. INTRODUCTION TO GUST ANALYSIS

The response of any vehicle due to atmospheric turbulence may be treated by considering the atmosphere as a series of discrete gusts or as continuously random turbulence. The latter method as discussed in Section IV and Appendix G is a more realistic representation of the atmosphere tthan the former.

To determine if the passage of any vehicle through atmospheric turbulence is critical some measure of load must be obtained. Usually the bending moment distribution is satisfactory, but for a delta-winged glider a better, though more complicated, measure is panel loads.

Since for our particular case the glider loads due to the atmospheric turbulence are not critical, the bending moment at station 327 is taken for demonstrative purposes. In one case, however, the panel loads are determined to show the method and the results. If the loads are critical more cases can be considered. For some cases the acceleration of the center of gravity of the vehicle is determined in addition to the bending moment.

2. FORMULATION OF PROBLEM

The glider is represented by as many as four degrees of freedom, i.e., rigid body translation, rigid body pitch, and the first two coupled flexible degrees of freedom. The glider is assumed to be cool, and not to have suffered permanent deformations during re-entry.

The aerodynamic forces acting on the glider have been determined by assuming that the lift acting on each panel depends only on the local motion with a modified lift curve slope determined from a combination of experimental and theoretical work. This assumption neglects the effects of pressure interaction between a given panel and another. In addition, no aerodynamic lag effects are included, and the glider controls are assumed to be locked.

The perturbation equations of motion have been developed using the wind tunnel axes as described in Appendix D.

$$
\begin{bmatrix} \sum m & & & \\ & \sum mx^2 & & \\ & & M_1 & \\ & & & M_2 \end{bmatrix} \begin{Bmatrix} \ddot{q}_T \\ \ddot{q}_\bullet \\ \ddot{q}_1 \\ \ddot{q}_2 \end{Bmatrix} + \begin{bmatrix} 0 & & & \\ & 0 & & \\ & & 2M_1 \zeta_1 \omega_1 & \\ & & & 2M_2 \zeta_2 \omega_2 \end{bmatrix} \begin{Bmatrix} \dot{q}_T \\ \dot{q}_\bullet \\ \dot{q}_1 \\ \dot{q}_2 \end{Bmatrix}
$$

$$
+ \begin{bmatrix} 0 & & & \\ & 0 & & \\ & & \omega_1^2 M_1 & \\ & & & \omega_2^2 M_2 \end{bmatrix} \begin{Bmatrix} q_T \\ q_\bullet \\ q_1 \\ q_2 \end{Bmatrix} = \begin{Bmatrix} Q_{q_T}(A) \\ Q_{q_\bullet}(A) \\ Q_{q_1}(A) \\ Q_{q_2}(A) \end{Bmatrix} \tag{VI-1}
$$

where:

$$
\begin{aligned}
Q_{q_T}(A) &= q \, C_{L_\alpha} \sum s \alpha \\
Q_{q_\bullet}(A) &= q \, C_{L_\alpha} \sum s x \alpha \\
Q_{q_1}(A) &= q \, C_{L_\alpha} \sum s \phi_1 \alpha \\
Q_{q_2}(A) &= q \, C_{L_\alpha} \sum s \phi_2 \alpha
\end{aligned} \tag{VI-2}
$$

Σ : Represents Summation Over the Vehicle

$$\alpha = q_\theta + \frac{V}{V}g - \frac{\dot{q}_z}{V} - \frac{\dot{q}_\theta x}{V} - \phi_1 \frac{\dot{q}_1}{V} - \frac{\phi_2 \dot{q}_2}{V} + \phi_1' q_1 + \phi_2' q_2 \qquad (VI-3)$$

$$\gamma_1 = \gamma_2 = .02$$

q : Dynamic Pressure

V_g : Velocity of Gust

S : Panel Area

C_{L_α} : Lift-curve Slope

x : Distance From Mass Center to Panel

The force summation has been used to determine the various loads.

The vehicle properties are represented by constants for each altitude band considered, and the constants are evaluated at the midpoint of each band. The values that are used can be found in Table VI- 2. The value of the lift-curve slope is determined by using Fig. IV-2.

TABLE VI-2 — VEHICLE PROPERTIES

Altitude Band Feet	Dynamic Pressure lb/ft^2	Air Speed ft/sec	Speed of Sound ft/sec	Mach Number	Lift-curve Slope
0 - 10,000	214	457	1098	.416	1.788
10,000 - 20,000	214	535	1058	.506	1.825
20,000 - 30,000	214	634	1017	.623	1.875
30,000 - 40,000	214	762	973	.783	1.925

3. **RESULTS**

a. **RANDOM GUSTS**

In order to determine the number of degrees of freedom that are necessary for accuracy, a two degree of freedom and a four degree of freedom system have been examined using the continuous atmospheric turbulence approach as outlined in Section IV. The bending moment expected once in a hundred flights at an average altitude of 1000 feet and at a speed of 430 fps for station 327 has been determined. The results can be seen in Table VI-3.

TABLE VI-3 - EFFECTS OF FLEXIBILITY

Number of Degrees of Freedom	Bending Moment Station 327
2	45.48×10^3 in-lbs
4	48.72×10^3 in-lbs

The addition of the flexible degrees of freedom results in approximately a 7% increase in bending moment. For this glider the frequencies of the flexible degrees of freedom are 6.57 and 14.06 cps. The flexible degrees of freedom will be more important if the frequencies are of the order of one or two cycles per second. For the vehicle studied two degrees of freedom seem adequate for demonstrative purposes.

Using two degrees of freedom and assuming that the glider travels approximately 100,000 feet in each altitude band, the bending moment at station 327 and the center of mass acceleration expected once in one hundred flights for each altitude band have been calculated and are shown in Table VI-4.

TABLE VI-4 - RESPONSES DUE TO CONTINUOUS TURBULENCE

Altitude Band Feet	Bending Moment Station 327 10^3 in-lbs	Center of Mass Acceleration ft/sec^2
0 - 10,000	45.0	28.57
10,000 - 20,000	38.88	25.17
20,000 - 30,000	37.56	24.26
30,000 - 40,000	29.40	19.00

As can be seen both measures of response are smaller at the higher altitudes and increase as the glider approaches sea level.

In order to determine the bending moment expected once in one hundred flights the procedure outlined in Section IV has been used. The results are presented in Figure VI-4 which gives the exceedance curve for the total flight. Fig. VI-4 shows that the bending moment expected once in one hundred flights is 48,120 in-lbs.

b. DISCRETE GUSTS

As previously mentioned only one case is considered in determining the panel loads. The vehicle is assumed to be flying with a

speed of 430 fps, a dynamic pressure of 214 lb/ft^2 and at an altitude of 1,000 feet. The loads equations have been written for thirty panel points, and they have been solved along with the equations of motion for three degrees of freedom on the analog computor using a $(1-\cos\omega t)$ forcing function. The frequency used corresponds approximately to the pitch frequency which is six-tenths cycle per second.

Typical responses to the $(1-\cos\omega t)$ input are shown in Fig. VI-5.

The panel loads for a one foot per second gust are reduced to a pressure distribution in pounds per square inch per panel. Since some of the load peaks are 180° out-of-phase, two loading conditions corresponding to the first and second peaks of time history of loads have been computed. The results can be seen in Fig. VI-6 and VI-7. To determine the loads for any gust magnitude it is only necessary to multiply each load by the gust magnitude.

Temperature, °F

$\alpha = 45°$

Altitude = 230,000 Ft.
Velocity = 21,400 fps
Turbulent Flow, Lower Surface
Laminar Flow, Stagnation Point
and Leading Edge

FIG. VI-1 EQUILIBRIUM TEMPERATURES

Temperature, °F

$\alpha = 20°$

Altitude = 220,000 Ft.
Velocity = 21,400 fps
Turbulent Flow, Lower Surface
Laminar Flow, Stagnation Point
and Leading Edge

FIG. VI-2 EQUILIBRIUM TEMPERATURES

Panel Load per g , Lb/In²

FIG. VI-3 MANEUVER LOADS

FIG. VI-4   BENDING MOMENT EXCEEDANCES DUE TO ATMOSPHERIC TURBULENCE
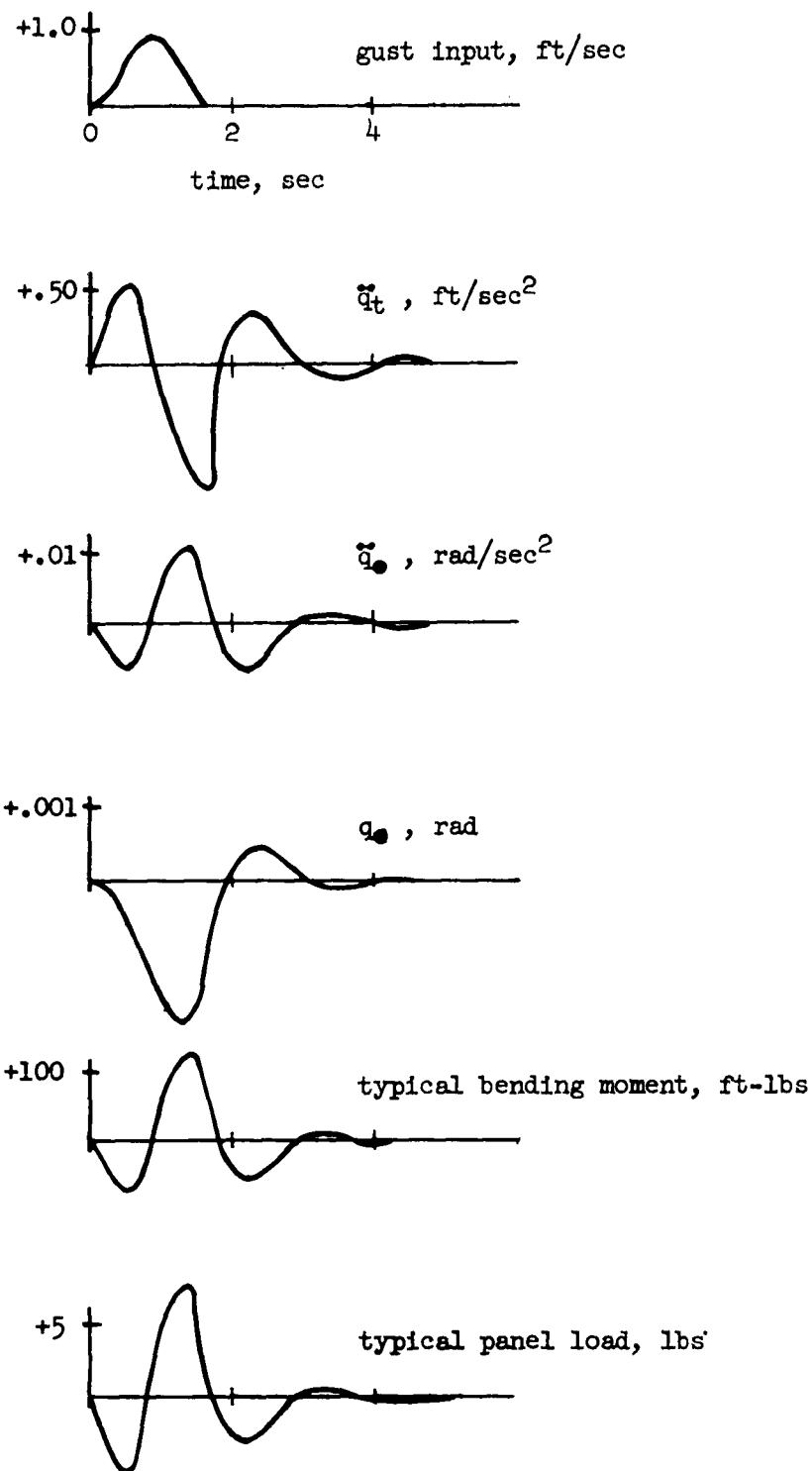
FIG. VI-5 TYPICAL RESPONSES TO GUST INPUT

Panel Loads, 10^3 Lbs/In^2
Inertia Loads plus Aerodynamic Loads

One Foot per Second (1-COS ω t) Gust
ω = .6 CPS
First Peak
V = 430 Ft/Sec
h = 1000 Ft

								-1.24	-1.91
						1.43	1.58	1.43	1.35
				1.79	1.72	1.75	-.556	1.27	1.43
		1.79	1.57	1.03	.873	.794	.675	.556	.476
.866	-.238	-5.56	-7.94	-8.41	.476	0	.159	-4.60	-14.3
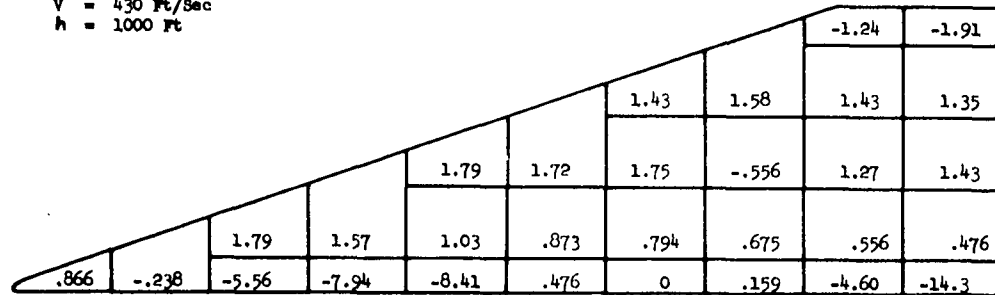
FIG. VI-6 DISCRETE GUST LOADS

Panel Loads, 10^3 Lbs/In^2
Inertia Loads plus Aerodynamic Loads

One Foot per Second (1-COS ω t) Gust
ω = .6 CPS
Second Peak
V = 430 Ft/Sec
h = 1000 Ft

								2.15	2.86
						-2.38	-2.17	-2.46	-2.38
				-2.71	-2.51	-2.54	.556	-2.46	-2.38
		-2.98	-2.38	-1.59	-1.39	-1.23	-1.11	-.913	-.794
.866	-.381	8.25	12.4	12.5	- .635	0	- .222	6.98	22.2
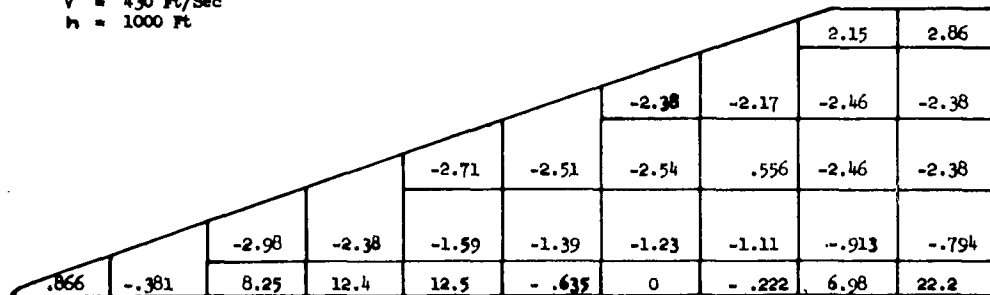
FIG. VI-7 DISCRETE GUST LOADS

VII. LANDING AND RECOVERY

A. GENERAL DISCUSSION

1. INTRODUCTION

Landing might be defined as the cessation of the relative motion between a vehicle and a solid or liquid at or near the boundary of the medium. While crude, this definition serves to describe, in many cases, the landing of airborne vehicles. One of the major problems encountered in landing is confined, though not solely, to the determination of the component normal to the boundary of the landing surface of the time rate of change of the relative momentum of the vehicle. Although it is possible to gradually reduce this component to zero at contact of the vehicle with the boundary in the case of some vehicles (dirigibles) such is not the case in the more conventional craft which attain a nominal terminal velocity in normal landing (as in the flare-out condition of a winged vehicle, the "free-fall" of a ballistic missile, or a parachuted body). For vehicles of the latter type, it is at and subsequent to contact that the large landing loads are induced.

2. MECHANICS OF LANDING

Those laws of physics which are pertinent to the investigation of the landing problem are:

> Conservation of mass
> Conservation of momentum
> Conservation of energy
> Clausius-Duheim inequality

It is rather significant to note that a change in the momentum of the landing vehicle need not necessarily imply a change in the energy of the vehicle, but merely a conversion of the energy to a different form. On the other hand, the converse, as related to external forces, is not true. This occurs for the simple reason that the application of a force F will always be accompanied by an impulse, $\int F \, dt$, but it is possible that no work $\int F \cdot dr$ will be done if the force is transverse to the displacement or, what is more applicalbe in the case of landing, if the forces act through no displacement. Consider, as a comparative set of examples, the following:

i. A translating rigid vehicle lands on a rigid frictionless surface in such manner as to cause the rear gear to first come into contact with the surface. The contact force F acts through zero displacement. Hence no work is done on the vehicle by F; there is a change in the linear momentum in the amount of $\int F_n \, dt$ and there is a change in the angular momentum. Neglecting dissipative forces, the energy is conserved and whereas, before the vehicle was translating, it is now translating (in general) and rotating.

ii. If the rear gear is provided with a deformable mechanism on one end of which acts the landing force $\bar{F}_1$ and on the other end a force $\bar{F}_2$ transmitted in turn to the vehicle, then while the work done by $\bar{F}_1$

(for a rigid frictionless landing surface) would be zero, the work done by F_2 would not be zero.

Hence, part of the energy now appears in the work of deforming the landing mechanism, the remainder occurring in rigid body translation and rotation just as before. If the landing mechanism is partially elastic, some of the work done by $\bar{F}_2$ has simply converted the rigid body energy into the potential energy of the elastic mechanism, the remainder of the work done by $\bar{F}_2$ in permanently deforming the mechanism appears as a change in internal energy of material (rise in temperature thus satisfying the Clausius-Duheim inequality). This landing mechanism illustrates only one of many ways in which the energy of a body may change form (kinetic to potential in the case of elastic mediums, and kinetic to thermal in the case of dissipative mediums). Note that in no instance has the total energy of the vehicle been decreased, rather it has been transformed. Only in the event that the forces external to the vehicle act through finite displacements is the total energy of the vehicle changed (e.g. aerodynamic, hydrodynamic, gravitational, landing surface).

At the instant of impact and for a short duration thereafter, the external forces, normal to the landing surface, acting on the vehicle serve to dissipate energy, save one, the gravitational forces about which little can be done in ordinary cases. Although significant quantities of energy can be removed from the system (vehicle) by these forces (aerodynamic, hydrodynamic, friction), so, too, can significant quantities of gross kinetic energy be transformed into heat by dissipative landing mechanisms. The latter method, while not removing energy from the vehicle, does transform it into internal energy of the material of the vehicle, an irreversible process which decreases the kinetic energy and transforms it in a manner such that once transformed, this energy (heat) will not reappear as kinetic energy. Insofar as the heat thus produced does not result in prohibitive temperatures, the "dissipative landing mechanism" provides an effective method for decreasing the kinetic energy. Similar remarks apply to other mechanisms in the vehicle which are capable of providing irreversible transformations of energy.

3. BOUNDS ON THE ACCELERATION

Bounds on the maximum acceleration of the mass center induced during landing can be set independent of the type of mechanism employed. Consider a vehicle having mass M and a velocity of the mass center $\bar{V}$. The resultant force acting on the vehicle normal to the boundary at any instant is:

$$\bar{n} \cdot \bar{F} = \bar{n} \cdot \frac{d}{dt} (M\bar{V}) \qquad (VII-1)$$

In scalar notation:

$$F_n = \frac{d}{dt} (MV)_n \qquad (VII-2)$$

where

$\bar{n}$: defines the normal to landing surface, and it is assumed that $d\bar{n}/dt = 0$.

If $\int_0^{\tau} F_n \, dt < - M V_n(0)$ then the vehicle will continue toward or penetrate the boundary of the landing medium; now let τ_1 be the first instant such that:

$$\int_0^{\tau_1} F_n dt = - MV_n(0) \qquad\qquad (\text{VII-3})$$

and let S_n be the distance traveled normal to the boundary by the mass center from the instant of contact:

$$S_n(\tau_1) = \int_0^{\tau_1} V_n dt \qquad\qquad (\text{VII-4})$$

It would follow from the relation $V_n \, d\, V_n = a_n \, dS_n$ that

$$\left[a_n(t)\right]_{max} \geq \frac{V_n^2(0)}{2\, S_n(\tau_1)} \quad ; \; 0 \leq t \leq \tau_1 \qquad\qquad (\text{VII-5})$$

and that $\left[a_n(t)\right]_{max} = \dfrac{V_n^2(0)}{2\, S_n(\tau_1)}$ (VII-6)

if and only if $a_n(t) = \left[a_n(\tau)\right]_{max} = $ constant

where $\left[\quad\right]_{max}$ means "maximum value of."

Hence, a lower bound on the maximum acceleration can be easily set by knowing the initial normal velocity $V_n(0)$ and the displacement of the mass center.

Unfortunately, no rational basis exists for placing an upper bound on the acceleration of the mass center without detailed knowledge of the structure, landing gear, etc. However, acceleration displacement histories chosen arbitrarily might provide a rough estimate (142).

Consider a landing on a linear elastic medium.

Assume $a_n = k\, S_n$, then

$$\int a_n dS_n = \tfrac{1}{2} k\, S_n^2(\tau_1) = \tfrac{1}{2} a_n(\tau_1)\, S_n(\tau_1) = \tfrac{1}{2} V_n^2(0) \qquad (\text{VII-7})$$

Hence,

$$a_n(\tau_1) = \frac{V_n^2(0)}{S_n(\tau_1)} \qquad\qquad (\text{VII-8})$$

Comparison of Eqns VII-5 and VII-8 indicates that, for comparable conditions, the maximum normal acceleration of a vehicle landing on a linear elastic medium will be twice that obtained for a lower bound.

4. SPECIFIC MECHANISMS USED IN LANDING

The landing problem is critically dependent on the square of the normal component of velocity at the instant of contact, $V_n^2(0)$; hence mechanisms such as flaps, parachutes and reaction jets are significant in the successful solution to the overall landing problem. For indeed, the lower bound on the acceleration is primarily determined by $\bar{V}_n(0)$, Eqn. (VII-5).

Having $V_n(0)$ and $S_n(\mathcal{T}_1)$, the upper bound will depend on the specific landing mechanism. The mechanics of several landing mechanisms are described below:

i. In the conventional approach, only part of the total kinetic energy is associated with the normal component of velocity, the other part (often large) is associated with the tangential component of velocity. Hence, if the flight path is primarily tangential to the surface, the terminology of tangential landing is employed. In a conventional approach, oleo struts are often used; energy of deformation is irreversibly transformed into heat by flow of a viscous fluid through an orifice. Plastic straps may be used (replaceable after each landing) to perfor... the same function, the deformation of a plastic material being the irreversible process used to transform kinetic energy into heat.

Either of these struts can be used with tires or skids in the case of landing on a solid surface or with skis or pontoons in the case of landing on a fluid surface.

The amount of energy associated with the normal component of velocity dissipated into a solid surface is generally insignificant; however, in the case of landing on a fluid, considerable portions of this energy can be transferred from the vehicle to the fluid at a variety of rates (depending on the geometry of the ski or pontoon).

ii. The "normal" approach is characterized by the flight path being nearly normal to the landing surface. The nose spike has been used in the terminal phase of recovery of vehicles; the kinetic energy of the vehicle using a nose spike is dissipated into the medium on which the vehicle lands, solid or fluid; some kinetic energy is dissipated by deformation of the spike itself. The hydraulic limiter can be used alone or in series to modify the deceleration-time history, by providing a dissipative mechanism in which the deformation rate versus energy transformed is known. The airbag is much the same as hydraulic limiter, the controlled dissipative mechanism being attached to either the landing surface or the vehicle (52).

B. GROUND LANDING

1. DESCRIPTION OF THE SYSTEM STUDIED

The glide vehicle is idealized as a plate having two flexible modes, fitted with a single conventional oleo-pneumatic strut and wheel (forward gear) and two symmetrically placed plastic-elastic yield straps and skid (after gears), and acted upon by an aerodynamic lift and damping moment. The analog computer has been employed to solve the resulting nonlinear equations of motion; electronic representation of the oleo-pneumatic strut and the plastic-elastic yield strap have been made by means of a collection of relatively simple circuit elements (see Appendix G).

The landing surface is presumed to be fixed with respect to a suitable inertial reference frame. Three auxiliary variables are introduced in addition to the generalized coordinates shown in Fig. VII-6.

y_1 : deformation of the oleo-pneumatic strut

y_2 : displacement of the center of the wheel of the forward gear.

Y_3 : displacement of the upper end of the after gear strut

Also two body fixed coordinates ξ, η, in the plane of the wing are introduced for the purpose of specifying the gear locations; see Fig. VII-6.

The Lagrangian equations governing the motion are:

$$
\begin{bmatrix}
\Sigma m & & & \\
& \Sigma mx^2 & & \\
& & M_1 & \\
& & & M_2
\end{bmatrix}
\begin{Bmatrix}
\ddot{q}_z \\
\ddot{q}_\theta \\
\ddot{q}_1 + \omega_1^2 q_1 \\
\ddot{q}_2 + \omega_2^2 q_2
\end{Bmatrix}
=
\begin{Bmatrix}
Q_{q_z}(A) + Q_{q_z}(L) \\
Q_{q_\theta}(A) + Q_{q_\theta}(L) \\
Q_{q_1}(A) + Q_{q_1}(L) \\
Q_{q_2}(A) + Q_{q_2}(L)
\end{Bmatrix}
\qquad \text{(VII-9)}
$$

where,

Σm : mass of the glider

Σmx^2 : mass moment of inertia about the mass center

M_1, M_2, q_1, q_2, ω_1, ω_2 : generalized masses, generalized coordinates and characteristic frequencies, respectively, associated with the symmetrical normal modes of glider flexibility.

$Q(A)$, $Q(L)$: generalized forces associated with aerodynamic and landing forces respectively.

2. GENERALIZED FORCE ARISING FROM AERODYNAMIC FORCES, $Q_x(A)$

The aerodynamic lift $\bar{L}_1$ is assumed to act through the mass center of the vehicle and normal to the landing surface and is dependent only on the rigid body angle of attack. The aerodynamic moment L_2 is dependent only on the body rotational motion. The terms arising from $Q_x(L)$ are given by:

$$Q_{q_z}(A) = -1/2 \rho \left[\dot{q}_x(0)\right]^2 S + C_{L_\alpha}\left[\frac{+\dot{q}_z - \dot{q}_z(0)}{\dot{q}_x(0)} + q_\Theta - q_\Theta(0)\right] \tag{VII-10}$$

$$Q_{q_\Theta}(A) = -1/4 \rho \left[\dot{q}_x(0)\right]^2 SC^2 C_{M_{\dot{\Theta}}} \dot{q}_\Theta \tag{VII-11}$$

$$Q_{q_n}(A) = 0 \tag{VII-12}$$

where

ρ : air density (standard

C_{L_α} : slope of the lift-angle of attack curve (assumed constant)

S : reference area (plan form area of the glider)

C_{M_Θ} : coefficient of aerodynamic damping moment (assumed constant).

C : reference length (length of glider)

Obviously no great effort has been expended to account in detail for the aerodynamic forces, the reason being that upon landing , the attitude, ψ (equilibrium glide) is abruptly changed, so as to cause $L_1 \longrightarrow 0$, adding to the impact a force almost equal to the weight. To include this effect seemed highly significant, but the manner in which $L_1 \longrightarrow 0$ as $\psi \longrightarrow 0$ is estimated to be of little significance; hence a simple aerodynamic theory is used. The dissipation of energy resulting from aerodynamic damping provides a refinement in the analysis without a disproportionate amount of additional labor.

3. GENERALIZED FORCE ARISING FROM LANDING GEAR CONTACT (137) $Q_x(L)$

The forward gear is composed of a linear elastic tire of neglible mass, mounted on the end of a massless oleo strut which acts as a rigid rod until a fixed preload is exceeded; thereafter it acts as an energy absorber by metering a viscous flow of oil through an orifice and allows an isothermal compression of the gas in the strut column. The forward gear force (assumed normal to landing surface) acting on the glider is given by:

$$F_1 = \begin{cases} 0, & y_2 \leq 0 \\[2ex] ky_2, & 0 < y_2 < \dfrac{P_1 A_a}{k}, \ y_1 \leq 0 \\[3ex] ky_2 = \dfrac{\rho_o A^3 |\dot{y}_1| \dot{y}_1}{2C_D^2 \ a^2(y_1)} + P_1 A_a \ \dfrac{\ell_1}{\ell_1 - y_1}, & y_2 \geq \dfrac{P_1 A_a}{k}, \ y_1 > 0 \end{cases} \qquad \text{(VII-13)}$$

where

k :   tire spring constant

A :   net area of the oleo pneumatic cylinder

$a(y_1)$:   net orifice area

C_D :   orifice coefficient

$P_1 A_a$:   gas-spring preload

ρ_o :   mass density of oil

P_1 :   air pressure in fully extended strut

ℓ_1 :   length of air column

While the assumption that the compression of the gas column in the strut takes place isothermally is probably not as sound physically as an assumption of adiabatic compression, fair correlation is obtained using the isothermal assumption in practice; moreover, the problem of simulating the compression is somewhat   simplified by using the isothermal assumption.

The components of the force acting on the rear gears (plastic-elastic yield strap) normal to the landing surface, F_2, as a function of deformation y_3 are described in FIG. VII-7. Let $f(y_3)$ be the ordinate of the curve in FIG. VII-7; then,

$$F_2 = \begin{cases} 0, & y_3 \leq y_{3_{max}} - \dfrac{f(y_{3_{max}})}{k_E} \\[3ex] f(y_{3_{max}}) - k_E(y_{3_{max}} - y_3), & y_{3_{max}} - \dfrac{f(y_{3_{max}})}{k_E} < y_3 \leq y_{3_{max}} \\[3ex] f(y_3), & y_{3_{max}} \leq y_3 \end{cases} \qquad \text{(VII-14)}$$

where $y_{3_{max}}$ is the maximum of the positive values of y_3 obtained up to the instant in question, and k_E is the slope of the elastic recovery portion of the curve shown in Fig. VII-7.

The horizontal component of the force acting on the rear gears, F_3, results from friction between the skids and the landing surfaces:

$$F_3 = -\mu F_2 \tag{VII-15}$$

where μ : coefficient of friction

Having defined these forces, Q_x (L) becomes:

$$Q_{q_z}(L) = F_1 + F_2 \tag{VII-16}$$

$$Q_{q_\theta}(L) = -F_3 d_2 - F_1 a + F_2 b \tag{VII-17}$$

$$Q_{q_n}(L) = \phi_n(\xi_1, \eta_1) F_1 + \phi_n(\xi_2, \eta_2) F_2 \tag{VII-18}$$

$$+ \phi_n'(\xi_2, \eta_2) F_3 d_2$$

4. **GEOMETRICAL CONSTRAINTS**

The various coordinates are not all independent; certain obvious geometrical constraints are necessary; see Fig. VII-6.

$$q_z + bq_\theta + \sum \phi_j(\xi_2, \eta_2) q_j + y_3 = 0 \tag{VII-19}$$

$$q_z - aq_\theta + \sum \phi_j(\xi_1, \eta_1) q_j + y_1 + y_2 + (d_2 + (a+b) \sin \psi_o - d_1) = 0 \tag{VII-20}$$

5. **INITIAL CONDITIONS**

An equilibrium glide approach, at a specified sinking speed requires:

$$q_z(0) = 0 \tag{VII-21}$$

$$\dot{q}_z(0) : \text{ specified sinking speed} \tag{VII-22}$$

$$\ddot{q}_z(0) = 0 \tag{VII-23}$$

$$q_\theta(0) = 0 \tag{VII-24}$$

$$\dot{q}_\theta(0) = 0 \tag{VII-25}$$

$$\ddot{q}_\theta(0) = 0 \tag{VII-26}$$

Presuming that the modal displacement and modal velocity of the vehicle are zero at the instant of contact requires:

$$q_n(0) = \dot{q}_n(0) = 0 \text{ for each n.} \qquad \text{(VII-27)}$$

The zero datum of y_3 is specified such that at the instant of contact of the after gear with the landing surface, i.e. $t = 0$:

$$y_3(0) = 0; \qquad \text{(VII-28)}$$

and the zero datum of y_2 is specified at the instant of initial contact of the forward gear with the landing surface, i.e., $t = \tilde{\mathcal{L}}$:

$$y_2(\tilde{\mathcal{L}}) = 0 \qquad \text{(VII-29)}$$

6. SOLUTION OF THE EQUATIONS

The nonlinear equations of motion thus obtained present a difficult problem, if one were to use ordinary methods of digital solution; however, the solution is easily obtained by electronic analog, as described in Appendix G.

7. RESULTS

The influence of the flexibility of the glider, the location of after gear $(\mathcal{F}_2, \eta_2)$, the metering pin shape $(a(y_1))$, Eqn. (VII-13) and the ultimate load on the yield strap load-deformation curve Fig. VII-7 on the load induced in the gears and at the pilot station are given in Table VII-1 and VII-2 respectively.

Typical traces obtained from the analog study are shown in Figs. VII-8 and VII-9.

The influence of the metering pin shape on the force F_1 is explicitly illustrated in Figs. VII-10 and VII-11.

8. CONCLUSIONS

The analysis given is believed to be adequate for the purpose of determining the force environment of the vehicle under conventional landing conditions. The use of an analog provides a simple experimental method of changing the parameters and minimizing the loads. For the particular vehicle studied, it would seem that a rigid body analysis would be quite adequate; and one might extend this conclusion to vehicles of similar configuration in which the first characteristic frequency is of the order of 6.5 cps.

C. SEA LANDING (148)

1. GENERAL DISCUSSION

The purpose of this discussion is to present the state of the art of solving hydrodynamic impact problems (163).

a. Formulation of the Problem

Consider a system ,S, having two elements:

    1. A rigid body

    2. An ideal fluid

If the rigid body has a velocity $\bar{V}_0$ initially, and the fluid is
motionless initially, and if the mass of S is conserved, then
the conservation of momentum states that:

$$M\bar{V} - M\bar{V}_0 + \int_{\text{vol. fluid}} \rho \bar{v} d\mathcal{V} = 0 \qquad \text{(VII-30)}$$

where   M : mass of rigid body

           $\bar{V}$: velocity of M

           $\bar{v}$: velocity field of fluid

           ρ : density of fluid

           $d\mathcal{V}$: incremental volume of fluid

Consider a single direction, say the vertical, then (1) can be
written:

$$\bar{a} \cdot (M\bar{V} - M\bar{V}_0) + \bar{a} \cdot \int_{\text{vol. fluid}} \rho \bar{v}\, d\mathcal{V} = 0 \qquad \text{(VII-31)}$$

where $\bar{a}$: unit vector in the vertical direction.

Let $mV = \bar{a} \cdot \int \rho \bar{v} d\mathcal{V}$ (VII-32)

Eqn. (VII-32) serves to define m, the virtual mass; that is, a
mass having the same velocity component as M during the impact,
and hence m appears mathematically to act with M. The virtual
mass has little or no physical reality. If for a given rigid
body and a given fluid one can estimate by a prescribed rule
the value of m, then a convenient "dodge" of the rather form-
idable problem of evaluating the integral in Eqn. (VII-30) is
effected. If the fluid is considered ideal, then the problem
of finding the virtual mass is reduced to one of geometry, and
the force of impact is obtained by quadrature

$$\int_0^x \left(1 + \frac{m}{M}\right)\, dx = \int_0^t dt \qquad \text{(VII-33)}$$

where

           x : penetration into the fluid
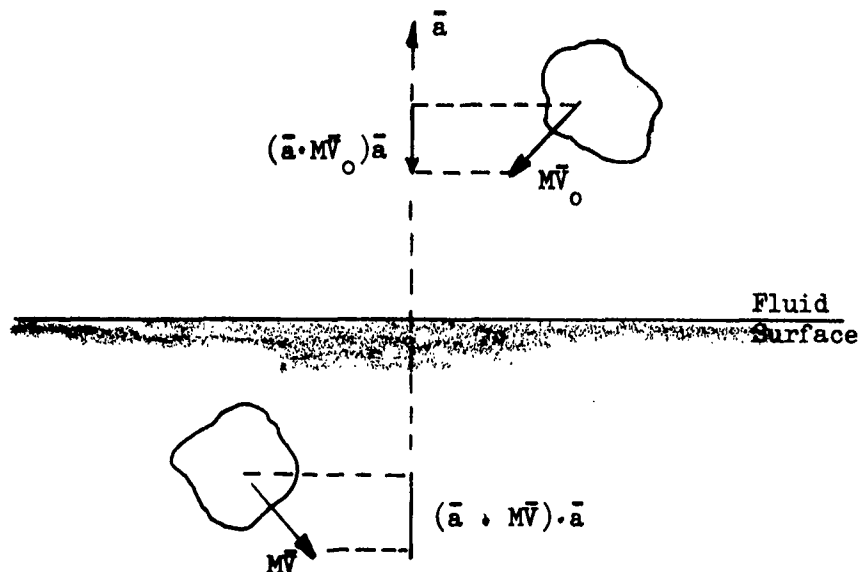
Figure VII-1

b. Solutions to the Problem (152)

1. T. von Karman estimated that for an infinite wedge entering
the fluid vertically and symmetrically (2 dimensional problem),
the virtual mass was that enclosed in a semicircular cylinder
as shown in Fig. VII-2a.

2. H. Wagner used a semicircular cylinder approximation but
calculated the water rise on the sides of the wedge, see
Fig. VII-2b, and used the corresponding width to determine
the diameter of the semicircular cylinder. Wagner also
solved for the virtual mass associated with the potential
flow under a wedge immersing at constant speed.

(a)   (b)
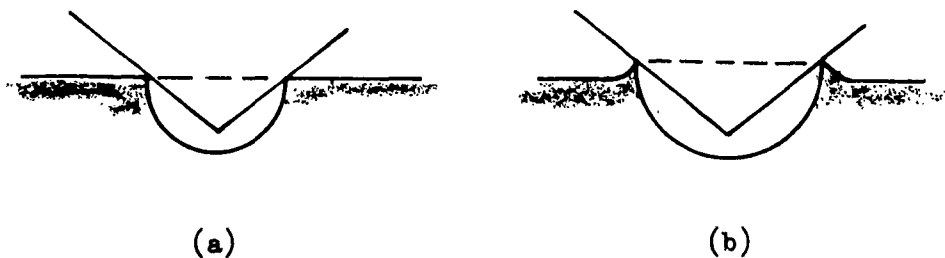
FIG. VII-2

3. Sydow extended the usefulness of Wagner's results by obtaining a virtual mass valid for variable velocity.

4. Bisplinghoff and Doherty (135), obtained an expression for the virtual mass associated with the potential flow past an immersing wedge by assuming a free surface potential of zero. Using a two-dimensional analysis and applying the divergence theorem:

$$\int_v \rho \, \bar{V} \, dv \; = \; \int \rho \, \bar{V} \, \phi \, dv \; = \; \int \rho \frac{\partial \phi}{\partial n} \, dS \qquad\qquad (VII\text{-}34)$$

where

$\dfrac{d\phi}{dn}$: normal derivative of the potential on the surface

dS : element of surface

The last integral in Eqn. VII-34 need only be evaluated on the common surface S_1 between the solid and the fluid, evaluation on S_2 and S_3 being zero, Fig. VII-3. This analysis was also extended to give the force on an immersing, symmetrical two dimensional body. Further, the work of Bisplinghoff and Doherty is significant in that:

i)   A concise review of previous (1952) work is given.

ii) A set of accurate experimental data is presented which serves to establish the applicability of two-dimensional analysis.

iii) A rational procedure is detailed for the reverse problem; that is, given the desired force-time relation, what should be the geometry of the body.
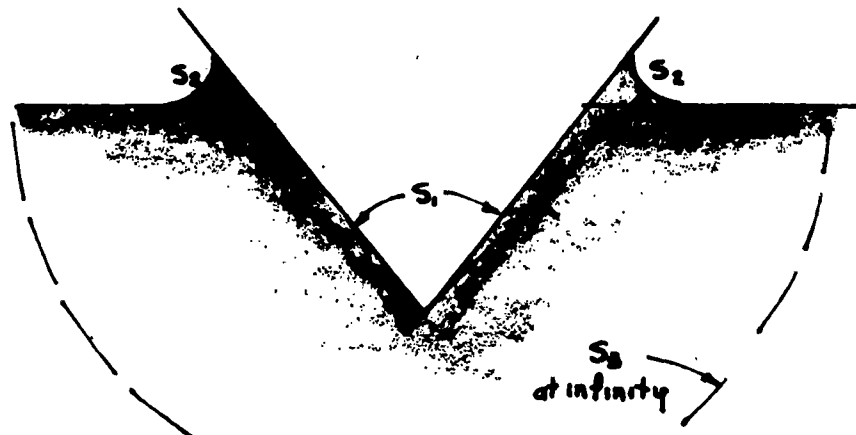
Figure VII-3

5. Shiffman and Spencer (161) present a method for solving the impact of an axially symmetric cone entering the fluid normally (essentially a two-dimensional problem). The analysis makes use of similarity of flow, potential theory and the exact free surface condition (Fig. VII-3.), namely,

$$\frac{\partial^2 \bar{r}}{\partial t^2} \cdot \frac{\partial \bar{r}}{\partial s} = 0 \qquad\qquad (VII-35)$$

where $\bar{r}$ position vector of a particle, taken in the Lagrangian sense

this analysis indicates clearly the difficulties involved, for to obtain a solution, one must (i) estimate the shape of the free surface and (ii) calculate a Green's function satisfying the boundary condition, (iii) then re-estimate the shape of the free surface, etc. So difficult is the procedure that only one cone angle is investigated numerically.

An approximate, theory is presented, by taking the virtual mass to be that fluid enclosed in an ellipsoid enveloping the portion of the cone which penetrates beneath the fluid surface.

6. In conclusion, then, the exact formulation of the impact problem does not admit of a simple solution. Using two dimensional potential flow and relaxing some of the boundary conditions (namely, letting the potential at the free surface be zero) estimates of the integral of Eqn. VII-30 and hence the virtual mass can be made which show fair to good agreement with the experimental data. In no instance is a general theory of hydrodynamic impact proposed, rather particular theories are applied to certain cases in which the geometry is very simple.

Few instances exist in which the compressibility and viscosity of the fluid are considered, and not then neglected. In practically all instances the immersing body is considered to be rigid.

2. TANGENTIAL LANDING ON A FLUID SURFACE EMPLOYING SKIS

The theories presented by Mayo (152) for the nonchine immersed case, Fig. VII-4a and by Schnitzer (160) for the chine immersed case, Fig. VII-4 b, show good agreement with the respective experimental data.

Figure VII-4

In Fig. VII-5, the potential cross-flow planes normal to the keel, and the coordinates relative to a horizontal fluid surface are shown. The virtual mass in each cross-flow plane is obtained from a simple two dimensional potential theory. In the case of nonchine immersion, the virtual mass is that given by Sydow modified by a factor determined by an experiment reported by Mayo; in the case of chine immersion, the virtual mass is that obtained by adding to the virtual mass before chine immersion the virtual mass given by Bobyleff for penetration equal to the perpendicular distance from the chine to the free fluid surface.
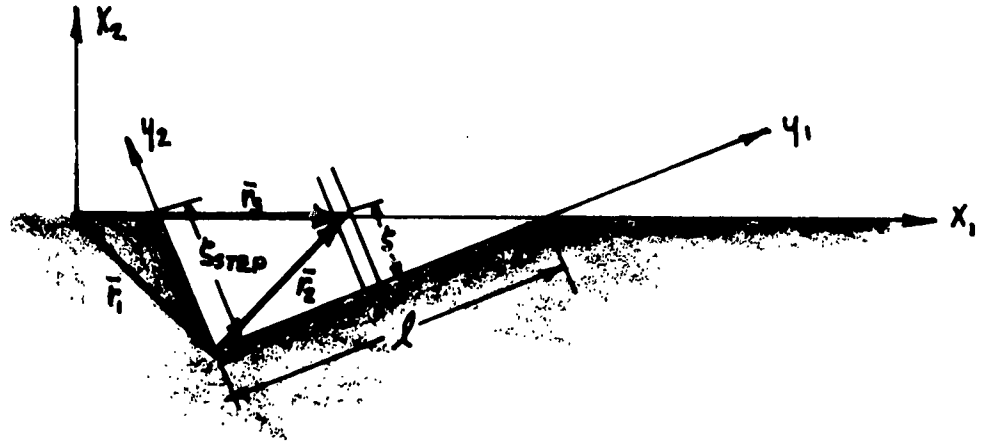
Figure VII-5

Consider the fluid to be inviscid and incompressible. If one views the flow plane as remaining stationary in space, then as the ski translates (at a fixed angle of trim τ) in both the y_1 and y_2 direction, the cross-section of the ski normal to the keel effectively penetrates the fluid in the flow plane, giving rise to an increment of force in each flow plane. The sum of all such increments of force yield the resultant force normal to the keel.

To account for the force exerted on a finite length of the ski, force is multiplied by a correction factor given by Pabst,

$$\phi(\lambda) = \left(\frac{1}{1 + \frac{1}{\lambda^2}}\right)^{\frac{1}{2}} \left(1 - \frac{.425}{\lambda' + \frac{1}{\lambda'}}\right) \qquad \text{(VII-36)}$$

where

$$\lambda = \frac{\text{LENGTH, L}}{\text{MEAN BEAM, B}} \qquad \text{(VII-37)}$$

Using the procedure outlined above the relation between the force exerted on the ski and the penetration can be obtained.

In each flow plane

$$dF = \frac{\partial}{\partial t}(m_\omega \dot{\zeta}) \, ds \qquad\qquad (\text{VII-38})$$

$$F = \phi(\lambda) \int \frac{\partial}{\partial t}(m_\omega \dot{\zeta}) \, ds \qquad\qquad (\text{VII-39})$$

$$F = \phi(\lambda)\left[\int_0^l \dot{\zeta}\, \frac{\partial m_\omega}{\partial t}\, ds + \ddot{\zeta}\int_0^l m_\omega \, ds \right]$$

$$F = \phi(\lambda)\left[\dot{\zeta}^2 \int_0^l \frac{\partial m_\omega}{\partial \zeta}\, ds + \ddot{\zeta}\int_0^l m_\omega \, ds \right] \qquad (\text{VII-40})$$

where

$$m_\omega = \tfrac{1}{2}\rho\pi\zeta^2\, f^2(\beta), \qquad 0 \leq \zeta \leq \tfrac{1}{2}\, b \tan\beta \qquad (\text{VII-41})$$

$$m_\omega = 1/8\, \rho\pi b^2 \left[f(\beta) \tan\beta \right]^2 + \tfrac{1}{2} B \rho b^2 (\tfrac{\zeta}{b} - \tfrac{\tan\beta}{2}), \qquad (\text{VII-42})$$

$$\tfrac{1}{2}\, b \tan\beta < \zeta < \zeta \text{ step}$$

and

$$\lambda = \frac{1}{\tan\tau\, f(\beta)}, \qquad\qquad \frac{\zeta_s}{b} \leq \frac{\tan\beta}{2} \qquad (\text{VII-43})$$

$$\lambda = \frac{\left(\frac{\zeta_s}{b}\right)^2}{\tan\tau\left[\frac{\zeta_s}{b} - \frac{1}{4f(\beta)}\right]}, \qquad \frac{\zeta_s}{b} > \frac{\tan\beta}{2} \qquad (\text{VII-44})$$

$$f(\beta) = \frac{\pi}{2\beta} - 1 \qquad\qquad (\text{VII-45})$$

An illustration of a typical acceleration-time history one might expect from a fixed-trim, nonchine immersed ski landing of the glider studied herein is shown in Fig. VII-12 along with the pertinent data. The method suggested by Mayo (153), as outlined above, is used; $\phi(\lambda) = 1$, is assumed.

D. **PARACHUTES**

Analytical methods of predicting the force exerted by a parachute during and after deployment are at best semiempirical (141). In the final analysis one must depend upon experimental data. Fortunately, however, there exists sufficient data in ordinary flight regimes that a successful parachute recovery system can be designed (139); see references on this subject, Appendix H.

TABLE VII-1

PEAK FRONT GEAR LOADS DUE TO LANDING IMPACT, SHOWING EFFECTS OF
FLEXIBILITY AND OF A SIMPLE VARIABLE-DIAMETER METERING PIN

REAR GEAR YIELD STRAP PEAK LOAD = 12,000 lbs.

Rear gear location	Constant diameter metering pin			Variable diameter metering pin
	Rigid-body representation	One flexible mode in representation	Two flexible modes in representation	Two flexible modes in representation
	lbs.	lbs.	lbs.	lbs.
A	15,800	15,000	14,000	12,300
B	10,300	10,300	10,300	8,250
C	6,900	6,900	6,900	6,250

REAR GEAR YIELD STRAP PEAK LOAD = 6,000 lbs

Rear gear location	Constant diameter metering pin			Variable diameter metering pin
	Rigid-body representation	One flexible mode in representation	Two flexible modes in representation	Two flexible modes in representation
	lbs.	lbs.	lbs.	lbs.
A	12,970	13,100	12,750	11,300
B	8,500	8,500	8,500	7,600
C	No values were obtained for this case as the rear gear static load was over 6,000 lbs.			

TABLE VII-2

PEAK PILOT STATION ACCELERATIONS DUE TO LANDING IMPACT, SHOWING EFFECTS
OF FLEXIBILITY AND OF A SIMPLE VARIABLE DIAMETER METERING PIN

REAR GEAR YIELD STRAP PEAK LOAD = 12,000 lbs.

Rear gear location	Constant diameter metering pin			Variable diameter metering pin
	Rigid-body representation	One flexible mode in representation	Two flexible modes in representation	Two flexible modes in representation
	g	g	g	g
A	4.34 (4.81)*	4.25 (3.65)	4.76 (3.18)	3.95 (2.50)
B	3.40 (2.86)	3.35 (2.70)	3.35 (2.77)	2.68 (2.04)
C	2.32 (1.75)	2.31 (1.66)	2.48 (2.23)	2.08 (1.57)

*(The second peak of the acceleration trace is shown in parenthesis
for each case. Note that for only one case, the rigid representation
with the rear gear in the most aft location, was the second peak
higher than the first.)

aft gear (ξ_2, η_2)

location A

alternate locations:

location B

location C

fwd. gear
(ξ_1, η_1)

ξ

η
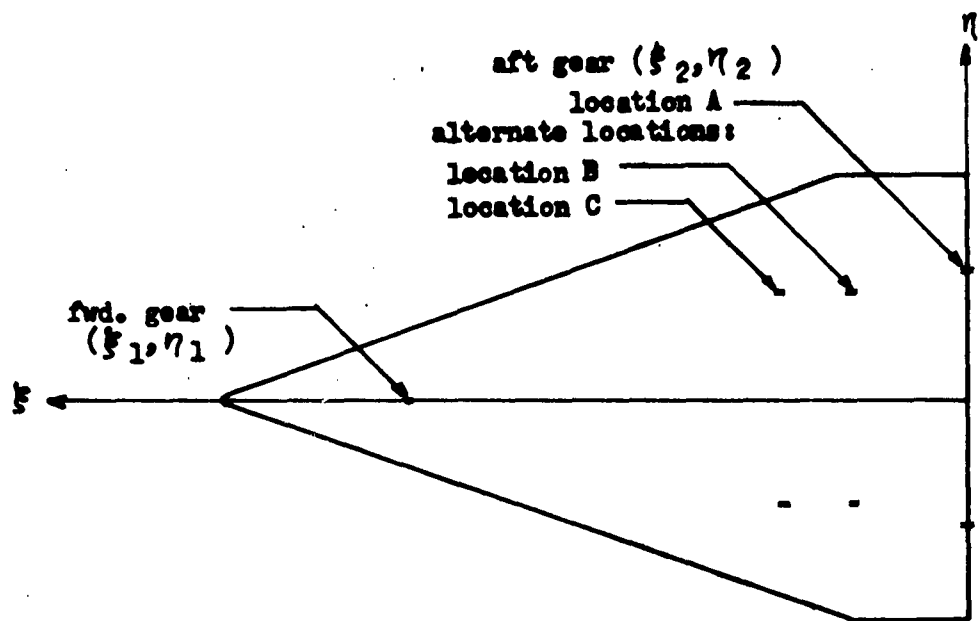
equilibrium glide position shown

ψ_0

γ_1 d_1

q_x

q_3

q_0

d_2 γ_3

γ_2
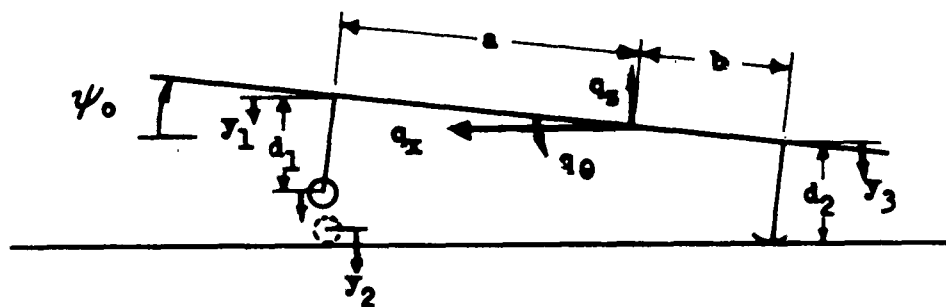
FIG. VII-6   PLANFORM AND SIDE VIEWS OF GLIDER SHOWING GEAR LOCATIONS
AND COORDINATE SYSTEM
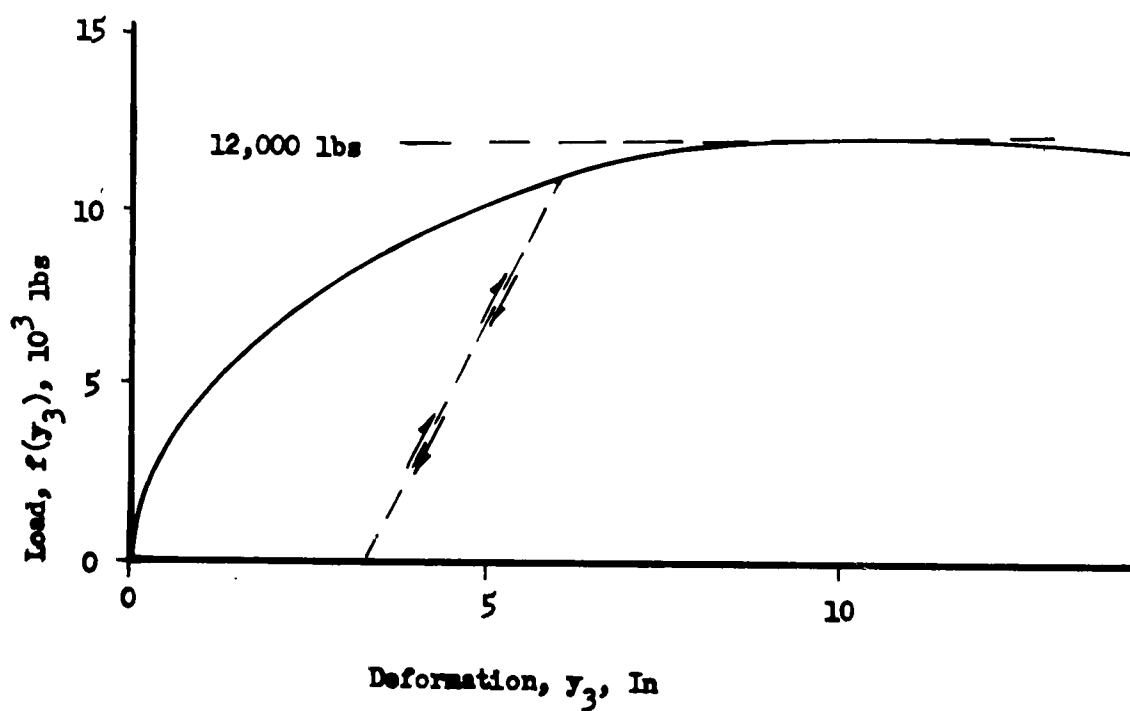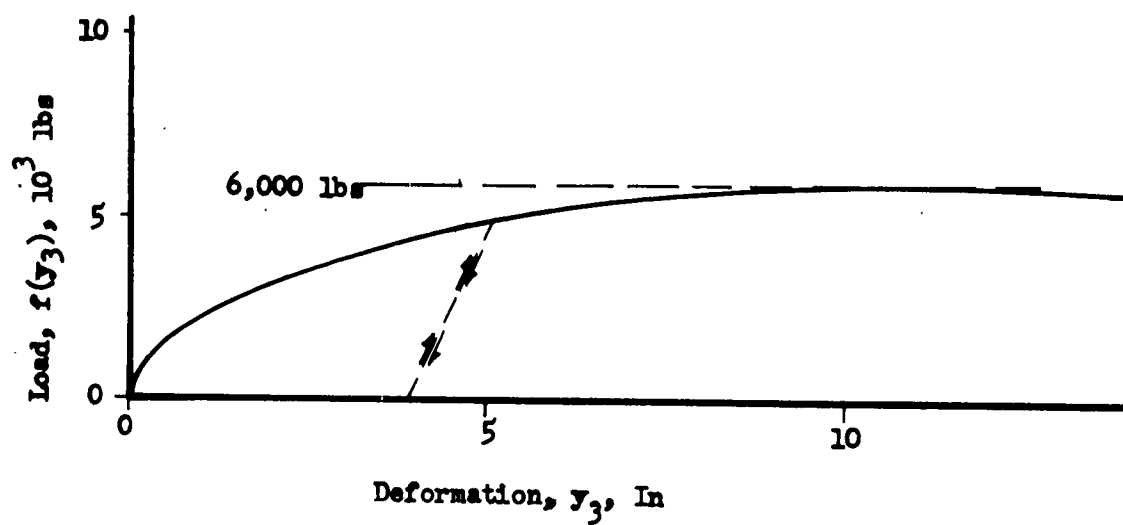
FIG. VII-7 PLASTIC-ELASTIC YIELD STRAP LOAD DEFORMATION FUNCTIONS FOR COMBINED REAR GEARS
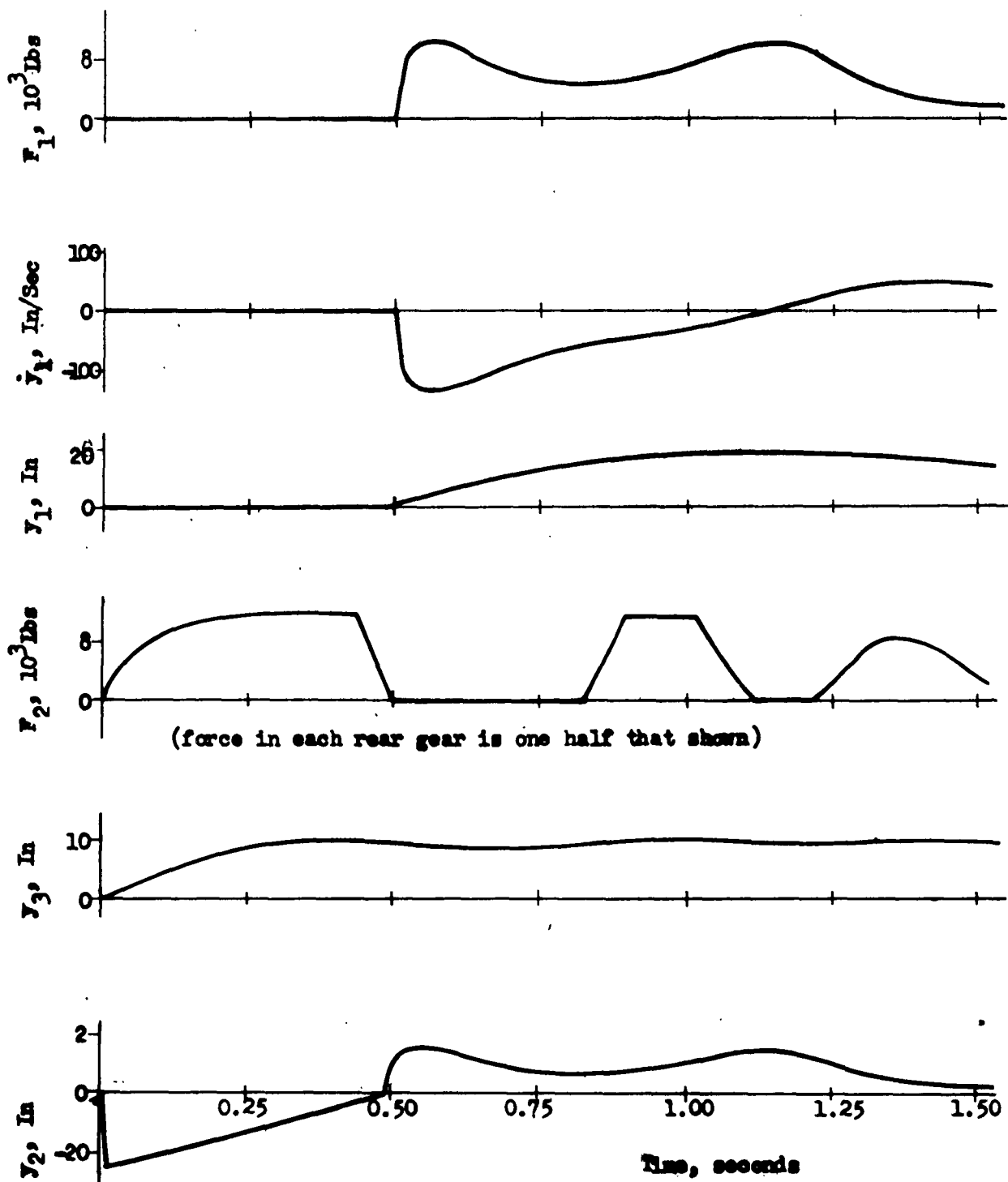
FIG. VII-8 TYPICAL ANALOG TIME-HISTORIES FOR GROUND LANDING
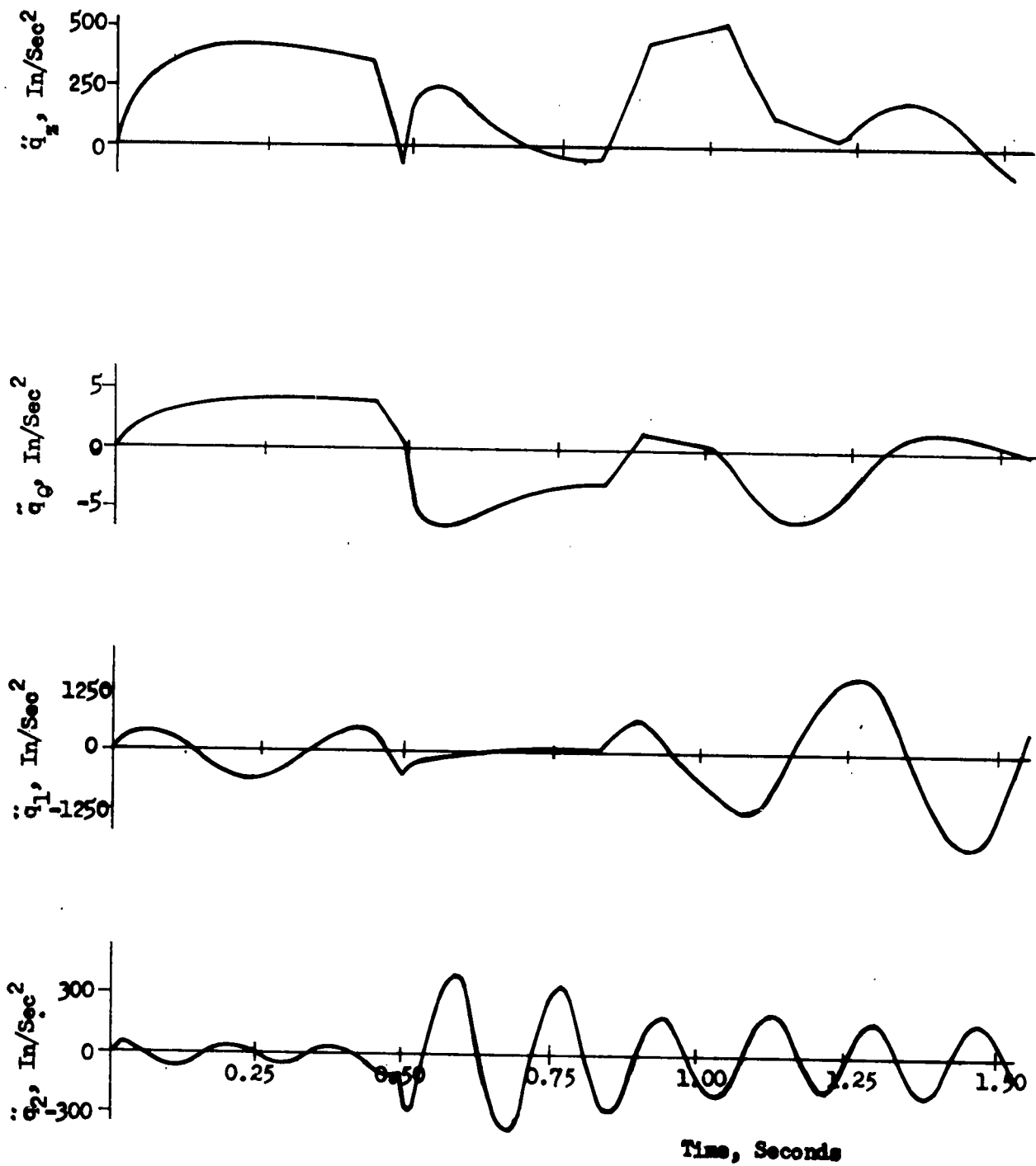
FIG. VII-9 TYPICAL ANALOG TIME-HISTORIES FOR GROUND LANDING
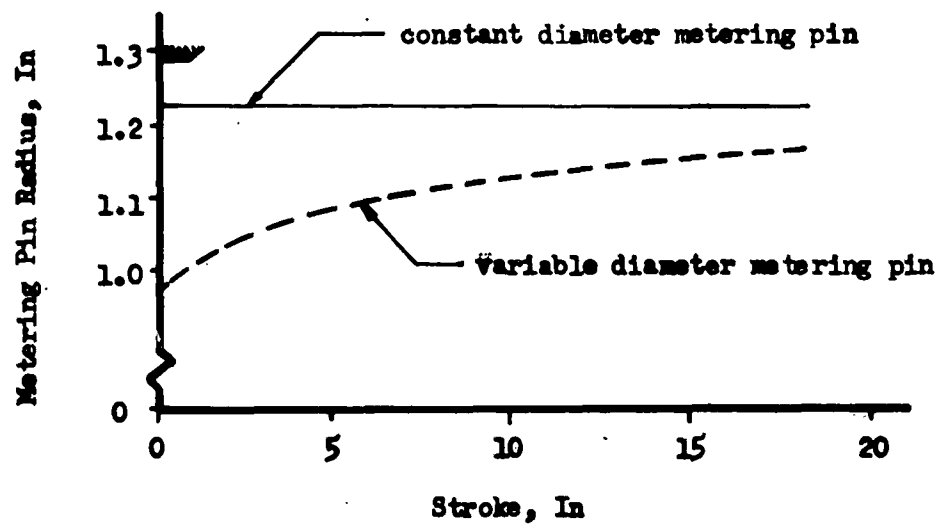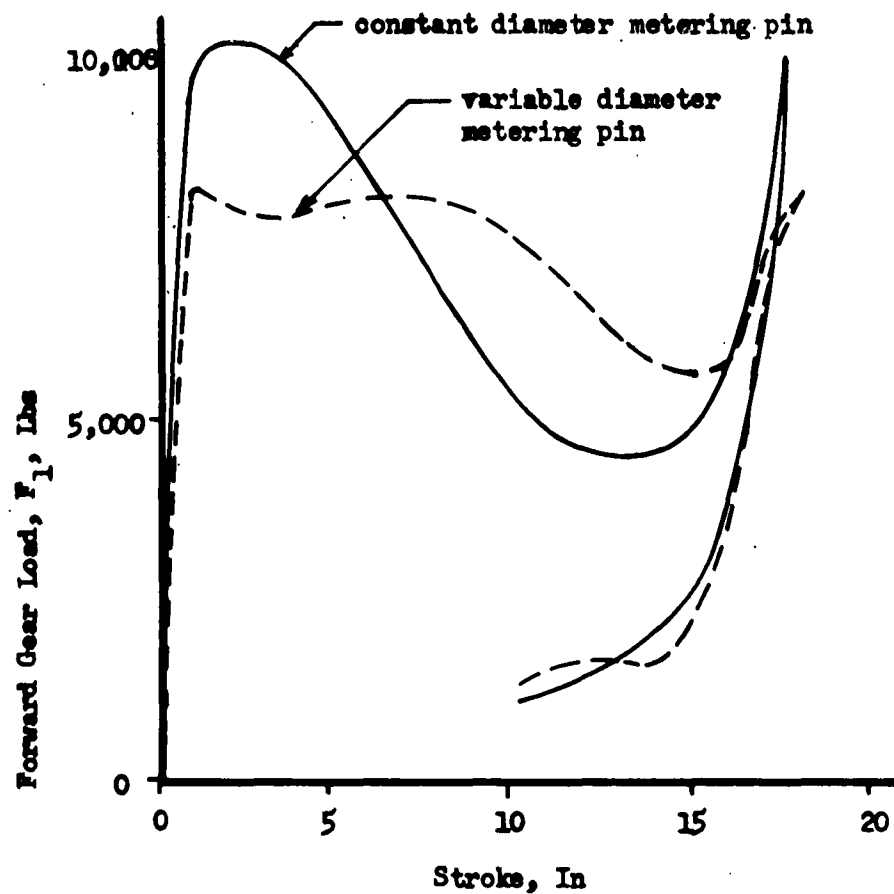
FIG. VII-10   TYPICAL CURVES OF FORWARD GEAR LOAD, F_1, VS. STROKE FOR
CONSTANT AND VARIABLE DIAMETER METERING PINS

$$\frac{\rho_o \lambda^3}{2C_D^2 \left[a(y_1) \right]^2} = 2$$

$$\frac{\rho_o \lambda^3}{2C_D^2 \left[a(y_1) \right]^2} = 1.5$$

$$\frac{\rho_o \lambda^3}{2C_D^2 \left[a(y_1) \right]^2} = 1.0$$

$$\frac{\rho_o \lambda^3}{2C_D^2 \left[a(y_1) \right]^2} = .5$$

Time, Seconds
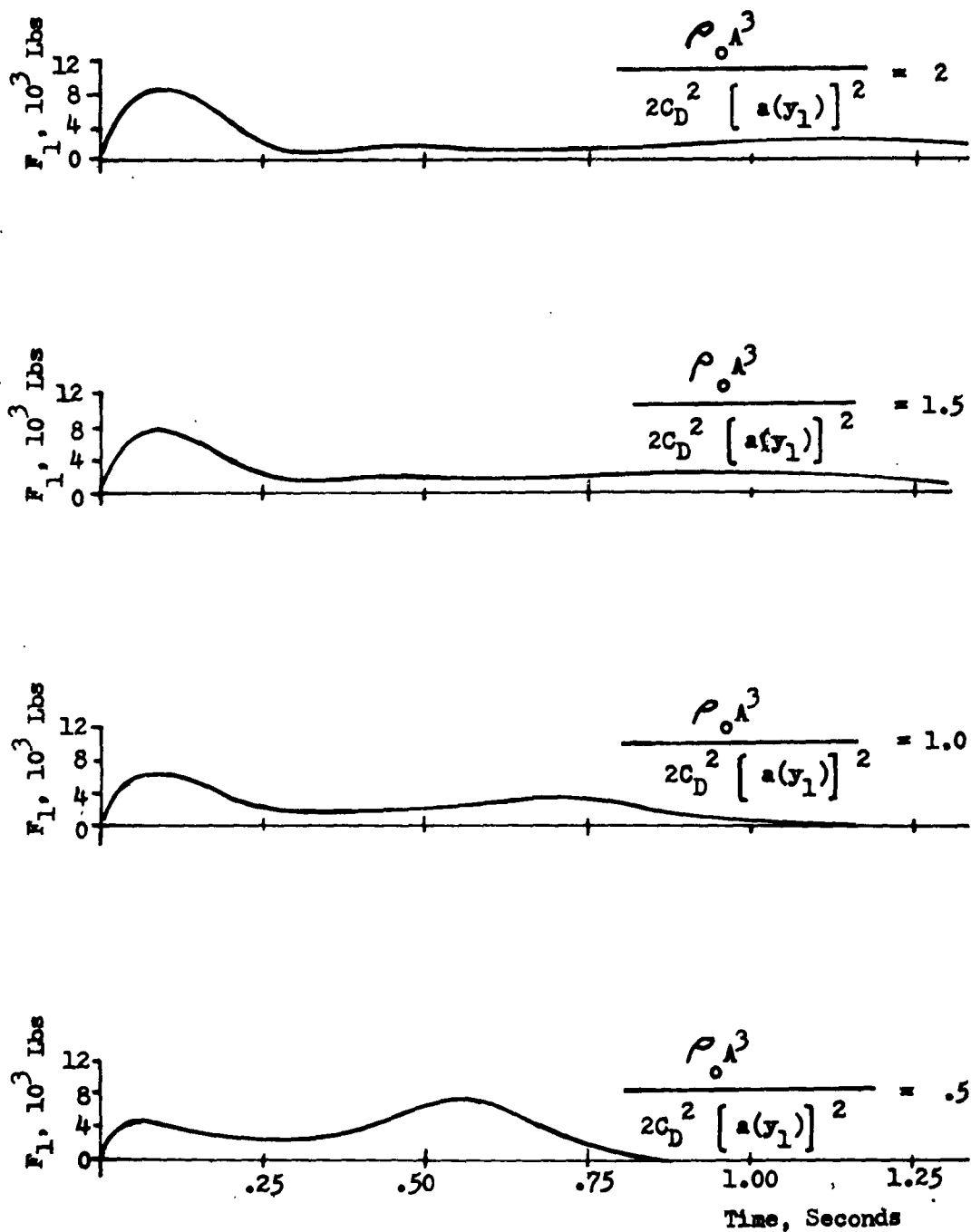
FIG. VII-11   LOAD-TIME CURVES SHOWING EFFECTS OF VARIOUS ORIFICE
AREAS ON FORWARD GEAR LOAD, F_1

(THE PARAMETER $\dfrac{\rho_o \lambda^3}{2C_D^2 \left[a(y_1) \right]^2}$ IS DEFINED IN EQN. VII-13)

FIG. VII-12   SKI LANDING
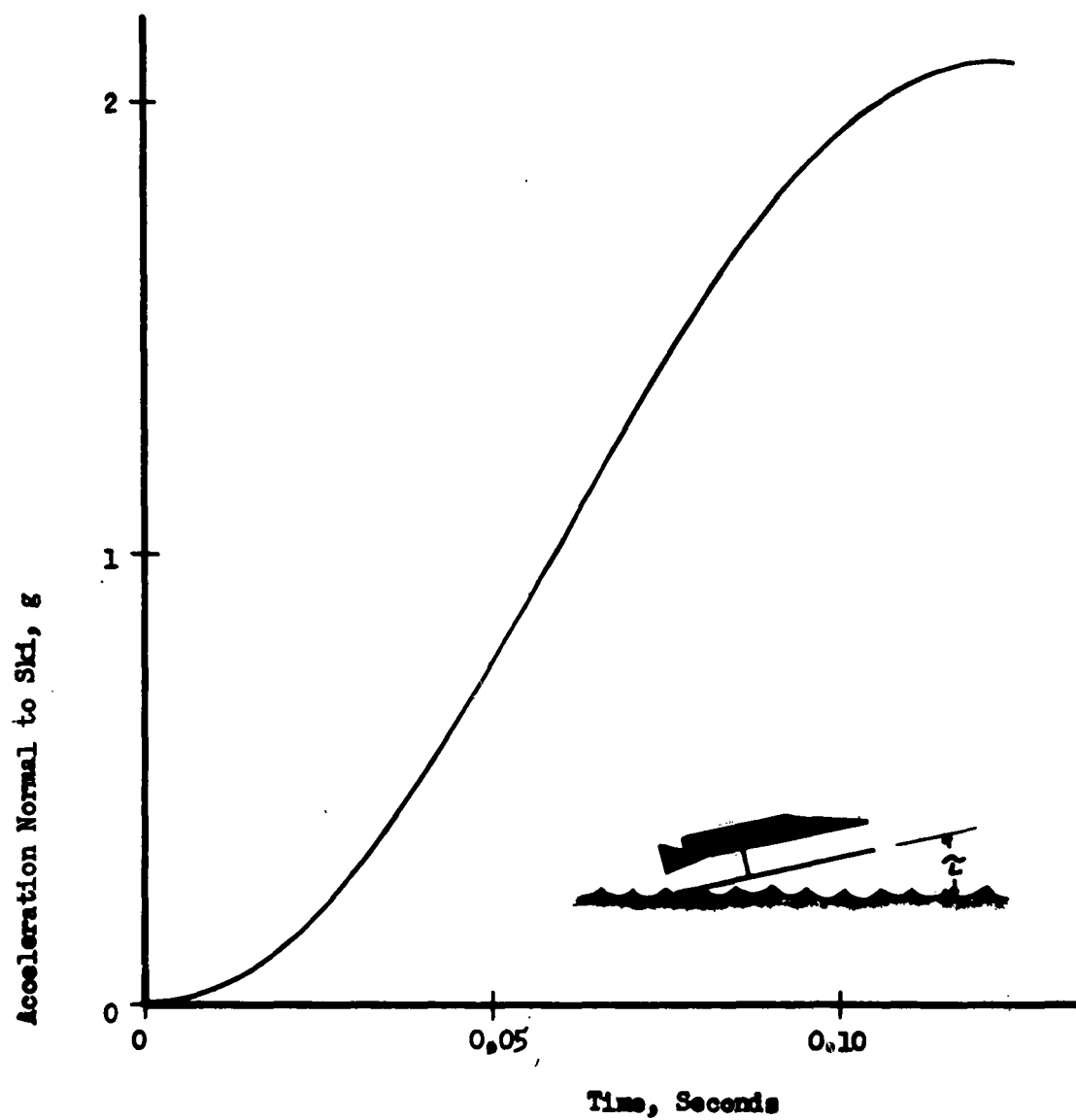
τ : trim $(6°)$
β : deadrise angle $(25°)$
$\dot{y}_g(0)$: sink speed normal to ski (19.3 fps)

APPENDIX A

CONFIGURATION AND TRAJECTORY

This Appendix contains the data upon which the studies in the report are based. The geometry, weight, and stiffness data are given in Fig. A-1 through A-6. It should be emphasized that these data do not represent the result of an extensive configuration study but rather they are chosen as being representative of a typical advanced vehicle.

The trajectory data are given in Fig. A-7 and A-8. These data are representative of a first-stage gravity turn boost trajectory, and a typical equilibrium glide re-entry trajectory. Except during the initial tilt from the vertical, the angle of attack during first stage boost is zero, and for second stage boost it is twenty-five degrees.

The thrust of the first stage engines is considered to vary with altitude as given by Eqn. A-1 while the thrust of the second stage engines is constant and equal to 20,000 pounds.

$$T = T_o + A (p_o - p) \qquad\qquad (A-1)$$

where T : Thrust at altitude h in pounds

T_o : Motor thrust at sea level = 500,000 pounds

A : Exit Area = 5442 square inches

p_o : Atmospheric pressure at sea level = 14.7 lb/in^2

p : Atmospheric pressure at any altitude in lb/in^2
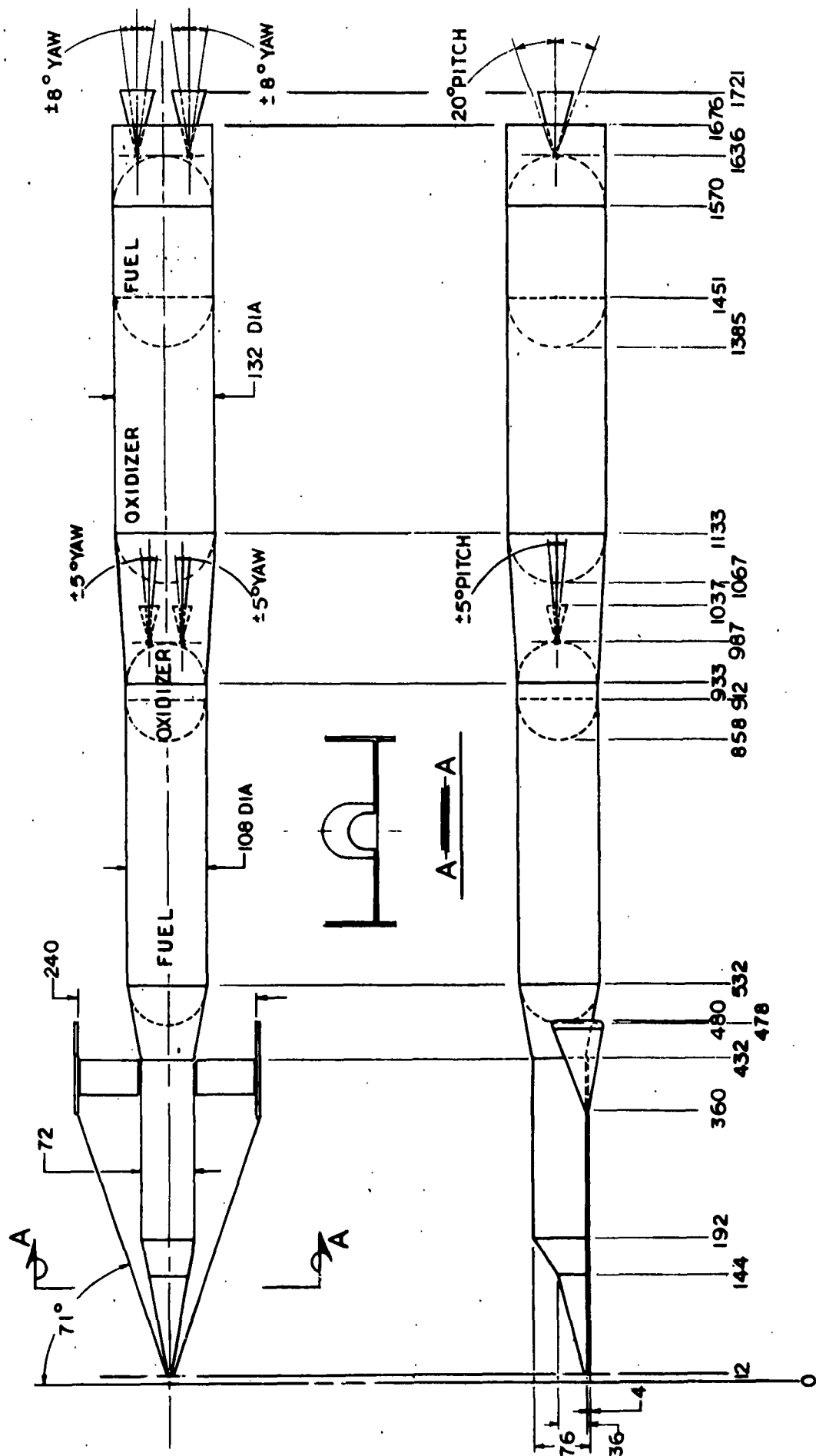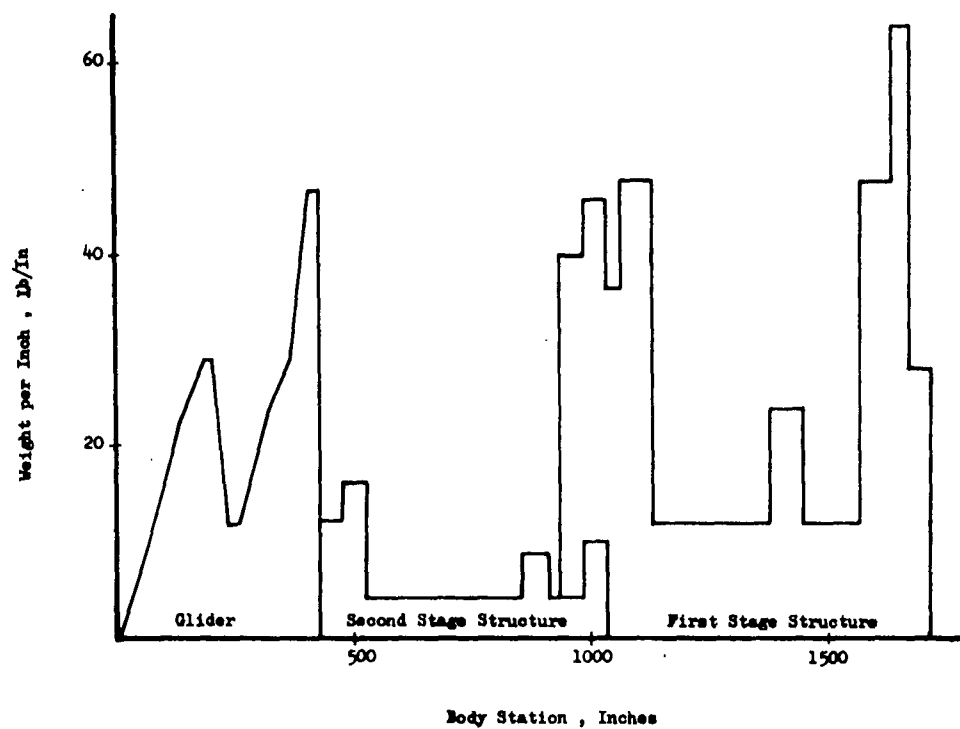
FIG. A-2   WEIGHT EMPTY
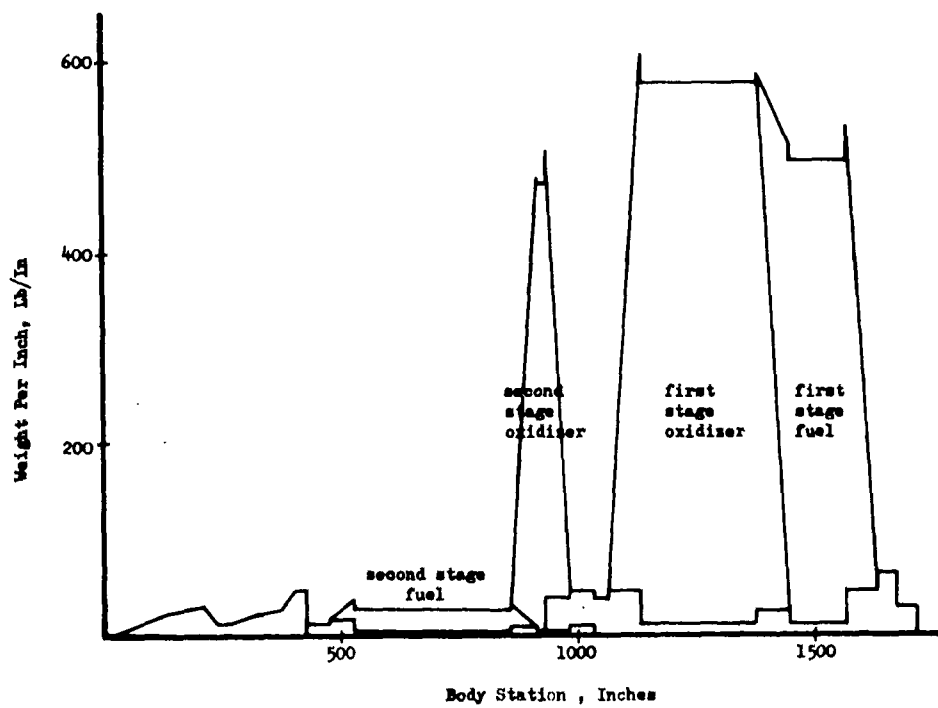
FIG. A-3   WEIGHT FULLY LOADED
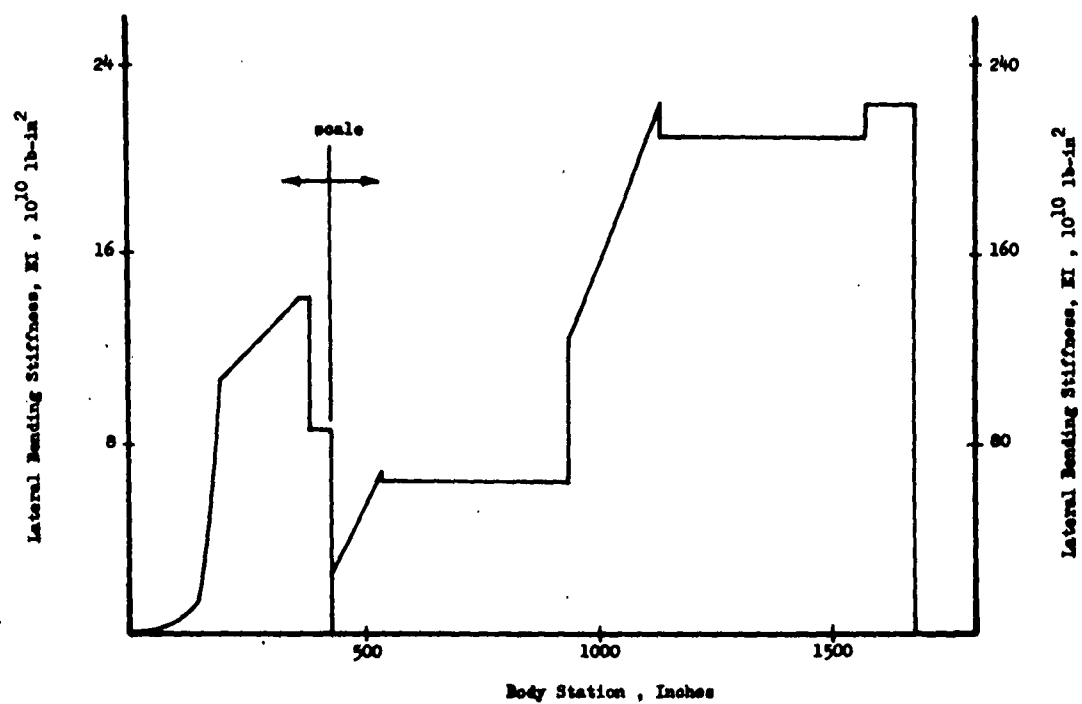
FIG. A-4   LATERAL BENDING STIFFNESS
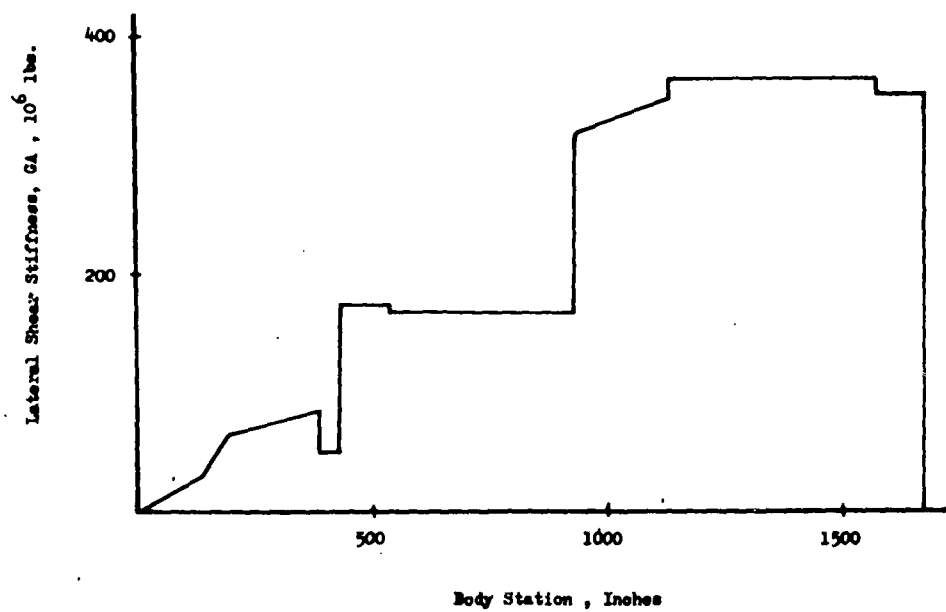
FIG. A-5   LATERAL SHEAR STIFFNESS

Body Station , Inches

FIG. A-6 EXTENSIONAL STIFFNESS
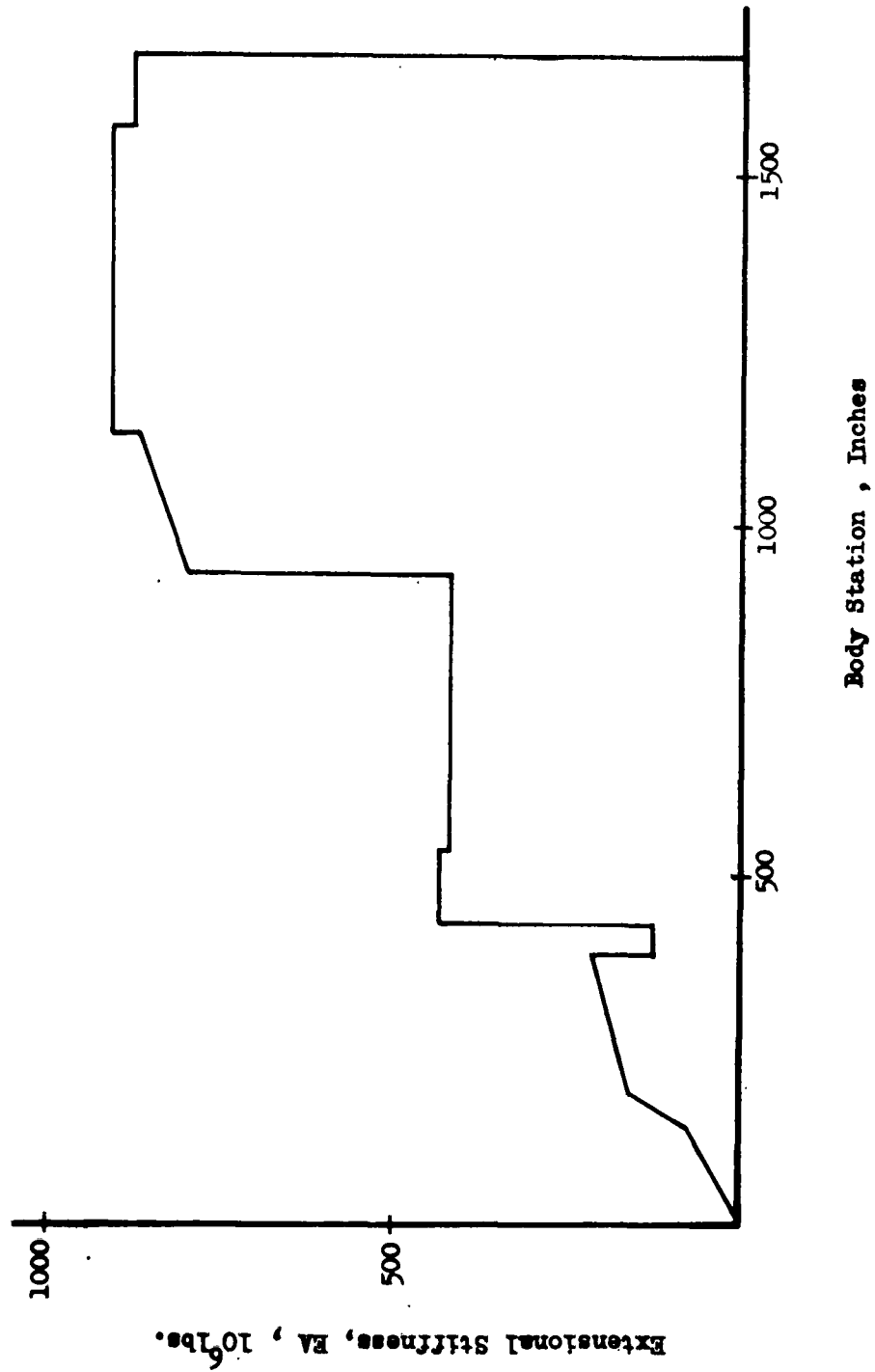
Extensional Stiffness, EA , 10^6 lbs.
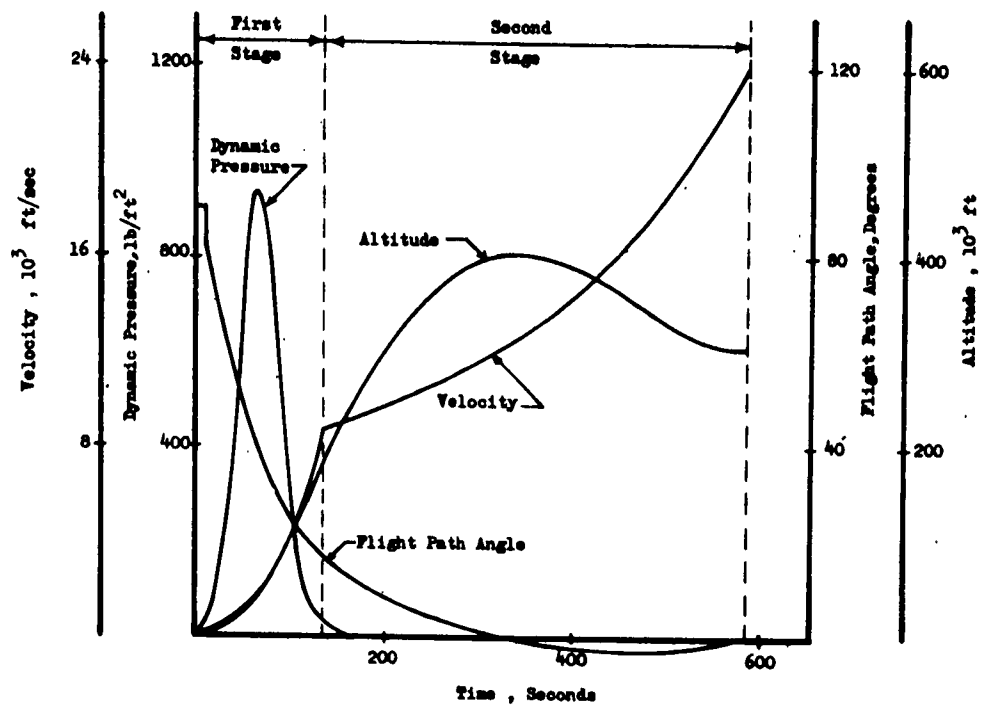
FIG. A-7   BOOST TRAJECTORY DATA
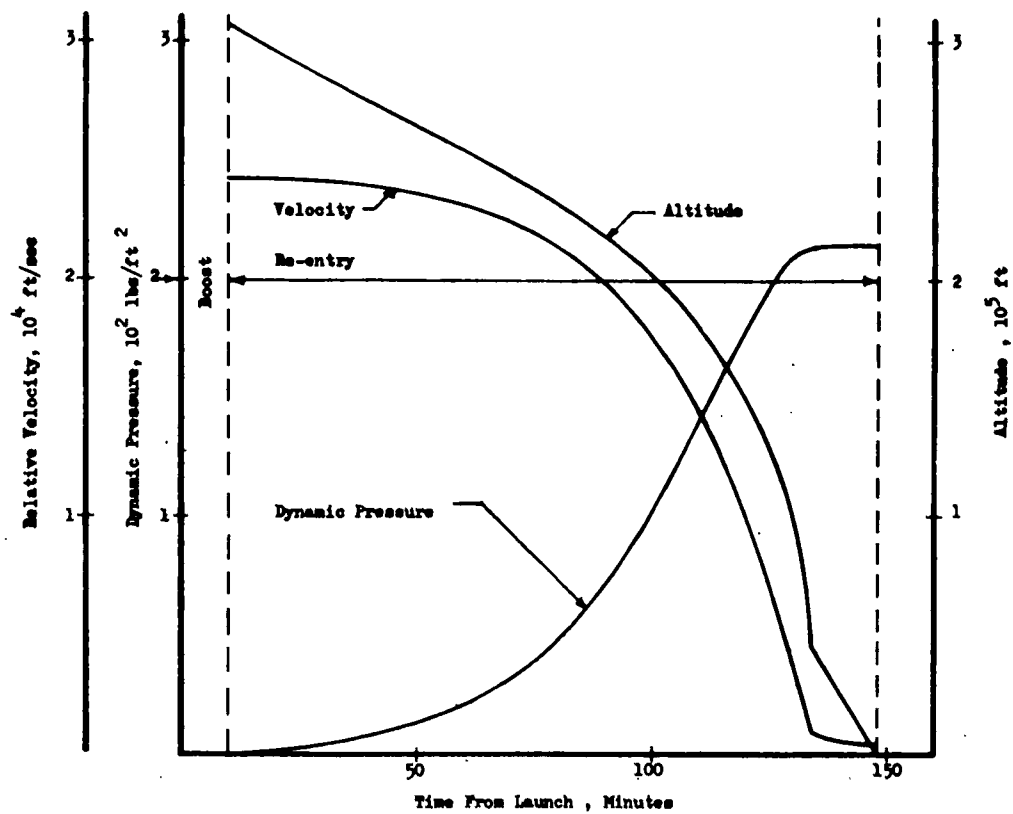
FIG. A-8   RE-ENTRY TRAJECTORY DATA

APPENDIX B

MODE DETERMINATION

1. INTRODUCTION

The well known classical theory of small vibrations sets an important
framework upon which the dynamicist can rely in the treatment of mechanical
systems possessing freedom to undergo infinitesimal or small displacements
from a state of equilibrium. Both the formal and the practical techniques
of solving the characteristic equation for the eigen vectors (or modes) and
the characteristic frequencies and the process of orthogonalization of the
eigen vectors have been studied since before the time of Lord Rayleigh;
descriptions of these techniques and the theory can be found in many texts
and papers (see references 41 and 168 to 177 inclusive).

The utility of the modal method (and it is true of all other analytical
methods) is directly related to one's ability to obtain the influence
coefficients or the stiffness matrix, the Green's function, as it is variously
called. It is here that known elementary and simple solutions of the theory
of elasticity for the static load-deformation relations play an important
role; most of these solutions are for simple structural elements. The
challenge of either approximating a complex structure with structural
elements whose load-deformation relationships are known or solving the
complex structure for these relationships directly is one that has been
met with fair success in some cases.

At the time this study was initiated the programs available to the
contractor made it necessary to determine the natural modes in three parts.
Part one consisted of determining the natural modes considering the vehicle
as a flexible beam. Part two determined the natural modes of the glider
clamped along the centerline; part three coupled the natural modes determined
in parts one and two. Each part will be described in some detail.

The modes are determined by considering the liquid fuel frozen and
the engine nozzle locked. It is realized that the natural modes may be
determined by incorporating the fuel and engine as separate degrees-of-
freedom. In fact, many other degrees-of-freedom can be included; however,
it is much more desirable to determine the natural modes of the basic system
and to couple the various other effects when desired.

2. BEAM MODES

If a vibrating beam is put in equilibrium using D'Alembert's principle,
the free body diagram of a segment of the beam is as pictured in Fig. B-1
and the basic beam equations are (5):

$$m\ddot{w} + (EI\,\delta'')'' - (\mu\,\ddot{\delta}')' = 0 \tag{B-1}$$

$$\Theta' = \frac{1}{KG}\left[\mu\,\ddot{\delta}' - (EI\,\delta'')'\right] \tag{B-2}$$

where:

m : mass per unit length

w : total lateral deflection

EI : bending stiffness of cross section

δ : lateral deflection due to bending

μ : moment of inertia per unit length

Θ : lateral deflection due to shear

KG : shear stiffness of cross section

$\ddot{w}$: second time derivative of w

δ'' : second derivative of δ with respect to Y
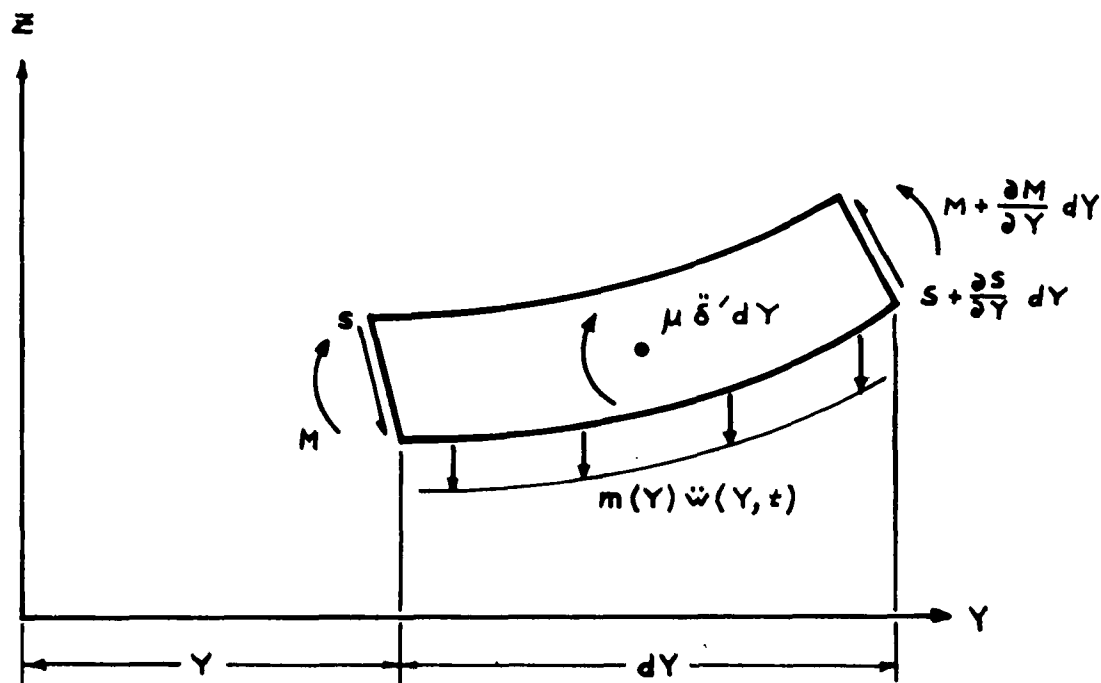
FIG. B-1

These equations of motion can be solved for arbitrary variations in elastic and inertial properties of the beam for many practical boundary conditions. Several approximate methods (44) are available to solve the Eqn. (B-1) and (B-2).

The program used to determine the beam modes is described in Appendix G.

The stiffness matrix of a beam including bending deformations, shear deformations, rotary inertia, and static unbalances that is used in this study is the following:

$$
\begin{bmatrix} K_1 & K_2 \\ \hline K_3 & K_4 \end{bmatrix}
\begin{Bmatrix} w_1 \\ \vdots \\ w_N \\ \alpha_{1b} \\ \vdots \\ \alpha_{Nb} \end{Bmatrix}
$$

$$(B\text{-}3)$$

$$
\begin{array}{cc}
(EI)_1 & (EI)_N \\
(K'GA)_1 & (K'GA)_N
\end{array}
$$

$$
\begin{array}{ccccc}
x_1 & & & & x_N \\
w_1 & & & & w_N \\
\alpha_1 & & & & \alpha_N \\
m_1 & & & & m_N \\
I_1 & & & & I_N \\
S_1 & & & & S_N
\end{array}
$$

where:

$$
K_1 : \begin{bmatrix}
\dfrac{12(EI)_1}{\ell_1^3 \, \Upsilon_1} & & & & & \text{SYM.} \\[2ex]
-\dfrac{12(EI)_1}{\ell_1^3 \, \Upsilon_1} & 12\left[\dfrac{(EI)_1}{\ell_1^3 \, \Upsilon_1} + \dfrac{(EI)_2}{\ell_2^3 \, \Upsilon_2}\right] & & & & \\[2ex]
0 & -\dfrac{12(EI)_2}{\ell_2^3 \, \Upsilon_2} & \cdot & & & \\[2ex]
\cdot & & \cdot & \cdot & & \\[1ex]
\cdot & & & \cdot & \cdot & \\[1ex]
\cdot & & & & \cdot & \cdot \\[1ex]
0 & & & & -\dfrac{12(EI)_{N-1}}{\ell_{N-1}^3 \, \Upsilon_{N-1}} & \dfrac{12(EI)_{N-1}}{\ell_{N-1}^3 \, \Upsilon_{N-1}}
\end{bmatrix}
$$

$$K_3 = K_2' : \begin{bmatrix} \dfrac{6(EI)_1}{\ell_1^2 b \, \gamma_1} & -\dfrac{6(EI)_1}{\ell_1^2 b \, \gamma_1} & 0 & \bullet & \bullet & \bullet \\[4mm] \dfrac{6(EI)_1}{\ell_1^2 b \, \gamma_1} & -\dfrac{6(EI)_1}{\ell_1^2 b \, \gamma_1} + \dfrac{6(EI)_2}{\ell_2^2 b \, \gamma_2} & -\dfrac{6(EI)_2}{\ell_2^2 b \, \gamma_2} & & & \\[4mm] 0 & \dfrac{6(EI)_2}{\ell_2^2 b \, \gamma_2} & \bullet & \bullet & & \\[3mm] \bullet & & \bullet & \bullet & \bullet & \\[2mm] \bullet & & & \bullet & \bullet & \\[2mm] \bullet & & & & \dfrac{6(EI)_{N-1}}{\ell_{N-1}^2 b \, \gamma_{N-1}} & \dfrac{6(EI)_{N-1}}{\ell_{N-1}^2 b \, \gamma_{N-1}} \end{bmatrix}$$

where the prime on K_2 means transpose

$$K_4 : \begin{bmatrix} \dfrac{4(EI)_1 R_1}{\ell_1 \gamma_1 b^2} & & & & \text{SYM.} \\[4mm] 6(1-\tfrac{2}{3}R_1)\dfrac{(EI)_1}{\ell_1 \gamma_1 b^2} & \dfrac{4}{b}\left(\dfrac{(EI)_1 R_1}{\ell_1 \, \gamma_1} + \dfrac{(EI)_2 R_2}{\ell_2 \, \gamma_2}\right) & & & \\[4mm] 0 & \bullet & \bullet & & \\[3mm] \bullet & & \bullet & \bullet & \\[2mm] \bullet & & & \bullet & \bullet \\[2mm] \bullet & & & \dfrac{6\left(1-\tfrac{2}{3}R_{N-1}\right)(EI)_{N-1}}{\gamma_{N-1}\,\ell_{N-1}\,b^2} & \dfrac{4(EI)_{N-1}R_{N-1}}{b^2 \ell_{N-1}\gamma_{N-1}} \end{bmatrix}$$

where

$$\ell_i = x_{i+1} - x_i$$

$$b = \frac{x_N - x_1}{N}$$

$$\gamma_i = 1 + \frac{12(EI)_i}{\ell_i^2 K'(GA)_i}$$

$$R_i = \frac{\gamma_i + 3}{4}$$

In this study the configuration is such that the rotary inertias can be neglected, and there are no static unbalances.

In Tables B-1, B-2, and B-3 are tabulated the values necessary to compute the beam modes. The effective shear area constant ,k', is 1/2. Fig. B-4 shows the first three computed free-free beam modes at first stage start burn.

3. PLATE MODES

Solutions of the plate equations have been attempted by imposing constraints on the streamwise deformations (174, 175) by using Rayleigh-Ritz methods (169, 171) and by directly attacking the differential equations by finite difference methods (168, 170, 177).

A stiffness matrix for thin plates bending under lateral forces and edge couples suitable for the analysis of the elastic characteristics of plates of variable thickness which is used is presented below. The method used in this study, however, may become obsolete quickly as new and perhaps better methods of attack are formulated.

The expression of the bending strain energy ,U, for a plate of uniform flexural rigidity and isotropic material is

$$U = \frac{D}{2} \iint (w_{xx}^2 + w_{yy}^2 + 2\nu \, w_{xx} \, w_{yy} + 2(1 - \nu) \, w_{xy}^2) \quad dA \tag{B-4}$$

where:

$$D \quad : \quad \frac{Eh^3}{12(1-\nu)}$$

ν :   Poisson's ratio

w :   Displacement function

$$w_{xx} \quad : \quad \frac{\partial^2 w}{\partial x^2} \, , \text{ etc.}$$

dA :   Differential area

The four terms of the energy expression (B-4) may be defined by analogy with the elementary beam as X bending stiffness, Y bending stiffness, bending coupling, and torsional stiffness, respectively. If the x axis is along the chord and the y axis along the span, scalars may be applied to the first and second terms to approximate the effects of varying the amounts of chordwise and spanwise bending material on elastic response. Similarly, wing cutout effects can be approximated. Normally, where cutouts are made, additional bending material is placed in the spars and ribs to replace the lost normal stress carrying capability of the skin. The loss of shear carrying capability can be approximated by multiplying the torsional stiffness matrix by one-half before combining it with the bending terms since a shear flow analysis would attribute half of the rigidity to the spars and half to the skin panels.

In deriving the plate stiffness matrix, the bending curvatures are obtained by assuming the displacement along the edges of the panel as third order polynomials. The bending coupling is obtained by integrating the products of these cubics over a quadrant of the plate and the torsion term is based on simple torsion of the rectangular cell. Thus writing the displacement along line 1-2, FIG. B-2:

$$w = A_3 x^3 + A_2 x^2 + A_1 x + A_0 \qquad (B-5)$$

$$w_x = 0 = 3A_3 x^2 + 2A_2 x + A_1 \qquad (B-6)$$

$$w_{xx} = 2(3A_3 x + A_2) \qquad (B-7)$$
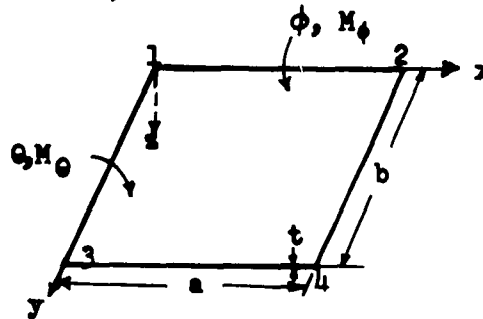
FIG. B-2 THIN PLATE NOTATIONS

The four constants of the displacement expression A_i are evaluated by requiring that this function give the displacements and slopes of the nodes 1 and 2 at $x = 0$ and $x = a$. Then in matrix form, the expression for the curvature becomes:

$$w_{xx} = 2/a \left[\frac{3x}{a} - 2 \;\middle|\; \frac{6x}{a^2} - \frac{3}{a} \;\middle|\; \frac{3x}{a} - 1 \;\middle|\; -\frac{6x}{a^2} + \frac{3}{a} \right] \left\{ \begin{array}{c} \theta_1 \\ w_1 \\ \theta_2 \\ w_2 \end{array} \right\} \qquad (B-8)$$

w_{xx}^2 is obtained by multiplying this expression by its transpose. The total strain energy contributed by w_{xx} is found by integrating the result over x between 0 and a and multiplying by b/2, assuming the w_{xx}^2 term varies linearly with y. Then using Castigliano's first theorem gives:

$$\left\{ \begin{array}{c} M_{\theta_1} \\ F_{z_1} \\ M_{\theta_2} \\ F_{z_2} \end{array} \right\} = \frac{Db}{a^2} \left[\begin{array}{cccc} 2a & & \text{sym.} & \\ 3 & 6/a & & \\ a & 3 & 2/a & \\ -3 & -6/a & -3 & 6/a \end{array} \right] \left\{ \begin{array}{c} \theta_1 \\ w_1 \\ \theta_2 \\ w_2 \end{array} \right\} \qquad (B-9)$$

Since a similar matrix to B-9 can be written in terms of the angular rotations and vertical displacements of nodes 3 and 4, one can get:

$$
\begin{Bmatrix}
M_{\theta_1} \\
F_{z_1} \\
M_{\theta_2} \\
F_{z_2} \\
M_{\theta_3} \\
F_{z_3} \\
M_{\theta_4} \\
F_{z_4}
\end{Bmatrix}
=
\frac{Db}{a^2}
\begin{bmatrix}
2a & & & & & & & \\
3 & 6a & & & \text{SYM} & & & \\
a & 3 & 2a & & & & & \\
-3 & -6/a & -3 & 6/a & & & & \\
0 & 0 & 0 & 0 & 2a & & & \\
0 & 0 & 0 & 0 & 3 & 6/a & & \\
0 & 0 & 0 & 0 & a & 3 & 2a & \\
0 & 0 & 0 & 0 & -3 & -6/a & -3 & 6/a
\end{bmatrix}
\begin{Bmatrix}
\theta_1 \\
w_1 \\
\theta_2 \\
w_2 \\
\theta_3 \\
w_3 \\
\theta_4 \\
w_4
\end{Bmatrix}
\qquad \text{(B-10)}
$$

If cubics of the same form as used to express w_{yy} are selected in the Y direction as well, Y bending stiffness matrix can be written immediately from symmetry of the previous matrix:

$$
\begin{Bmatrix}
M_{\phi_1} \\
F_{z_1} \\
M_{\phi_2} \\
F_{z_2} \\
M_{\phi_3} \\
F_{z_3} \\
M_{\phi_4} \\
F_{z_4}
\end{Bmatrix}
=
\frac{Da}{b^2}
\begin{bmatrix}
2b & & & & & & & \\
3 & 6/b & & & \text{SYM} & & & \\
0 & 0 & 2/b & & & & & \\
0 & 0 & 3 & 6/b & & & & \\
b & 3 & 0 & 0 & 2b & & & \\
-3 & -6/b & 0 & 0 & -3 & 6/b & & \\
0 & 0 & b & 3 & 0 & 0 & 2b & \\
0 & 0 & -3 & -6/b & 0 & 0 & -3 & 6/b
\end{bmatrix}
\begin{Bmatrix}
\phi_1 \\
w_1 \\
\phi_2 \\
w_2 \\
\phi_3 \\
w_3 \\
\phi_4 \\
w_4
\end{Bmatrix}
\qquad \text{(B-11)}
$$

To obtain the bending coupling energy the transpose of w_{xx} is multiplied by w_{yy}, integrated, and differentiated as before. A product can be taken at each node, integration performed over a quadrant of the plate, and the sum of the four products used to represent the coupling energy, using this method the final expression for bending coupling stiffness is in matrix form:

$$
\begin{Bmatrix}
\Sigma M_{\theta_1} \\
\Sigma M_{\phi_1} \\
\Sigma F_{z_1} \\
\Sigma M_{\theta_2} \\
\Sigma M_{\phi_2} \\
\Sigma F_{z_2} \\
\Sigma M_{\theta_3} \\
\Sigma M_{\phi_3} \\
\Sigma F_{z_3} \\
\Sigma M_{\theta_4} \\
\Sigma M_{\phi_4} \\
\Sigma F_{z_4}
\end{Bmatrix}
=
\frac{\nu D}{16}
\begin{bmatrix}
0 & & & & & & & & & & & \\
25 & 0 & & & & & & & & & & \\
30/b & 30/a & 72/ab & & & & & & & \text{SYM} & & \\
0 & 5 & 0 & 0 & & & & & & & & \\
-5 & 0 & -30/a & -25 & 0 & & & & & & & \\
-6/b & -30/a & -72/ab & -30/b & 30/a & 72/ab & & & & & & \\
0 & -5 & -30/b & 0 & -1 & 6/b & 0 & & & & & \\
5 & 0 & 6/a & 1 & 0 & -25 & 0 & 0 & & & & \\
-30/b & -6/a & -72/ab & -6/b & 6/a & 72/ab & -30/a & -30/a & 72/ab & & & \\
0 & -1 & -6/b & 0 & 5 & 30/b & 0 & -5 & 6/b & 0 & & \\
-1 & 0 & -6/a & -5 & 0 & 6/a & 0 & 5 & 30/a & 25 & 0 & \\
6/b & 6/a & 72/ab & 30/b & -6/a & -72/ab & -6/a & 30/a & -72/ab & -30/b & -30/a & 72/ab
\end{bmatrix}
\begin{Bmatrix}
\theta_1 \\
\phi_1 \\
w_1 \\
\theta_2 \\
\phi_2 \\
w_2 \\
\theta_3 \\
\phi_3 \\
w_3 \\
\theta_4 \\
\phi_4 \\
w_4
\end{Bmatrix}
\qquad \text{(B-12)}
$$

Considering the simple torsion of cell a-b, the curvature can be defined as:

$$W_{XY} = \frac{1}{ab} \begin{bmatrix} 1 & -1 & -1 & 1 \end{bmatrix} \begin{Bmatrix} W_1 \\ W_2 \\ W_3 \\ W_4 \end{Bmatrix} \tag{B-13}$$

Performing premultiplication, integration over ab, and differentiation the stiffness form can be found:

$$\begin{Bmatrix} F_{z_1} \\ F_{z_2} \\ F_{z_3} \\ F_{z_4} \end{Bmatrix} = \frac{2(1-Y)D}{ab} \begin{bmatrix} +1 & & & \\ -1 & +1 & & \\ -1 & +1 & +1 & \\ +1 & -1 & -1 & +1 \end{bmatrix} \begin{Bmatrix} W_1 \\ W_2 \\ W_3 \\ W_4 \end{Bmatrix} \tag{B-14}$$

Summing all the relations (Eqns. B-11 through B-14), one finds the stiffness matrix for a thin rectangular plate as given in Eqn.(B-15). With the change of displacement coordinates and moment normalizing, the elements of the matrix become nondimensional quantities. One may also observe that a given column of the matrix defines a set of forces which satisfy the three equilibrium equations.

This stiffness matrix is closely related to the evaluation of stiffness by Levy's torque tube and beam analogy. Here, however, the Poisson ratio coupling has been retained and a single matrix includes both bending and torsion.

$$
\begin{Bmatrix}
M_{\theta_1}/b \\[2pt]
M_{\phi_1}/a \\[2pt]
R_1 \\[2pt]
M_{\theta_2}/b \\[2pt]
M_{\phi_2}/a \\[2pt]
R_2 \\[2pt]
M_{\theta_3}/b \\[2pt]
M_{\phi_3}/a \\[2pt]
R_3 \\[2pt]
M_{\theta_4}/b \\[2pt]
M_{\phi_4}/a \\[2pt]
R_4
\end{Bmatrix}
=
\frac{D}{ab}
\left[\;\;\text{SYM}\;\;\right]
\begin{Bmatrix}
\Theta_1 b \\[2pt]
\Phi_1 a \\[2pt]
W_1 \\[2pt]
\Theta_2 b \\[2pt]
\Phi_2 a \\[2pt]
W_2 \\[2pt]
\Theta_3 b \\[2pt]
\Phi_3 a \\[2pt]
W_3 \\[2pt]
\Theta_4 b \\[2pt]
\Phi_4 a \\[2pt]
W_4
\end{Bmatrix}
\tag{B-15}
$$

where

$$\alpha = \nu/16$$
$$\beta = 2(1-\nu)$$
$$P = a/b$$

Matrix (lower triangle; symmetric):

	$\Theta_1 b$	$\Phi_1 a$	W_1	$\Theta_2 b$	$\Phi_2 a$	W_2	$\Theta_3 b$	$\Phi_3 a$	W_3	$\Theta_4 b$	$\Phi_4 a$	W_4
M_{θ_1}/b	2											
M_{ϕ_1}/a	25α	2										
R_1	$3P^{-1}+30P\alpha$	$3P+30P^{-1}\alpha$	$6P^{-2}+6P^2+72\alpha+\beta$									
M_{θ_2}/b	1	5α	$3P^{-1}+6P\alpha$	2								
M_{ϕ_2}/a	-5α	0	$-30P^{-1}\alpha$	-25α	2							
R_2	$-3P^{-1}-6P\alpha$	$-30P^{-1}\alpha$	$-6P^{-2}-72\alpha-\beta$	$-3P^{-1}-30P\alpha$	$3P+30P^{-1}\alpha$	$6P^{-2}+6P^2+72\alpha+\beta$						
M_{θ_3}/b	0	-5α	$-30P\alpha$	0	α	$6P\alpha$	2					
M_{ϕ_3}/a	5α	1	$3P+6P\alpha$	α	0	$-6P^{-1}\alpha$	-25α	2				
R_3	$-30P\alpha$	$-6P^{-2}-72\alpha-\beta$	$-6P^{-2}-72\alpha-\beta$	$6P^{-1}\alpha$	$72\alpha+\beta$	$3P^{-1}+30P\alpha$	$-3P^{-1}-30P\alpha$	$6P^{-2}+6P^2+72\alpha+\beta$				
M_{θ_4}/b	0	$-\alpha$	$30P\alpha$	0	-5α	$30P\alpha$	-5α	0	$30P\alpha$	2		
M_{ϕ_4}/a	$-\alpha$	0	$-6P^{-1}\alpha$	-5α	0	$30P^{-1}\alpha$	5α	0	$30P^{-1}\alpha$	25α	2	
R_4	$6P\alpha$	$6P^{-1}\alpha$	$72\alpha+\beta$	$30P\alpha$	$-3P^{-1}-6P\alpha$	$-6P^{-2}-72\alpha-\beta$	$-3P^{-1}-6P\alpha$	$30P\alpha$	$-6P^{-2}-72\alpha-\beta$	$3P^{-1}+30P\alpha$	$3P+30P^{-1}\alpha$	$6P^{-2}+6P^2+72\alpha+\beta$

If a complex structure may be thought of as a collection of plates
this approach may be used. With the help of a high speed computer the
stiffness matrix of the complete structure may be assembled. In addition,
beams in bending running in any direction along the node lines may be
added. The program used to determine the mode shapes of this type of
structure is described in Appendix G.

Table B-4 shows the glider mass distribution. The fuselage stiff-
ness is approximated by using a plate and a beam as shown in Fig. B-5.
Because of machine limitations only the deflections, w, are used so the
appropriate terms (Θ and Φ terms) in the stiffness matrix are set to zero.

Fig. B-6 shows the first three mode shapes determined.

4. COUPLING

Coupling is a typical eigenvalue problem which for our case is
followed by orthogonalizing the resulting eigenvectors. The uncoupled
mode shapes are related to the coupled mode shapes by the modal matrix
of the orthogonalized coupled system.

Shown in Figs. B-7, B-8, and B-9 are typical coupled mode shapes.

5. MODE SHAPES USED

Presented in Tables B-5 through B-12 are the modal values that are
used in this study.

The difference between beam modes and coupled modes is that the beam
modes are determined by representing the vehicle as an elastic line while
the coupled modes are determined by coupling the beam modes with the glider
plate modes.

Since only the deflections have been calculated in the coupling pro-
gram, the slopes have been determined by the method which is illustrated
below. In addition, for modal values other than start burn, 1/4 burnout,
1/2 burnout, 3/4 burnout, and burnout for both stages, a linear interpre-
tation is used.

For the release problem as well as the separation problem the coupled
modes are used, but only the modal values along the centerline are used.
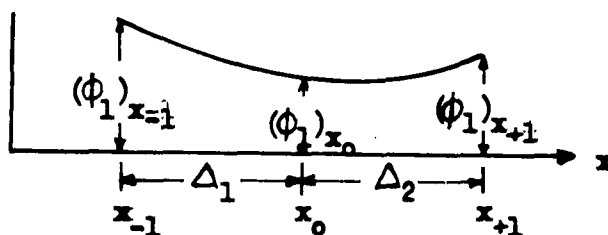
FIG. B-3

$$(\phi_1)'_{x_0} = 1/2 \left[\frac{(\phi_1)_{x_{-1}} - (\phi_1)_{x_0}}{x_0 - x_{-1}} + \frac{(\phi_1)_{x_0} - (\phi_1)_{x_{+1}}}{x_{+1} - x_0} \right]$$

TABLE B-1

FIRST – STAGE BOOST

27 MASS POINTS

Station Number	EI, 10^{10} in-lbs.	K'GA, 10^6 lbs.	Weight in Pounds				
			t = 0	t = 1/4	t = 1/2	t = 3/4	Burn-Out
33	.25	10	147				
75	.65	21	440				
117	1.2	32	773				
159	7.5	55	1082				
201	11.1	67.5	1177				
243	12.1	72.5	596				
285	12.9	77.5	693				
327	13.7	82	1005				
369	11.3	50	1245				
411	19.2	50	1842				
455	41.5	87	555				
505	56.5	86	1384				
587	64	84	3035				
696	64	84	3035				
804	64	84	3009				
896	92	122	23401				
960	152.5	164	15025				
1027	188	169	3365	3159	3159	3159	3159
1100	209	177	21837	22233	1007	1007	1007
1175	209	182	48555	48555	24781	1007	1007
1259	209	182	48555	48555	48555	27329	1007
1343	209	182	48555	20261	20261	20261	1583
1418	209	182	36315	23463	963	720	720
1481	209	182	29909	29411	29411	7154	708
1541	209	182	29411	19213	19213	19213	3159
1603	216	179	19213				
1656	223	176	3841				

SECOND-STAGE BOOST

23 MASS POINTS

Station Number	EI,10^{10} in-lbs	K'GA 10^6 lbs	Launch	1/4 burn	1/2 burn	3/4 burn	burnout
				Weight in pounds			
33			147				
75	.25	10	440				
117	.65	21	773				
159	1.2	32	1082				
201	7.5	55	1177				
243	11.1	67.5	596		same as launch		
285	12.1	72.5	693				
327	12.9	77.5	1005				
369	13.7	82	1245				
411	11.3	50	1842				
455	19.2	50	555				
505	41.5	87	1384	861	861	861	861
560	56.5	86	1518	222	222	222	222
614	64	84	1517	1136	221	221	221
669	64	84	1518	1518	223	222	222
723	64	84	1517	1517	1517	221	221
777	64	84	1505	1505	1505	612	220
831	64	84	1504	1504	1504	1504	219
872	64	84	3962	623	623	623	231
899	64	84	9710	4249	362	362	231
923	64	84	9909	9909	4996	83	83
947	64	84	9458	9458	9458	5571	110
974	64	84	3943	3943	3943	3943	604

TABLE B-3
GLIDER ALONE

10 MASS POINTS

Station Number	EI,10^{10} in-lbs	K'GA, 10^6 lbs	Weight lbs
33	.25	10	147
75	.65	21	440
117	1.2	32	773
159	7.5	55	1082
201	11.1	67.5	1177
243	12.1	72.5	596
285	12.9	77.5	693
327	13.7	82	1005
369	11.3	50	1245
411			1842

GLIDER WEIGHT DISTRIBUTION

Point Number	Body Station Number Inches	Distance from Centerline Inches	Weight Pounds
1	33	0	73.5
2	75	0	220
3	117	0	330.5
4	159	0	417.65
5	201	0	403.8
6	243	0	81.3
7	285	0	91.8
8	327	0	83.3
9	369	0	227.8
10	411	0	515.3
11	117	30	56
12	159	30	123.35
13	201	30	130.7
14	243	30	130.7
15	285	30	130.7
16	327	30	130.7
17	369	30	130.7
18	411	30	130.7
19	201	69	54
20	243	60	86
21	285	60	70
22	327	60	205
23	369	60	70
24	411	60	70
25	285	90	54
26	327	90	83.5
27	369	90	70
28	411	90	70
29	369	97.5	124
30	411	97.5	135

TABLE B-5

NORMALIZED CANTILEVER BEAM MODES

Body Station Inches	ϕ_1	ϕ'_1 $10^3/\text{inch}$	ϕ_2	ϕ'_2 $10^3/\text{inch}$	ϕ_3	ϕ_4	ϕ_5
33	1.000	.987	1.000	2.193	1.000	1.000	1.000
75	.959	.981	.908	2.160	.810	.718	.623
117	.917	.969	.818	2.087	.630	.462	.300
159	.877	.950	.731	1.967	.468	.253	.069
201	.837	.943	.649	1.924	.324	.087	-.083
243	.797	.934	.568	1.871	.189	-.060	-.202
285	.758	.921	.489	1.796	.065	-.185	-.289
327	.720	.904	.415	1.697	-.045	-.283	-.339
369	.682	.883	.345	1.574	-.137	-.350	-.350
411	.645	.849	.280	1.385	-.208	-.379	-.316
455	.608	.822	.220	1.240	-.258	-.371	-.241
505	.567	.804	.158	1.147	-.294	-.339	-.149
587	.501	.775	.066	1.003	-.328	-.260	.006
696	.418	.728	-.036	.781	-.325	-.124	.178
804	.341	.664	-.101	.499	-.274	.007	.252
896	.282	.594	-.146	.213	-.197	.084	.212
960	.245	.552	-.155	.062	-.128	.095	.095
1027	.208	.521	-.156	-.033	-.055	.085	-.029
1100	.170	.487	-.150	-.116	-.019	.062	-.139
1175	.134	.450	-.138	-.187	-.083	.025	-.182
1259	.096	.399	-.116	-.250	.128	-.023	-.094
1343	.064	.338	-.088	-.282	.139	-.059	.070
1418	.039	.272	-.062	-.276	.122	-.070	.180
1481	.023	.209	-.040	-.242	-.092	-.061	.203
1541	.011	.141	-.022	-.182	-.058	-.043	.163
1603	.003	.067	-.007	-.095	-.023	-.019	.077
1656	.000	.000	.000	.000	.000	.000	.000
ω in cps	.956		2.495		5.76	9.41	13.63

TABLE B-6

FLEXIBLE BASE NORMALIZED BEAM MODES

Body Station Inches	ϕ_1	ϕ_1' $10^3/\text{inch}$	ϕ_2	ϕ_2' $10^3/\text{inch}$	ϕ_3	ϕ_4
33	1.000	.650	1.000	1.820	1.000	4.120
75	.973	.648	.923	1.806	.827	3.980
117	.946	.646	.848	1.750	.662	3.680
159	.918	.643	.775	1.670	.512	3.220
201	.891	.642	.705	1.640	.377	3.060
243	.864	.641	.636	1.600	.248	2.880
285	.838	.640	.569	1.550	.129	2.620
327	.811	.639	.504	1.480	.022	2.310
369	.784	.637	.443	1.400	-.070	1.930
411	.757	.634	.385	1.260	-.145	1.370
455	.729	.632	.330	1.160	-.201	.975
505	.698	.631	.272	1.090	-.247	.738
587	.646	.629	.184	.988	-.298	.411
696	.578	.625	.081	.822	-.322	-.016
804	.510	.620	.000	.605	-.296	-.442
896	.453	.615	-.049	.380	-.236	-.774
960	.414	.612	-.070	.256	-.172	-.881
1027	.373	.610	-.086	.172	-.102	-.886
1100	.328	.607	-.096	.093	-.028	-.819
1175	.283	.604	-.100	.015	.041	-.685
1259	.232	.599	-.098	-.070	.099	-.454
1343	.182	.594	-.087	-.149	.130	-.168
1418	.138	.588	-.071	-.208	.130	.092
1481	.101	.582	-.055	-.246	.110	.283
1541	.066	.572	-.037	-.272	.080	.421
1603	.030	.568	-.017	-.285	.039	.502
1656	.000	.561	.000	-.286	.000	.519
ω in cps	.242		2.03		5.15	

TABLE B-7

COUPLED MODES -- FIRST STAGE START BURN

Body Station Inches	ϕ_1	ϕ_2	ϕ_3	ϕ_4	ϕ_5	ϕ_6	ϕ_7	ϕ_8
33	.991	-.240	.666	.989	-.137	.887	1.000	.161
75	.898	-.196	.513	.689	-.076	.522	.473	.092
117	.807	-.154	.378	.419	-.032	.209	.068	-.001
159	.720	-.119	.256	.202	-.012	-.012	-.142	-.046
201	.636	-.090	.149	.032	-.010	-.154	-.209	-.068
243	.555	-.063	.048	-.116	-.013	-.264	-.228	-.082
285	.476	-.038	-.044	-.239	-.020	-.340	-.211	-.086
327	.401	-.018	-.124	-.333	-.030	-.379	-.165	-.083
369	.331	-.001	-.189	-.394	-.041	-.379	-.098	-.073
411	.267	.010	-.238	-.415	-.053	-.334	-.015	-.054
455	.210	.012	-.272	-.396	-.066	-.252	.065	-.032
505	.148	.021	-.286	-.349	-.069	-.147	.129	-.006
587	.060	.023	-.294	-.250	-.070	.017	.192	.025
696	-.036	.019	-.267	-.092	-.055	.186	.171	.041
804	-.101	.016	-.204	-.048	-.025	.242	.065	.029
896	-.129	.004	-.131	.118	.002	.178	-.033	.004
960	-.130	.000	-.072	.113	.014	.042	-.051	-.012
1027	-.123	-.003	-.015	.084	.019	-.086	-.057	-.018
1100	-.107	-.006	.038	.043	.020	-.189	-.012	-.018
1175	-.083	-.007	.075	-.004	.012	-.195	.019	-.003
1259	-.049	-.007	.086	-.047	-.004	-.031	.026	.017
1343	-.007	-.004	.064	-.060	-.015	.154	-.004	.007
1418	-.033	.000	.019	-.038	-.014	.185	-.026	-.013
1481	.069	.003	-.030	-.002	-.005	.095	-.022	-.016
1541	.103	.007	-.080	.039	-.006	-.051	-.001	-.003
1603	.138	.011	-.129	.080	.018	-.201	.026	.015
1656	.168	.014	-.169	.111	.030	-.345	.043	.026
ω in cps	2.60	5.72	6.83	10.48	14.04	16.13	21.02	24.80

NORMALIZED BEAM MODES -- FIRST STAGE BOOST AT $t=56$ SEC FROM LAUNCH

Body Station Inches	Φ_1	Φ_1' 10^2/inch	Φ_2	Φ_2' 10^2/inch
33	1.0	.241	1.0	.587
75	.898	.240	.767	.534
117	.798	.237	.551	.478
159	.699	.219	.366	.409
201	.614	.204	.208	.360
243	.527	.204	.064	.326
285	.443	.194	-.065	.283
327	.364	.182	-.174	.231
369	.290	.167	-.260	.170
411	.223	.150	-.317	.099
455	.162	.131	-.344	.040
505	.101	.115	-.353	-.008
587	.012	.098	-.338	-.040
696	-.083	.072	-.271	-.077
804	-.145	.041	-.171	-.098
896	-.167	.010	-.076	-.101
960	-.164	-.012	-.013	-.090
1027	-.151	-.024	.042	-.073
1100	-.130	-.033	.089	-.053
1175	-.102	-.042	.121	-.027
1259	-.062	-.049	.130	.011
1343	-.020	-.054	.102	.057
1418	.023	-.058	.042	.091
1481	.060	-.061	-.023	.107
1541	.098	-.062	-.090	.111
1603	.135	-.060	-.158	.105
1656	.167	-.061	-.212	.096
ω in cps	2.80		7.28	

COUPLED MODES -- FIRST STAGE BOOST AT t=56 SEC FROM LAUNCH

Body Station Inches	Distance from Centerline	ϕ_1	ϕ_1' 10^2/in	ϕ_2	ϕ_2' 10^2/in	ϕ_3	ϕ_3' 10^2/in
33	0	.992	.224	-.214	-.099	.791	.476
75	0	.892	.235	-.174	-.090	.601	.436
117	0	.795	.227	-.138	-.080	.425	.392
159	0	.702	.217	-.107	-.068	.272	.338
201	0	.612	.210	-.081	-.060	.141	.300
243	0	.525	.203	-.057	-.054	.020	.272
285	0	.442	.194	-.036	-.048	-.088	.234
327	0	.363	.182	-.016	-.038	-.176	.197
369	0	.289	.167	-.004	-.026	-.253	.151
411	0	.222	.149	.006	-.016	-.303	.090
455	0	.161	.130	.010	-.008	-.329	.039
505	0	.100	.115	.013	-.003	-.338	-.006
587	0	-.012	.097	.013	.003	-.329	-.057
696	0	-.083	.072	.007	.005	-.273	-.068
804	0	-.145	.041	.003	.005	-.182	-.075
896	0	-.167	.011	-.003	.004	-.091	-.100
960	0	-.166	-.012	-.005	.003	-.026	-.093
1027	0	-.152	-.025	-.006	.002	.031	-.078
1100	0	-.130	-.033	-.007	.001	.082	-.059
1175	0	-.103	-.041	-.008	0	.118	-.016
1259	0	-.064	-.049	-.007	-.002	.132	.008
1343	0	-.020	-.055	-.005	-.004	.105	.056
1418	0	.023	-.059	-.001	-.005	.045	.093
1481	0	.061	-.061	.002	-.005	-.021	.110
1541	0	.098	-.061	.005	-.005	-.090	.114
1603	0	.136	-.060	.009	-.005	-.160	.108
1656	0	.168	-.059	.011	-.005	-.215	.097
117	30	.795	.227	-.138	-.080	.425	.392
159	30	.702	.217	-.107	-.068	.272	.338
201	30	.612	.210	-.081	-.060	.141	.300
243	30	.525	.203	-.057	-.054	.020	.272
285	30	.492	.194	-.035	-.047	-.088	.238
327	30	.363	.182	-.017	-.039	-.180	.196
369	30	.289	.167	-.003	-.028	-.252	.146
411	30	.222	.149	.006	-.022	-.302	.095
201	60	.615	.201	-.084	-.076	.142	.300
243	60	.531	.195	-.049	-.097	.027	.244
285	60	.451	.183	-.002	-.127	-.063	.173
327	60	.377	.171	.058	-.162	-.118	.076
369	60	.307	.159	.133	-.160	-.127	.009
411	60	.243	.145	.192	-.131	-.126	-.060
285	90	.471	.156	.074	-.329	-.030	-.042
327	90	.407	.146	.242	-.443	.041	-.233
369	90	.348	.138	.446	-.455	.167	-.304
411	90	.292	.130	.625	-.408	.296	-.357
369	97.5	.384	.120	.732	-.640	.441	.142
411	97.5	.334	.116	1.008	-.616	.680	-.142

| ω in cps | | 2.79 | | 5.74 | | 7.465 | |

TABLE B-10
COUPLED MODES— FIRST STAGE BOOST
MODES NORMALIZED TO STATION 33

Body Station Inches	0 ϕ_1	20 ϕ_1	20 $10^2\phi_1'/in$	33.75 ϕ_1	33.75 $10^2\phi_1'/in$	45.5 ϕ_1	45.5 $10^2\phi_1'/in$	50.9 ϕ_1	50.9 $10^2\phi_1'/in$	53 ϕ_1	53 $10^2\phi_1'/in$
33	1.0	1.0	.228	1.0	.250	1.0	.250	1.0	.250	1.0	.250
75	.908	.902	.232	.899	.237	.900	.237	.900	.237	.900	.237
117	.814	.806	.222	.801	.227	.801	.228	.801	.229	.801	.230
159	.726	.716	.211	.709	.214	.708	.217	.707	.218	.707	.219
201	.642	.629	.203	.621	.206	.619	.209	.618	.210	.618	.211
243	.559	.545	.196	.536	.199	.532	.202	.531	.204	.530	.204
285	.480	.464	.188	.454	.190	.449	.193	.447	.195	.446	.195
327	.405	.388	.177	.376	.179	.370	.181	.367	.183	.366	.183
369	.334	.315	.163	.303	.165	.297	.167	.293	.168	.292	.168
411	.270	.251	.109	.238	.147	.230	.149	.226	.150	.225	.150
455	.290	.223	.125	.177	.130	.169	.131	.165	.131	.164	.131
505	.149	.130	.147	.116	.111	.108	.115	.104	.115	.102	.116
587	.061	.041	.098	.028	.098	.019	.098	.015	.098	.013	.098
696	-.036	-.055	.074	-.068	.073	-.076	.073	-.081	.073	-.082	.073
804	-.102	-.119	.044	-.131	.042	-.139	.042	-.113	.042	-.115	.041
896	-.130	-.144	.011	-.155	.012	-.163	.012	-.166	.011	-.168	.011
960	-.132	-.116	-.007	-.151	-.009	-.161	-.011	-.165	-.011	-.166	-.012
1027	-.124	-.135	-.020	-.142	-.022	-.148	-.024	-.151	-.025	-.152	-.025
1100	-.108	-.117	-.029	-.123	-.031	-.128	-.032	-.130	-.033	-.131	-.033
1175	-.084	-.091	-.038	-.097	-.039	-.100	-.041	-.102	-.041	-.102	-.041
1259	-.049	-.056	-.047	-.060	-.048	-.063	-.049	-.064	-.049	-.064	-.049
1343	-.008	-.013	-.054	-.016	-.055	-.018	-.055	-.020	-.055	-.020	-.056
1418	.033	.029	-.057	.027	-.059	.025	-.060	.024	-.059	.024	-.059
1481	.069	.066	-.059	.064	-.060	.063	-.061	.062	-.061	.062	-.061
1541	.104	.102	-.059	.101	-.060	.100	-.061	.099	-.061	.099	-.061
1603	.139	.139	-.058	.138	-.060	.138	-.060	.137	-.061	.137	-.061
1656	.169	.169	-.052	.169	-.053	.169	-.053	.169	-.054	.169	-.054
ω in cps	2.599	2.661		2.709		2.750		2.769		2.777	

Time in seconds

TABLE B-10 (continued)
COUPLED MODES — FIRST STAGE BOOST
MODES NORMALIZED TO STATION 33

Time in seconds

Body Station Inches	55.02 ϕ_1	55.02 ϕ_1' $10^2/in$	56.95 ϕ_1	56.95 ϕ_1' $10^2/in$	58.82 ϕ_1	58.82 ϕ_1' $10^2/in$	60.62 ϕ_1	60.62 ϕ_1' $10^2/in$	67.5 ϕ_1	67.5 ϕ_1' $10^2/in$
33	1.0	.250	1.0	.250	1.0	.250	1.0	.250	1.0	.250
75	.900	.237	.900	.237	.900	.237	.900	.237	.900	.236
117	.801	.230	.801	.230	.801	.230	.801	.230	.801	.231
159	.707	.219	.707	.219	.707	.220	.707	.220	.706	.222
201	.617	.211	.617	.211	.617	.212	.616	.213	.615	.215
243	.530	.205	.530	.205	.529	.206	.528	.206	.526	.208
285	.445	.195	.445	.196	.444	.196	.443	.197	.440	.198
327	.366	.183	.365	.184	.364	.184	.363	.185	.360	.186
369	.291	.169	.291	.169	.290	.169	.288	.170	.284	.171
411	.224	.150	.223	.150	.222	.151	.221	.151	.216	.152
455	.162	.131	.162	.131	.160	.132	.159	.132	.154	.132
505	.101	.116	.100	.116	.099	.116	.098	.116	.092	.116
587	.012	.098	.011	.098	.010	.098	.008	.098	.003	.098
696	-.084	.073	-.084	.073	-.086	.073	-.087	.073	-.093	.073
804	-.146	.041	-.147	.041	-.148	.041	-.150	.041	-.155	.041
896	-.169	.011	-.170	.011	-.171	.011	-.172	.011	-.177	.011
960	-.167	-.012	-.168	-.012	-.169	-.012	-.171	-.013	-.176	-.013
1027	-.153	-.026	-.153	-.026	-.151	-.026	-.155	-.027	-.159	-.028
1100	-.131	-.034	-.132	-.034	-.133	-.034	-.133	-.034	-.136	-.035
1175	-.103	-.042	-.103	-.042	-.104	-.042	-.105	-.042	-.107	-.043
1259	-.065	-.049	-.065	-.050	-.065	-.050	-.066	-.050	-.068	-.050
1343	-.020	-.056	-.020	-.056	-.021	-.056	-.021	-.056	-.022	-.056
1418	.024	-.060	.024	-.060	.024	-.060	.023	-.060	.022	-.060
1481	.0619	-.061	.062	-.061	.062	-.061	.061	-.062	.060	-.062
1541	.099	-.062	.099	-.062	.099	-.062	.098	-.062	.098	-.062
1603	.137	-.061	.137	-.061	.137	-.061	.137	-.061	.136	-.062
1656	.169	-.054	.169	-.054	.169	-.054	.169	-.054	.169	-.054
ω in cps	2.785		2.792		2.800		2.807		2.833	

TABLE B-11

NORMALIZED COUPLED MODES - FIRST STAGE BURNOUT AND SECOND STAGE START BURN

First Stage Burnout		Second Stage Start Burn	
Body Station Inches	ϕ	Body Station Inches	ϕ
33	1.000	33	-.249
75	.884	75	-.205
117	.771	117	-.165
159	.665	159	-.129
201	.565	201	-.097
243	.468	243	-.068
285	.376	285	-.041
327	.290	327	-.019
369	.211	369	-.001
411	.141	411	.011
455	.079	455	.017
505	.020	505	.020
587	-.062	560	.020
696	-.142	614	.019
804	-.180	669	.017
896	-.176	723	.013
960	-.151	777	.008
1027	-.113	831	.002
1100	-.064	872	-.003
1175	-.007	899	-.006
1259	.062	923	-.009
1343	.136	947	-.011
1418	.206	974	-.014
1481	.266		
1541	.323		
1603	.384		
1656	.435		

ω in cps 3.34   5.72

COUPLED MODES - GLIDER FREE-FREE

Body Station Inches	Distance from Centerline	ϕ_1	ϕ'_1 10^2/Ft	ϕ_2	ϕ'_2 10^2/Ft	ϕ_3	ϕ_4	ϕ_5	ϕ_6
33	0	.107	1.484	-.110	-1.276	.987	.518	-.223	-.063
75	0	.069	1.060	-.077	-.840	.440	.200	-.027	-.009
117	0	-.032	1.008	-.051	-.589	-.038	-.026	.076	.016
159	0	-.002	.946	-.036	-.280	-.151	-.121	.071	.005
201	0	-.034	.905	-.031	-.068	-.183	-.128	.021	-.014
243	0	-.065	.882	-.031	-.085	-.165	-.108	-.012	-.049
285	0	-.096	.861	-.037	.290	-.108	-.080	-.035	-.081
327	0	-.125	.844	-.052	.550	-.020	-.050	-.057	-.098
369	0	-.155	.836	-.076	.843	.084	-.019	-.090	-.091
411	0	-.184	.835	-.110	.995	.193	.021	-.139	-.063
117	30	.032	.975	.051	-.427	.038	-.026	.072	.016
159	30	-.002	.946	-.036	-.281	-.151	-.121	.071	.005
201	30	-.034	.905	-.031	-.077	-.184	-.128	.018	-.012
243	30	-.065	.881	-.031	.064	-.166	-.107	-.017	-.045
285	30	-.096	.856	-.036	.271	-.109	-.077	-.035	-.080
327	30	-.125	.836	-.050	.560	-.021	-.048	-.052	-.100
369	30	-.154	.829	-.075	.889	.084	-.019	-.083	-.088
411	30	-.183	.831	-.112	1.055	.193	.021	-.131	-.051
201	60	-.035	.693	-.019	-3.101	-.280	-.113	-.360	.293
243	60	-.050	.458	.090	-3.717	-.378	.125	-.700	.535
285	60	-.067	-.051	.241	-2.930	-.323	.279	-.266	.139
327	60	-.066	-.666	.295	2.024	-.084	.141	.498	-.391
369	60	-.021	-.824	.100	8.812	.122	-.038	.363	.185
411	60	.002	-.643	-.322	12.049	.121	.097	.666	1.238
285	90	000	-3.421	.818	-4.640	-.738	.990	.825	.632
327	90	.119	-4.137	.980	4.474	-.132	.362	.840	-.595
369	90	.289	-4.544	.505	22.47	.229	-.185	.313	.340
411	90	.437	-4.234	-.593	31.36	-.079	.175	.770	1.182
369	97.5	.575	-7.231	.919	46.69	.398	-.467	-.473	.259
411	97.5	.828	-7.231	-.716	46.69	-.269	.171	-.230	-.653
ω in cps		6.58		14.06		22.35	24.70	38.21	40.05
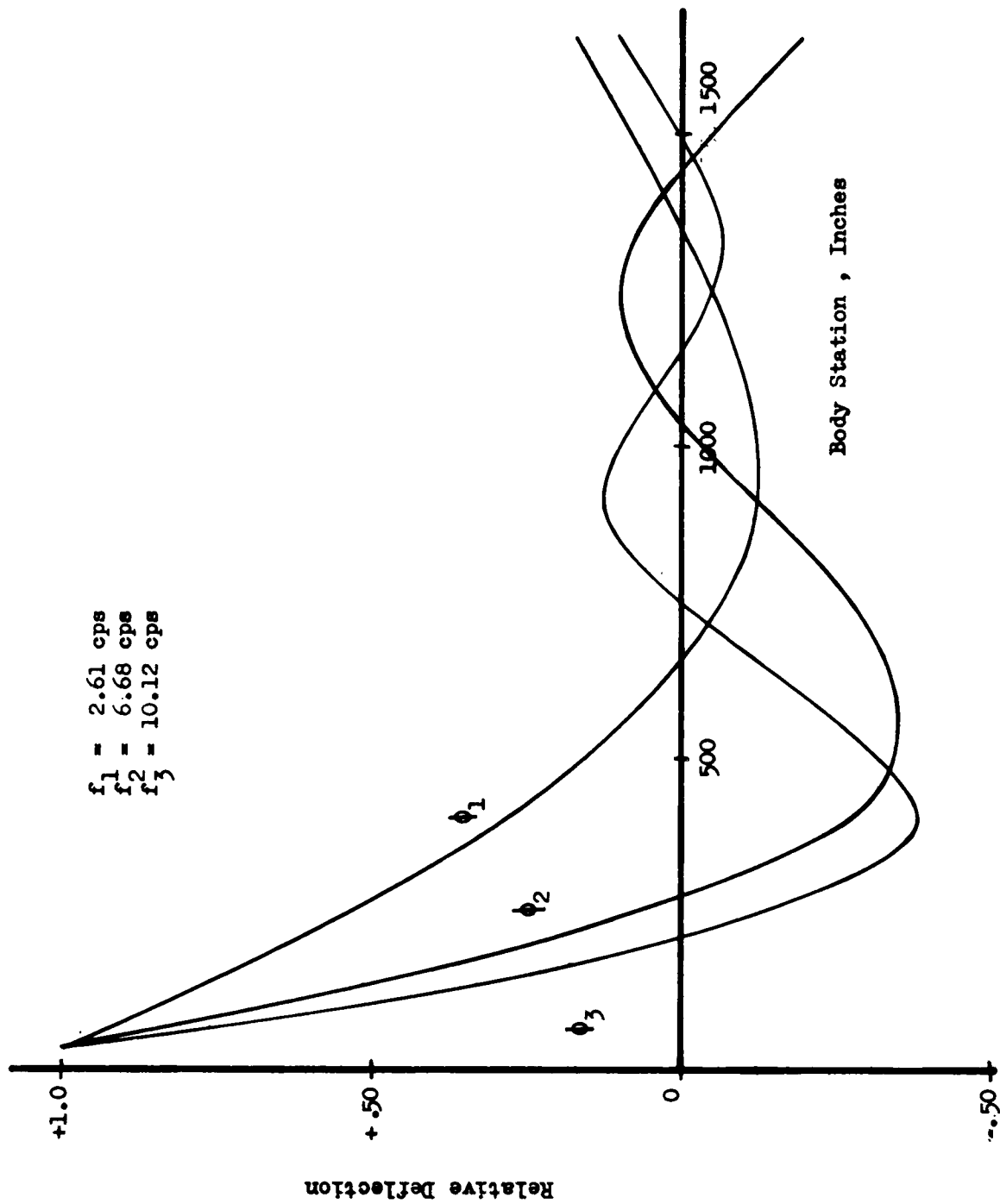
FIG. B-4   TYPICAL BEAM MODES -- FIRST STAGE START BURN

Station "O"

Station 159

Station 360

Station 432

30

35.6

C

C

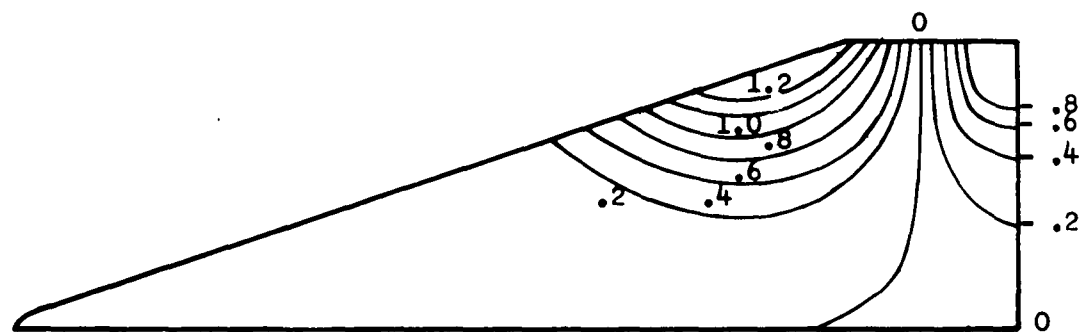$t = .01$ inch
$E = 29 \times 10^6$ lb/in^2
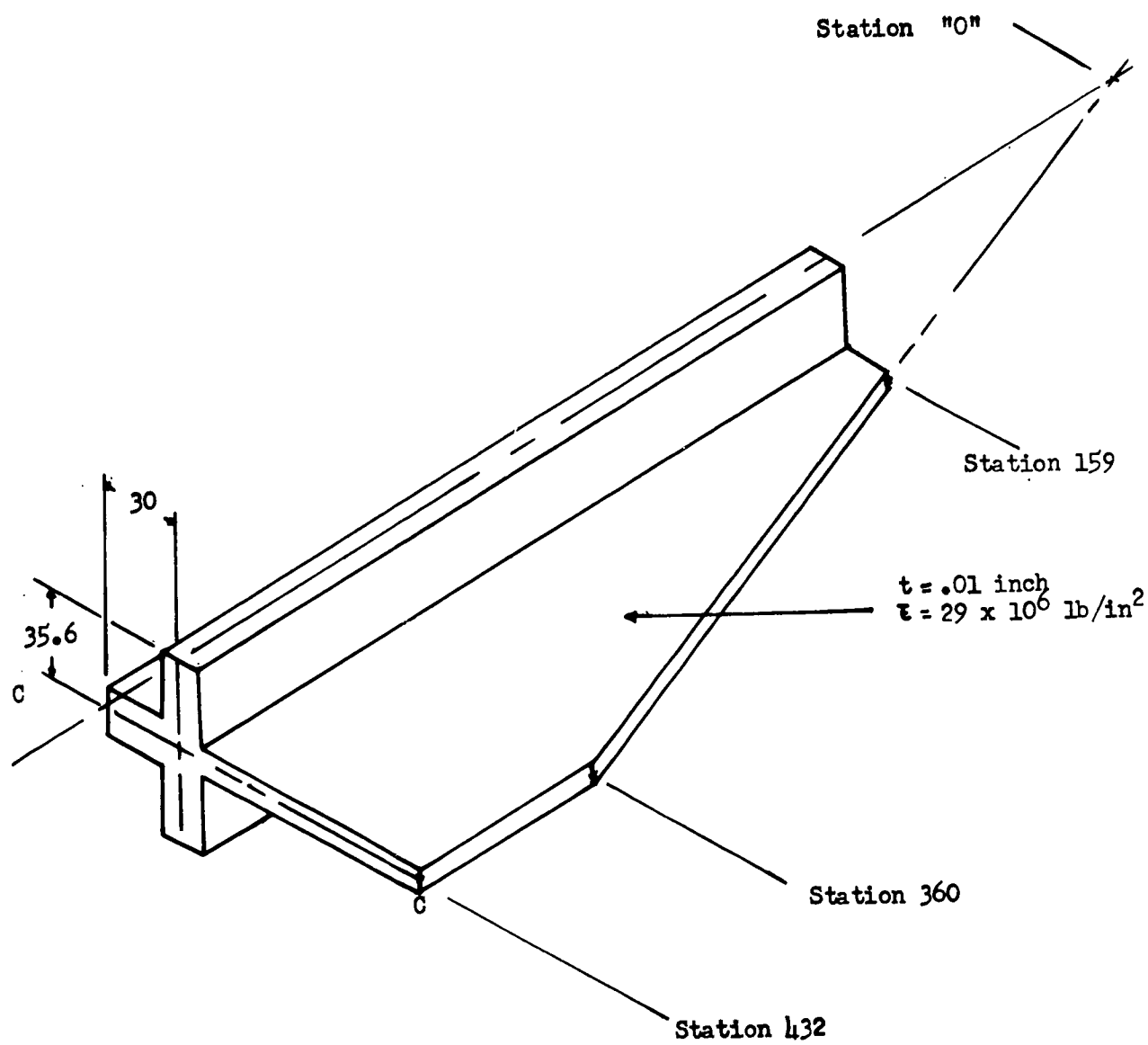
Icc Beam $= 300$ In^4
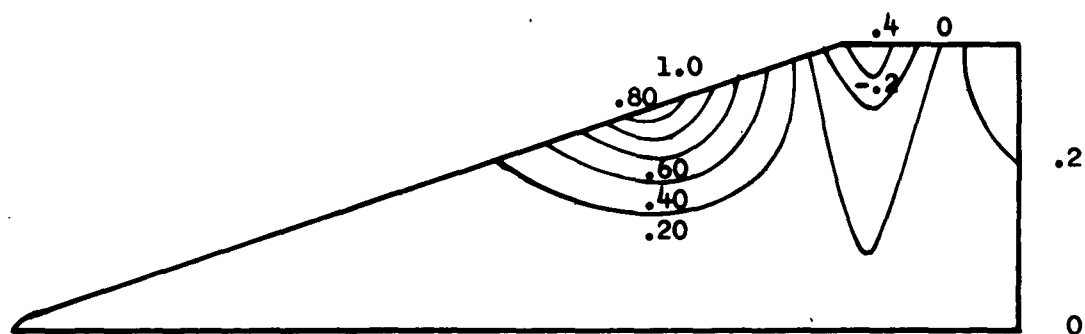
Icc Plate $= 1610$ In^4

FIG. B-5 EQUIVALENT GLIDER
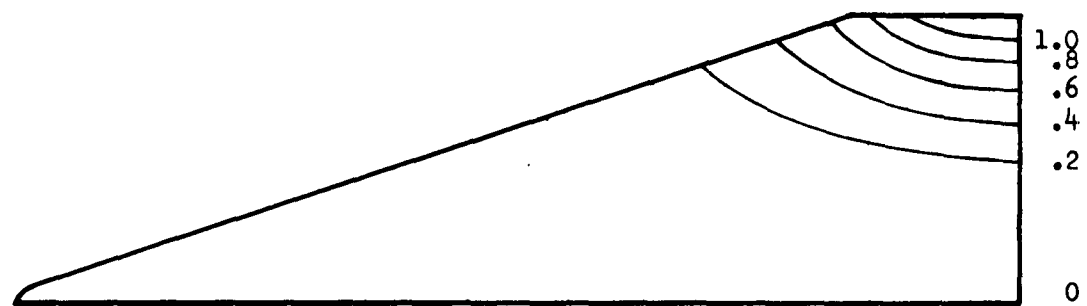
First Mode
ω = 5.73 cps

Second Mode
ω = 13.96 cps

Third Mode
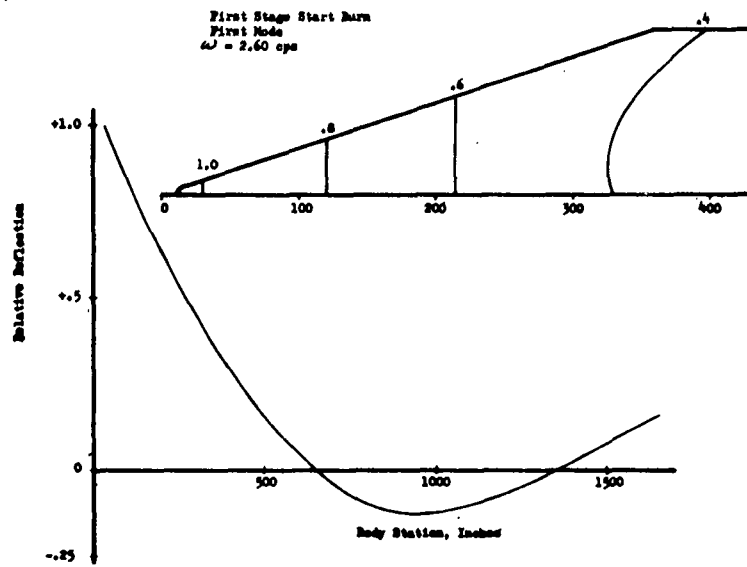ω = 23.76 cps

FIG. B-6   TYPICAL PLATE MODES
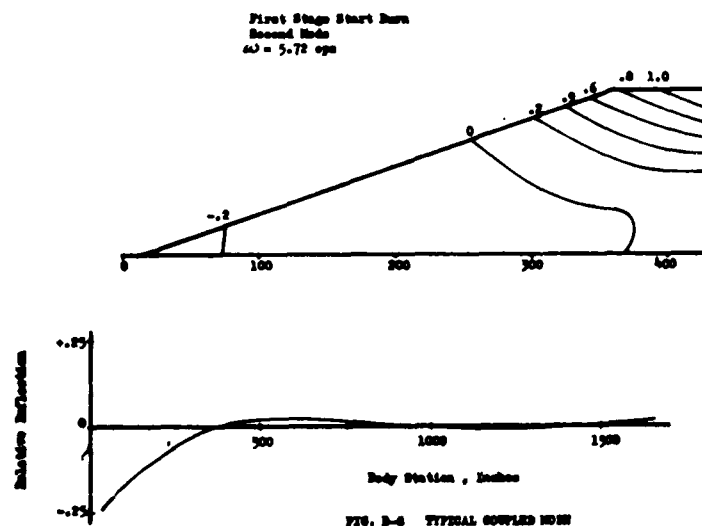
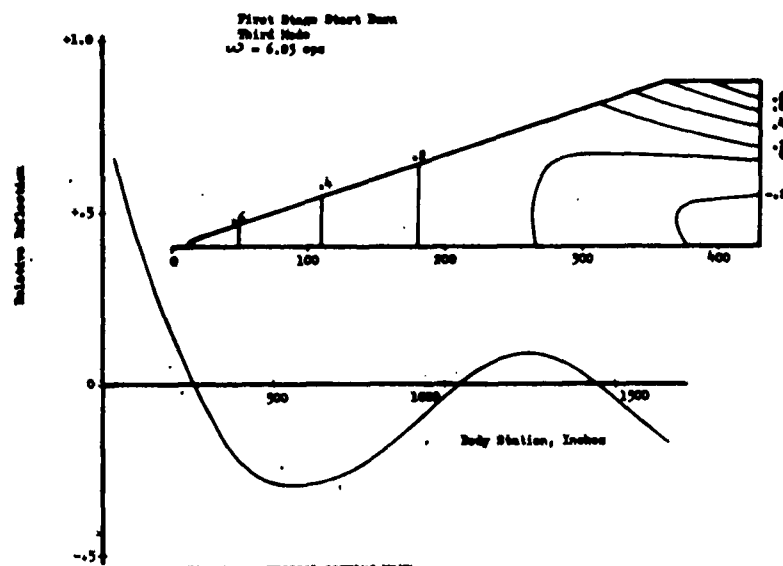Fig. B-7 TYPICAL COUPLED MODE

Fig. B-8 TYPICAL COUPLED MODE

Fig. B-9 TYPICAL COUPLED MODE

APPENDIX C

FLIGHT EQUATIONS OF MOTION

The purpose of the following is to discuss some of the physics employed in the modeling of the actual boost-glide system studied and to display the equations governing the motion of the modeled system in flight.

1.   EQUATIONS OF MOTION GOVERNING A SYSTEM HAVING A MASS EFFLUX

   a. Application of Newton's Equation

   We define the system ,S, to be considered as all that within the closed envelope E, the surface of which is coincident with the surface of the vehicle together with planes at the exit area of the nozzles. Since the mass in E is not conserved, the "principle of mass center" cannot be applied directly to S. The first task taken in modeling the actual system is to show that the effect of the time rate of mass efflux from S can be replaced by a force. In doing this the propulsion system (its chemical, hydrodynamic and thermodynamic effect) is replaced by a mechanical force.

   Have a partition of S such that at any future time τ, $S_1(\tau)$ represents the system of particles in and on E and $S_2(\tau) = S(0) - S_1(\tau)$. $S_2(\tau)$ represents the system of particles ejected from S(0) during the interval τ.

Let ($\overline{}$)   :   designation of a vector

   m   :   mass

   m_E :   mass within and on E

   $\overline{r}$:   inertial position vector of mass m

   $\overline{R}_E$:   inertial position vector of center of mass within and on E

   $\overline{R}_S$:   inertial position vector of center of mass within S

   $\overline{F}$:   resultant external force acting on S_1

   $\overline{M}$:   resultant external moment acting on S_1 with respect to the mass center of S_1

   $\overline{H}_E$:   angular momentum of S_1 with respect to mass center of S_1

$m \equiv - \dfrac{dm_E}{dt}$:   mass rate of efflux

   $\overline{\rho}_E$:   position vector with respect to mass center of S_1

   σ_E :   surface of E

The linear momentum of S (t) is given by

$$\bar{L}_s(t) = \sum_s m \dot{\bar{r}} = \sum_{S_1} m \dot{\bar{R}}_\varepsilon(t) + \sum_{S_2} m \dot{\bar{R}}_\varepsilon(t) \qquad (C-1)$$

and of $S(t + \Delta t)$:

$$\bar{L}_s(t + \Delta t) = \sum_{S_1} m \dot{\bar{r}}(t + \Delta t) + \sum_{S_2} m \dot{\bar{r}}(t + \Delta t)$$

$$\bar{L}_s(t + \Delta t) = \sum_{S_1} m \dot{\bar{R}}_\varepsilon(t + \Delta t) + \sum_{S_2} m \dot{\bar{R}}_{S_2}(t + \Delta t) \qquad (C-2)$$

since

$$\dot{\bar{R}}_{S_1}(t + \Delta t) = \dot{\bar{R}}_\varepsilon(t + \Delta t) \qquad (C-3)$$

Application of Newton's second law to S yields

$$\bar{F} = \lim_{\Delta t \to 0} \left[\frac{\Delta \bar{L}}{\Delta t}\right] = \lim_{\Delta t \to 0} \left(\sum_{S_1} \frac{m \Delta \dot{\bar{R}}_\varepsilon}{\Delta t}\right) + \lim_{\Delta t \to 0} \left(\sum_{S_2} \frac{m[\dot{\bar{R}}_s(t + \Delta t) - \dot{\bar{R}}_\varepsilon(t)]}{\Delta t}\right) \quad (C-4)$$

Observe that for the system under consideration we assume:

$$\lim_{\Delta t \to 0} \sum_{S_2} m = 0 \qquad (C-5)$$

Further, that unless

$$\left| \int_{t_1}^{t + \Delta t} \left\{ \lim_{\Delta t \to 0} \left[\dot{\bar{R}}_{S_2}(\tau + \Delta \xi) - \dot{\bar{R}}_\varepsilon(\tau)\right] \right\} d\tau \right| > d \qquad (C-6)$$

where d is the minimum distance of some particle in S_2 from the walls of the envelope, the system S_2 will be void, and the features considered here trivial; in short a "flow" of mass through the envelope is presumed to take place.

Define $\bar{V}_r$ such that:

$$\lim_{\Delta t \to 0} \left[\dot{\bar{R}}_{S_2}(t + \Delta t) - \dot{\bar{R}}_\varepsilon(t) \right] = \bar{V}_r \qquad (C-7)$$

Then $(C-4)$ becomes:

$$\bar{F} = \frac{d\bar{L}_\varepsilon}{dt} + \bar{V}_r \lim_{\Delta t \to 0} \left(\frac{\sum_{S_2} m}{\Delta t}\right) \qquad (C-8)$$

The mass of $S(t)$ is conserved, hence:

$$\lim_{\Delta t \to 0} \left(\frac{\Delta M}{\Delta t}\right) = \lim_{\Delta t \to 0} \left(\frac{\Delta \sum_{S_1} m}{\Delta t} + \frac{\sum_{S_2} m}{\Delta t}\right) = 0 \qquad (C-9)$$

Since $\sum_S m \rightarrow \sum_{\mathcal{E}} m$ $\quad$ as $\quad \Delta t \rightarrow 0 \quad$ then

$$\lim_{\Delta t \to 0} \left(\frac{\Delta \sum_{S_i} m}{\Delta t} \right) = \frac{dm_{\mathcal{E}}}{dt} = -\lim_{\Delta t \to 0} \left(\frac{\sum_{S_i} m}{\Delta t} \right) \tag{C-10}$$

Finally then (C-8) can be written in the form:

$$\bar{\bar{F}} + \frac{dm_{\mathcal{E}}}{dt} \bar{V}_r = \frac{d\bar{L}_{\mathcal{E}}}{dt} \tag{C-11}$$

In conclusion, the mass efflux across the boundary of an envelope which defines a system acts on the system in the same manner as an externally applied force as indicated in Eqn. C-11.

A similar development reveals that the efflux produces a moment on the system within E.

$$\bar{M} = \frac{d\bar{H}_{\mathcal{E}}}{dt} - \sum_{\sigma_{\mathcal{E}}} \bar{\rho}_{\mathcal{E}} \times \dot{m}_{\mathcal{E}} \bar{V}_r \tag{C-12}$$
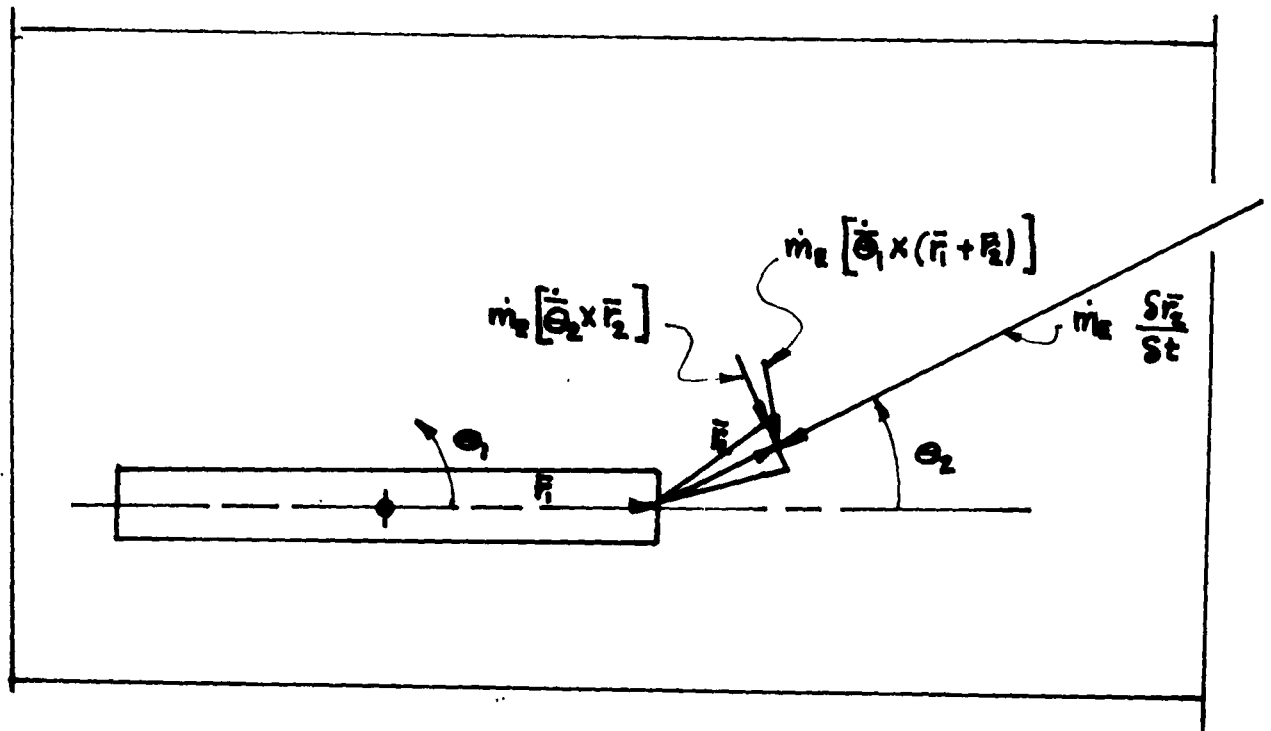

FIG. C-1

EXAMPLE OF FORCES EFFECTED BY A MASS EFFLUX

b. <u>Nature of the Force Effected by a Mass Efflux</u>

Given below is an illustration, having direct application to the system considered in this report, of the nature of the force effected by a mass efflux.

Consider a rigid body idealization of the system as pictured, Fig. C-1. Assume that the mass efflux of the system occurs at point P and is constrained to flow along the axis of the motor nozzle. The force caused by the efflux is:

$$\vec{f} = \dot{m}_E \vec{V}_r = \dot{m}_E \left[\dot{\vec{\theta}}_1 \times (\vec{r}_1 + \vec{r}_2) + \frac{\delta \vec{r}_1}{\delta t} + \dot{\vec{\theta}}_2 \times \vec{r}_2 + \frac{\delta \vec{r}_1}{\delta t}^{0} \right] \qquad (C-13)$$

since $\dfrac{\delta \vec{r}_1}{\delta t} = 0$ (rigid body).

The first and third terms on the right hand side of Eqn. C-13 results from pitch and nozzle rotational velocities respectively; the second term, $\dot{m}_E (\delta \vec{r}_2 / \delta t)$, is that part of $\vec{f}$ normally considered as the "motor thrust" resulting from a mass efflux since it acts along the axis of the motor nozzle.

Refinements in $\vec{f}$ can be made by considering a flexible vehicle in which case:

$$\frac{\delta \vec{r}_1}{\delta t} = \left| \frac{\delta \vec{r}_1}{\delta t} \cdot \vec{u}_a \right| \vec{u}_a + \left| \frac{\delta \vec{r}_1}{\delta t} \cdot \vec{u}_n \right| \vec{u}_n \qquad (C-14)$$

where

$\vec{u}_a$: unit vector along the body axis

$\vec{u}_n$: unit vector transverse to the body axis

$\dfrac{\delta}{\delta t}$: local derivative

the first term on the right-hand side of (C-14) being the relative velocity resulting from axial motion, and the second term being the relative velocity resulting from transverse (or bending) motion.

It seems obvious, then, that the calculation of $\dot{m}\, \vec{V}_r$ in Eqn. C-11 can be made as complex and detailed as one's patience might allow.

2. MODELING OF THE SYSTEM

a. Reduction of the System From a Continuum to a Discrete Set of Masses

The distribution of the masses in S does not admit throughout E of a simple continuous analytical function of the space coordinates, but an approximation may be obtained by a lumping of the masses into discrete rigid collections at a set of points. To each point one must assign six quantities: namely, a mass, any two of the three principal directions of the ellipsoid of inertia and the three mass moments of inertia associated with each of the axes of the ellipsoid. If the point associated with a particular lumped collection lies at the mass center of the collection and the ellipsoid of inertia of the actual distributed mass reckoned with respect to this point is the same as that assigned to the point, then the mass center and ellipsoid of inertia associated with the system are the same as that reckoned for the collection of points so defined; this is an obvious mechanical necessity. The finer the subdivision of the mass distribution of the system, the lesser will become the importance of the ellipsoid of inertia, especially for systems in which the local rotational velocities and accelerations are small. Such is the case for the system here considered except for the motor nozzles each of which is considered as a rigid body.

The relations of force vs. displacement between the lumped mass points should imitate as nearly as possible the force-displacement relations which exist between the same points in the actual system, and under a specified motion involving relative displacement, velocity and acceleration among the particles, the energy stored or the energy dissipated by the point model should be nearly the same as that in the actual system under the same conditions.

b. Kinetic Energy of the Modeled System

If the system considered is one which under the action of no external forces possesses an equilibrium position, then a convenient rigid reference frame is provided from which the displacements of the mass points may be measured. To determine the position of any mass point in the system relative to an inertial reference frame, one need only to determine the position of one point P of the equilibrium reference frame relative to the inertial frame, $\mathbf{F}$, the equilibrium position $\bar{r}_a$ (i) of a particular mass point i relative to P, and the displacement u_i from equilibrium at a given time t_1.

The inertial position vector $\overline{R}_i$ of any mass point, i, then is given by:

$$\overline{R}_i = \overline{r} + \overline{r}_a(i) + \overline{u}_i \qquad (C-15)$$

and the kinetic energy of the system is

$$T = 1/2 \sum_s m \; \dot{\overline{R}}^2 \qquad (C-16)$$

The exact form taken by $\overline{R}_i$, Eqn. (C-15), is dependent on the methods used to describe the displacement of various masses from the equilibrium position. The modal approach discussed in Appendix B and employed for the system considered assumes that the mass of the fuel and the motor nozzles are rigidly attached to the elastic line of flexure; hence the total kinetic energy is made up of two parts: the kinetic energy of the masses attached to the elastic line plus the kinetic energy resulting from motion relative to the elastic line of those masses which are not in fact rigidly attached to the elastic line.

c. Modeling of Masses Possessing Freedom to Displace from the

Elastic Line

The particles of the fuel are free to oscillate about the elastic line. For small translatory and rotary disturbances, the sloshing motion of the fuel can be replaced (using a rigorous analysis) by a mass fixed on the tank axis (coincident with elastic line) and a set of pendulae or spring supported masses at specified distances from the mass center of fluid in the tank (measured along the tank axis). The motor nozzles are free to rotate about a point (nozzle hinge point) fixed to the elastic line, but no special modeling is necessary.

d. Potential Energy of the Modeled System

The potential energy of the system obtains from two sources: (1) the elastic potential of flexure and (2) the potential of the displaced fluid in an acceleration field. If the fuel is modeled by a set of pendulae, the potential energy is given in terms of the relative angular displacement from the axis, the axial acceleration field and the pendulum mass; see part 4 of this Appendix. The orthogonalization of the flexural modes reduces the description of the flexural behavior of the system to a set of simple mass-spring systems, the spring constant in each member of the set being well defined. An analogous set of masses and springs can be obtained which represent the modes of the fuel slosh under an axial acceleration field. The familiar form

$$V = 1/2 \sum k \; q^2 \qquad (C-17)$$

takes account of the potential energy of the system.

e. Energy Dissipation in the Modeled System

A problem which has plagued many dynamic investigations is: "What sort of analytical representation will adequately describe the internal dissipation of energy of a given system?" For a simple mass-spring system the Rayleigh dissipation function, $\mathcal{F}$, as expressed as a fraction of the critical damping, ζ, each characteristic frequency, ω, generalized mass, M, and velocity, q, offers a relatively simple method of accounting for structural damping by means of an equivalent viscous damping;

$$\mathcal{F} = \sum M \omega \zeta \dot{q}^2 \qquad (C-18)$$

f. External Forces Acting on the System

Having defined the modeled system, S, the effect of the environment on it is discussed; this effect can be completely described by identifying and describing the nature of the body and surface forces acting on S.

The gravitational field produces the only body force acting on the system; no substantial variations in the gravitational field over the extension of the system are assumed at any point on the trajectory.

The surface forces acting on the system result from (1) hydrostatic atmospheric pressure (2) aerodynamic forces resulting from motion relative to the air (3) pressure at the exit area of the motor nozzles.

It is interesting to note that the term "thrust" as used in practice is not given solely by the term $\dot{m}\, \delta\bar{r}/\delta t$ in Eqn. (C-13) but is augmented by the surface forces (1) and (3) described above. The term "thrust" is generally defined for each engine by:

$$\bar{T} = \dot{m}\, \frac{\delta \bar{r}_s}{\delta t} + \left(p_e - p_a \right) \bar{A} \qquad (C-19)$$

where P_e : exit nozzle pressure

P_a : atmospheric pressure

$\bar{A}$: vector having the magnitude of the exit area and the direction of the inward normal to this area.

Detailed discussion of aerodynamic theories applicable in each instance of relative motion between the system and the air are discussed in the separate sections or problem areas.

g. Work Done on the System by the Control Mechanism

Within the vehicle there is provided a mechanism to produce a change in relative angular position of the motor nozzles from the tangent to the elastic axis at the hinge point of the motor nozzles. The control moment M_c is governed by attitude sensed Θ_s, attitude rate sensed $\dot{\Theta}_s$, programmed pitch attitude, Θ_1, time lags, T_i, resulting from the hydraulic actuating mechanism, electronic shaping networks, and springs ,k, representing the elastic stiffness of the control mechanism; the relation

$$M_c = M_c(\Theta_s, \dot{\Theta}_s, \Theta_1, T_i, K) \tag{C-20}$$

is called the control law and is specified in each problem area.

The work done by M_c arises from a change in the chemical and electrical potential of the system. Since only mechanical potential is given explicit treatment herein, mechanical effects resulting from nonmechanical causes must be treated separately, such is the case here.

3. EQUATIONS OF MOTION

a. Derivation

The Lagrangian form

$$\frac{d}{dt}\left(\frac{\partial T}{\partial \dot{\chi}}\right) - \frac{\partial T}{\partial \chi} + \frac{\partial V}{\partial \chi} + \frac{\partial \mathcal{F}}{\partial \dot{\chi}} = Q_\chi \tag{C-21}$$

is applicable to the system described herein, and is subject to the following definitions.

b. Kinetic Energy, T.

$$T = 1/2\ m_i\ (\dot{\bar{r}} + \dot{\bar{r}}_a + \dot{\bar{u}})^2$$

$$+ 1/2\ (m_o)\left[\ \dot{\bar{s}}_o^2 + 2(\dot{\bar{r}} + \dot{\bar{r}}_a + \dot{\bar{u}})\cdot\dot{\bar{s}}_o\ \right]$$

$$+ 1/2\ \sum_\ell \sum_k\ m_{\ell k}\left[\ \dot{\bar{s}}_{\ell k}^2 + 2(\dot{\bar{r}} + \dot{\bar{r}}_a + \dot{\bar{u}})\cdot\dot{\bar{s}}_{\ell k}\ \right] \tag{C-22}$$

$$+ 1/2\ (I_o)\left[\ \sum_i\ \phi_i'\ \dot{q}_i + \dot{q}_s + \dot{\psi}\ \right]^2$$

The kinetic energy of local rotary motion of the masses m_i has been neglected.

c. <u>Potential Energy, V</u>

$$V = \frac{1}{2} \sum_j M_j \omega_j^2 \, q_j^2 + \frac{1}{2} \sum_\ell \sum_k m_{\ell k} \, a_c \, q_{\ell k}^2 \qquad \text{(C-23)}$$

The first term represents the potential energy of the elastic structure and the second term, the potential energy of the sloshing fluid (see part 4 of this Appendix).

d. <u>Dissipation Function, $\mathcal{F}$</u>

$$\mathcal{F} = \sum_j M_j \omega_j \, \mathcal{J}_j \dot{q}_j^2 \qquad \text{(C-24)}$$

The fuel is assumed to be ideal and hence dissipates no energy; only the structure dissipates energy.

e. <u>Generalized Force, Q_χ</u>

The term Q_χ given by

$$Q_\chi = \sum_s \bar{F}_s \cdot \frac{\partial \bar{R} \, (\bar{F}_s)}{\partial \chi} \qquad \text{(C-25)}$$

can be decomposed in terms depending on the origin of the force, $\bar{F}_s$, as follows:

e_1) Gravitational Forces

$$Q_\chi(\bar{G}) = \sum m_i \bar{g} \cdot \frac{\partial}{\partial \chi} (\bar{r} + \bar{r}_a + \bar{u})$$
$$+ \; m_o \bar{g} \cdot \frac{\partial \bar{s}_o}{\partial \chi} + \sum_\ell \sum_k m_{\ell k} \, \bar{g} \cdot \frac{\partial \bar{s}_{\ell k}}{\partial \chi} \qquad \text{(C-26)}$$

e_2) Forces effected by thrust:

$$Q_\chi(\bar{T}) = \bar{T} \cdot \frac{\partial}{\partial \chi} (\bar{r} + \bar{r}_a + \bar{r}_T) \qquad \text{(C-27)}$$

e_3) Aerodynamic forces: $Q(A)$, which are discussed in each problem area.

e_4) Control force: $Q_\chi(C)$ is the generalized force resulting from the control moment and is discussed in the separate problem areas. Note that $Q_\chi(C)$ is nonzero only for $\chi = q_5$.

The following list, together with Fig. C-2, displays the definition of the terms appearing in equations.

i : mass station point located

m_i : lumped mass at station i; numerical value given in Appendix B.

m_o : mass of both motor nozzles

$m_{\ell k}$: $k^{\underline{th}}$ slosh mass in the $\ell^{\underline{th}}$ tank

I_o : mass moment of inertia of both motor nozzles

χ : generic notation for the generalized coordinates

$\bar{r}$: inertial position vector of the equilibrium mass center of the system

$\bar{r}_a$: axial position vector with respect to equilibrium mass center

$\bar{u}_i$: displacement vector of m_i transverse to the equilibrium axis

$\dot{q}_z$: transverse component of velocity of equilibrium mass center with respect to body fixed axes

$\dot{q}_x$: longitudinal component of velocity of equilibrium mass center with respect to body fixed axes

$\bar{s}_o$: displacement vector (measured from the corresponding point on the elastic axis) of the mass center of the motor nozzles

$\bar{s}_{\ell k}$: displacement vector (measured perpendicular to the elastic axis) of the mass, $m_{\ell k}$

ψ : attitude

x_1 : Cartesian component of $\bar{r}$ in the x_1 direction

x_2 : Cartesian component of $\bar{r}$ in the x_2 direction

x, z : body fixed coordinates

$\bar{I}', \bar{J}'$: unit vectors associated with body fixed coordinates

q_θ : perturbed angular displacement measured with respect to the programmed pitch attitude

θ_1 : programmed pitch attitude

q_j : generalized coordinate corresponding to the $j^{\underline{th}}$ flexural mode of the structure

$q_{\ell k}$: k^{th} slosh coordinate in the ℓth tank

ϕ_j : modal value associated with q_j

ϕ_j' : $\dfrac{\partial \phi_j}{\partial x}$

$\bar{g}$: gravitational field

a_c : carried acceleration field (see part 4 of this Appendix)

x_A : body fixed axial coordinate of the attitude sensor

x_R : body fixed axial coordinate of the rate sensor

ω_j : characteristic frequency associated with the orthogonal mode q_j

$\bar{F}_s$: generic notation for forces acting on the system

$\bar{r}_T$: position vector from hinge point to centroid of nozzle exit area

$\bar{R}(\bar{F}_s)$: position vector of the point of attack of $\bar{F}_s$

$\displaystyle\sum_s$: summation over s

$\sum$: summation of the terms in the summand over the entire vehicle

$\mathcal{Y}_j$: fraction of critical damping in the jth flexural mode

γ : flight path angle

x_p : body fixed axial coordinate associated with the hinge point of the motor nozzles

M_j : $\sum m \phi_j^2$, generalized mass in the, j^{th} flexural mode

$x_{\ell k}$: body fixed axial coordinate associated with the hinge point of the kth slosh mass in the ℓth tank

$\mathcal{L}$: distance from nozzle hinge point to mass center of nozzle

ℓ_1 : distance from nozzle hinge point to centroid of nozzle exit area

The evaluation of ϕ_j, ϕ_j', and x is to be made at that point on the axis corresponding to mass with which the term is associated, unless otherwise specified.

f. Linearization of the Equations of Motion

A priori, no general theory of linearization of the equations of motion exists. For a holonomic system in which the kinetic energy is composed of terms of the form $\dot{\bar{r}}_1 \cdot \dot{\bar{r}}_2$, the operator $\frac{d}{dt}(\frac{\partial}{\partial \dot{\chi}}) - \frac{\partial}{\partial \chi} \equiv L_\chi$ yields:

$$L_{\chi_i} (\dot{\bar{r}}_1 \cdot \dot{\bar{r}}_2) = \left[\frac{\partial^2 \bar{r}_1}{\partial \chi_j \partial \chi_m} \cdot \frac{\partial \bar{r}_2}{\partial \chi_i} + \frac{\partial^2 \bar{r}_2}{\partial \chi_j \partial \chi_m} \cdot \frac{\partial \bar{r}_1}{\partial \chi_i} + \frac{\partial^2 \bar{r}_2}{\partial \chi_i \partial \chi_m} \cdot \frac{\partial \bar{r}_1}{\partial \chi_j} \right.$$

$$\left. + \frac{\partial^2 \bar{r}_1}{\partial \chi_i \partial \chi_m} \cdot \frac{\partial \bar{r}_2}{\partial \chi_j} \right] \dot{\chi}_j \dot{\chi}_m \qquad\qquad (C-28)*$$

$$+ \left[\frac{\partial \bar{r}_1}{\partial \chi_j} \cdot \frac{\partial \bar{r}_2}{\partial \chi_i} + \frac{\partial \bar{r}_1}{\partial \chi_i} \cdot \frac{\partial \bar{r}_2}{\partial \chi_j} \right] \ddot{\chi}_j$$

Linearization as employed in this study implies: (1) the deletion of the terms involving $\dot{\chi}_j \dot{\chi}_m$; and (2) deletion of terms wherein the coefficient of $\ddot{\chi}_j$ contains the generalized coordinates (or products thereof) which are of small order; (3) the approximation $\sin \psi \simeq \psi$, $\cos \psi \simeq 1$, for ψ small.

One observes that if $\bar{r}$ is a linear combination of the generalized coordinates then $\dfrac{\partial^2 \bar{r}}{\partial \chi_i \partial \chi_j} = 0$ and no terms of the form $\chi_i \chi_j$ occur:

and $\dfrac{\partial \bar{r}_1}{\partial \chi_i}$, $\dfrac{\partial \bar{r}_2}{\partial \chi_j}$, etc. represent the cosine between the i$\underline{th}$ and j$\underline{th}$ coordinate which, if the argument is small, can be approximated by 1 and if the argument is large represent nonlinear terms in the equations of motion, as reflected by a term of comparatively small order in the kinetic energy since,

$$\dot{\bar{r}}_1 \cdot \dot{\bar{r}}_2 = \frac{\partial \bar{r}_1}{\partial \chi_j} \cdot \frac{\partial \bar{r}_2}{\partial \chi_i} \dot{\chi}_i \dot{\chi}_j \qquad\qquad (C-20)$$

Hence in certain special cases the justification for linearization might be easily carried over from a justification of the neglect of certain terms in the kinetic energy.

* Summation on the repeated indices is understood in this notation.

One sees also, that nonlinearities are not inherent in the kinematics of the system studied here; further, that the nonlinearities which do arise, come from the generalized forces or the employment of special coordinate systems. We see this more clearly in the following paragraphs where body fixed coordinates are introduced.

g. Equations Referred to Body Fixed Axes

The equations of motion as determined by direct substitution of Eqns. C-22, C-23, C-24 and C-25 into C-21 yield a set of equations in which the trajectory is imbedded. Inasmuch as a nominal trajectory is presumed known, these equations governing the rigid body motions can be modified so as to produce equations governing the perturbed motion resulting from forces tending to deviate the vehicle from its nominal trajectory. To do this we define the velocity of the mass center with respect to "airplane axes" (body fixed axes), z and x as shown in Fig. C-2. The only term affected by this mode of description is $\bar{r}$ in Eqn. (C-22);

$$\dot{\bar{r}} = \dot{q}_z \, \bar{i}' + \dot{q}_x \, \bar{j}' \tag{C-30}$$

where $\bar{i}'$ and $\bar{j}'$ are base vectors in the body fixed axes system. The equations of motion so obtained are given at the end of this Appendix.

h. Transformation to Obtain Perturbation Equations of Motion

Under no perturbing forces the only force which acts normal to the vehicle trajectory is that of gravity. The normal acceleration of the mass center is related to the force in the normal direction by Newton's law:

$$mg \cos \psi = m \dot{\psi} |\bar{v}| \tag{C-31}$$

where

$$|\bar{v}| = \sqrt{\left[\dot{q}_x \cos(\psi - \gamma) \right]^2 + \left[\dot{q}_z \sin (\psi - \gamma) \right]^2} \simeq \dot{q}_x$$

Application of the condition expressed in Eqn. (C-31), that is the "zero gravity turn condition", to the terms in Eqns. C-35, C-39, C-40 which involve the transverse acceleration and gravity is shown below:

$$\ddot{q}_z + \dot{q}_x \dot{\psi} + g \cos \psi = \ddot{q}_z + \dot{q}_x \dot{q}_\theta - g \sin \Theta_1 q_\theta \tag{C-32}$$

where

$$q_\bullet + \Theta_1 = \psi$$

$$\cos q_\bullet \simeq 1$$

$$\sin q_0 \simeq q_\bullet \tag{C-33}$$

$$q_\bullet \ll \pi$$

Finally, we replace $\sin \psi$ by

$$\sin \Theta_1 \cos q_\bullet + \sin q_\bullet \cos \Theta_1 \simeq \sin \Theta_1 + \cos \Theta_1 \, q_\bullet \tag{C-34}$$

and neglect terms involving the products of perturbed quantities.

Having a nominal trajectory specified, the values of $\dot{q}_x$ and Θ_1 at any time are predetermined; hence the resulting left hand side of the equations become linear functions of perturbed coordinates.

$$(\sum m_i)(\ddot{q}_{\bar{e}} + \dot{q}_{x}\dot{\psi}) - m_o\ell\ddot{q}_s - \sum\sum m_{\mu k}\ddot{q}_{\mu k}h_{\mu k} = -\sum m_i g\cos\psi + \dot{m}[\dot{\psi}(\ell_i - x_{p_i}) - \sum\phi_i\dot{q}_j + \ell_i(\dot{q}_s + \sum\phi'_i(x_{p_i})\dot{q}_j)] + [I_o + (P_e - P_o)A](q_s + \sum\phi'_i(x_{p_i})q_j) + Q_{q_{\bar{e}}}(A)$$

$$\text{(C-35)}$$

$$(\sum m_i)(\ddot{q}_x - \ddot{q}_{\bar{e}}\dot{\psi}) = -\sum m_i g\sin\psi + [T_o + (P_e - P_o)A] + Q_{q_x}(A)$$

$$\text{(C-36)}$$

$$(\sum m_i z^2)\ddot{\psi} + m_o[\ell(\ddot{q}_{\bar{e}} - \ddot{q}_x\dot{\psi})q_s - \ell x\ddot{q}_s] + \sum\sum m_{\mu k}h_{\mu k}(q_{\mu k}(\ddot{q}_{\bar{e}} - \ddot{q}_x\dot{\psi}) - \ddot{q}_{\mu k}x) + I_o(\ddot{q}_s + \phi'_i(x_{p_i})\ddot{q}_j + \ddot{\psi})$$
$$= -\dot{m}[\dot{\psi}(\ell_i - x_{p_i}) - \sum\phi_i\dot{q}_j + \ell_i(\dot{q}_s + \sum\phi'_i(x_{p_i})\dot{q}_j)](\ell_i - x_{p_i}) + x_{p_i}[T_o + (P_e - P_o)A](q_s + \sum\phi'_i(x_{p_i})q_j) + Q_\psi(A) - m_o\ell g\sin\psi\,q_s$$
$$-\sum\sum m_{\mu k}q_{\mu k}g\sin\psi$$

$$\text{(C-37)}$$

$$M_n[\ddot{q}_n + 2\omega_n S_n\dot{q}_n + \omega_n^2 q_n] - m_o\ell[\phi'_n(x_{p_i})(\ddot{q}_x - \ddot{q}_{\bar{e}}\dot{\psi}) + \ddot{q}_{\bar{e}}\phi_n] - \sum\sum m_{\mu k}h_{\mu k}[q_{\mu k}(\ddot{q}_x - \ddot{q}_{\bar{e}}\dot{\psi})\phi_n(x_{\mu k}) + \ddot{q}_{\mu k}\phi_n] - I_o(\ddot{q}_s + \sum\phi'_j\ddot{q}_j + \ddot{\psi})\phi_n(x_{p_i})$$
$$= [m_o g\ell\ddot{q}_s\phi'_n(x_{p_i}) + \sum\sum\dot{m}_{\ell k}h_{\mu k}q_{\mu k}g\phi'_n(x_{\mu k})]\sin\psi + \dot{m}[\dot{\psi}(\ell_i - x_{p_i}) - \sum\phi_i\dot{q}_j + \ell_i(\dot{q}_s + \sum\phi'_i(x_{p_i})\dot{q}_j)](\phi_n(x_{p_i}) + \ell_i\phi'_n(x_{p_i}))$$
$$+ [T + (P_e - P_o)A](q_s + \sum\phi'_j(x_{p_i})q_j)\phi_n(x_{p_i}) + Q_{q_n}(A) \quad ; \quad n = 1, \cdots, j$$

$$\text{(C-38)}$$

$$m_{\ell k}[\ddot{q}_{\mu k}h_{\ell k}^2 + (\ddot{q}_{\bar{e}} - \ddot{q}_x\dot{\psi})q_{\mu k}h_{\ell k} - (\ddot{q}_{\bar{e}} + \ddot{q}_x\dot{\psi})h_{\ell k} - x\ddot{\psi}h_{\mu k} - \sum\phi_j\ddot{q}_j h_{\ell k} + (\ddot{q}_x - \ddot{q}_{\bar{e}}\dot{\psi})h_{\mu k}\sum\phi'_j(x_{\ell k})q_j] = m_{\mu k}g h_{\mu k}(\cos\psi - \sin\psi\sum\phi'_j(x_{\mu k})q_j) - m_{\ell k}g\,h_{\mu k}\sin\psi\,q_{\ell k}$$

$$\text{(C-39)}$$

$$m_o[\ddot{q}_s\ell^2 - (\ddot{q}_{\bar{e}} + \ddot{q}_x\dot{\psi})\ell - x\ddot{\psi}\ell - \sum\phi_j\ddot{q}_j\ell + (\ddot{q}_x - \ddot{q}_{\bar{e}}\dot{\psi})\ell(q_s + \sum\phi'_j(x_{p_i})q_j)] + I_o[\ddot{q}_s + \sum\phi'_j(x_{p_i})\ddot{q}_j + \ddot{\psi}] = m_o g\ell[\cos\psi - (q_s + \sum\phi'_j(x_{p_i})q_j)\sin\psi]$$
$$-\dot{m}\ell_i[\dot{\psi}(\ell_i - x_{p_i}) - \sum\phi_i\dot{q}_j + \ell_i(\dot{q}_s + \sum\phi'_i(x_{p_i})\dot{q}_j)] + Q_{q_s}(C)$$

$$\text{(C-40)}$$

NOTE THAT $\psi = q_{\theta} + \theta_i$ AND $\ddot{\theta}_i \ll \ddot{q}_{\theta}$

FIG. C-2   COORDINATE SYSTEM : FLIGHT EQUATIONS OF MOTION

4. <u>FUEL SLOSH ANALOGY FOR TRANSVERSE DISTURBANCES ONLY</u> *

We temporarily omit the subscript ℓ indicating the tank under consideration with the understanding that the values are obtained by using the physical constants that pertain to the $\ell^{\underline{th}}$ tank.

In FIG. C-3 is shown the actual tank, the equivalent circular cylindrical tank, the two common mechanical analogies and the geometrical relations involved in the analogies. The equivalent tank is of the same radius and contains the same volume of fluid.
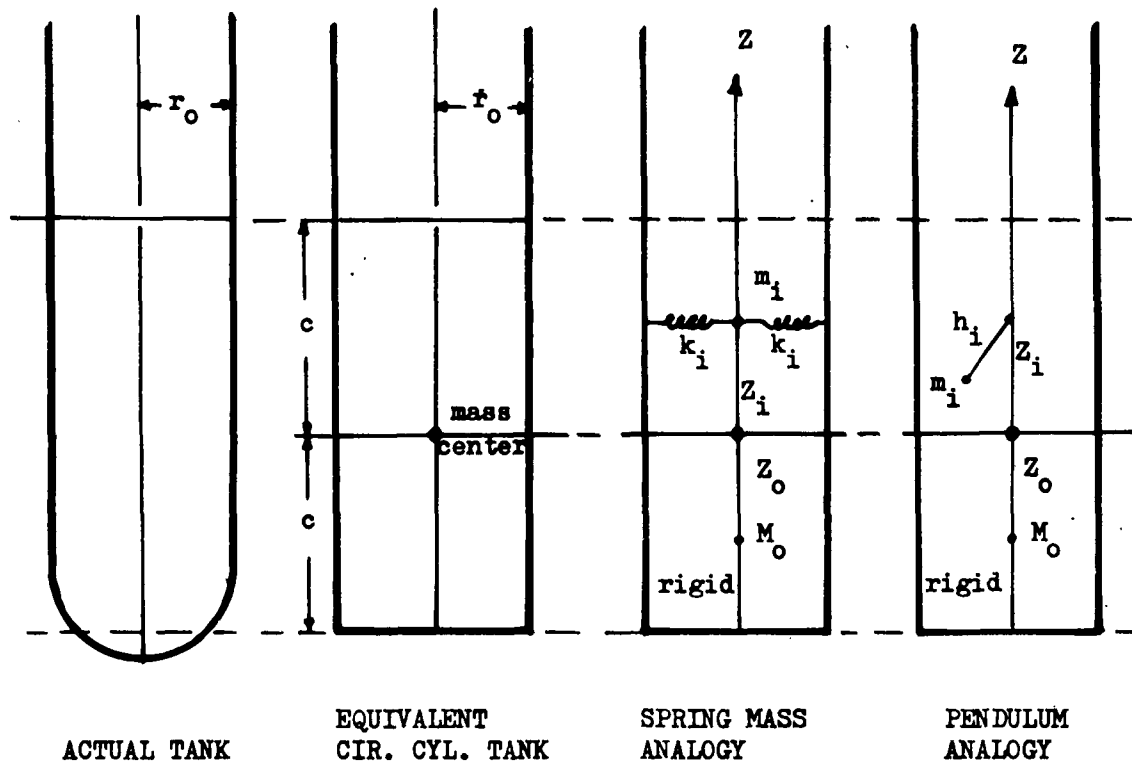

| ACTUAL TANK | EQUIVALENT CIR. CYL. TANK | SPRING MASS ANALOGY | PENDULUM ANALOGY |

FIG. C-3

---

* More complete analyses can be had in which translatory and rotary disturbances are considered; see references on fuel slosh.

Let ρ : density of fluid

SPRING MASS ANALOGY

$$M_o = M \left(1 - \sum A_i\right)$$

$$m_i = M A_i$$

$$Z_i = \frac{4c\, D_i}{A_i}$$

$$Z_o = \frac{\left(\dfrac{r_o^2}{8c} - 4c \sum D_i\right)}{\left(1 - \sum A_i\right)}$$

$$k_i = 1/2\,\omega_i^2\, m_i$$

PENDULUM ANALOGY

$$M_o = M \left(1 - \sum A_i\right)$$

$$m_i = M A_i$$

$$Z_i = \frac{4c\, D_i}{A_i}$$

$$Z_o = \frac{\left(\dfrac{r_o^2}{8c} - 4c \sum D_i\right)}{\left(1 - \sum A_i\right)}$$

$$h_i = \frac{A_c}{\omega_i^2}$$

where

$$M = \rho \, (2c) \pi r_o^2$$

$$A_i = \frac{2 \tanh K_i}{K_i \left(\beta_i^2 - 1\right)}$$

$$D_i = \frac{\frac{K_i}{2} \sinh K_i - \cosh K_i + 2}{K_i^2 \left(\beta_i^2 - 1\right) \cosh K_i}$$

$$K_i = \frac{\beta_i}{r_o} \quad (2c)$$

$$J_o' \left(\beta_i\right) = 0 \quad \text{where } J_o' \text{ is the derivative of the}$$
$$\text{Bessel function of the zero order}$$

$$\omega_i^2 = A_c \frac{K_i}{2c} \tanh K_i$$

$$A_c : \quad \text{axial acceleration}$$

$$A_c = \ddot{q}_x - \dot{q}_z \dot{\psi} + y \sin \psi$$

4. FUEL SLOSH ANALOGIES

Many studies have been made of fuel slosh following the assumption of small displacement made by Lamb (24). For right circular cylinders and, conical and spherical shells the solutions are well known. For containers having a geometry less simple than these, and in which the equilibrium fluid surface is not oriented with respect to the container in an appropriate manner, the solutions are not known. No solutions are known for even the simplest geometry if the slosh amplitude is large.

The propellents generally considered for advanced vehicles act as ideal liquids and in this respect the classic ideal fluid assumption is well satisfied. The propellants, however, are often cryogenic materials which tend to "boil" at the uninsulated vehicle walls.

Interesting and difficult problems are introduced if one wishes to consider the thermodynamic aspects of fuel slosh; research in this area seems warranted.

METHOD OF CHOOSING CONTROL GAIN SETTINGS TO PROVIDE A DESIRED
PITCH FREQUENCY AND DAMPING INCLUDING THE EFFECTS OF FLEXIBILITY

It was necessary specify a pitch control system and select gain
settings before flight loads could be analyzed, since the vehicle is statically
unstable without controls. The type of control system postulated here is only
one of several possibilities and is not necessarily the best design for a
vehicle of this type. The emphasis in this study is on the dynamic response
of the vehicle as a whole and not on the control system itself. No claim is
made that the criterion used for choosing gain settings is the best one for
design purposes.

Control gain settings which provide approximately the desired pitch
frequency and damping could be determined by trial and error on the analog
computer, but this would be time consuming and rather inaccurate. On the
digital computer the trial and error method would be prohibitively expensive.
Therefore, a method of calculating the proper gain settings from the
equations of motion has been developed.

In order to be able to examine the pitch degree of freedom separately,
the equations of motion used in the boost flight loads analysis (Eqn. IV-8)
have been transformed referring motions to so-called wind tunnel axes instead
of body axes. The homogeneous equations with no wind or gust forcing function
have been considered. The transformation to wind tunnel axes is made as
follows:

Let
$$\dot{q}_T = \dot{q}_Z + V q_\theta \qquad (D-1)$$

$$\ddot{q}_T = \ddot{q}_Z + V\dot{q}_\theta + \dot{V}q_\theta \qquad (D-2)$$

The rigid body angle of attack, assuming no wind and small angle of attack
is

$$\alpha = -\frac{\dot{q}_Z}{V} \qquad (D-3)$$

Solving Eqn. (D-1) for this quantity yields

$$-\frac{\dot{q}_Z}{V} = q_\theta - \frac{\dot{q}_T}{V} \qquad (D-4)$$

The true acceleration normal to the body axes with respect to fixed
space is

$$a_Z = \ddot{q}_Z + V\dot{q}_\theta \qquad (D-5)$$

Note that for no wind and small angle of attack $\dot{q}_X = V$. From Eqn. (D-2)

$$\ddot{q}_Z + V\dot{q}_\Theta = \ddot{q}_T - \dot{V}q_\Theta \qquad (D-6)$$

If a constant forward speed is assumed, as in the final gliding approach during re-entry, the $\dot{V}q_\Theta$ term vanishes and $\ddot{q}_T$ is the true acceleration with respect to fixed space. During boost the $\dot{V}q_\Theta$ term remains since $\dot{V}$ is not zero. However, if the coefficients of the equations of motion are assumed constant, as in the analog solutions, a rather artificial situation exists. In this case, in order to get the same solutions of the equations of motion using wind tunnel coordinates as are obtained using coordinates referred to body axes, the assumption that $\dot{V} = 0$ must be made in transforming to wind tunnel axes. Considerations such as these make it inadvisable to use wind tunnel axes in the derivation of equations of motion for vehicles in accelerated flight. However, as mentioned above, the transformation to wind tunnel axes permits the examination of the pitch mode separately.

The transformation to wind tunnel axes is effected by making the substitutions indicated in Eqns. (D-4 and D-6). After the transformation, the equations of motion appear in matrix form as follows:

$$
\begin{bmatrix} M & & & \\ & I & & \\ & & m_1 & \\ & & & m_2 \end{bmatrix}
\begin{Bmatrix} \ddot{q}_T \\ \ddot{q}_\Theta \\ \ddot{q}_1 \\ \ddot{q}_2 \end{Bmatrix}
+
\begin{bmatrix} 0 & & & \\ & 0 & & \\ & & m_1 \omega_1^2 & \\ & & & m_2 \omega_2^2 \end{bmatrix}
\begin{Bmatrix} q_T \\ q_\Theta \\ q_1 \\ q_2 \end{Bmatrix}
=
$$

$$
\begin{bmatrix} b_{11} & b_{12} & b_{13} & b_{14} \\ b_{21} & b_{22} & b_{23} & b_{24} \\ b_{31} & b_{32} & b_{33} & b_{34} \\ b_{41} & b_{42} & b_{43} & b_{44} \end{bmatrix}
\begin{Bmatrix} \dot{q}_T \\ \dot{q}_\Theta \\ \dot{q}_1 \\ \dot{q}_2 \end{Bmatrix}
+
\begin{bmatrix} 0 & c_{12} & c_{13} & c_{14} & c_{15} \\ 0 & c_{22} & c_{23} & c_{24} & c_{25} \\ 0 & c_{32} & c_{33} & c_{34} & c_{35} \\ 0 & c_{42} & c_{43} & c_{44} & c_{45} \end{bmatrix}
\begin{Bmatrix} q_T \\ q_\Theta \\ q_1 \\ q_2 \\ q_\delta \end{Bmatrix}
\qquad (D-7)
$$

where M : total mass of the vehicle

I : pitching moment of inertia

m_1, m_2 : generalized masses of the first and second flexible modes

ω_1, ω_2 : natural frequencies of the first and second flexible modes

$\begin{bmatrix} b_{ij} \end{bmatrix}$: $\dot{q}_j$ coefficient matrix

$\begin{bmatrix} c_{ij} \end{bmatrix}$: q_j coefficient matrix

The sloshing and nozzle swiveling degrees of freedom are not shown in Eqn. (D-7), since they are not needed in the development of the formulas for the calculation of gain settings.

The following control system representations are considered:

1)
$$q_\delta = K_\Theta q_\Theta + K_{\dot{\Theta}} \dot{q}_\Theta \tag{D-8}$$

2)
$$q_\delta = K_\Theta \Theta_s + K_{\dot{\Theta}} \dot{\Theta}_s \tag{D-9}$$

where
$$\Theta_s = q_\Theta + \sum_j \phi'_{jA} q_j \tag{D-10}$$

$$\dot{\Theta}_s = \dot{q}_\Theta + \sum_j \phi'_{jR} \dot{q}_j \tag{D-11}$$

and

3)
$$\frac{q_\delta(S)}{\Theta_s(S)} = \frac{K_\Theta + K_{\dot{\Theta}} S}{(1+T_1 S)(1+T_2 S)(1 + \frac{2\zeta_*}{\omega_*} + \frac{S^2}{\omega_*^2})} \tag{D-12}$$

In the third representation above, one, two, or all three lags are considered.

For the rigid vehicle with the control system of Eqn. (D-8), the required gains are calculated by considering the pitch degree of freedom only.

$$I\ddot{q}_\Theta = b_{22}\dot{q}_\Theta + c_{22}q_\Theta + c_{25}q_\delta \tag{D-13}$$

Substituting Eqn. (D-8) into Eqn. (D-13) and dividing through by I yields:

$$\ddot{q}_\Theta = \frac{b_{22} + c_{25} K_{\dot{\Theta}}}{I} \dot{q}_\Theta + \frac{c_{22} + c_{25} K_\Theta}{I} q_\Theta \tag{D-14}$$

Equation (D-14) is also written as:

$$\ddot{q}_\Theta = - 2\zeta_\Theta \omega_\Theta \dot{q}_\Theta - \omega_\Theta^2 q_\Theta \tag{D-15}$$

where ω_Θ = desired pitch frequency

ζ_Θ = desired pitch damping ratio

Equating coefficients and solving for K_Θ and $K_{\dot\Theta}$ yields

$$K_\Theta = \frac{-\omega_\Theta^2 I - c_{22}}{c_{25}} \qquad \text{(D-16)}$$

$$K_{\dot\Theta} = \frac{-2\,\mathcal{S}_\Theta\,\omega_\Theta I - b_{22}}{c_{25}} \qquad \text{(D-17)}$$

Although gains computed by Eqns. (D-16 and D-17) are based on a single degree of freedom, solution for the roots of the characteristic equation of the two degree of freedom system which include the translation mode show that the frequency and damping ratio are not significantly changed by the inclusion of the translation freedom. In other words the gains calculated by Eqns. (D-16 and D-17) provide the desired short period response for the rigid vehicle. However, as indicated in Section IV-C-1, the gains calculated by Eqns. (D-16 and D-17) do not prove at all satisfactory when flexible modes and control system refinements are added. As a matter of fact, in many cases these gains do not even provide stability. In the first analog studies the gains were adjusted by trial and error on the analog until a satisfactory response was obtained, and then loads were recorded usir; these gains. The flexible mode response was primarily a static deflection under load at the pitch frequency containing very small components at the frequencies of the flexible modes. This suggested the method of accounting for the effects of flexibility in the original selection of gains which will now be discussed.

Consider the system represented by translation, pitch, two flexible modes, and a simple nonlagged control system as defined by Eqn. (D-8). First, the assumption is made that the flexible modes deflect statically, thus dropping out all the time derivatives of the generalized coordinates for the flexible modes. Next, q_ς is replaced in the equations of motion by the expression given in Eqn. (D-8). The equations for pitch and the flexible modes now appear as

$$I\ddot{q}_\Theta = (b_{22} + c_{25} K_{\dot\Theta})\,\dot{q}_\Theta + (c_{22} + c_{25}K_\Theta)\,q_\Theta + c_{23}q_1 + \dot{c}_{24}q_2 \qquad \text{(D-18)}$$

$$m_1\omega_1^2 q_1 = (b_{32} + c_{35}K_{\dot\Theta})\,\dot{q}_{\bar\Theta} + (c_{32} + c_{35}K_\Theta)q_\Theta + c_{33}q_1 + c_{34}q_2 \qquad \text{(D-19)}$$

$$m_2\omega_2^2 q_2 = (b_{42} + c_{45}K_{\dot\Theta})\dot{q}_\Theta + (c_{42} + c_{45}K_\Theta)q_\Theta + c_{43}q_1 + c_{44}q_2 \qquad \text{(D-20)}$$

Terms involving $\dot{q}_m$ are omitted since they do not enter into the calculation of gain settings.

Eqns. (D-19 and D-20) are then solved simultaneously for q_1 and q_2. The solutions have the following form:

$$q_1 = (A + B K_{\dot{\Theta}}) \dot{q}_{\Theta} + (C + D K_{\Theta}) q_{\Theta} \qquad (D\text{-}21)$$

$$q_2 = (E + F K_{\dot{\Theta}}) \dot{q}_{\Theta} + (G + H K_{\Theta}) q_{\Theta} \qquad (D\text{-}22)$$

The expressions for q_1 and q_2 given in Eqns. (D-21 and D-22) are then substituted into Eqn. (D-18):

$$I\ddot{q}_{\Theta} = \left[(b_{22} + c_{23}A + c_{24}E) + (c_{25} + c_{23}B + c_{24}F) K_{\dot{\Theta}} \right] \dot{q}_{\Theta} \qquad (D\text{-}23)$$

$$+ \left[(c_{22} + c_{23}C + c_{24}G) + (c_{25} + c_{23}D + c_{24}H) K_{\Theta} \right] q_{\Theta}$$

Using the approach described earlier for the rigid case (see Eqns. (D-13 through D-17), expressions for K_{Θ} and $K_{\dot{\Theta}}$ may now be written.

$$K_{\Theta} = \frac{-\omega_{\Theta}^2 I - (c_{22} + c_{23}C + c_{24}G)}{c_{25} + c_{23}D + c_{24}H} \qquad (D\text{-}24)$$

$$K_{\dot{\Theta}} = \frac{-2 \mathcal{F}_{\Theta}\omega_{\Theta} I - (b_{22} + c_{23}A + c_{24}E)}{c_{25} + c_{23}B + c_{24}F} \qquad (D\text{-}25)$$

In these expressions A, B, C, D, E, F, G, and H are algebraic functions of the coefficients of the equations of motion.

$$A = -\frac{b_{32}(m_2\omega_2^2 - c_{44}) + c_{42}c_{34}}{(c_{33}' - m_1\omega_1^2)(m_2\omega_2^2 - c_{44}) + c_{43}c_{34}} \qquad (D\text{-}26)$$

$$B = D \qquad (D\text{-}27)$$

$$C = -\frac{c_{32}(m_2\omega_2^2 - c_{44}) + c_{42}c_{34}}{(c_{33} - m_1\omega_1^2)(m_2\omega_2^2 - c_{44}) + c_{43}c_{34}} \qquad (D\text{-}28)$$

$$D = -\frac{c_{35}(m_2\omega_2^2 - c_{44}) + c_{45}c_{34}}{(c_{33} - m_1\omega_1^2)(m_2\omega_2^2 - c_{44}) + c_{43}c_{34}} \qquad (D\text{-}29)$$

$$E = -\frac{b_{42} - c_{43}A}{m_2\omega_2^2 - c_{44}} \qquad (D\text{-}30)$$

$$F = H \tag{D-31}$$

$$G = -\frac{c_{42} - c_{43}\, C}{m_2\omega_2^2 - c_{44}} \tag{D-32}$$

$$H = -\frac{c_{45} - c_{43}\, D}{m_2\omega_2^2 - c_{44}} \tag{D-33}$$

Although two flexible modes are used in the above example, the same method may be used to predict gains for systems having more or less than two flexible modes. However, if more than two flexible modes are considered, the simultaneous solution of the quasi-static equations for q_1, q_2, q_3, etc., may become unduly complicated. The effect of the higher modes on gains required will probably be small. In the case analyzed even the second mode has very little effect on the predicted gains, although the effect of the first mode is large. If only one mode is considered the expressions for calculating K_Θ and $K_{\dot{\Theta}}$ become quite simple.

$$K_\Theta = -\frac{\omega_\Theta^2 I + c_{22} + \dfrac{c_{32}\, c_{23}}{m_1\omega_1^2 - c_{33}}}{c_{25} + \dfrac{c_{35}\, c_{23}}{m_1\omega_1^2 - c_{33}}} \tag{D-34}$$

$$K_{\dot{\Theta}} = -\frac{2\omega_\Theta \mathcal{J}_\Theta I + b_{22} + \dfrac{b_{32}\, c_{23}}{m_1\omega_1^2 - c_{33}}}{c_{25} + \dfrac{c_{35}\, c_{23}}{m_1\omega_1^2 - c_{33}}} \tag{D-35}$$

Gain settings calculated using Eqns. (D-24) and (D-25) or Eqns. (D-34) and (D-35) apply only for the simplest control system representation described by Eqn. (D-8). If the sensors sense bending as well as rigid pitch (as they must in any real system), the effective gains of the control system are different from the gain settings, since the sensor outputs which are amplified contain components proportional to the slopes in the flexible modes. If the response in the flexible modes is essentially static, as is assumed in calculating the gains required, the slopes in the flexible modes are approximately proportional to the incremental pitch angle. In this case the gain settings which will give the required effective gains may be calculated. The following conditions must be met:

$$\overline{K}_\Theta\, \Theta = K_\Theta\, q_\Theta \tag{D-36}$$

$$\overline{K}_{\dot{\Theta}}\, \dot{\Theta} = K_{\dot{\Theta}}\, \dot{q}_\Theta \tag{D-37}$$

where

$\overline{K}_\Theta$ = attitude gain setting

K_Θ = effective gain required

$\overline{K}_{\dot\Theta}$ = rate gain setting

$K_{\dot\Theta}$ = effective gain required

Rewriting Eqns. (D-10 and D-11)

$$\Theta_s = q_\Theta + \phi'_{1A} q_1 + \phi'_{2A} q_2 \qquad (D-38)$$

$$\dot\Theta_s = \dot q_\Theta + \phi'_{1R} \dot q_1 + \phi'_{2R} \dot q_2 \qquad (D-39)$$

From Eqns. (D-21 and D-22), assuming q_1 and q_2 are proportional to q_Θ,

$$q_1 = (C + D K_\Theta) q_\Theta \qquad (D-40)$$

$$q_2 = (G + H K_\Theta) q_\Theta \qquad (D-41)$$

Substituting Eqns. (D-40 and D-41) into Eqn. (D-38)

$$\Theta_s = q_\Theta + \phi'_{1A} (C + D K_\Theta) q_\Theta + \phi'_{2A} (G + H K_\Theta) q_\Theta \qquad (D-42)$$

Substituting Eqn. (D-42) into Eqn. (D-36) and simplifying,

$$\overline{K}_\Theta = K_\Theta \frac{1}{1 + \phi'_{1A} (C + D K_\Theta) + \phi'_{2A} (G + H K_\Theta)} \qquad (D-43)$$

Differentiating and substituting Eqns. (D-40 and D-41) into Eqn. (D-39)

$$\dot\Theta_s = \dot q_\Theta + \phi'_{1R} (C + D K_\Theta) \dot q_\Theta + \phi'_{2R} (G + H K_\Theta) \dot q_\Theta \qquad (D-44)$$

Substituting Eqn. (D-44) into Eqn. (D-37) and simplifying,

$$\overline{K}_{\dot\Theta} = K_{\dot\Theta} \frac{1}{1 + \phi'_{1R} (C + D K_\Theta) + \phi'_{2R} (G + H K_\Theta)} \qquad (D-45)$$

Using the gain settings $\overline{K}_\Theta$ and $\overline{K}_{\dot\Theta}$ will provide approximately the effective gains desired.

When lags are included in the control system representation it is found that each additional lag necessitates an increase in $K_{\dot\Theta}$. It is possible to predict the increase necessary by the following method. Consider the nonlagged system transfer function.

$$\frac{q_\delta(s)}{q_\Theta(s)} = K_\Theta + s\, K_{\dot\Theta} \qquad (D\text{-}46)$$

Replacing the Laplace operator with $i\omega$, the frequency response function is obtained:

$$\frac{q_\delta}{q_\Theta} = K_\Theta + i\omega\, K_{\dot\Theta} \qquad (D\text{-}47)$$

The amplitude and phase angle may be written as a function of frequency:

$$\frac{q_\delta}{q_\Theta} = \left(K_\Theta^2 + \omega^2\, K_{\dot\Theta}^2\right)^{1/2} \underline{/\tan^{-1} \frac{\omega\, K_{\dot\Theta}}{K_\Theta}} \qquad (D\text{-}48)$$

It is the positive phase shift, $\tan^{-1} \dfrac{\omega\, K_{\dot\Theta}}{K_\Theta}$, which provides the required damping. In the more complicated control system representation described by Eqn. (D-12) each of the lags produces a negative phase shift which tends to cancel the positive phase shift provided by the $(K_\Theta + K_{\dot\Theta}\, s)$ term in the numerator. Therefore, it is necessary to increase $K_{\dot\Theta}$ until the net positive phase shift is equal to that which is present in the nonlagged system. The increase in $K_{\dot\Theta}$ required is of course a function of the frequency. The damped frequency desired for the short period mode for the boost-glide vehicle of this analysis is $\omega_\Theta \sqrt{1 - \mathcal{J}_\Theta^2}$. This frequency is used in the calculation of the increase in $K_{\dot\Theta}$ required. To determine the new value of $K_{\dot\Theta}$, designated as $K_{\dot\Theta}'$, equate the phase shift of the nonlagged control system to the phase shift of the lagged system and solve for $K_{\dot\Theta}'$.

$$\tan^{-1} \frac{\omega\, K_{\dot\Theta}'}{K_\Theta} - \tan^{-1}T_1\, \omega_1 - \tan^{-1}T_2\, \omega_2 - \tan^{-1} \frac{2\, \mathcal{J}_\Theta\, \omega_b\, \omega}{\omega_o^2 - \omega^2} = \tan^{-1} \frac{\omega\, K_{\dot\Theta}}{K_\Theta} \qquad (D\text{-}49)$$

The left hand side of Eqn. (D-49) represents the phase shift of the lagged system; the term on the right hand side is the phase shift of the nonlagged system. Having the effective gain required for the lagged system, $K_{\dot\Theta}'$, the gain setting $\overline{K}_{\dot\Theta}'$ is found by applying Eqn. (D-45).

The gain settings predicted by the methods described in the preceding paragraphs agreed quite well with the settings determined by trial and error on the analog. Given the desired pitch frequency and damping, the methods

described can be used to select gain settings for use in a digital solution where the determination of gain settings by trial and error would be uneconomical.

A SIMPLIFIED SOLUTION TO THE WIND SHEAR PROBLEM

A simplified method of obtaining wind shear bending loads for a boost-glide vehicle which is subjected to a typical design wind profile such as the revised Sissenwine 1% wind shear profile (Fig. IV-2) is presented herein. The method utilizes an assumed typical first bending mode and the assumption that the aerodynamic lift acts only on the glider and is concentrated at the centroid of the glider area. Typical first bending modes for liquid and solid propellant vehicles are shown in Fig. E-1. First bending mode frequency as a function of weight and fineness ratio is plotted in Fig. E-2. The configuration parameter, $K W^{1/3}(L/D)^{2/3}$, for a particular vehicle is calculated using the weight of the booster at maximum q/v. The center of gravity is calculated at maximum q/v and is assumed to remain fixed in the vehicle throughout the flight. A simple control system is used in which gains are calculated to give a pitch frequency of .5 cps and a damping ratio of .6 critical.

The first part of the method employs a hand solution by which the loads due to the slow time-varying portion of the wind profile are found. For this part of the solution the vehicle can be considered to be a rigid body which is free to translate and pitch. The equations of motion referred to wind tunnel axes (see Appendix D) can be written in the form:

$$
\begin{bmatrix} M & 0 \\ 0 & I \end{bmatrix} \begin{Bmatrix} \ddot{q}_T \\ L\ddot{q}_\Theta \end{Bmatrix} + \begin{bmatrix} C_{11} & C_{12} \\ C_{21} & C_{22} \end{bmatrix} \begin{Bmatrix} \dot{q}_T \\ L\dot{q}_\Theta \end{Bmatrix} + \begin{bmatrix} 0 & k_{12} \\ 0 & k_{22} \end{bmatrix} \begin{Bmatrix} q_T \\ Lq_\Theta \end{Bmatrix} = \begin{Bmatrix} c_{11} \\ c_{21} \end{Bmatrix} V_w \sin \psi \qquad (E-1)
$$

Where M   : Total mass

I   : Pitching moment of inertia

$\begin{bmatrix} C_{ij} \end{bmatrix}$, $\begin{bmatrix} K_{ij} \end{bmatrix}$, and $\begin{Bmatrix} C_{ij} \end{Bmatrix}$: matrices of coefficients

L   : Overall length of the vehicle

V   : Wind velocity

ψ : Inclination of vehicle from horizontal

q_T : Normal translation coordinate

q_Θ : Perturbation pitch angle

The control forces are embedded in Eqn. (E-1) as functions of q_{Θ} and $\dot{q}_{\Theta}$.

It is assumed that over small time intervals the coefficients in Eqn. (E-1) can be considered constants and $V_w \sin \psi$ can be approximated by linear functions of time. It is also assumed that $\ddot{q}_{\Theta} = \dot{q}_{\Theta} = 0$. Under these assumptions, a Laplace Transform solution of the equations of motion for conditions at the end of a time interval t_1 yields.

$$\dot{q}_T(t_1) = \left[\dot{q}_T(0) + \frac{K_2}{\beta} - K_1 \right] e^{-\beta t_1} + K_2 t_1 - (\frac{K_2}{\beta} - K_1) \qquad (E-2)$$

$$Lq_{\Theta}(t_1) = \alpha \left(\left[K_1 - \frac{K_2}{\beta} - \dot{q}_T(0) \right] e^{-\beta t_1} + \frac{K_2}{\beta} \right) \qquad (E-3)$$

where:

$$\alpha = \frac{C_{21}}{k_{22}}$$

$$\beta = \frac{k_{22} C_{11} - k_{12} C_{21}}{M k_{22}}$$

$$V_w \sin \psi = K_1 + K_2 t$$

The process is repeated for a number of time intervals until conditions at the altitude of the spike are obtained. Five such intervals are usually sufficient. The loads due to the slow time-varying portion of the wind profile can be calculated from the above responses.

Loads due to the wind spike alone are calculated by solving the constant coefficient equations of motion and loads equations calculated at maximum q/v. For this part of the solution, a flexible vehicle is considered which is free to translate, pitch, and bend in its first mode shape.

The total responses and loads in the vicinity of the wind spike can be found by adding the responses and loads due to the slow time-varying portion of the wind profile to those found due to the wind spike alone.

The use of the above method permits a very rapid determination of wind shear loads, since no time is required for calculating modes or aerodynamic load distributions. The results in the cases tested are considered sufficiently accurate for preliminary design purposes. A comparison of bending moment diagrams calculated by the simplified method and by a three degree of freedom digital solution of the equations with time varying coefficients is shown in Fig. E-3.
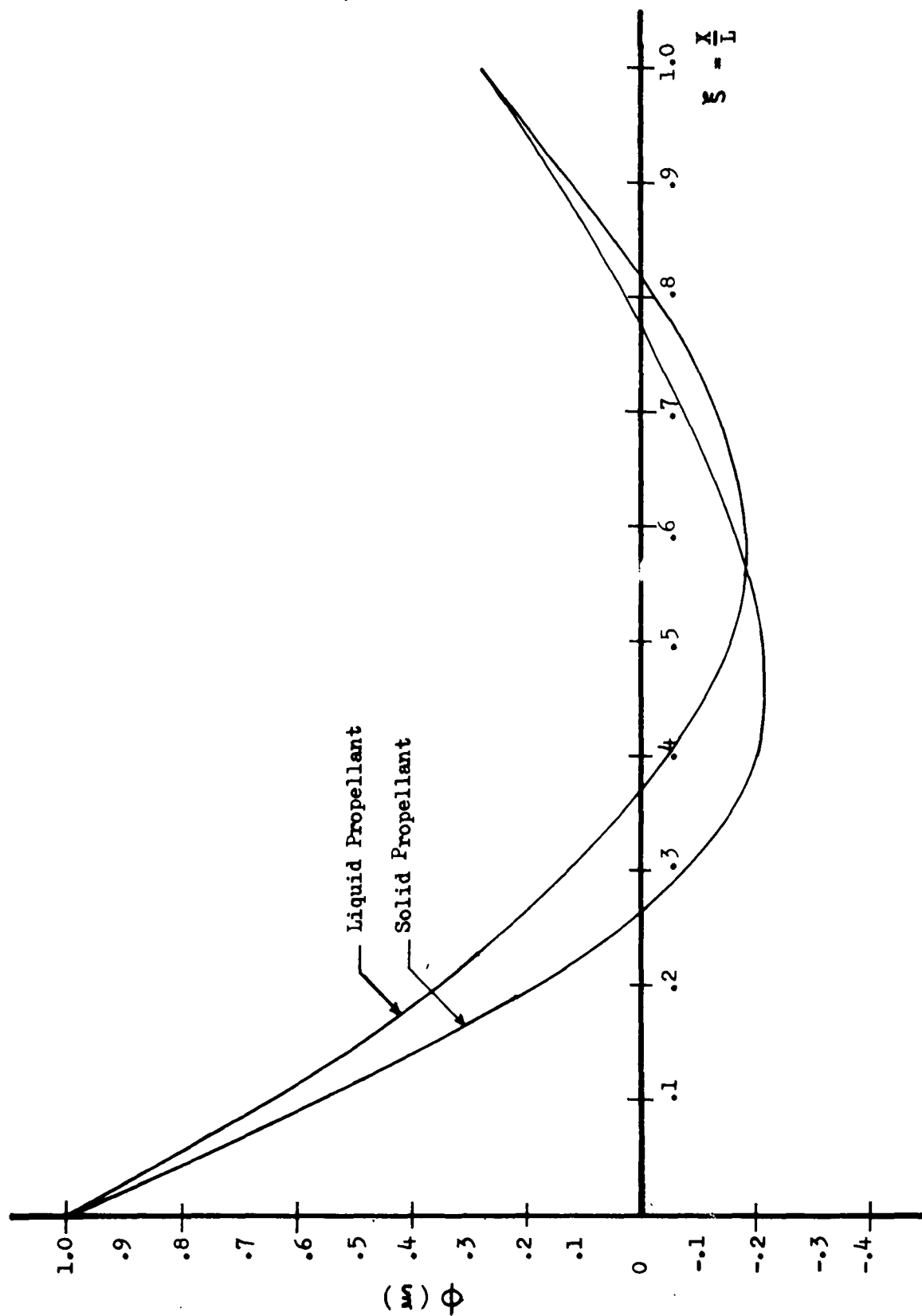
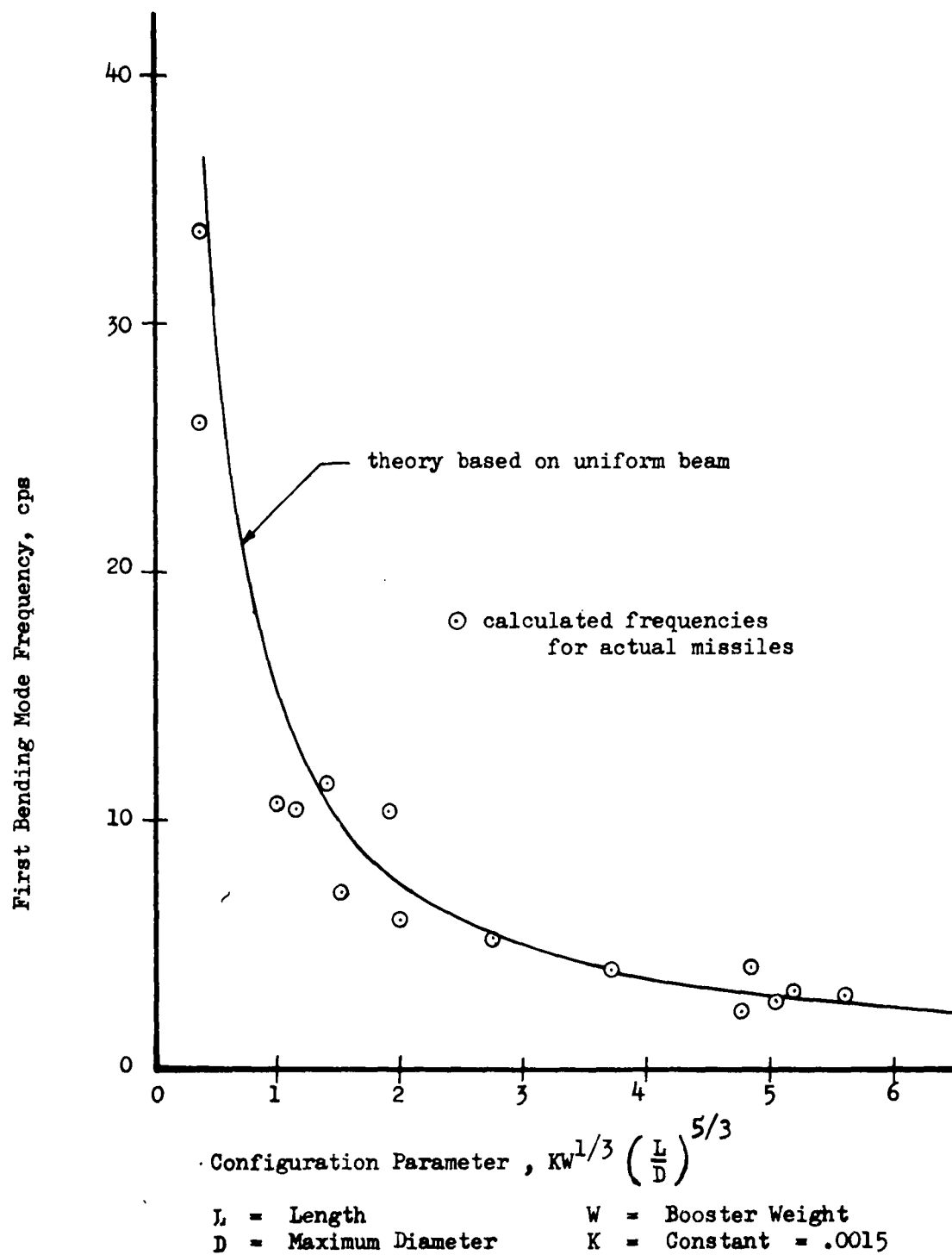FIG. E-1   TYPICAL FIRST MODE SHAPES NEAR MAXIMUM q/v

FIG. E-2 FIRST BENDING MODE FREQUENCY
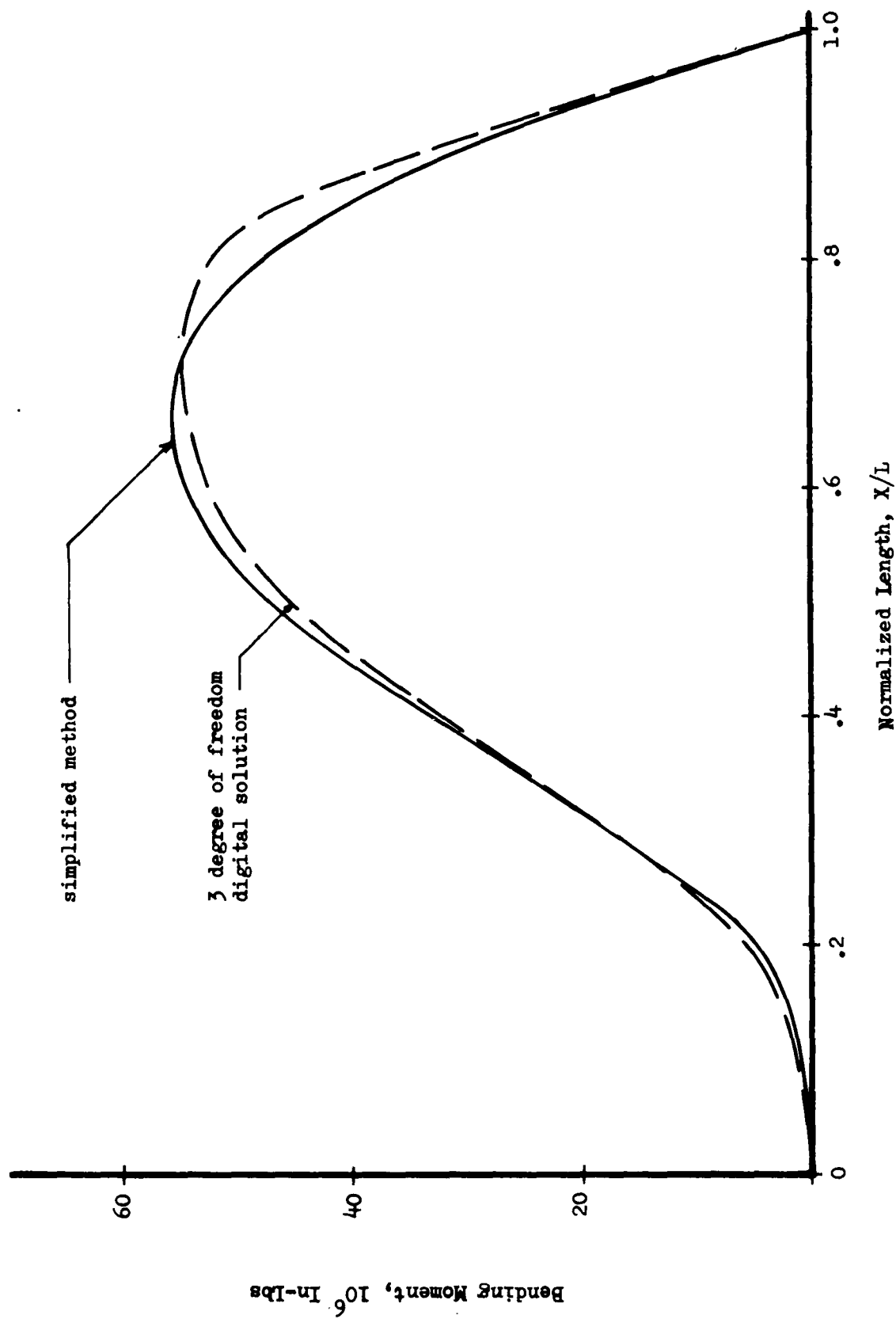AS A FUNCTION OF WEIGHT AND FINENESS RATIO

Normalized Length, X/L

FIG. E-3   COMPARISON OF MAXIMUM BENDING MOMENTS--
SIMPLIFIED METHOD WITH 3 DEGREE OF FREEDOM
DIGITAL SOLUTION

simplified method

3 degree of freedom
digital solution

Bending Moment, 10^6 In-lbs

DRAG RESPONSE TO CONTINUOUS RANDOM TURBULENCE

This Appendix describes the criteria used to determine the drag response of the vehicle to continuous random turbulence. Although the purpose of this study was not to establish environmental criteria, it must be recognized that rational criteria should specify both the environment to be used and the method of analysis to be employed. In the area of ground wind response it is felt that criteria have not been well defined, and it is not possible to evaluate dynamic response effects without further describing the nature of the ground wind.

In specifying a design ground wind, one must be concerned with both magnitude and shape or frequency content of the wind. Design winds in the past (85) have usually been specified to consist of a steady wind velocity plus a gust increment which is 50% of the steady wind velocity. However the specifications have not indicated whether the gust increment is to be a step, ramp, tent, or one-minus-cosine shaped gust. Actually the gust increment has probably been selected from meteorological measurements of gust factors (defined as the peak wind speed in a five minute period divided by the mean speed in that period) which has often been measured to be approximately 1.5 (66). Therefore, rather than choosing an arbitrary gust shape and gradient as has been formerly done, power spectral techniques will be used to model the meteorological ground wind description.

1. GROUND WIND MODEL

The design wind description should be influenced both by the large quantity of meteorological data collected over the years (66) and by the more recent power spectral data gathered by current investigators (67, 73). It has been shown that a great deal of data is needed to fix the magnitudes of gust disturbances; however, relatively small samples are sufficient to determine the spectral content of the ground winds.

The magnitudes are, therefore, determined by the large amount of available meteorological data. The gust factor of 1.5 will be used for the present and the choice of 60-90 or 40-60 m.p.h. or some other set of values will depend upon the particular vehicle being studied.

The form of the turbulence to be added to the mean wind speed will be taken from Reference 67. Fig. F-1 shows a number of measured power spectra with the suggested spectrum superimposed upon it. Analytically,

$$\phi(\Omega) = \frac{2L\sigma_r^2}{\pi}\left[\frac{1}{1 + L^2\Omega^2}\right] \tag{F-1}$$

where   L   : the scale of turbulence = 1200 feet.

   Ω : the reduced frequency in radians/ft.

   σ_r : standard deviation of turbulence.

By applying Taylor's Hypothesis, (83) the spatial spectrum of Eqn.(F-1)can be changed to a time spectrum by the relationship

$$\omega = V \cdot \Omega \tag{F-2}$$

where ω : frequency in radians/sec.

V : average wind velocity

The power spectrum in the time domain will therefore be

$$\phi(\omega) = \left(\frac{2\sigma_u^2}{\pi}\right)\left(\frac{L}{V}\right)\left(\frac{1}{1+\left(\frac{L}{V}\omega\right)^2}\right) \tag{F-3}$$

The amplitude of the turbulence should be chosen to give approximately the desired gust factor (1.5 as per References 85 and 66).

2. RESPONSE SIMULATION

The response of a vehicle in the launch position has been described in detail (Eqns. II-1 and II-2) and only the form is given here. By dropping the terms involving products of response velocities, we have:

$$\left[M\right]\{\ddot{q}\} + \left[c\right]\{\dot{q}\} + \left[M\omega^2\right]\{q\} = \{K_1\}\ V^2 - \left[K_2\right]\{\dot{q}\}\ V \tag{F-4}$$

It can be seen that Eqn. F-4 is nonlinear and the classical power spectral approach based on the superposition principle does not apply. Nevertheless the power spectral description of turbulence still can be used to form the input to the nonlinear problem. This is accomplished on nonlinear analog equipment as described in Appendix G.

3. INTERPRETATION OF STATISTICAL DATA

The problem of choosing a design load from a random load trace is not a simple one. At first thought, one might suggest simply taking the highest observed value. However, the question of sample length would not be easy to determine. Secondly the influence of gust amplitude must be considered carefully. The gust factor is generated from a random signal and, therefore, will vary in a range about 1.5. The vehicle load associated with a larger gust factor will be too high for design. In short, if the absolute values of load obtained are used for design, the inference would be made that the gust factors obtained from the electronic simulation are more reliable than the large amount of meteorological data which has been gathered.

In view of the above difficulty the analog simulation is used to obtain dynamic magnification factors rather than absolute values. By this method the suggested gust factor of 1.5 can be used as a basic part of the calculation. The loads determination is then summarized in Eqn.(F-5).

$$\begin{bmatrix} \text{Dynamic Wind} \\ \text{Loads} \end{bmatrix} = \begin{bmatrix} \text{Static Loads} \\ \text{Computed for} \\ \text{Steady Wind} \\ \text{Plus Gust} \end{bmatrix} \times \begin{bmatrix} \text{Dynamic} \\ \text{Magnification} \\ \text{Factor} \end{bmatrix} \qquad (F\text{-}5)$$

The dynamic magnification factor is found by comparing the dynamic loads as obtained from the solution of Eqn.(F-4) with the static loads as obtained from Eqn.(F-6).

$$\left[M\omega^2 \right] \left\{ q \right\} = \left\{ K_1 \right\} v^2 \qquad (F\text{-}6)$$

The comparison is made by considering the distribution of maximum values of both the static and dynamic loads. The sets of maximum values are obtained by dividing the random records into a number of small time increments and reading the maximum value in each increment. The mean value and variance of each set is then computed:

$$\bar{\mathcal{L}} \equiv \frac{1}{N} \sum_{i=1}^{N} \mathcal{L}_i \qquad (F\text{-}7)$$

$$\sigma^2 \equiv \frac{1}{N} \sum_{i=1}^{N} \mathcal{L}_i^2 - \bar{\mathcal{L}}^2 \qquad (F\text{-}8)$$

where

$\mathcal{L}_i$: maximum load in i$\underline{\text{th}}$ time interval

$\bar{\mathcal{L}}$: mean value of maximum load

N : number of time intervals

σ : variance of maximum load distribution

The comparison can now be made by comparing mean values of the maximum loads or by comparing more extreme values of the load distributions. For most distributions there will probably be little difference in the various comparisons. However it appears that extreme values are of more interest to the designers and hence "three-sigma" loads are used in defining the magnification factor as follows:

$$\text{D.M.F.} \equiv \frac{(\bar{\mathcal{L}} + 3\sigma)_{\text{dynamic}}}{(\bar{\mathcal{L}} + 3\sigma)_{\text{static}}} \qquad (F\text{-}9)$$
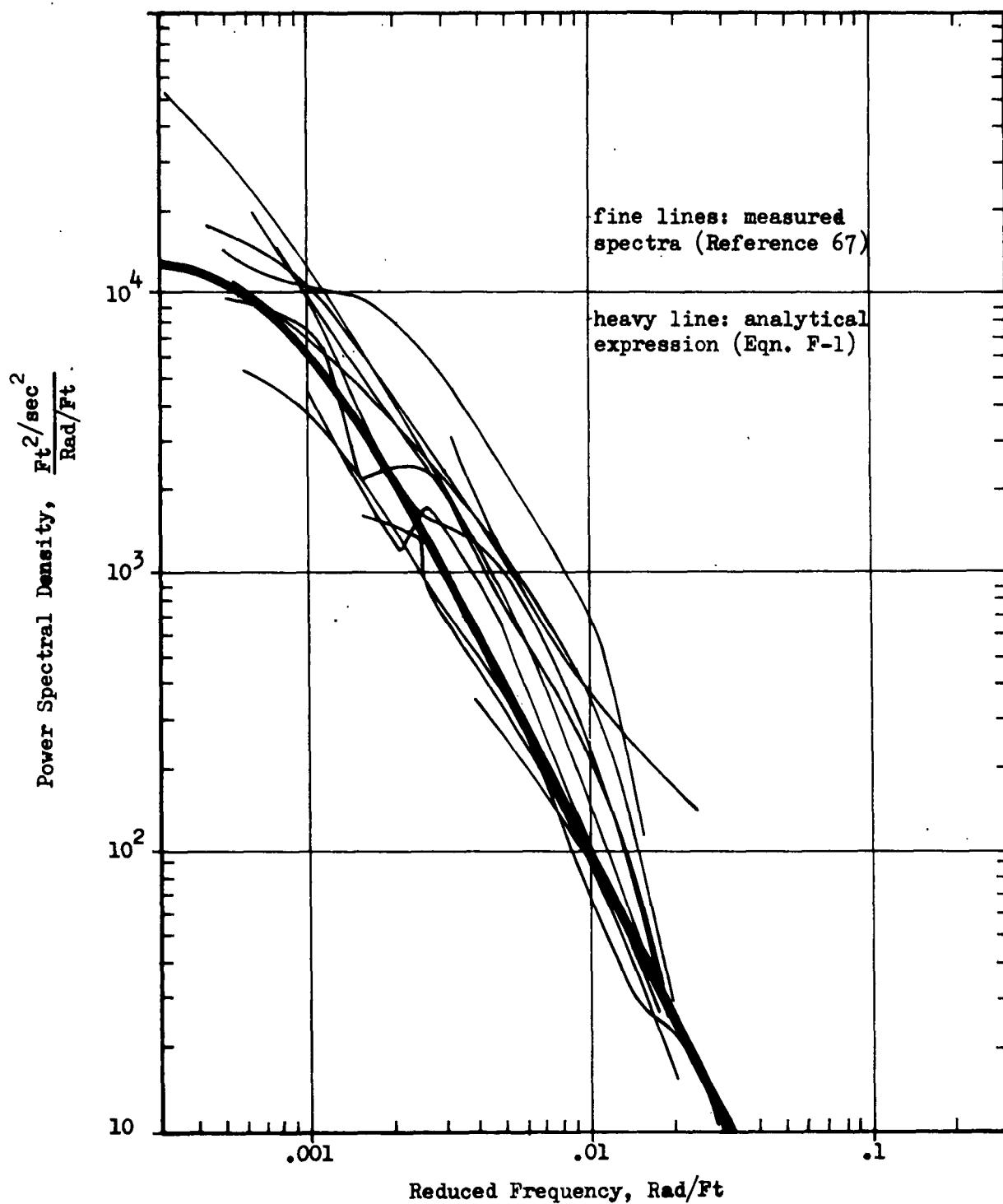
FIG. F-1   POWER SPECTRA OF HORIZONTAL
TURBULENCE NEAR GROUND IN THE DIRECTION OF THE MEAN WIND

APPENDIX G

COMPUTERS

The determination of the dynamic response of a system requires two basic
steps - (1) establishing a model of the system and (2) obtaining the response
of the model. In this study the system is modeled analytically by sets of
mathematical equations and the responses are obtained as the solution of the
equations. The mathematical model of vehicle systems is usually too complex
to be solved in closed form or by use of a hand calculator. Therefore,
computing aides such as high speed digital computers and analog computers
must be used. In this appendix a discussion will be given of the applicability
of digital computers, differential analyzers, and direct analog computers in
the solution of dynamic response problems.

1. DIGITAL COMPUTERS

Digital computers are an invaluable tool in the solution of dynamics
problems because of their ability to perform standard calculations at a high
rate of speed with equally high accuracy. However, time required to program
a given problem is generally long. Therefore, digital programs are most often
written to solve standard types of problems which arise repeatedly, thus
justifying the effort required to write the program.

A brief description of the programs used in this study is given below.
These are programs which are in general use in dynamics and were not developed
under this contract. Special problems, such as nonlinearities peculiar to
this study, are better handled by analog equipment.

a. Modes and Frequencies of Beams

This program calculates the first few natural modes and frequencies
of an arbitrarily supported nonuniform beam on an elastic foundation.
The beam is assumed divided into pieces; for each piece the
stiffness matrix is calculated. The individual pieces are merged
together to obtain the stiffness matrix for the whole beam. The
support conditions are then imposed by simply striking out appropriate
rows and columns of the stiffness and mass matrices. The resulting
eigenvalue problem for the frequencies and mode shapes is solved by
matrix iteration. The generalized mass can be optionally calculated
as a check on the orthogonality of those modes that have been
calculated. In theory, this should be a diagonal matrix.

b. Structural Analysis

This program is intended to do a complete structural analysis of a
general built-up structure. The program first forms stiffness
matrices for the simple pieces into which the engineer chooses to
break up his structure. The individual pieces are put together to
form a stiffness matrix for the complete structure. Having the
stiffness matrix the modes and frequencies are then obtained by
matrix iteration.

c. <u>Matrix Algebra</u>

This program is a compilation of SHARE matrix programs put together with a suitable control program. It is able to do almost any matrix operation, such as add, multiply, invert, transpose, find roots, partition, etc. The calculation of the coefficients for the equations of motion was accomplished by this program.

d. <u>Solution of Simultaneous Linear Differential Equations</u>

This program solves the system of ordinary differential equations shown below for the unknown vector $\{q(t)\}$:

$$\left[M \right]\{\ddot{q}\} + \left[C \right]\{\dot{q}\} + \left[K \right]\{q\} = \{\alpha\}\, f(t), \tag{G-1}$$

with initial conditions $\{q\}\big|_{t=0} = \{q_0\}$, $\{\dot{q}\}\big|_{t=0} = \{\dot{q}_0\}$

where $\left[M \right]\left[C \right]\left[K \right]\{\alpha\}$ are matrices whose elements are arbitrary

function of time, $\{q_0\}$, $\{\dot{q}_0\}$ are columns of constants, and

the forcing function f(t) is an arbitrary function of time. The program solves the equations using a four point Adams-Moulton predictor corrector numerical integration method. A modified Euler method is used to start the process off. The program automatically adjusts the time step at each stage by keeping track of a measure of the truncation error. If this error gets too large, the step size is halved; if the error gets too small, the step size is doubled. Once the $\{q\}$'s have been obtained, the program will optionally calculate a linear combination of the $\{\ddot{q}\}$, $\{\dot{q}\}$, and $\{q\}$ as shown below:

$$\left[A \right]\{\ddot{q}\} + \left[B \right]\{\dot{q}\} + \left[C \right]\{q\} + \left[\beta \right]\, f(t)$$

The elements of the matrices A, B, C, β are again arbitrary functions of time. The reason for this operation is that the q's may represent response of a system to some loading, and the linear combination may be desired to calculate internal loads throughout the system.

e. <u>Power Spectral Density Program</u>

This program calculates the frequency response function for a linear constant coefficient system that can be represented by the following set of equations:

$$\left[M_1 \right]\{\ddot{q}\} + \left[M_2 \right]\{\dot{q}\} + \left[M_3 \right]\{q\} + \left[M_4 \right]\{\ddot{q} * g(t)\}$$

$$+ \left[M_5 \right]\{\dot{q} * g(t)\} + \{C_1\}\,\alpha_g + \{C_2\}\dot{\alpha}_g * f(t) = 0 \tag{G-2}$$

where $\left[M_i \right]$: matrices

C_1 and C_2 : columns,

α_g : forcing function

$g(t)$, $f(t)$: the Wagner and Kussner functions respectively,

and where the symbol $*$ signifies convolution. The program first finds the $\{q\}$'s andthen uses these responses in an equation similar to (G-2) to calculate loads. Let $T(i\Omega)$ be the frequency response function of the loads. Finally, the program performs two numerical integrations.

$$\{A\} = \left[\int_0^\infty \left\{ |T(i\Omega)|^2 \right\} \phi(\Omega)\, d\Omega \right]^{1/2}$$

$$\{N(0)\} = \frac{1}{2\pi\{A\}} \left[\int_0^\infty \Omega^2 \left\{ |T(i\Omega)|^2 \right\} \phi(\Omega)\, d\Omega \right]^{1/2}$$

where for turbulence studies $\phi(\Omega)$ is usually as given below:

$$\phi(\Omega) = \frac{L}{\pi} \left[\frac{1 + 3L^2\Omega^2}{(1 + L^2\Omega^2)^2} \right]$$

L : scale length of turbulence

Ω : frequency in rad/ft.

Thus one obtains the R.M.S. value of output load and a measure of the number of times the output load exceeds a given value.
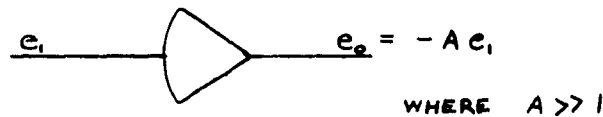
2. DIFFERENTIAL ANALYZERS

The differential analyzer, commonly referred to as an analog computer, is an electronic computer used to solve differential equations. It is a highly versatile computer well adapted to the solution of dynamic response problems. Among its advantages are the following: (1) The dynamics engineer can establish his own circuit analogy with little or no help from electronics or mathematical experts, thus eliminating time delays and communication errors. (2) The dynamics engineer can observe the results as they are being obtained and thus can make decisions as to the best method of varying parameters. (3) Most types of nonlinear differential equations can be solved with relative ease.

Whereas the differential analyzers cannot compare with digital computers in accuracy, they are considered to be adequate for engineering work. In modern electronic differential analyzers, the individual elements are accurate to within approximately .01%. A single differential equation can be expected to have no more than .1% error. With larger systems or in systems involving differences of large numbers, the accuracy would of course be less. Non-linearities may introduce more inaccuracies, especially when unusual functions need to be generated.
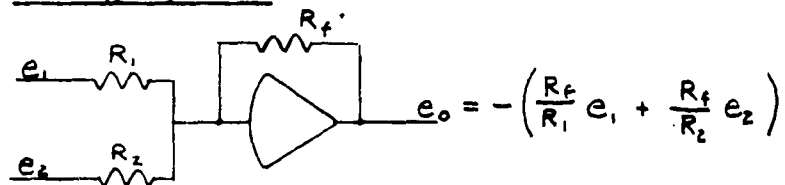
a. <u>Basic Analog Elements</u>

The basic analog elements used in the solution of the dynamic equations in this report will now be described. The solutions of all the equations are represented by voltages at various points in the circuit.
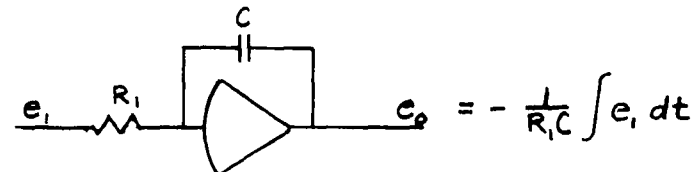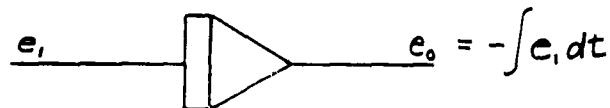
<u>High Gain Amplifier</u>

$$e_o = -A e_i$$

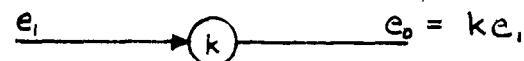$$\text{WHERE} \quad A \gg 1$$

<u>Summing Amplifier</u>

$$e_o = -\left(\frac{R_f}{R_1} e_1 + \frac{R_f}{R_2} e_2\right)$$

or symbolically

$$e_o = -(e_1 + e_2)$$

<u>Integrating Amplifier</u>

$$e_o = -\frac{1}{R_1 C} \int e_i \, dt$$

or symbolically

$$e_o = -\int e_i \, dt$$

<u>Potentiometer</u>

$$e_o = k e_i$$

Multiplier

$$e_1$$
$$e_2$$
$$e_o = -\frac{e_1 e_2}{100}$$

Divider

$$e_1$$
$$e_2 \quad \boxed{D}$$
$$e_o = -100\,\frac{e_1}{e_2}$$

Function Generator

$$e_1 \qquad \boxed{\begin{array}{c} f(e_1) \\ \hline \\ e_1 \end{array}} \qquad f(e_1)$$

Diode

$$+e \qquad \overset{i=0}{\vartriangleleft} \qquad -e$$
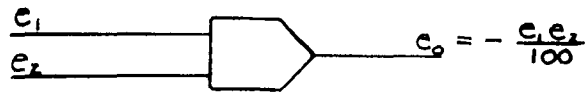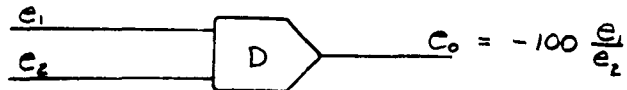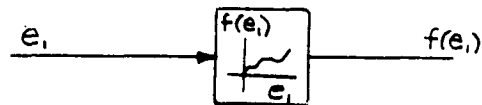
$$+e \qquad \overset{i\rightarrow}{\vartriangleright} \qquad -e$$
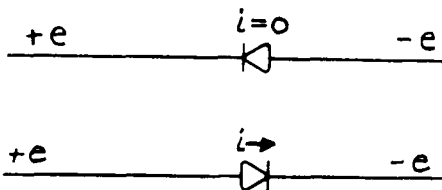
b. ## Analog Circuits

In this section, representative circuits will be presented which will demonstrate to the reader the method of analog application. This will be done for general cases, and such details as scaling the variables will not be included. It is sufficient to say that if the problem is scaled properly, the voltages on the amplifiers will be as large as possible but less than the overload voltage.

Linear Differential Equations

Systems of second order differential equations form the foundations
of most dynamics studies. A typical wind shear problem with a two
degree of freedom system and a simplified control system will be
used for demonstration. Because analogs integrate much better than
they differentiate, the equations are first solved for the highest
order derivatives.

$$\begin{Bmatrix} \ddot{q}_1 \\ \ddot{q}_2 \end{Bmatrix} = -\left[\begin{bmatrix} C_{11} & C_{12} \\ C_{21} & C_{22} \end{bmatrix} \begin{Bmatrix} \dot{q}_1 \\ \dot{q}_2 \end{Bmatrix} + \begin{bmatrix} k_{11} & k_{12} \\ k_{21} & k_{22} \end{bmatrix} \begin{Bmatrix} q_1 \\ q_2 \end{Bmatrix} - \begin{Bmatrix} g_1 \\ g_2 \end{Bmatrix} v_w - \begin{Bmatrix} F_1 \\ F_2 \end{Bmatrix} \delta_T \right]$$

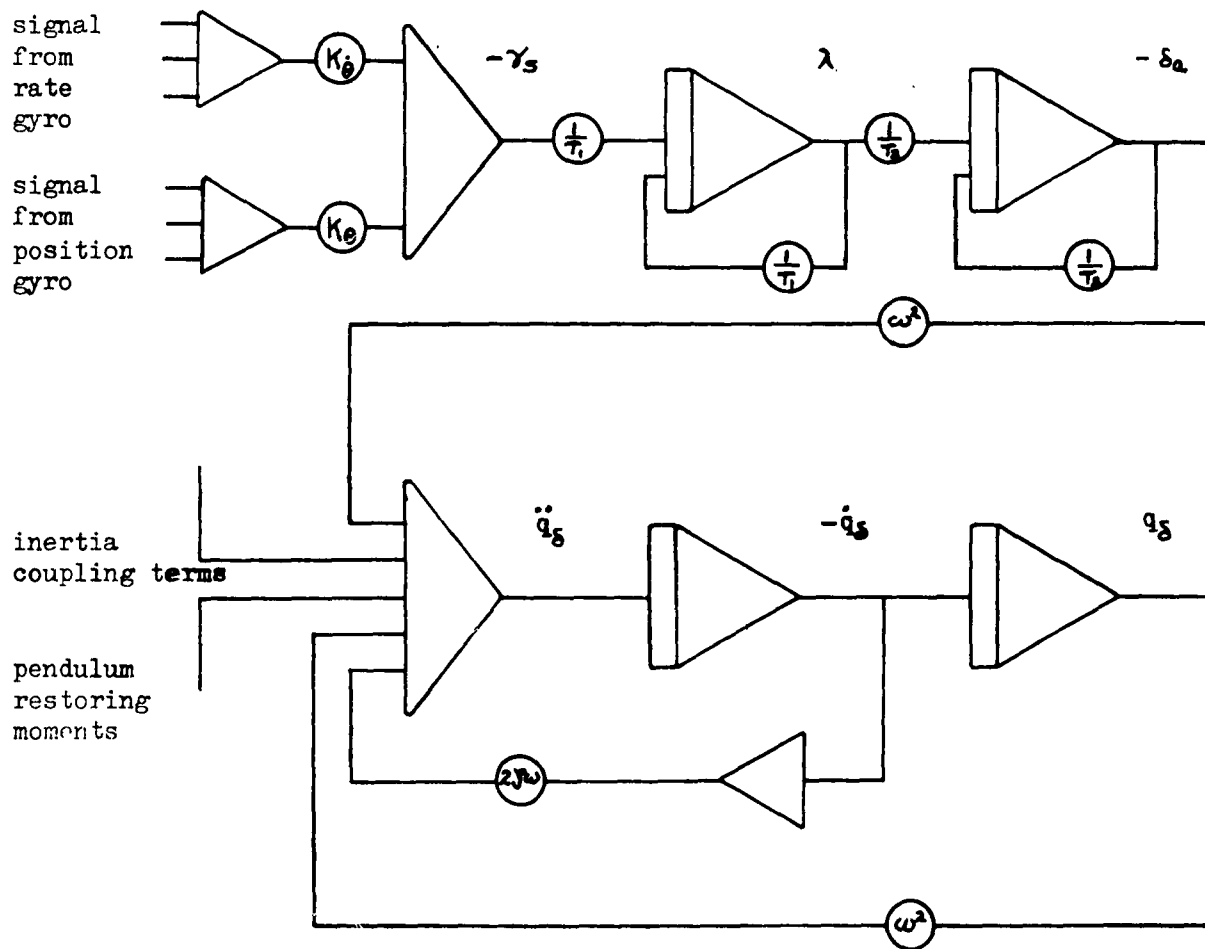$$-\delta_T = -\begin{bmatrix} G_1 & \dot{q}_2 & + & G_2 & q_2 \end{bmatrix}$$
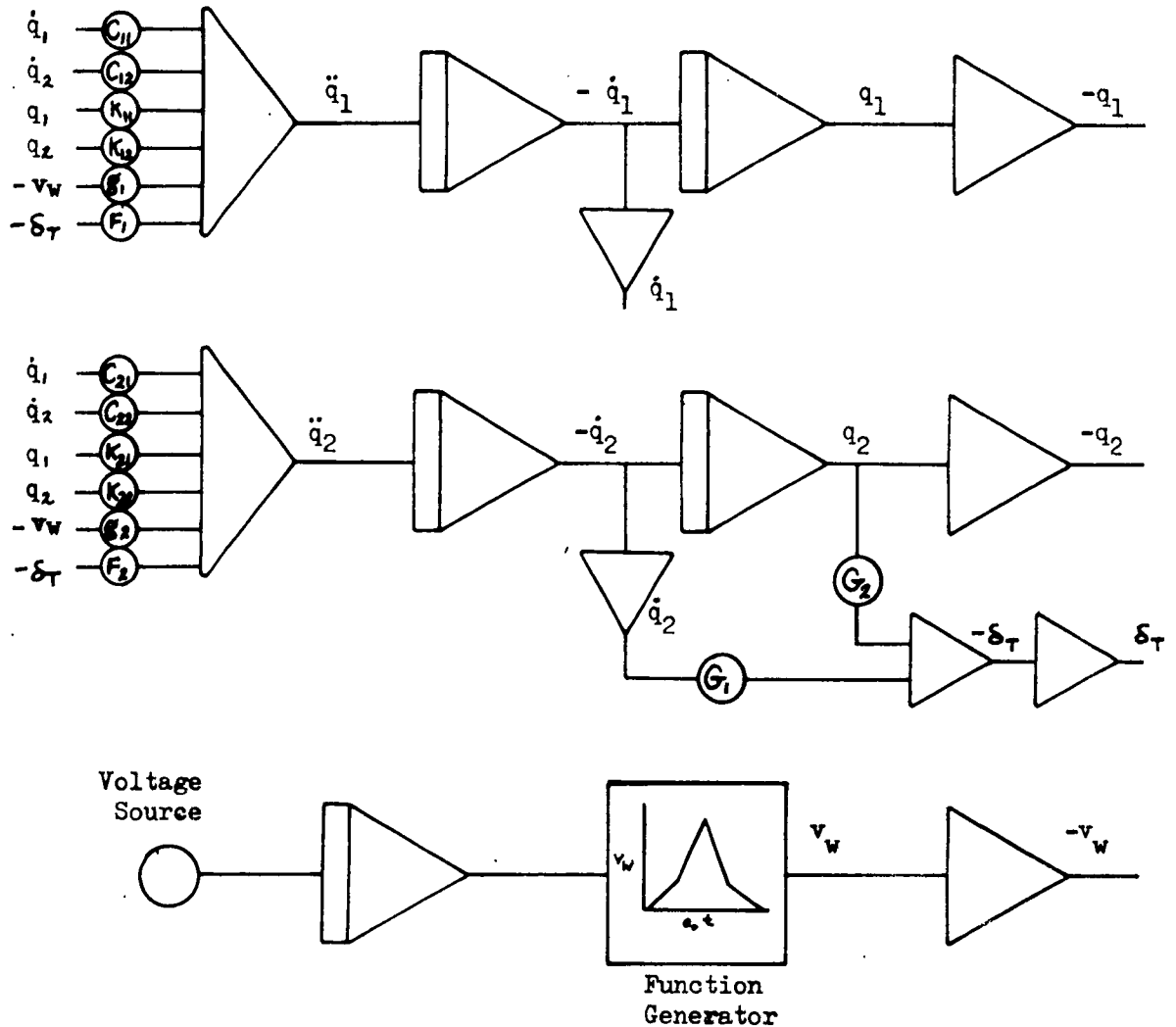
Control system simulation

The control system representation used in this study can be represented by the following transfer function:
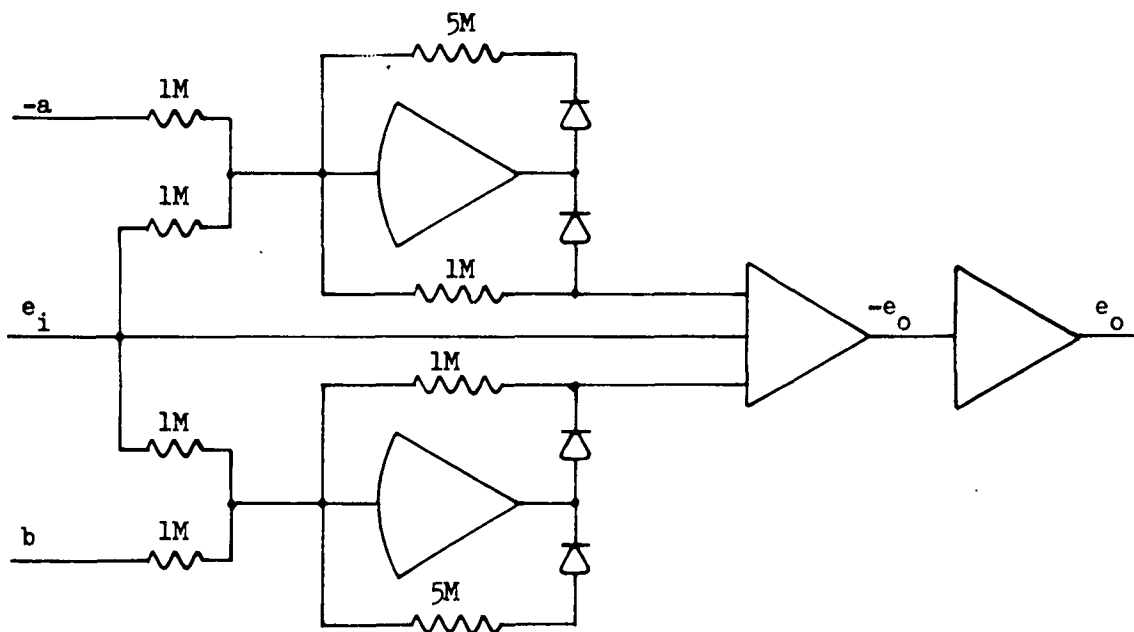
$$q_\delta / \Theta_s = \frac{(k_\Theta + k_{\dot{\Theta}} s)}{(1 + T_1 s)(1 + T_2 s)\left(1 + \frac{2\zeta}{\omega} s + \frac{s^2}{\omega^2}\right)}$$

The wiring diagram for the preceding equation is as follows.

Limiting circuits

For some applications, particularly in control system design,
certain variables have physical limits. A circuit for simu-
lating this effect is shown below.

$$e_o = a \qquad a < e_i$$

$$e_o = e_i \qquad -b < e_i < a$$

$$e_o = -b \qquad e_i < -b$$

Ground Wind Drag Simulation

The ground wind drag problem adds certain **nonlinearities** to the system and requires the generation of a random gust signal. This illustration shows how static and dynamic responses are obtained, although the actual study compared loads rather than responses. The basic equations are given below.

Dynamic: $\ddot{q} + 2\zeta\omega\dot{q} + \omega^2 q = f_1 V^2 - f_2 V\dot{q} + f_3\dot{q}^2$

Static: $\omega^2 q = f_1 V^2$

where $V = V_{steady} + V_{random}$

and V_{random} is characterized by its power spectrum

$$\Phi_v(\omega) = \sigma_v \frac{T}{\pi}\left(\frac{1}{1+T^2\omega^2}\right)$$
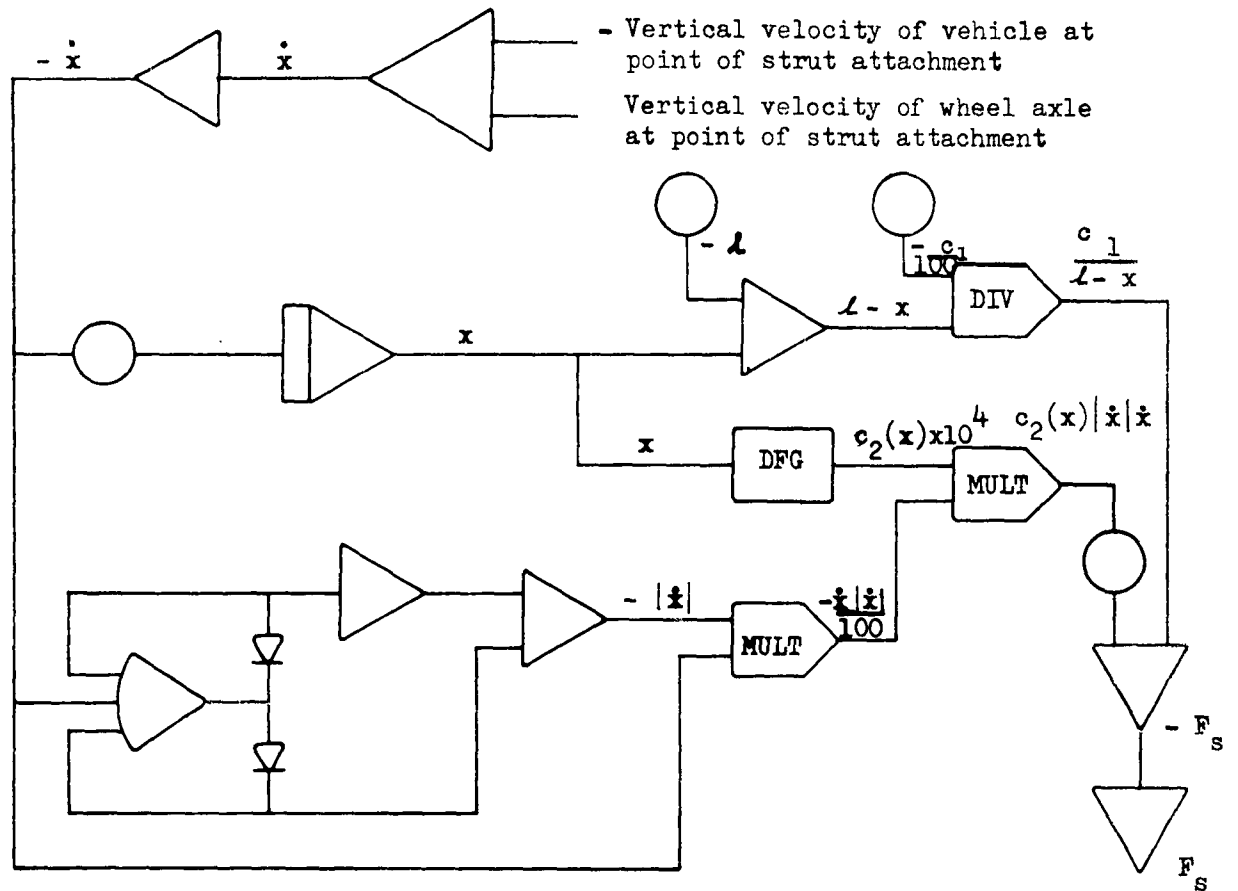

WADD TR 60-518   214
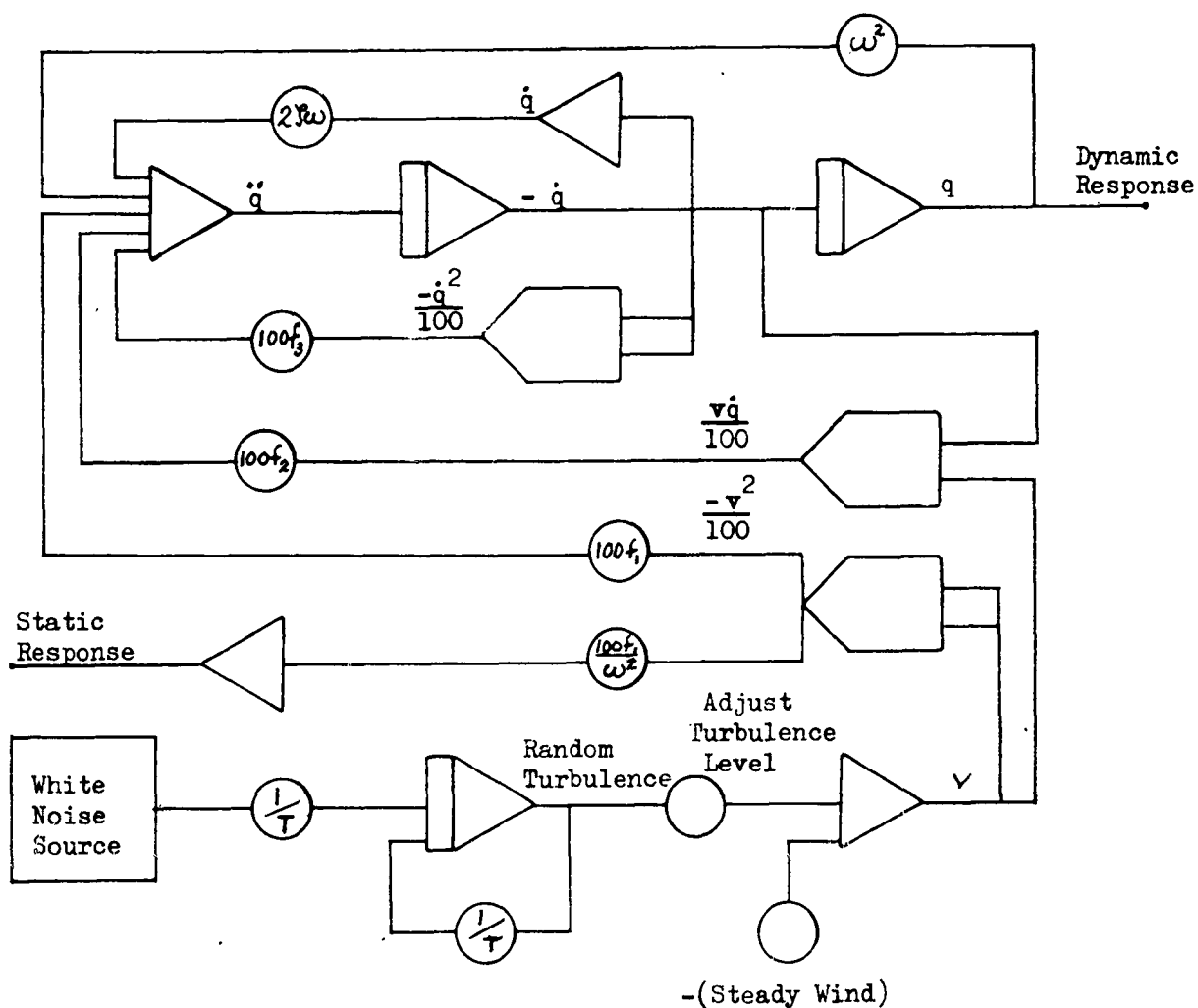
Oleo-pneumatic strut simulation

The oleo-pneumatic gear has a nonlinear airspring and hydraulic damping coefficient:

$$F_s = \frac{c_1}{\ell - x} + c_2(x) |\dot{x}| \dot{x}$$

This equation may be represented as shown below.

- Vertical velocity of vehicle at point of strut attachment

Vertical velocity of wheel axle at point of strut attachment

<u>Plastic – elastic yield strap</u>

The plastic – elastic yield strap force is a function of spring constant, k, load-deformation function, $f(y)$, and previous displacement time-history:

$$F_1 = \begin{cases} 0 & y < y_{max} - \dfrac{f(y_{max})}{k} \\[3mm] f(y_{max}) - k(y_{max} - y) & y_{max} - \dfrac{f(y_{max})}{k} \leq y \leq y_{max} \\[3mm] f(y_{max}) & y = y_{max} \end{cases}$$

where $\qquad y_{max} = \max\left[y(\tau)\right]$

$\qquad\qquad \tau \leq t$

$\qquad$ t: present instant.

This system may be simulated using the circuit below.
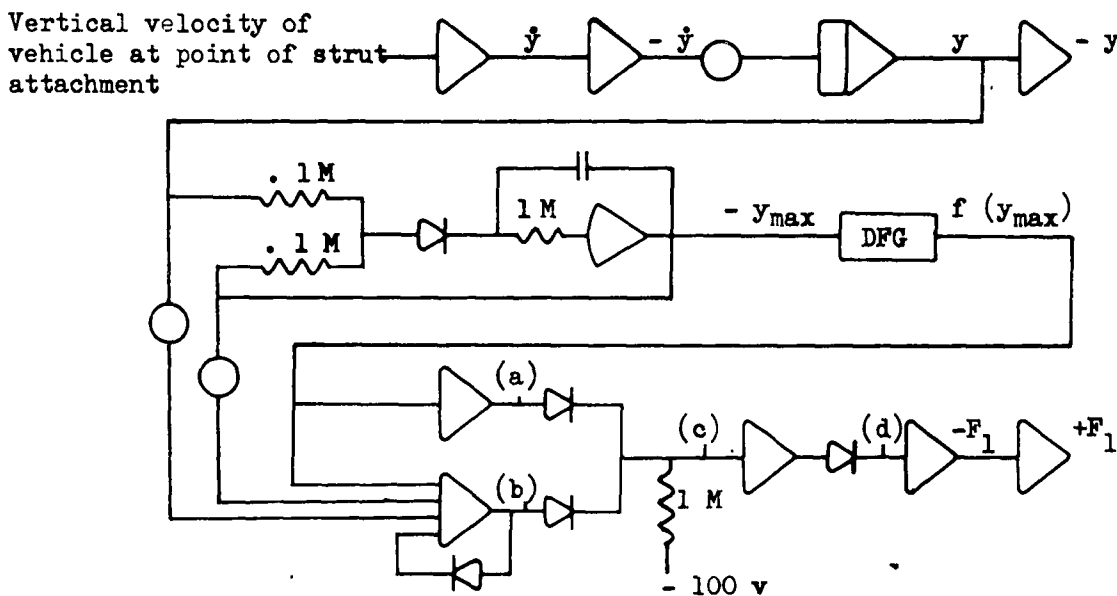
The voltage at (a) represents: $\quad - f(y_{max})$

The voltage at (b) represents: $\quad - f(y_{max}) + k(y_{max} - y)$

The voltage at (c) represents the largest, algebraically, of (a) or (b).

The voltage at (d) is always positive or zero since it is assumed that compression of the yield strap gives no negative force.

3. DIRECT ANALOGY COMPUTERS

A third type of computer--the direct analogy computer--will also be described although it was not used in this research study. In this approach a mathematical model is not established. Rather the physical system (masses, springs, dampers, forces, motions) are represented by analogous electrical variables such as inductances, capacitors, resistors, currents, and voltages.

The major use of direct analog computers is in the analysis of passive distributed parameter systems such as elastic structures. When a problem of this type is to be analyzed, a linear lumped-parameter idealization of the original system is designed. This idealized system is such that it can then be simulated exactly by a passive lumped-parameter electrical circuit. It can be shown that in most cases direct analogies can be constructed directly from the idealized structure without the necessity of writing equations.

There are many problems where passive and active analog equipment are used in conjunction. The most common examples are the analyses of elastic airfoil motions caused by aerodynamic forces which are dependent on the airfoil motion. In such an analysis the aircraft structure is simulated by passive analog elements and the aerodynamic forces are simulated by operational amplifiers.

Once the computer is wired according to the appropriate analog circuit, the computer can be regarded as an electrical model of the system. Parameter variations can be easily made and a variety of excitations can be applied. The response at any point of the system can be measured by metering the corresponding point in the circuit. A consequence, however, of using a physical system (analog) to describe another is that the results must be regarded in the same manner as test data, rather than mathematical. Computer errors other than those introduced by idealizing the problem are caused by lack of perfection of the computer elements and by the metering circuit which disturbs the thing it measures. The extent to which errors of this type can be minimized depends on the nature of the problem and the skill with which it is programmed.

APPENDIX H

REFERENCES

The following bibliography consists of (1) material referenced
in this study; and (2) articles, papers and texts which might provide
a useful starting point for a more detailed research into the various
aspects of missile dynamics.

I.   GENERAL

1.   Advances in Applied Mechanics, I, (1948), II (1951), Academic Press
     Inc., Publishers, New York.

2.   Bieber, R. E., "Missile Structural Loads by Nonstationary Statistical
     Methods", Lockheed Aircraft Corporation, Sunnyvale, California,
     April, 1959 (also available as ASTIA AD-225 595).

3.   Birkhoff, G., Hydrodynamics, Dover, 1950.

4.   Bisplinghoff, R. L., "Methods in Transient Stress Analysis", Journal
     of Aeronautical Science, Vol. 17, May, 1950.

5.   Bisplinghoff, Raymond L., Ashley, Holt, and Halfman, Robert L.,
     Aeroelasticity, Addison-Wesley Publishing Co., Inc., Cambridge,
     Mass., 1955.

6.   Bonney, E. A., Zucrow, M. J., Besserer, C. W., "Principles of Guided
     Missile Design, Vol. 2, Aerodynamics, Propulsion, Structures",
     D. Van Nostrand Co., Inc., 1956.

7.   Cheng, David K., "Analysis of Linear Systems", Reading, Mass.,
     Addison-Wesley, 1959.

8.   Clarkson, B. L., "The Effect of Jet Noise on Aircraft Structures",
     The Aeronautical Quarterly, Vol. X, Part 2, May, 1958.

9.   Crandall, S. H. (Editor), Random Vibrations, Cambridge Technology
     Press of MIT, 1958.

10. Dabies, E. F., "The Equations of Motion of a Tumbling Re-entry Body",
     California Institute of Technology, Jet Propulsion Laboratory
     Progress Report 20-339, November, 1957.

11. Donovan, A. F., and Lawrence, H. R. (Editors), Aerodynamic Components
     of Aircraft at High Speeds, Princeton University Press, 1957. (Vol. VII
     of High Speed Aerodynamics and Jet Propulsion, Princeton Series.)

12. Dryden, H. L., Murnaghan, F. P., Bateman, H., Hydrodynamics, Dover, 1956.

13. Ferri, Antonio, Elements of Aerodynamics of Supersonic Flows,
     MacMillan Company, 1949.

14. Fowler, John, "Lumped System Approximations for Lateral Vibrations" Space Technology Laboratories.

15. Goldstein, S. (Editor) Modern Developments in Fluid Dynamics, Vols. I, II, Oxford University Press (1938).

16. Hakkinen, Raime, J., Richardson, A. S., Jr., "Theoretical and Experimental Investigation of Random Gust Loads", NACA-TN 3878 (1957).

17. "High Speed Aerodynamics and Structures", 3rd Symposium, Vol. 3, March 25-27, 1958, sponsored by ARDC, USAF, University of California, Ryan Aeronautical Company and Convair.

18. Hilton, W. F., High-Speed Aerodynamics, Longmans, Green and Company, 1951.

19. Hoerner, Sighard F., Fluid Dynamic Drag, Published by the author, 1958.

20. Houbolt, J. C., "A Recurrence Matrix Solution for the Dynamic Response of Elastic Aircraft", Journal of the Aeronautical Sciences, Vol. 17, No. 9, (Sept. 1950): 540-550.

21. Jarmolow, K., "Dynamics of Spinning Rocket with Varying Moment of Inertia and Applied Moment", Journal of Applied Physics, Vol. 28, No. 3, March 1957.

22. Kachigan, K., "The General Theory and Analysis of a Flexible Bodied Missile with Autopilot Control", Nov. 11, 1955, Report No. ZU-7-048; AFBMD document No. 56-1067 (Contract AF 04(645)4) (Also available as ASTIA AD-218 758).

23. Kuethe, A. M., and Schetzer, J. D., Foundations of Aerodynamics, John Wiley and Sons, 1950.

24. Lamb, H., Hydrodynamics, Dover, 1945.

25. Laning, J. H. and Batten, R. H., Random Processes in Automatic Control, McGraw-Hill Book Co., Inc. 1956.

26. Leitmann G., "On the Equations of Motion", British Interplanetary Society Journal, July-September 1957.

27. Liepmann, Hans W., and Puckett, Allen E., Introduction to Aerodynamics of a Compressible Fluid, GALCIT Aeronautical Series, John Wiley & Sons 1947.

28. Liepmann, Hans W., and Roshko, A., Elements of Gas Dynamics, John Wiley & Sons, 1957.

29. Lin, C. C., "Theory of Hydrodynamic Stability", Proceedings of the Fifth Symposium in Applied Mathematics, Cambridge University.

30. Miles, E. R. C., Supersonic Aerodynamics, A Theoretical Introduction McGraw-Hill Book Company, 1950.

31. Milne-Thompson, L. M., Theoretical Aerodynamics, 2nd Edition., D. Van Nostrand Company, 1952.

32. Mirels, Harold, and Thornton, Philip R., "Effect of Body Perturbations on Hypersonic Flow Over Slender Power Law Bodies", NASA TR-R-45, 1959.

33. "Missiles, Rockets, and Satellites, Vols. I, II, III, IV, and V" (Bibliographical survey), Dept. of the Army, Pamphlet No. 70-5-1,2,3,4 and 5, June, 1958.

34. Ostwatitsch, Klaus, Gas Dynamics (Gasdynamik), Springer-Verlag, Berlin, 1952.

35. Pistiner, J. S., "Stability Criteria for the Airframe Dynamics of a Liquid Propellant Rocket", Journal of the Aero/Space Sciences, October, 1959.

36. Prandtl, L., and Tietjens, O. G., Fundamentals of Hydro-and Aero-mechanics, Dover Publications, 1957.

37. Press, H., et al, "Some Applications of Generalized Harmonic Analysis to Gust Loads on Airplanes", Journal of the Aeronautical Sciences, January, 1955.

38. Ramberg, W., "Transient Vibration in an Airplane Wing Obtained by Several Methods", Journal of Research, National Bureau of Standards , May, 1949.

39. Rayleigh, J. W. S., The Theory of Sound, Vols. I, II, (1894), (1896), Dover, 1945.

40. Roberson, R. E., "Torques on a Satellite Vehicle from Internal Moving Parts", Journal of Applied Mechanics, Vol. 25, June, 1958.

41. Rutherford, D. E., Classical Mechanics, Interscience Publishers, Inc., 1957.

42. Sandborn, V. A., "An Equation for the Mean Velocity Distribution of Boundary Layers", NASA Memo 2-5-59E.

43. Sauer, Robert, Introduction to Theoretical Gas Dynamics, Springer-Verlag, Berlin, 1943.

44. Scanlan, R. H., and Rosenbaum, R., Introduction to the Study of Aircraft Vibration and Flutter, The MacMillan Co., New York, 1951.

45. Sears, William R., (Editor), General Theory of High Speed Aerodynamics, Vol. 6, Princeton University Press, 1954.

46. Shapiro, Ascher H., The Dynamics and Thermodynamics of Compressible Fluid Flow, Vols. I and II, The Ronald Press Company., New York, 1953.

47. Sokolnikoff, I. S., Mathematical Theory of Elasticity, McGraw-Hill Book Co., New York, 1956.

48. Sommerfeld, A., Mechanics of Deformable Bodies, (1946), Academic Press Inc., New York, 1950.

49. Space Technology Laboratories, 7, April, 1958
    <u>Generalized Missile Dynamics Analysis</u>

    | I | "Development and Application", Barton, M. V., | EM 8-7 |
    | II | "Equations of Motion", Young, D. | EM 8-8 |
    | III | "Aerodynamics", Miles, J., and Young, D. | EM 8-9 |
    | IV | "Sloshing", Miles, J. W., and Young, D. | EM 8-10 |
    | V | "Bending Modes", Fowler, J. R. | EM 8-16 |
    | VI | "Control System Equations", Martin, D. C. | EM 8-14 |
    | VII | "Programming", Brooks, J. A. | EM 8-15 |

50. Trilling, Leon, et al, <u>Aerodynamics of Missiles</u>, Massachusetts
    Institute of Technology, 1957

51. Tsien, H. S., "Notes on Aerodynamics of Compressible Fluids"
    (unpublished) Massachusetts Institute of Technology, Cambridge, 1959

52. Varland, Walter B., et al "Study of Guided Missiles Structural Design
    Criteria", WADC Technical Report 57-140, Vol. I, February, 1959

53. von Karman., <u>Collected Works of Theodore von Karman</u>, Vols. I, II, III,
    IV., Butterworth's Scientific Publications, London, 1956

54. von Karman, T., "Some Significant Developments in Aerodynamics since
    1946", Journal of the Aero/Space Sciences, Vol. 26, No. 3, March, 1959

55. von Karman, Theodore, "Supersonic Aerodynamics, Principles and
    Applications", Journal of the Aeronautical Sciences, July, 1947

II. <u>PRELAUNCH</u>

56. Barton, M. V., "Ground Shock Environment -- Measurement and Application"
    Shock and Vibration Bulletin, Part I, Office of the Secretary of Defense
    Washington, D. C., Sept. 1958

57. Biot, M. A., "A Mechanical Analyzer for the Prediction of Earthquake
    Stresses", Bulletin Seismological Society of America, Vol. 31, 1941

58. Buell, D. A., and Kenton, G. C., "The Wind-Induced Loads on a
    Dynamically Scaled Model of a Large Missile in Launching Position",
    NASA TM X-109, Dec., 1959 (Confidential)

59. Court, A., "Wind Extremes as Design Factors", Journal of the Franklin
    Institute, July, 1953

60. Den Hartog, J. P., "Recent Technical Manifestations of von Karman
    Vortex Wake", Proceedings of the National Academy of Sciences, May 1954

61. Fung, Y. C., "Fluctuating Lift and Drag Acting on a Cylinder in a Flow
    at Supercritical Reynolds Numbers", Institute of the Aeronautical
    Sciences Paper Number 60-6, 1960

62. Fung, Y. C. and Barton, M. V., "Some Shock Spectra Characteristics
    and Uses", Journal of Applied Mechanics, Transactions, ASME, Sept., 1958

63. Goldman, R. L., "Karman Vortex Forces on the Vanguard Rocket",
     Shock and Vibration Bulletin, Part II, Dec., 1958

64. Hama, F. R., "Three Dimensional Vortex Pattern Behind a Circular
     Cylinder", Journal of the Aeronautical Sciences, Vol. 24, No. 2,
     February, 1952

65. Hama, F. R., Long, J. D., and Hegarty, J. C., "On Transition from
     Laminar to Turbulent Flow", Journal of Applied Physics, February, 1957

66. Handbook of Geophysics, Air Force Cambridge Research Center, Air
     Research and Development Center, 1957

67. Henry, Robert M., "A Study of the Effects of Wind Speed, Lapse Rate,
     And Altitude on the Spectrum of Atmospheric Turbulence at Low Altitude",
     IAS Pre-print 59-43, January, 1959

68. Housner, G. W., "Spectrum Intensities of Strong-Motion Earthquakes"
     Proceedings of the Symposium on Earthquake and Blast Effects in
     Structures, UCLA, Los Angeles, California, 1952

69. Housner, G. W. and McCann, G. D., "The Analysis of Strong-motion
     Earthquake Records with the Electric Analog Computer", Bulletin of the
     Seismological Society of America, Vol. 29, 1949

70. Housner, G. W., Martel, R. R., and Alford, J. L., "Spectrum Analysis
     of Strong-Motion Earthquakes", Bulletin of the Seismological Society
     Of America, Vol. 43, April, 1953.

71. Hudson, D. E. and Housner, G. W., "Structural Vibrations Produced by
     Ground Motion", Transactions of the ASCE, Vol. 122, 1957

72. Kovasznay, L. S. G., "Hot Wire Investigation of Wake Behind Cylinder
     at Low Reynolds Number", NACA TM 1130 (1947)

73. Lappe, U. O., Davidson, B., and Notess, C. B., "Analysis of Atmospheric
     Turbulence Spectra Obtained from Concurrent Airplane and Tower
     Measurements", IAS Preprint 59-44, January, 1959

74. Miles, J. W., "On the Disturbed Motion of a Plane Vortex", Journal
     of Fluid Mechanics, Vol. 4, Part 5, Sept. 1958 (Also NACA TN 2887)

75. Panofsky, H. A., and McCormick, R. A., "Properties of Spectra of
     Atmospheric Turbulence at 100 Meters", Quarterly Journal of the Royal
     Meteorological Society, Vol. 80, No. 346, Oct., 1954

76. Panofsky, H. A. and Van der Hoven, Isaac: "Structure of Small Scale
     and Middle Scale Turbulence at Brookhaven", Pennsylvania State University,
     Department of Meteorology, March, 1956

77. Rosenhead, L., Vortex Systems in Wakes, Advances in Applied Mechanics III,
     Academic Press Inc., New York, 1953

78. Roshko, A., "On the Development of Turbulent Wakes from Vortex Sheets",
     NACA TN 2413 (1953)

79. Roshko, A., "On the Drag and Shedding Frequency of Bluff Cylinders", NACA TN 3169 (July 1954)

80. Roshko, A., "On the Wake and Drag of Bluff Bodies", Journal of the Aeronautical Sciences, February, 1955

81. Rouse, H., Elementary Mechanics of Fluids, John Wiley & Sons, Inc., New York, 1946

82. Sacks, A. H., "Vortex Interference Effects on the Aerodynamics of Slender Airplanes and Missiles", Journal of the Aeronautical Sciences, Vol. 24, No. 6, June 1957

83. Taylor, G. I. "The Spectrum of Turbulence", Proceedings of the Royal Society, 164 (A), 1938

84. Townsend, A. A., "Diffusion in Turbulent Wake of a Cylinder", Proceedings of the Seventh International Congress of Applied Mechanics, 2, 227-248, (1948)

85. USAF Bulletin 106A, March 8, 1957

86. Van der Hoven, Isaac, and Panofsky, H. A., "Statistical Properties of the Vertical Flux and Kinetic Energy at 100 Meters", Pennsylvania State University, Department of Meteorology, June 1954

III. LAUNCH

87. Berman, K. and Cherey, S. H., "Rocket Motor Instability Studies", Jet Propulsion, Vol. 25, No. 10, October 1955

88. Crocco, L. and Grey, J., "Combustion Instability in Liquid Propellant Rocket Motors", Princeton University Aeronautical Engineering Report No. 216C, Appendix A, January 1953

89. Crocco, L,, Grey, J., and Harrje, D. T., "On the Importance of the Sensitive Time Lag in Longitudinal High Frequency Rocket Combustion Instability", Jet Propulsion, Vol. 28, No. 12, December 1958

90. Goodman, Theodore, "Launching of Airborne Missiles Under Water" Part III Note on Lateral Hydrodynamic Forces Due to the Free Surface. August 1959 (Available as ASTIA Ad-219 758)

91. E. V. Laitone, "Effect of Acceleration on the Longitudinal Dynamic Stability of a Missile", American Rocket Society, Vol. 29, Number 2 Feb. 1959

92. Levine, R. S., and Lawhead, R. W., "A Survey of Combustion Instability In Liquid Propellant Rocket Engine" North American Aviation, Inc.

93. Matthews, G. B., "Determination of Combustion Time Lag Parameter in a Liquid Bi-propellant Rocket Motor" Princeton University Aeronautical Report No. 372, Appendix C., March, 1957

94. Miesse, C. C., "The Effect of Ambient Pressure Oscillations on the Disintegration and Dispersion of a Liquid Jet", Jet Propulsion, Vol. 25 1955

95. Osborn, J. R., and Zucrow, M. J., "A Literature Survey on Combustion Pressure Oscillations in Liquid Propellant Rocket Motors", Purdue University Report TM 57-2, June 1957 (Confidential)

96. Osborn, J. R., and Zucrow, M. J., "An Unclassified Literature Survey on Combustion Pressure Oscillations in Liquid Propellant Rocket Motors", Purdue University Report TM 57-1, June 1957

97. Oswald, T. W., "Dynamic Behavior During Accelerated Flight with Particular Application to Missile Launching", Journal of the Aeronautical Sciences, Vol. 23, No. 8, August 1956

98. Oswald, T. W., "A Note on Missile Launching", Journal of the Aeronautical Sciences, Vol. 24, No. 1, January 1957

99. Price, E. W., "One Dimensional Steady Flow with Mass Addition and the Effect of Combustion Chamber Flow on Rocket Thrust", Jet Propulsion, Vol. 25, No. 10, October 1955

100. Reichel, R. H., "Dynamic Stability of Rocket Powerplants Using Liquid Propellants", Aero Digest, Vol. 73, No. 5, November 1956

101. Sanders, J. C., Novik, D., Hart, C. E., "Effect of Dynamic Characteristics of Rocket Components on Rocket Control", Aeronautical Engineering Review, Oct., 1957

102. Tonda, T. P., "Notes on Problems in Combustion Instability of Rocket Motor", Aeronautical Engineering Review, November 1957

103. Wick, R. S., "The Effect of Vehicle Structure on Propulsion System Dynamics and Stability", Jet Propulsion, Vol. 26, No. 10, Oct., 1956

IV.   BOOSTED FLIGHT

104. Boatright, William B., "Experimental Study and Analysis of Loading and Pressure Distributions on Delta Wings Due to Thickness and to Angle of Attack at Supersonic Speeds", NACA RM L56I14, Dec., 1956

105. Dvoskin, N., and Sissenwine, N., "Evaluation of AN/GMD-2 Wind Shear Data for Development of Missile Criteria", Air Force Surveys in Geophysics No. 99, AFCRC-TN-58-259 (Available as AD-152495), April 1958

106. Ellis, Macon C., Jr., and Hasel, Lowell E., "Preliminary Investigation at Supersonic Speeds of Triangular and Sweptback Wings", NACA TN 1955 October 1949

107. Foster, Gerald V., "Exploratory Investigation at Mach Number of 2.01 of the Longitudinal Stability and Control Characteristics of a Winged Re-entry Configuration", NASA TM X-178, De c., 1959.

108. Hobbs, N. P., Criscione, E. S. Massola, L. L., and Frassinelli, G. J., "Development of Interim Wind, Wind Shear, and Gust Design Criteria for Vertically-Rising Vehicles", AviDyne Research, Inc., Wright Air Development Center, July, 1959 (Secret)

109. Joseph, Lt. E., Unpublished Wind Shear and Gust Design Criteria, WADC, May, 1959

110. McDevitt, J. B., and Rakich, J. V., "The Aerodynamic Characteristics of Several Thick Delta Wings at Mach Numbers to 6 and Angles of Attack to 50°", NASA TM X-162, March 1960

111. Manton, F. E. S., and Renny, H. B., "A Solution of Missile Dynamics During Boost Phase (Fixed Controls)", ARDE (Gt. Brit.), December, 1959 (Available as ASTIA AD-231 671)

112. Perkins, C. D., and Hage, R. E., Airplane Performance Stability and Control, John Wiley & Sons, Inc., New York, 1949

113. Press, Harry, Meadows, May T., and Hadlock, Ivan, "A Reevaluation of Data on Atmospheric Turbulence and Airplane Gust Loads for Application In Spectral Calculations", NACA Report 1272, March 1956

114. Press, Harry, and Steiner, Roy, "An Approach to the Problem of Estimating Severe and Repeated Gust Loads for Missile Operations", NACA TN 4332, Sept., 1958

115. Sissenwine, N., "Development of Missile Design Wind Profiles for Patrick Air Force Base", Air Force Surveys in Geophysics No. 96, AFCRC-TN-58-216 (available as ASTIA AD-146870), March 1958

116. Sissenwine, N., GRD AFCRC Memorandum entitled "Revised 1% Synthetic Wind Profile", June, 1959

117. Sissenwine, N., "Windshear, and Gusts for Design of Guidance Systems for Vertically Rising Air Vehicles", Air Force Surveys in Geophysics No. 57, AFCRC-TN-58-216 (available as ASTIA AD-146870) November, 1954

118. Thorson, K. R.,and Bohne, Q. R., "Application of Power Spectral Methods in Airplane and Missile Design", Journal of the Aero/Space Sciences, Vol. 27, No. 2, February 1960

119. West, F. E., Jr., Trescot, C. D., Jr., and Wiley, A. N., Jr., "Aerodynamic Characteristics for Two Hypersonic Glider Models With and Without Wing and Vertical-Tail Trailing Edge Chord Extensions at a Mach Number of 0.94", NASA TM X-66, Feb., 1960

120. West, F. E., Jr., Trescot, C. D., Jr.,and Wiley, A. N., Jr., "Effects of Elevon Deflection on the Aerodynamic Characteristics of a Hypersonic Glider Model at Mach Numbers of About 0.62 and 0.96", NASA TM X-203, Feb., 1960

121. West, F. E., Jr., Trescot, C. D., Jr., and Wiley, A. N., Jr., "Effect of Vertical-Tail and Rudder Deflection on the Aerodynamic Characteristics of a Hypersonic Glider Model at Mach Numbers of About 0.62 and 0.93", NASA TM X-189, Feb., 1960

122. West, F. E., Jr., Trescot, C. D., Jr., and Wiley, A. N., Jr., "High Subsonic Investigation of the Aerodynamic Characteristics of A Hypersonic Glider Model With and Without Deflected Elevons and Body Flap", NASA TM X-204, Feb., 1960

123. Williams, J. J., and Bergst, G. L., Jr., "Design Wind Criteria for Air Force Missile Test Center", Lockheed Aircraft Corporation, Missile Systems Division Report LMSD-2933, 30 April, 1958

V. STAGING

124. Rodean, R. C., "Rocket Thrust Termination Transients", American Rocket Society Journal, Volume 29, No. 6, June 1959.

125. Spalding, D. B., "Combustion in Liquid Fuel Rocket Motors", Aeronautical Quarterly, Vol. X, Part 1, February 1959.

VI. RE-ENTRY

126. Belanger, J., "Effect of Wind on a Ballistic Missile Re-entry Trajectory", Canadian Armament Research and Development Establishment, October, 1959 (Available as ASTIA AD-232 313)

127. Boeing Airplane Company, "Handbook for Aerodynamic Heat Transfer Computation", Vol. I and II Document Number D2-5107.

128. Chapman, Dean R., "An Approximate Analytical Method for Studying Entry into Planetary Atmospheres", NASA TR R-11, 1959 (also available as ASTIA AD-231 530)

129. Grant, Frederick C., "Importance of Variation of Drag with Lift in Minimization of Satellite Entry Accelerations", NASA TN D-120, October, 1959 (also available as ASTIA AD-227-118)

130. Newman, B. G., "Flow in a Viscous Trailing Vortex", The Aeronautical Quarterly, Vol. X, Part 2, May 1959

131. Paulson, John W., and Shanks, Robert E., "Investigation of Low-Subsonic Flight Characteristics of a Model of a Flat-Bottom Hypersonic Boost-Glide Configuration Having a 78° Delta Wing", NASA TM X-201 October 1959 Confidential

132. Press, H., and Meadows, M. T., "A Re-evaluation of Gust-Load Statistics for Applications in Spectral Calculations", NACA TN 3540, August 1955

133. Rice, S. O., "Mathematical Analysis of Random Noise", Selected Papers on Noise and Stochastic Processes, edited by Nelson Wax, Dover Publications, 1954

VII. LANDING

134. Ayvazian, Mihran, and O'Brien, T. F., "Effect of Structural Flexibility on Aircraft Loading, Part XV, A Parametric Study of Symmetrical Landing and Taxiing Loads by Means of Analogue Computations" Air Force Technical Report No. 6358, Part XV, November 1953

135. Bisplinghoff, R. L., and Doherty, C. S., A Two Dimensional Study of the Impact of Wedges on a Water Surface", Contract No. NOa(s)-9921 Department of Aeronautical Engineering, M.I.T., March 20, 1950

136. Borg, S. F., "Three Dimensional Wedge Impact on a Compressible Fluid" Journal of Applied Physics, Vol. 31, No. 2, Feb., 1960

137. Cook, Francis E., and Milwitsky, Benjamin, "Effect of Interaction on Landing-Gear Behavior and Dynamic Loads in a Flexible Airplane Structure" NACA Report 1278, 1956

138. Cumberbatch, E., "Two-Dimensional Planing at High Froude Number" Journal of Fluid Mechanics, Vol. 4, September 1958

139. Downing, J. R., et al, "Recovery Systems for Missiles and Target Aircraft Part I, II, III", Air Force Technical Report 5853, Dec., 1956

140. Fabula, A. G., "Ellipse Fitting Approximation of Two-Dimensional Normal Symmetric Impact of Rigid Bodies on Water", Fifth Midwestern Conference on Fluid Mechanics, 1957

141. Foote, J. R., and Giever, J. B., "Study of Parachute Opening, Part II" WADC Technical Report 56-253 (available as ASTIA AD-205 541) June, 1958

142. Franklin, J. M., "Effects of Impact on Simple Elastic Structures", David Taylor Model Basin Report 481, April 1942

143. Fung, Y. C., "The Analysis of Dynamic Stresses in Aircraft Structures During Landing as Nonstationary Random Processes", Journal of Applied Mechanics, Transactions ASME, 1955

144. Heinrich, Helmut G., "Drag and Stability of Parachutes", Aeronautical Engineering Review, June, 1956

145. Hoerner, S. F., "Drag Characteristics of Parachutes", Air Force Technical Report No. 6201, October 1950

146. Hoffman, E. L., "Comparison With Theory of Landing Impacts of a Model of a Seaplane Incorporating a Hydro-ski With and Without Shock Absorber" NACA RM L56D26, July 11, 1956

147. Idomir, Kenneth, "TM-76 Mace Landing Mat Design", Aero/Space Engineering, Vol. 19, No. 2, February 1960

148. Kaplan, L., "Bibliography of References Related to Hydro-Ski Loads", (Available as ASTIA AD-216 363,) February 16, 1959

149. McKay, James M., "Measurements Obtained During the First Landing of the North American X-15 Research Airplane", NASA TM X-207 Oct., 1959 (Confidential)

150. Matranga, Gene J., and Menard, Joseph A., "Approach and Landing Investigation at Lift-Drag Ratios of 30 to 4 Utilizing a Delta-Wing Interceptor Airplane", NASA TM X-125, October 1959 (Also available as ASTIA AD-312 849) (Confidential)

151. May, Albert and Jean C. Woodhull, "The Virtual Mass of a Sphere Entering Water Vertically", Journal of Applied Physics, December 1950, Vol. 21, No. 12 pp. 1285-1289

152. Mayo, W. L., "Analysis and Modification of Theory for Impact of Seaplanes on Water", NACA Report 810, 1945 and NACA TN 1008, 1945.

153. Mayo, Wilber L., "Hydrodynamic Impact of a System with a Single Elastic Mode", NACA Report 1074, 1952

154. Milwitsky, B., "A Generalized Theoretical Investigation of Hydrodynamic Pitching Moments Experienced by V-Bottom Seaplanes During Steplanding Impacts and Comparisons with Experiment", NACA TN 1930, 1948

155. O'Bryan, Thomas C., and Hatch, Howard G., "Limited Investigation of Crushable Structures for Acceleration Protection of Occupants of Vehicles at Low Impact Speeds", NASA TN D-158, October, 1959.

156. Pierson, J. D., "The Penetration of a Fluid Surface by a Wedge", Stevens Institute of Technology Experimental Towing Tank Reports 381 and 382, 1950.

157. Powell, M. A. and Shepherd, J. V., "Development of a System for the 'Over Sea' Recovery of Guided Missiles", NACA TN GW 439, January 1957.

158. Reeder, J. P., "The Effect of Lift Drag and Speed on the Ability to Position a Gliding Aircraft for a Landing on a 5000 foot Runway", NASA Memo 3-12-59L.

159. Richardson, E. G., "The Impact of a Solid on a Liquid Surface", Proceedings of the Physical Society 61, 1948.

160. Schnitzer, E., "Theoretical Determination of Water Loads on Pitching Hulls and Shock-Mounted Hydro-skis", NASA TN D-392, May 1960.

161. Shiffman, M., Spencer, D. D., "The Force of Impact on a Sphere Striking A Water Surface" (Second Approximation)" AMP Report 42.2R, Applied Mathematics Group, New York University, No. 133, July 1945.

162. Smiley, Robert F., "A Theoretical and Experimental Investigation of the Effects of Yaw on Pressures, Forces, and Moments during Seaplane Landings and Planing", NACA TN 2817 November 1952.

163. Szebehely, V. G., "Hydrodynamic Impact", Applied Mechanics Review May 1959.

164. Topping, A. D., Marketos, J. D., and Costakos, N. C., "A Study of Canopy Shapes and Stresses for Parachutes in Steady Descent", WADC Tech. Report 55-294, October 1955.

165. Trilling, Leon, "The Impact of a Body on a Water Surface at an Arbitrary Angle", Journal of Applied Physics, Vol. 21, No. 2, February 1950, pp. 161-170 .

166. Weber, Richard J., and Pauson, Werner M., "Some Thrust and Trajectory Considerations for Lunar Landings", NASA TN D-134, November 1959, (Also available as ASTIA AD 228 814).

167. Widmayer, E, Jr., and Schwab, R. H., "Structural and Impact Loads for the Flexible Airplane During Water Landings", Journal of the Aeronautical Sciences, March 1958.

B. MODAL DETERMINATION

168. Benscoter, S. U. and MacNeal, R. H., "Equivalent Plate Theory for a Straight Multicell Wing", NACA TN 2786, September 1952 .

169. Duffin, R. J., Gustafson, P. N., and Warner, W. H., "Natural Vibrations of Cantilevered Triangular Plates", Carnegie Institute of Technology, September 1952. '

170. Fung, Y. C., "Bending of Thin Elastic Plates of Variable Thickness", Journal of the Aeronautical Sciences, Vol. 20, No. 7, July 1953.

171. Lubkin, J. L. and Luke, Y. L., "Modes and Frequencies of Wings of Triangular Planform", WADC Technical Report 56-335, June 1956.

172. Mahalingam, S., "An Improvement of the Myklestad Method for Flexural-Vibration Problems", Journal of the Aero/Space Sciences, Vol. 26, No. 1, January 1959.

173. Myklestad, N. O., "Numerical Analysis of Forced Vibrations of Beams", Journal of Applied Mechanics, Vol. 20, No. 1, March 1953.

174. Reissner, E., and Stein, M., "Torsion and Transverse Bending of Cantilever Plates", NACA TN 2369, June 1951.

175. Stein, M., and Sanders, L., "A Method for Deflection Analysis of Thin Low-Aspect-Ratio Wings", NACA TN 3604, June 1956.

176. Turner, M. J., Clough, R. W. Martin, H. C., and Topp, L. J., "Stiffness and Deflection Analysis of Complex Structures", Journal of the Aeronautical Sciences, Vol. 23, No. 9, September 1956.

177. Williams, D., "A General Method (Depending on the Aid of a Digital Computer) for Deriving the Structural Influence Coefficients of Aeroplane Wings", R.A.E. Report Number: Structures 168, Nov. 1954.

C. EQUATIONS OF MOTION

178. Abrason, H. N., An Introduction to the Dynamics of Airplanes, The Ronald Press Company, New York, 1958.

179. Baron, M. L., and Bleich, H. H., "The Dynamic Analysis of Empty and Partially Full Cylindrical Tanks. Part I. Frequencies and Modes of Free Vibration and Transient Response by Mode Analysis", Wiedlinger, Paul, New York, May 1959.

180. Berry, J. G. and Reissner, E., "The Effect of an Internal Compressible Fluid Column on the Breathing Vibrations of a Thin Pressurized Cylindrical Shell", Journal of the Aeronautical Sciences, Vol. 25, No. 5, May 1958.

181. Budiansky, Bernard, "Sloshing of Liquids in Circular Canals and Spherical Tanks", Journal of the Aero-Space Sciences, Vol. 27, March 1960.

182. Eulitz, Werner, R., "Theoretical Discussion of the Sloshing Phenomenon and a Proposed Method for Depressing of Sloshing in Fuel Containers", ABMA, TN No. ORDAB-DSM No. 45, 1957.

183. Fung, Y. C., et al, "On the Vibration of Thin Shells Under Internal Pressure", Journal of the Aeronautical Sciences, Vol. 24, No. 9, September 1957.

184. Hahne, H. V., "Oscillation of a Gas in an Elastic Cylinder Shell", Third U. S. National Congress of Applied Mechanics, December 1958.

185. Housner, G. W., "Dynamic Pressures on Accelerated Fluid Containers" Bulletin of the Seismological Society of America, Vol. 47, No. 1, January 1957.

186. Lawrence, H. R., et al, "Variational Solution of Fuel Sloshing Modes", Jet Propulsion, Vol. 28, No. 2, November 1958.

187. Levin, E., "Conical Sloshing", Ramo-Wooldridge Corporation, PA/M-553/1.

188. Love, A. E. H., The Mathematical Theory of Elasticity, 4th Edition, Dover Publication, New York, 1944.

189. Margenau, Henry, and Murphy, George M., The Mathematics of Physics and Chemistry, 2nd Edition, D. Van Nostrand Company, Inc. Princeton, New Jersey, 1956.

190. Miles, J. W., The Potential Theory of Unsteady Supersonic Flow, Cambridge University Press, 1959.

191. Miles, J. W., "Ring Damping of Free Surface Oscillations", Journal of Applied Mechanics, Vol. 25, No. 2, June 1958.

192. Sokolnikoff, I. S., Tensor Analysis, John Wiley & Sons, Inc., New York, 1951.

193. von Karman, Theodore, and Biot, Maurice A., Mathematical Methods in Engineering, McGraw-Hill Book Company, Inc., 1940.

G. COMPUTERS

194. Pruden, F. W., "Combined Analog-Digital Simulation of Engineering Problems", NASA CN-78952, February 18, 1960.

Boeing Airplane Co., Seattle, Wash.
THE DYNAMIC RESPONSE OF ADVANCED VEHICLES, by
Q. R. Bohne, B. E. Clingan, C. W. de Ceault, et al.
September, 1960. 230p. incl. illus. tables, 194
refs. (Proj. 1370; Task 14000) (WADD-TR-60-518)
(Contract AF 33(616)-6597)   Unclassified report

An analytical study program has been conducted in
order to determine dynamic load conditions and
governing parameters for the flight of advanced
vehicles; and an assessment of the adequacy and the
applicability of existing dynamic loads predictions
methods has been made.

A typical two stage liquid fuel boost-glide con-
figuration is assumed for the study, thus allowing
for the interaction of such variables as fuel slosh,
structural flexibility, aerodynamic forces and

control system forces. The report is divided into
sections which discuss dynamic loads in the follow-
ing areas: pre-launch, launch, boosted flight,
staging, re-entry and landing or recovery. Includ-
ed in the Appendices are discussions of modal de-
termination, simplified methods of analysis,
computational techniques, and ground wind criteria.
Also included is a development of flight equat'ons
of motion and an extensive bibliography of reference
material.